

# Ultraviolet-A activation of the transcription factor Nrf2 in human skin: Implications for the anti-apoptotic protein heme oxygenase-1

Edwards, Gavin Peter

*Award date:*
2007

*Awarding institution:*
University of Bath

UNIVERSITY OF
BATH

# Ultraviolet-A Activation of the Transcription Factor Nrf2 in Human Skin: Implications for the Anti-Apoptotic Protein Heme Oxygenase-1

**Gavin Peter Edwards**

*A Thesis Submitted to the University of Bath for the Degree of Doctor of Philosophy*

Department of Pharmacy and Pharmacology, University of Bath, Bath, UK

May 2007







ProQuest LLC
789 East Eisenhower Parkway
P.O. Box 1346
Ann Arbor, MI 48106-1346

**Acknowledgements**

*I wish to thank all of the family and friends that have supported my work over the past three years. I would like to thank all of the members of labs 2.14 and 2.20, both past and present, for all of the help and guidance I have received over the course of my PhD. Most of all, I would like to extend my deepest thanks to my project supervisor and friend Prof. Rex Tyrrell. I wish to thank Prof. Rex Tyrrell for allowing me the opportunity to study within a world renowned research group, but also for his constant enthusiasm, patience, and friendly approach towards my project.*

## ABSTRACT

Heme oxygenase-1 (HO-1) is the ultraviolet-A (UVA) (320-380 nm) inducible isoform of the rate-limiting enzyme involved in heme degradation. Up-regulation of HO-1 by UVA provides a crucial cellular defence mechanism against oxidative stress in human skin, but the events underlying HO-1 regulation by UVA remain poorly characterised in human cells. In murine models, work with other inducers (heavy metals, heme) has demonstrated that the HO-1 gene is transcriptionally activated by NF-E2-Related Factor 2 (Nrf2). In this study the oxidising UVA component of solar radiation has been employed as a model system to elucidate the molecular mechanisms involved in transcriptional up-regulation of the HO-1 gene by Nrf2 in human skin. Here evidence is provided showing that UVA causes immediate whole cell accumulation of Nrf2 in primary human skin fibroblasts. Previous work from this laboratory has shown that UVA treatment results in the release of the HO-1 substrate heme from heme-containing proteins. In relation to this, the results of this study indicate that treatment with heme results in Nrf2 accumulation in human skin cells, and furthermore, that depletion of intracellular heme prevents UVA-mediated Nrf2 accumulation. Moreover, it is shown that UVA generated reactive oxygen species influence the amount of cytoplasmic Nrf2, and that UVA enhances *NRF2* transcriptional activation. Based on these observations, a molecular regulatory system is proposed where UVA promotes nuclear translocation of Nrf2, enhances transcriptional activation of *NRF2*, and stabilises Nrf2 through the release of heme. Here, it is suggested, that the resultant accumulation of Nrf2 may initiate up-regulation of the HO-1 gene which in turn degrades heme. In this study, the hypothesis that HO-1 modulates apoptosis in human melanoma cells has also been investigated. It is known that HO-1 possesses potent anti-apoptotic activity in both human and murine models, and that human melanoma cells often lack apoptotic potential and prove highly resistant to cytotoxic cancer therapies. The results of this study show that HO-1 over-expression in human melanoma cells prevents UVA-apoptosis in a dose-dependant manner. These data indicate that HO-1 may prove a suitable therapeutic target for pharmacological modulation in order to increase the efficacy of cytotoxic cancer therapies.

## CONTENTS

## ABBREVIATIONS

| | |
|---|---|
| **8-oxodGuo** | 8-oxo-7,8,-dihydro-2'-deoxyguanosine |
| **APS** | Ammonium persulphate |
| **ARE** | Antioxidant response element |
| **AV** | Annexin V |
| **BR** | Bilirubin |
| **BSA** | Bovine serum albumin |
| **BV** | Biliverdin |
| **CBP** | CREB (cyclic AMP-response element binding protein) binding protein |
| **CHD** | Coronary heart disease |
| **CO** | Carbon monoxide |
| **CNC-bZIP** | Cap "n" collar basic leucine zipper |
| **$D_2O$** | Deuterium oxide |
| **DEM** | Diethyl maleate |
| **DMSO** | Dimethyl sulphoxide |
| **DTT** | 1,4-dithio-DL-threitol |
| **EDTA** | Ethylene-diaminetetraacetic acid |
| **EGTA** | Ethylene-glycoltetraacetic acid |
| **EMR** | Electromagnetic radiation |
| **EMEM** | Earle's modified essential medium |
| **ERK** | Extracellular signal-regulated kinase |
| **FBS** | Fetal bovine serum |
| **$Fe^{2+}$** | Ferrous iron |
| **FITC** | Fluorescein isothiocyanate |
| **FL1** | Fluorescence intensity 1 |
| **FL3** | Fluorescence intensity 3 |
| **GFP** | Green fluorescent protein |
| **GST** | Glutathione S-transferase |
| **$H_2O_2$** | Hydrogen peroxide |
| ***hmox1*** | Murine heme oxygenase-1 gene |
| ***HMOX1*** | Human heme oxygenase-1 gene |

| | |
|---|---|
| **HO-1** | Heme Oxygenase-1 |
| **HO-2** | Heme Oxygenase-2 |
| **HO-3** | Heme Oxygenase-3 |
| **HS** | Horse serum |
| **JNK** | c-Jun N-terminal kinase |
| **Keap1** | Kelch-like ECH-associated protein 1 |
| **MARE** | Maf associated recognition element |
| **NQO1** | NAD(P)H: quinine oxidoreductase |
| **Nrf2** | NF-E2-Related Factor 2 |
| ***NRF2*** | Human Nrf2 gene |
| **MAPK** | Mitogen-activated protein kinase |
| **$^1O_2$** | Singlet oxygen |
| **$O^{\bullet}_2^-$** | Superoxide anion |
| **OH•** | Hydroxyl radical |
| **PAGE** | Polyacrylamide gel electrophoresis |
| **PBS** | Phosphate buffered saline |
| **PDT** | Photodynamic therapy |
| **$PEG_{4000}$** | Polyethylene glycol |
| **PFA** | Para-formaldehyde |
| **PI** | Propidium iodide |
| **PMSF** | Phenylmethylsulfonyl fluoride |
| **PS** | Phosphatidylserine |
| **ROS** | Reactive oxygen species |
| **RT-PCR** | Reverse transcription polymerase chain reaction |
| **SA** | 4,6-dioxoheptanoic acid |
| **SDS** | Sodium dodecyl sulphate |
| **StRE** | Stress response elements |
| **TAE** | Tris-acetate buffer |
| **TBE** | Tris-borate buffer |
| **TEMED** | N,N,N',N'-tetramethylethylenediamine |
| **UVR** | Ultraviolet radiation |
| **UVA** | Ultraviolet-A (320 – 380 nm) |
| **UVB** | Ultraviolet-B (280 – 320 nm) |
| **UVC** | Ultraviolet-C (200 – 280 nm) |

# 1. Introduction

UNIVERSITY OF
BATH

# 1. Introduction

## 1.1 Electromagnetic Radiation

In 1874 the first law of photochemistry was proposed by Theodor Grotthuss and John W. Draper. It states that light must be absorbed by a chemical substance in order for a photochemical reaction to take place. However, at this time the properties and composition of light were not fully understood. It was during the early $20^{th}$ century that Max Planck first theorised that light was composed of energetic particles which he termed 'light quanta'. This resulted in the development of the second law of photochemistry. The second law of photochemistry (the photo equivalence or Stark-Einstein law), was formulated between 1908 and 1913 by the German born physicists Johannes Stark and Albert Einstein. It states that for each photon of light absorbed, one molecule is activated for a photochemical reaction. Crucially, these two laws were the first to state that the energy and momentum of light could be imparted to solid matter.

The early development of light quantum theory by Planck underlies our current understanding of electromagnetic radiation. It was the development of the idea of light particles by Planck that led to the concept of electromagnetic waves. Today, electromagnetic radiation is defined as a self-propagating wave in space that has both electric and magnetic components, and is now considered in terms of wave-speed, wave-length $\lambda$ (m), and wave-frequency v ($c^{-1}$); a relationship that is linked by the equation:

**Wave speed (c) = frequency x wavelength**

In this equation the frequency and wavelength of a beam of light are linked by the constant (c) which is equivalent to $3x10^3$ m/s, 'the speed of light'. The electromagnetic spectrum is divided into sub-categories dependent on the frequency of the light. In order of increasing frequency the categories are: radio waves, microwaves, terahertz radiation, infrared radiation, visible light, ultraviolet radiation, X-rays, and gamma rays. Ultraviolet radiation (UVR) is the primary concern of this study.

## 1.2 Ultraviolet Radiation

### 1.2.1 General remarks

The discovery of UVR is attributed to the German physicist Johann Wilhelm Ritter. In 1801 Ritter documented that an energy source at the violet end of the visible spectrum could darken silver chloride-soaked paper. Ritter referred to this uncharacterised energy source as "deoxidising rays", referring to the chemical properties of the rays. Later the term "chemical rays" was coined, and it wasn't until the early 20$^{th}$ century that the term ultraviolet radiation was adopted. The term ultraviolet radiation relates to a fraction of the electromagnetic spectrum between 200 and 380 nm. This range of ultraviolet wavelengths is sub-divided into ultraviolet-A (UVA) (320 – 380 nm), ultraviolet-B (UVB) (280 – 320 nm), and ultraviolet-C (UVC) (200 – 280 nm).

### 1.2.2 Ultraviolet-A

The majority of stars, as well as our own, emit electromagnetic radiation over a broad range of energies, including the ultraviolet range. However, only solar UVR with a wavelength in excess of 290 nm reaches the earth's surface (reviewed in Tyrrell, 1991); UVR with a wavelength less than 290 nm is filtered out by the stratospheric ozone layer. Consequently, only UVA and UVB radiation exert an influence on biological systems on this planet. It is UVA radiation that this study will focus on.

UVA radiation comprises the majority of all solar UV reaching the planet's surface, approximately 96 % (Wilkinson, 1983). Interestingly, it is believed that UVA radiation had a significant input into the origin of life on this planet. However, aside from a limited number of modern clinical therapeutic applications, UVA radiation has few beneficial effects for humans. UVA has been linked to deleterious effects such as erythema, immune suppression, photoaging, and skin cancer (Murphy, 1998; Soter, 1990; Tyrrell, 1994). Consequently UVA is widely regarded as detrimental to human health.

### 1.2.3 The oxidative nature of UVA

Oxygen is the second most common component of the Earth (28 % by mass), and is necessary for sustainable respiration in all animals. However, oxygen is toxic and can cause irreversible cell damage, the effects of which can lead to cell death. The damage caused to a biological system by oxygen is termed oxidative stress.

All living cells maintain an internal reducing environment. This reducing environment is preserved by enzymes through a constant input of metabolic energy. Exogenous agents can cause an excess production of oxygen derived free radicals and / or energised molecules, commonly referred to as reactive oxygen species (ROS). ROS cause disturbances in the normal cellular redox state, and this can lead to cellular damage if antioxidant defense systems become overwhelmed.

In 1970 work was published indicating that the effects of UVA may be dependent on oxygen in prokaryotes (Webb and Lorenz, 1970), findings that were confirmed in mammalian cells some years later (Danpure and Tyrrell, 1976). Crucially, these studies indicated that no such oxygen dependent relationship existed below 320 nm, therefore signifying that UVA exerts its influence by a unique photochemical mechanism. It is now understood that UVA irradiation initiates oxygen dependant photochemistry via endogenous chromophores. Consequently, although UVA is weakly absorbed by most bio-molecules, UVA exerts its effects indirectly by means of radicals and ROS (Tyrrell, 1996). Today, UVA is considered to be the primary source of oxidative stress to human skin.

### 1.2.4 Reactive oxygen species

Upon absorption of UVA photons, an electron within an unsaturated group on an absorbing chromophore is transferred to an orbital of higher energy. This electron can either maintain the same direction of spin, producing an unstable singlet species, or can undergo spin conversion to yield a more stable triplet species. As shown in figure 1.1, type I photosensitised oxidation can result in energy or electron transfer, or a direct addition reaction. In contrast, the favoured type II photosensitised oxidation results in the generation of reactive oxygen species (ROS) (Coohill *et al.*, 1987; Tyrrell and Keyse, 1990). Within mammalian cells, quinones, flavins (Krishna *et al*, 1991) and in particular reduced nicotinamide co-factors (Cunningham *et al.*, 1985;

Czochralska *et al.*, 1984), as well as porphyrins (Carraro and Pathak, 1988) can act as chromophores. All of these molecules can yield large amounts of ROS such as singlet oxygen ($^1O_2$) and superoxide anion ($O_2^{\bullet-}$) when UVA irradiated.

It has been shown that at least half of UVA-induced cell damage results from $^1O_2$ (Tyrrell and Pidoux, 1989). It is the highly energised state of this molecule which is responsible for its destructive nature. Singlet oxygen is not a radical; it is an energised but uncharged form of the diatomic molecule in which the valence electrons are spin paired. Singlet oxygen displays an atomic state in which the two spin angular moments of the electrons cancel each other out, creating zero net spin, and a state 94 kJ $mol^{-1}$ higher in energy than the ground state (Halliwell and Gutteridge, 1990). In 1988, Tyrrell published one of the earliest studies to implicate $^1O_2$ in UVA cytotoxicity (Tyrrell and Pidoux, 1989). The study employed a human fibroblast line (1BR/3) cultured from a skin biopsy of a normal adult human. In this study cells were treated at various UV wavelengths in the presence of the $^1O_2$ lifetime enhancer deuterium oxide ($D_2O$) (Lindig *et al.*, 1980). In the presence of $D_2O$, the study observed greatly reduced cell viability within the UVA and near visible spectrum, particularly around 365 nm, although no such relationship was observed outside of the UVA range; findings that were indicative of the unique oxygen dependent photochemistry of UVA. Further to this, Tyrrell and Pidoux showed that when cells were irradiated at 365 nm in the presence of sodium azide, a strong and reasonably specific quencher of $^1O_2$, the inverse relationship was observed. In the presence of sodium azide, a two-fold protection against radiation at 365 nm was observed; consistent with the interpretation that at least half of UVA induced cellular damage is $^1O_2$ dependent.

Superoxide anion ($O^{\bullet}{}_2^-$) is another ROS that is generated by UVA. Superoxide anion is a one-electron reduction of diatomic $O_2$, and is generated by type I or II photosensitised oxidation, particularly with respect to the UVA-mediated photo-oxidation of NADH and NADPH (Cunningham *et al.*, 1985; Czochralska *et al.*, 1984). Superoxide anion is relatively un-reactive towards most bio-molecules such as lipids and DNA (Fridovich, 1978); however, $O^{\bullet}{}_2^-$ does inactivate proteins that contain prosthetic groups such as heme or iron sulphur clusters (Garner *et al.*, 1995).

Hydrogen peroxide ($H_2O_2$) is yet another ROS that is generated by UVA. $H_2O_2$ is generated as a result of UVA-induced photo-oxidation of tryptophan (Czochralska *et al.*, 1984; McCormick *et al.*, 1976), macromolecules (Tyrrell *et al.*,

1991), and NADH / NADPH (Cunningham *et al.*, 1985; Czochralska *et al.*, 1984; McCormick *et al.*, 1976). Hydrogen peroxide is itself a reactive oxygen species, however, it is far more cytotoxic following its decomposition via the Fenton reaction which results in the generation of hydroxyl radicals (refer to figure 1.2). Hydroxyl radicals ($OH^{\cdot}$) are a three-electron reduction of diatomic oxygen, they are highly reactive, and have been implicated in UVA inactivation of cells (Tyrrell *et al.*, 1991). It is believed that $OH^{\cdot}$ are primarily generated by the Fenton reaction (Walling, 1975), a reaction that is driven by a transition metal ion, particularly iron, and $O^{\bullet}{}_2^{-}$. As with any reaction, the Fenton reaction proceeds at a rate dictated by its limiting factor. As stated, UVA generates $H_2O_2$ and $O_2^{-}$. It would therefore seem likely that iron would present as the limiting factor. However, work has shown that there is a substantial increase in intracellular free iron following UVA treatment, the result of UVA-induced proteolytic degradation of ferritin (Pourzand *et al.*, 1999). UVA therefore has the ability to generate large quantities of highly destructive $OH^{\cdot}$ which serve to inactivate cells.

**Type I**
(Photosensitised Oxidation)

$^3X + {}^1Substrate \rightarrow {}^1X + {}^3Substrate$ *(Energy Transfer)*

$^3X + Substrate \rightarrow X^{\cdot+} + Substrate^{-\cdot}$ *(Electron Transfer)*

$^3X + Substrate \rightarrow Adduct$ *(Addition Reaction)*

X = Chromophore

**Type II**
(Photosensitised Oxidation)

$^3X + {}^3O_2 \rightarrow {}^1X + {}^1O_2$ *(Singlet Oxygen Generation)*

$^3X + {}^3O_2 \rightarrow X^{\cdot+} + O_2^{-\cdot}$ *(Superoxide Anion Generation)*

X = Chromophore

**Figure 1.1: The photochemistry of a Type I and Type II photosensitised oxidation**

The Fenton Reaction

[1] $H_2O_2 + Fe^{2+} \rightarrow OH^{\cdot} + OH^- + Fe^{3+}$

[2] $O_2^{-\cdot} + Fe^{3+} \rightarrow O_2 + Fe^{2+}$

**Figure 1.2: The chemistry of the Fenton Reaction**

[1]: The reduction of hydrogen peroxide driven by the oxidation of iron.

[2]: The reduction of iron driven by oxidation of superoxide anion.

### 1.2.5 Cellular damage

DNA has extremely low absorption in the UVA range (Kielbassa *et al.*, 1997). Accordingly, UVA exerts genotoxicity by means of photosensitisers, which upon absorption of UVA photons, transfer energy via oxygen to other biomolecules, including DNA. UVA can introduce genetic damage in one of three forms: strand breaks, base modification, and base deletion. Base deletion is observed at a far lower incidence with respect to UVA when compared to other wavelengths of ultraviolet radiation (Cadet *et al.*, 1992), and therefore warrants no further discussion. Base modification and strand breaks are the most common forms of genetic damage introduced by UVA.

Oxidation of guanine, induced in human skin by electromagnetic radiation ranging from 312 to 434 nm, is reputed to be the predominant form of UVA-induced DNA damage (Douki *et al.*, 1999; Kvam and Tyrell, 1997; Pflaum *et al.*, 1994; Zhang *et al.*, 1997). The oxidative product of the reaction, 8-oxo-7,8,-dihydro-2'-deoxyguanosine (8-oxodGuo), is highly mutagenic, and results in non Watson-Crick base-pairing during replication. Studies have shown that it is UVA-generated $^1O_2$ that is the cause of 8-oxodGuo (Devasgayam *et al.*, 1991). Another form of base modification that has been attributed to UVA is pyrimidine photoproducts. Pyrimidine photoproducts are observed in two different forms, (6-4) photoproducts and cyclobutane pyrimidine dimers (CPDs). With respect to UVA, only the cyclobutane ring structures are observed (Applegate *et al.*, 1999; Kuluncsics *et al.*, 1999; Mori *et al.*, 1988; Tyrell, 1973; Umlas *et al.*, 1985). UVA induced CPDs, although observed at a lower frequency than oxidative products of guanine, are at least equally cytotoxic, and result in the insertion of erroneous bases during replication. Accordingly, CPDs correlate with cell death and often tumorgenicity (Hart *et al.*, 1977; Sutherland *et al.*, 1985), an effect that has been demonstrated *in vivo* (Ley *et al.*, 1991; Vandaberg *et al.*, 1994).

Strand breaks, both single and double, also result from UVA irradiation (Peak *et al.*, 1987; Peak and Peak, 1990). Strands breaks however play a less significant role in UVA cytotoxicity. Endogenous endonucleases generate strand breaks to induce apoptosis, a key function in cell regulation. It is the introduction of erroneous strand breaks which is detrimental to cell health. Such strand breaks often occur as a

result of deoxyribose degradation, the incidence of which has been linked to intracellular ROS (Murata-Kamiya *et al.*, 1995). Both $^1O_2$ and $OH^{\cdot}$ possess the ability to cause such damage, the former of which is widely considered to be the principal mediator. In addition to this, work has shown that $^1O_2$ has the capacity to break covalent bonds within DNA (Blazek *et al.*, 1989), particularly at guanine residues (Devasgayam *et al.*, 1991).

### 1.2.6 UVA activation of signalling pathways

In mammalian cells, UVR initiates a complex web of signalling pathways. The distinct photochemical mechanisms associated with the different wavelengths of UVR result in the activation of different signal transduction pathways. UVC wavelengths, which do not generate active oxygen intermediates, are strongly absorbed by bio-molecules such as DNA. These short UVR wavelengths initiate transduction events the majority of which involve stress- and mitogen- activated protein kinase cascades (for review see Bode and Dong, 2003). Although UVB wavelengths do contain some oxidative components, the signalling pathways stimulated by this intermediate wavelength solar UVR exhibit greater similarity to the signal transduction pathways associated with UVC radiation rather than those associated with UVA.

In various models, experimental evidence has shown that UVB radiation is able to: stimulate the release of a wealth of immunomodulating cytokines (Hunt *et al.*, 2006; Jiang *et al.*, 2005), initiate expression of cell adhesion molecules (Cornelius *et al.*, 1994; Kirnbauer *et al.*, 1992), activate transcriptional up-regulation of proto-oncogene transcription factors (Soriani *et al.*, 2000), as well as lead to the stabilisation of p53 (Chouinard *et al.*, 2002; She *et al.*, 2000). In addition to this, UVB radiation is reputed to activate proteins that are involved in an abundance of signal transduction pathways such as mitogen-activated protein kinases (MAPK), extracellular signal-regulated kinases (ERK), and c-Jun N-terminal kinases (JNK) (Fisher *et al.*, 1998).

The unique oxidant dependent photochemistry that is associated with UVA has been shown to initiate signalling pathways that are not stimulated in response to the shorter UVB and UVC wavelengths. The literature suggests that following a physiological, non-cytotoxic, dose of UVA radiation, UVA induced gene expression is modulated through active oxygen intermediates. UVA has been shown to regulate

expression of several genes; these include, amongst others, matrix metalloproteinases (Herrmann *et al.*, 1993), the nuclear proto-oncogenes c-fos and c-jun (Bose *et al.*, 1999; Soriani *et al.*, 2000), and heme oxygenase-1 HO-1 (Keyse and Tyrrell, 1989). Previous studies have shown that UVA gene-regulation can be influenced by removing the intracellular antioxidant glutathione or enhancing $^1O_2$ lifetime. The literature indicates that it is $^1O_2$ that is the primary effector in UVA gene regulation.

## 1.3 Heme Oxygenase

### 1.3.1 General remarks

At present three mammalian isoforms of heme oxygenase (HO) have been identified, HO-1, HO-2, and HO-3 (Maines, 1988; McCoubrey *et al.*, 1997; Shibahara, 1988). Of the two catalytically active forms of HO, HO-1 and HO-2, it is the former that has been shown to be inducible, whilst HO-2 is constitutively expressed.

HO-1 is classified as a heat shock protein (HSP32). A wealth of physiological, pathophysiological, and non-physiological agents have now been shown to induce HO-1. These include, acute exercise (Thompson *et al.*, 2005), the HO-1 substrate heme (Balla *et al.*, 1995; Yoshida *et al.*, 1988), hypoxia (Motterlini *et al.*, 2000), heavy metals (Mitani *et al.*, 1993), heat shock (Shibahara *et al.*, 1987; Ewing and Maines, 1991), ROS such as $H_2O_2$ (Keyse and Tyrrell, 1989), and UVA radiation (Keyse and Tyrrell, 1989). In recent years it has become apparent that HO-1 possesses potent cytoprotective properties, and it is now recognised that the protein is a crucial mediator of cellular homeostasis under conditions of stress. Consequently, considerable scientific endeavour has been expended elucidating the biological mechanisms that regulate *HMOX1*. Elucidation of the mechanisms underlying UVA regulation of *HMOX1* is a primary concern of this study.

### 1.3.2 HO-1 structure and localisation

The human *HMOX1* locus is located on chromosome 22 (22q12.3). The post-spliced transcript is composed of 5 exons which code for a 288 residue 32 000 $M_r$ protein (Yoshida *et al.*, 1988). HO-1 is preferentially localised in endoplasmic

reticulum and microsomes. Studies have shown that the structure of HO-1 is largely ά-helical (Schuller *et al.*, 1999) and that the hydrophobic C-terminus functions as a microsomal membrane anchor protein (Yoshida and Sato, 1989). The conserved core of HO-1 is completely novel when compared to other known structures in the Protein Data Bank. The core consists of hydrophobic inner chamber composed of two ά – helices which form a pocket in which the HO-1 substrate heme resides and undergoes enzymatic degradation.

### 1.3.3 The crucial defence enzyme HO-1

HO-1 is the rate limiting step in heme catabolism (Tenhunen *et al.*, 1969). Equimolar amounts of three products are produced as a result of heme degradation: biliverdin, which is rapidly converted to bilirubin through the action of biliverdin reductase (Singleton and Laster, 1965; O'Carra and Colleran, 1971), ferrous iron ($Fe^{2+}$), and carbon monoxide (CO) (Tenhunen *et al.*, 1969) (refer to figure 1.3). The cytoprotective action of HO-1 is, at least in part, derived from its ability to degrade free cellular heme; a polar molecule with the ability to destabilise proteins, lipids, and nucleic acids. Further to this, the cytoprotective action of HO-1 has been related to the catabolites of heme which have been shown to possess anti-inflammatory, anti-apoptotic, anti-oxidant, as well as cell signalling properties (for review see: Maines, 1997; Morse and Choi, 2002; Otterbein *et al.*, 2003).

The heme catabolite biliverdin and its derivative bilirubin are known to possess powerful anti-oxidant activity *in vitro* (Stocker *et al.*, 1987). Studies have indicated that bilirubin can reduce peroxyl radicals and that biliverdin can act as a peroxyl radical 'trap'. Further to this, studies have related the potent cytoprotective action of bilirubin to the prevention of lipid peroxidation in liposomes (Stocker and Ames, 1987), the prevention of depletion of endogenous antioxidants (Neuzil and Stocker, 1997), and inactivation of ROS such as $O^{\bullet}_2{}^-$ and $^1O_2$ (Stevens and Small, 1979), as well as the inhibition of photo-oxidative damage to proteins (Pederson, 1977).

Carbon monoxide is another product of heme catabolism. Studies have shown that CO can act as a soluble second messenger (Furchgott and Jothianandam, 1991; Maines, 1997; Verna *et al.*, 1993). The actions of CO have been implicated in a number of intracellular and extracellular effects, these largely include anti-

inflammatory, anti-apoptotic, and anti-proliferative actions (for reviews see: Christova *et al.*, 2000; Heiman and Delbro, 2005; Herman 1997). Interestingly, work has shown that CO confers an inhibitory action on most heme containing proteins, including the heme-HO complex that may have generated the molecule. Carbon monoxide may therefore serve to inhibit HO-1 heme degradation.

The final catabolite of heme degradation is $Fe^{2+}$. HO-1 releases $Fe^{2+}$ from the core of the heme molecule, resulting in the up-regulation of the iron-sequestering protein ferritin, as well as the activation of ATPase pumps that serve to remove $Fe^{2+}$ from the cell (Ferris *et al.*, 1999). As stated previously, $Fe^{2+}$ is extremely reactive towards oxygen, and can catalyse the conversion of un-reactive species into highly reactive species by means of the Fenton reaction. This results in the generation of ROS. Ferrous iron is therefore considered detrimental towards biological systems. The role of $Fe^{2+}$ in biological systems has been reviewed elsewhere (Taketani, 2005; Torti and Torti, 2002).

**Figure 1.3: Diagrammatic representation of the HO-1 catalysed degradation of heme**

*(next page)*

The diagram shows the reduction of the $\alpha$-Meso carbon bridge of the heme molecule by HO-1. The reaction requires NAPDH and the presence of oxygen to proceed. Biliverdin, ferrous iron, and carbon monoxide are the products of the reaction. Biliverdin is itself rapidly reduced to bilirubin through the action of bilverdin reductase.

(Chemical structures adapted from: Kirkby and Adin, 2006)

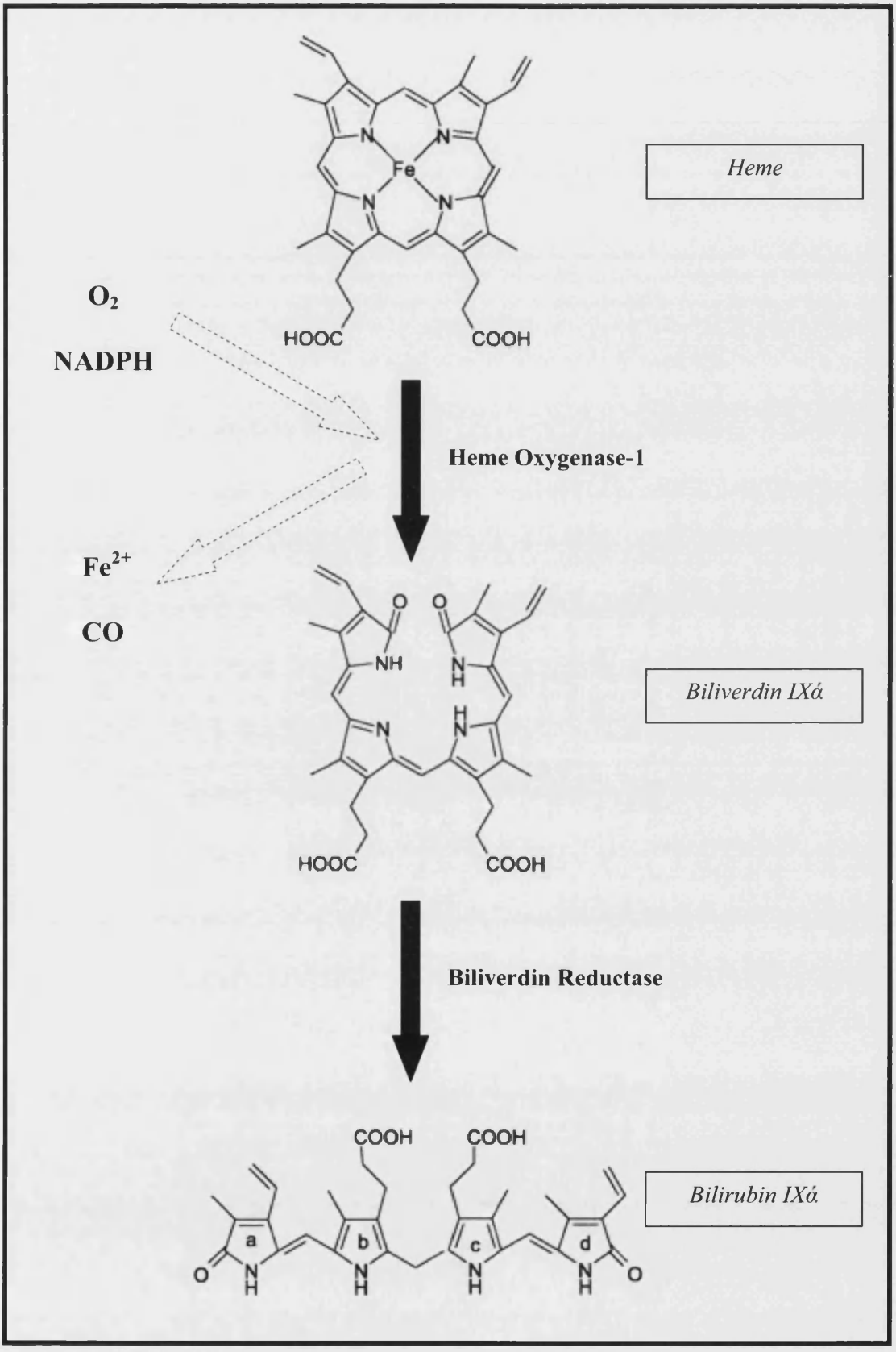
Heme
$O_2$
NADPH
Heme Oxygenase-1
$Fe^{2+}$
CO
Biliverdin IXά
Biliverdin Reductase
Bilirubin IXά

### 1.3.4 The physiological importance of HO-1

HO-1 is the most dramatic example of oxidant-inducible gene expression in mammalian cells (Applegate *et al.*, 1991; Keyse and Tyrrell, 1989). Increased expression of the protein has been shown to be crucial for protection against cell damage (Otterbein and Choi, 2000; Poss and Tonegawa, 1997; Ryter and Tyrrell, 2000), and has been linked to resistance to tissue injury in a wealth of pathologies. This protection against tissue injury has been attributed to the removal of the pro-oxidant heme, as well as the products of heme degradation, bilirubin and CO. Most of our current understanding relating to the functional significance and therapeutic benefits of HO-1 has been generated in a rodent model (for review see: Immenschuh and Ramadori, 2000), either through specific over expression of HO-1 by gene transfer, pharmacological modulation, or through targeted gene knock-out. However, few studies have addressed the functional importance of HO-1 in humans.

In 2002 the first autopsy findings relating to a HO-$1^{-/-}$ human were published (Kawashima *et al.*, 2002). The autopsy notes describe a 6 year-old boy who weighed only 13 kg and measured 86.5 cm in height. The findings of the autopsy describe a long list of pathologies. These included: anaemia; leukocytosis; thrombocytosis; coagulation abnormalities; elevated levels of serum haptoglobin, heme, and ferritin; low serum albumin concentration; as well as hyperlipidemia. In addition to this, the autopsy notes describe amyloid deposits in the liver as well as kidney glomerular dysfunction. The boy also exhibited an irregular distribution of macrophages as well as fatty streaks and fibrous plaques around the heart. Reverse transcription polymerase chain reaction (RT-PCR) found that the HO-1 gene was mutated in both alleles. A two-nucleotide deletion within exon 3 was detected in the paternal band, and a complete loss of exon 2 was found in the maternal band (Saikawa *et al.*, 2000; Yachie *et al.*, 1999). Interestingly, the boy presented with a number of pathologies that are not observed in HO-$1^{-/-}$ mice, and which often exhibit extremely long survival.

Accumulating evidence has indicated the possible therapeutic value of pharmacological modulation of HO-1 by virtue of its anti-inflammatory (for review see Alcaraz *et al.*, 2003; Immenschuh and Schroder, 2006), anti-apoptotic (for review see Fang *et al.*, 2004), and pro-proliferative actions (for review see Durante, 2003). Clinical application of the enzyme has been proposed in a wealth of pathological

states. These include: atherosclerosis (Ishikawa *et al.*, 1997; Morita, 2005; Siow *et al.*, 1999; Wang *et al.*, 1998), hypertension (Ishizaka *et al.*, 1997; Vera *et al.*, 2006), acute renal injury (Akagi *et al.*, 2005; Goncalves *et al.*, 2006), toxic nephropathy (Agarwal *et al.*, 1995; Horikawa *et al.*, 1998), endotoxic shock (Lee and Chau, 2002), chronic obstructive lung disease (Carter *et al.*, 2004; Xia *et al.*, 2006), gastrointestinal diseases (Guo *et al.*, 2000), Alzheimer's disease (Calabrese *et al.*, 2004; Ishizuka *et al*, 2002; Smith *et al.*, 1994), transplant rejection (Bach, 2006; Hancock *et al.*, 1998; Soares *et al.*, 1998; Woo *et al.*, 2000) and others (Chen *et al.*, 1999; Horvath *et al.*, 1998; Levere *et al.*, 1993; Otterbein *et al.*, 1999)

Depending on the pathology, activation or suppression of *HMOX1* may hold therapeutic value. One example of a disease state where *HMOX1* up-regulation may be beneficial is coronary heart disease (CHD). Each year, in excess of 250 000 individuals die globally as a result of CHD. Coronary heart disease is the consequence of an inflammatory process which results in the accumulation of atherosclerotic plaques within the walls of the arteries that supply the myocardium. Clinical studies have observed strong accumulation of HO-1 mRNA and protein in both animal and human atherosclerotic plaques (Wang *et al.*, 1998). Therefore, owing to the anti-inflammatory properties of HO-1, pharmacological activation of the HO-1 gene may prove a hugely effective therapeutic tool in preventing plaque formation (for review see: Morita, 2005). Studies have also shown that pathologies such as Alzheimer's disease (for review see: Calabrese *et al.*, 2004) and acute renal failure (for review see: Akagi *et al.*, 2005) may also benefit from over-expression of this gene. Furthermore, studies have shown that up-regulation of *HMOX1* may hold significant protection against allograft and xenograft transplant rejection (Hancock *et al.*, 1998; Soares *et al.*, 1998; Woo *et al.*, 2000).

An increasing amount of evidence indicates a vital role for HO-1 in both cell growth and cell death. Hence, the potential of the protein as a target in anticancer treatment is being evaluated (for review see; Fang *et al.*, 2004). In contrast to other pathologies, the pro-proliferative and anti-apoptotic properties of HO-1 suggest that it is suppression of *HMOX1* that may prove beneficial in order to increase the efficacy of existing cytotoxic cancer therapeutics.

### 1.3.5 UVA up-regulation of HO-1

In 1987 it was shown that the oxidising component of solar radiation (UVA) could induce a 32 KDa stress protein in human skin fibroblasts (Keyse and Tyrrell, 1987). It was later shown by molecular cloning that the protein was the oxidant inducible microsomal protein HO-1 (Keyse and Tyrrell, 1989). Up-regulation of HO-1 by UVA radiation is now known to represent a crucial cellular defence mechanism against oxidative stress, but the events underlying HO-1 regulation by UVA remain poorly characterised in human cells.

At present, ROS are reputed to be the principal mediator of UVA up-regulation of HO-1. Work from this laboratory has shown that it is $^1O_2$ that is the primary effector in UVA regulation of the HO-1 gene in primary human fibroblasts (Basu-Modak and Tyrrell, 1993). Basu-Modak and Tyrrell (1993) observed that UVA fluence-dependent up-regulation of *HMOX1* is enhanced in the presence of deuterium oxide ($D_2O$), a strong and reasonably specific $^1O_2$ lifetime enhancer (Lindig *et al.*, 1980). Further to this, in the presence of sodium azide, a $^1O_2$ quencher (Singh, 1982), this study observed a substantial decrease in UVA fluence-dependent HO-1 mRNA accumulation. Moreover, this study observed that other UVA generated ROS such as $O^{\bullet}_2^-$ and $OH^{\cdot}$ marginally influence UVA-regulation of *HMOX1*. Researchers from this laboratory have also shown that the carotenoid beta-carotene, one of the most potent $^1O_2$ quenchers in nature, can suppress UVA-induced *HMOX1* up-regulation in human cells (Trekli *et al.*, 2003). Trekli and co-workers observed a concentration-dependent suppression of UVA-induced transcriptional activation of *HMOX1* at carotenoid concentrations that have been documented in human plasma after dietary supplementation; further evidence of the involvement of $^1O_2$ in the UVA-regulation of *HMOX1*. The HO-1 substrate heme has also been implicated in UVA up-regulation of *HMOX1* in human cells (Kvam *et al.*, 1999). Kvam and co-workers observed a cyclooxygenase dependent release of micromolar amounts of heme from microsomal hemoproteins following UVA treatment. Furthermore, Kvam and co-workers documented a high degree of correlation between the amount of heme released and the subsequent degree of *HMOX1* activation.

Taken together these studies indicate both an oxidant and substrate dependent mechanism for *HMOX1* gene activation in human skin cells. Based on the observation that heme release from heme-proteins also occurs in response to $H_2O_2$

(Kvam *et al.*, 1999), and therefore indicating that the release of heme from heme-containing proteins is itself oxidant dependent, these two mechanisms for *HMOX1* gene activation appear to be intrinsically linked.

Work from this laboratory has established that there is a refractoriness of the HO-1 gene to re-induction by UVA irradiation (Noël and Tyrrell, 1997). Crucially, it has been shown that the development of a refractory period to re-induction of *HMOX1* is limited to UVA and heme, and is not observed using other known inducers of the HO-1 gene (unpublished observations, this laboratory). This refractoriness to re-induction therefore suggests that the molecular mechanism that underlies UVA-regulation of *HMOX1* is unique. Studies have shown that neither UVA (Keyse *et al.*, 1990) nor heme (Srivastava *et al.*, 1993) influence the half-life of HO-1 mRNA. Hence, the refractoriness event is not attributable to messenger stability. The products of heme catabolism have been shown to be involved in this effect, and thus a feedback mechanism may be present (Noël and Tyrrell, 1997). However, it was shown that HO-1 enzymatic activity is not the sole cause of this refractory period. Results have been obtained consistent with the notion that it is in fact insufficient intracellular heme containing proteins that is responsible for the refractoriness to induction of *HMOX1* by UVA. Complete refractoriness to reinduction of *HMOX1* by UVA was observed for 48 hrs following the initial UVA treatment. In relation to this, work has shown that more than half of the total detectable cellular microsomal hemoprotein is degraded by UVA, and that the amount of heme-containing protein does not recover for 48 hrs (Kvam *et al.*, 1999).

These results indicate that both heme and ROS are involved in UVA up-regulation of *HMOX1*. A major focus of this study will be the role of heme in UVA regulation of *HMOX1*.

### 1.3.6 *HMOX1* regulation

Deletion studies using a murine model have shown that *hmox-1* transcriptional regulation is dependent on conserved 10-bp sequences termed stress response elements (StRE) (Inamder *et al.*, 1996). Two StRE with the consensus sequence TGA(C/G)TCA(T/C) have been identified in the upstream region of the murine *hmox1* promoter. These StRE are known to have a sequence that closely resembles the consensus sequence of several previously characterised response elements. These

include the antioxidant response element (ARE), and the Maf associated recognition element (MARE) which is known to act as a binding site for the activating transcription factor Nrf2. To some extent the terms StRE, ARE, and MARE have been used inter-changeably within the literature, but for the purposes of this discussion these *cis*-acting elements will be referred to as MARE sites.

MARE containing enhancer regions termed E1 and E2 have been identified in the murine genome situated approximately 3.85 and 9.65 kb upstream of the *hmox1* transcriptional start site (Alam *et al.*, 1989, Alam *et al.*, 1995, Alam *et al.*, 1999). Searches of human chromosome 22 have identified two similar *cis*-acting elements upstream of the *HMOX-1* transcriptional start site (Takeda *et al.*, 1994; Raval and Tyrrell, unpublished observations this laboratory). MARE are known to be recognised and bound by small Maf proteins (either MafK, MafG, or MafF) (Kataoka *et al.*, 1994), and evidence has been provided indicating that various basic leucine zipper factors, specifically NF-E2-related factors, heterodimerise with Maf proteins and influence MARE-driven gene expression. Heterodimers comprising of a small Maf protein and Nrf2 have been shown to activate the HO-1 gene (Itoh *et al.* 1997, Alam *et al.*, 1999, Alam *et al.*, 2000, Ishii *et al.*, 2000, Kataoka *et al.*, 2001). Bach1, another basic leucine zipper protein, has been shown to form heterodimeric complexes with small Maf proteins which serve to negatively regulate the HO-1 gene (Oyake *et al.*, 1996; Igarashi *et al.*, 1998, Sun *et al.*, 2002). Much of our current understanding of HO-1 gene regulation is derived from work in mice, and few studies have addressed the issue in a human model. The conserved positioning of MARE between the murine and human genome indicates that similar regulatory mechanisms may exist between humans and mice; however, this has not been fully investigated. A primary concern of this study is to explore the regulation of *HMOX1* in a human model.

**Figure 1.4: Diagrammatic representation of the upstream enhancer elements in the human and mouse heme oxygenase-1 promoter**

*(next Page)*

Figure 1.4(a): The human *HMOX1* promoter.
Searches of chromosome 22 upstream of *HMOX1* have identified two MARE-containing enhancer elements situated approximately 4.0 and 9.1 kb upstream of the *HMOX1* transcriptional start site.

Figure 1.4(b): The murine *hmox-1* promoter.
Two MARE-containing enhancer elements situated at approximately 3.85 and 9.65 kb upstream of the *hmox-1* transcriptional start site have been identified in the murine genome.

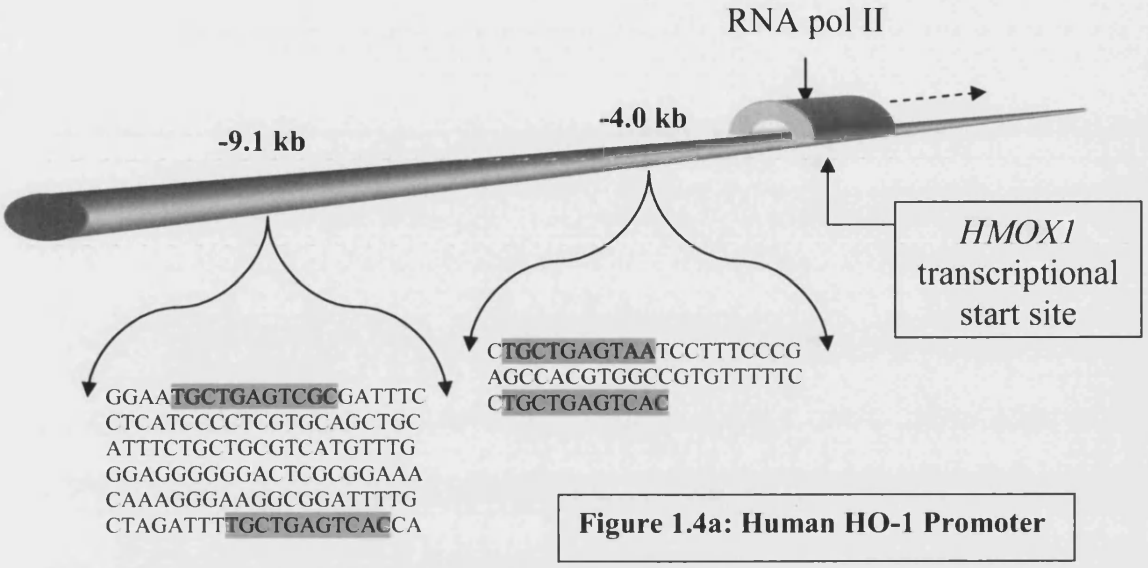


**Figure 1.4a: Human HO-1 Promoter**

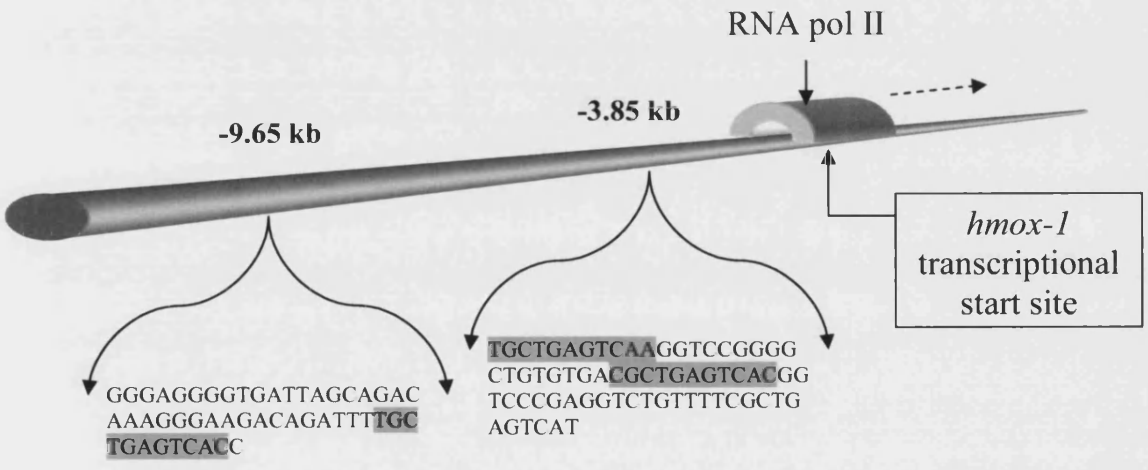


**Figure 1.4b: Murine HO-1 Promoter**

## 1.4 Nrf2

### 1.4.1 General remarks

The NF-E2-related family of proteins includes Nrf1, Nrf2, and Nrf3. These transcription factors are Cap 'n' Collar (CNC)-containing leucine zipper (b-Zip) proteins (Itoh *et al.*, 2004; Jaiswal, 2004; Nguyen *et al.*, 2004). NF-E2-related transcription factors are known to form heterodimers with small Maf proteins (Motohashi *et al.*, 2002). These heterodimeric complexes are reputed to bind to MARE sites in the 5'-flanking region of phase II detoxifying enzymes (Rushmore *et al.*, 1991), including the subject of this study, *HMOX1*. Of the three known Nrf proteins, Nrf2 has been shown to be the most potent inducer of MARE-regulated genes (Jaiswal, 2004), and many studies have shown that Nrf2 provides substantial protection against cellular oxidative stress. Crucially, using a murine model, investigators have shown that Nrf2 plays a principle role in up-regulation of the oxidant inducible gene *hmox-1* (Alam *et al.*, 1999).

### 1.4.2 The physiological importance of Nrf2

Chemical and endogenous insult brought upon by environmental toxicants result in the expression of enzymes involved in detoxification (Primano *et al.*, 1997). The cellular detoxification process is divided into phase I and phase II reactions. Phase I reactions are catalysed by the P-450 mono-oxygenase system, whist phase II reactions incorporate a larger cohort of enzymes that include NAD(P)H: quinone oxidoreductase 1 (NQO1), glutathione S-transferase (GST), and HO-1. In some instances phase I catalysed reactions produce chemical species that are potentially more toxic than the parental species; thus, phase II catalysed reactions are a requirement for complete detoxification and generally result in less toxic products. Under physiological (reducing) conditions, phase II enzymes are expressed constitutively at a relatively low level. It is endogenous or xenobiotic chemical insult that results in enzyme accumulation. It is now known that accumulation of enzymes involved in phase II detoxification is dependent on activating transcription factors. These activating transcription factors are known to up-regulate phase II genes through association with *cis*-acting regulatory elements. A recent study has demonstrated the

importance of Nrf2 in phase II gene activation. Hayes *et al.*, (2000) observed reduced phase II gene activation in *nrf2* knock-out mice. In relation to this, investigators have shown that insufficient induction of phase II enzymes results in increased susceptibility to xenobiotic chemicals (Aoki et al., 2001; Enomoto *et al*, 2001; Chan and Kan, 1999; Goldring *et al.*, 2004; Iizuka *et al.*, 2005; Khor *et al.*, 2006); and that Nrf2 plays a key role in cancer prevention (auf dem Keller *et al.*, 2006; Ramos-Gomez *et al.*, 2001; Yates *et al.*, 2006).

Genome-wide screening has now implicated Nrf2 in the activation of in excess of 200 genes, and much of our current understanding of the physiological importance of Nrf2 is derived from work in murine models. However, the physiological implications of defective Nrf2 in humans are not yet fully understood.

### 1.4.3 Nrf2 structure and regulation

Nrf2 has six functional Neh [Nrf2-ECH (erythroid cell-derived protein with CNC homology) homology] domains (refer to figure 1.5). All six domains exhibit inter-species conservation (Itoh *et al.*, 1999; Katoh *et al*, 2001; McMahon *et al.*, 2004). The Neh1 domain located at the proteins C-terminus contains the CNC-bZIP region, and confers both MARE binding and dimerisation with small Maf proteins. The 100 residue Neh2 domain situated in the N-terminal region confers binding to the actin associated protein Keap1 which serves to negatively regulate Nrf2 (McMahon *et al.*, 2004). The domains Neh4 and Neh5 interact with CBP [CREB (cyclic AMP-response element binding protein) binding protein] and synergistically contribute to transcriptional activation of the protein (Katoh *et al*, 2001). The redox-insensitive Neh6 domain has been shown to be essential in the degradation of the protein in oxidatively stressed cells (McMahon *et al.*, 2004).

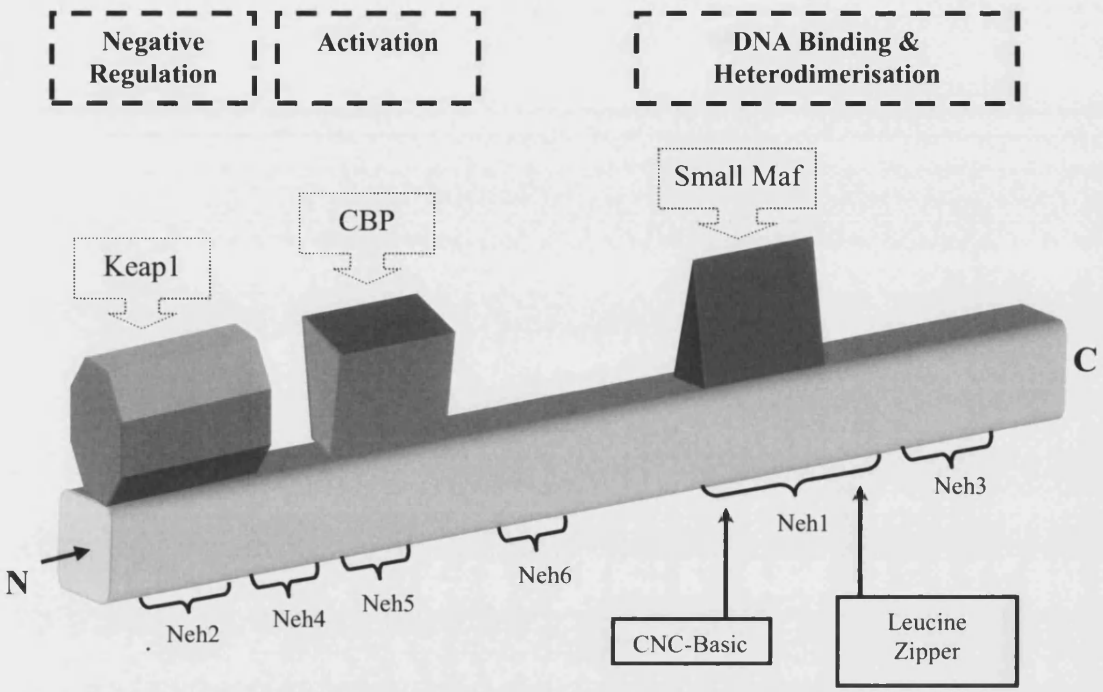


**Figure 1.5: Diagrammatic representation of the functional domains of Nrf2**

Nrf2 has six functional Neh [Nrf2-ECH (erythroid cell-derived protein with CNC homology) homology] domains. Each of the six domains is conserved inter species. The C-terminus of Nrf2 contains a basic leucine zipper structure which aids in both MARE binding and dimerisation with small Maf proteins. Nrf2 is negatively regulated by binding to the actin associated protein Keap1 at the Neh2 domain. The domains Neh4 and Neh5 interact with CBP [CREB (cyclic AMP-response element binding protein) binding protein] which synergistically contribute to transcriptional activation of the protein.

1.4.3 Nrf2 structure and regulation (*cont*)

Transcriptional up-regulation of *nrf2* has been reported previously (Kwak *et al.*, 2002). However, studies have shown that Nrf2 is primarily regulated by two post-translational mechanisms: cytoplasmic retention (anchoring), and modulation of protein half-life (Dhakshinamoorthy and Jaiswal, 2001; Itoh *et al.*, 1999; Jaiswal, 2004). Studies have shown that the cytoplasmic actin-binding protein Kelch-like ECH-associated protein 1 (Keap1) plays the co-ordinating role in the Nrf2 stress response mechanism. Under basal 'reducing' conditions Keap1 is tightly complexed with Nrf2, anchoring Nrf2 within the cytoplasm (Kang *et al.*, 2004), and therefore preventing transcriptional activation of phase II genes. It is now understood that Keap1 acts as a sensor of oxidative and electrophilic stress, releasing Nrf2 in response to such stimuli. In addition to this, it has been reported that oxidative stress can initiate the release of Nrf2 from Keap1 by phosphorylation of Nrf2 at serine 40. This has been related to the activation of protein kinase C and other cytosolic factors (for review see Jaiswal, 2004). A recent *in vivo* study using a murine model has evaluated the functional importance of Keap1 (Wakabayashi *et al.*, 2003). Wakabayashi and co-workers observed that Keap1 mutation leads to postnatal lethality due to constitutive Nrf2 activation, therefore underlining the importance of this negative regulator of phase II gene activation.

Studies have shown that while complexed with Keap1, Nrf2 is rapidly degraded by means of the ubiquitin (Ub)- proteasome proteolysis system (Itoh *et al.*, 2003; Kobayashi *et al.*, 2006; Nguyen *et al.*, 2003; Sekhar *et al.*, 2002; Stewart *et al.*, 2003; Zhang and Hannink, 2003). Two distinct molecular mechanisms by which Keap1 modulates total cellular levels of Nrf2 have been proposed: Firstly, cytoplasmic localisation of Nrf2 through binding to the actin associated protein Keap1 may increase the proximity of Nrf2 to the proteasome system (Itoh *et al.*, 2003; McMahon *et al.*, 2003), thus increasing the probability of ubiquitination. Secondly, Keap1 may effectively promote Nrf2 proteasomal degradation through active recruitment of proteasome subunits (Cullinan *et al.*, 2004; Kobayashi *et al.*, 2004). Devling *et al.*, (2005), elegantly demonstrated the role of Keap1 in Nrf2 degradation by means of RNAi. Using human keratinocytes, Devling and co-workers lowered the

level of endogenous Keap1 mRNA to < 30 % of control levels. The Keap1 targeted RNAi markedly enhanced levels of Nrf2 protein and increased transcription of an ARE-driven reporter gene 2.3-fold.

A degree of complexity surrounds the possible mechanisms involved in ROS / electrophile induced separation of Nrf2 from Keap1. It has been proposed that sulfhydryl groups on cysteine residues within Keap1 may mediate a conformation change of Keap1 in response to cellular stress, releasing Nrf2 and resulting in nuclear accumulation of the transcription factor (Dinkova-Kostova *et al.*, 2002; Itoh *et al.*, 1999). Indeed both murine and human Keap1 are known to contain 25 highly conserved cysteine residues. However, more recent data have shown that modification of these residues does not cause dissociation of the Nrf2-Keap1 complex (Eggler *et al.*, 2005), rather that modification of these residues inhibits ubiquitin conjugation to Nrf2 (Kobayashi *et al.*, 2006). Studies have also shown that phosphorylation of Nrf2 results in release from Keap1. However, the complex web of signalling cascades that may culminate in phosphorylation of Nrf2 cannot be fully explored within the confines of this discussion, and have recently been reviewed elsewhere (Giudice and Montella, 2006).

It is known that phase II gene activation by Nrf2 can be negatively regulated by Keap1, and that dissociation of Nrf2 from Keap1 results in Nrf2 nuclear accumulation. Nuclear localisation of Nrf2 may decrease the rate of proteasomal degradation, favouring accumulation of the protein, and therefore increasing phase II genes activation (refer to figure 1.6). However, further research is required to fully elucidate all aspects of this regulatory mechanism.

**Figure 1.6: Diagrammatic representation of the Nrf2-Keap1 regulatory system**

*(next page)*

The diagram shows activation of Nrf2 by ROS and electrophiles. In an 'un-stimulated' cell, Nrf2 is localised to the cytoplasm through association with the cytoskeleton binding protein Keap1. In response to electrophiles or ROS Keap1 and Nrf2 dissociate, this results in nuclear translocation of Nrf2. Nrf2 subsequently forms heterodimers with small Maf proteins which subsequently bind to MARE sites in the 5'-flanking region of phase II genes (including *HMOX1*). The Nrf2-Maf heterodimers activate phase II genes through the recruitment of proteins required for assembly of the pre-transcription complex. The cytoplasmic anchor protein Keap1 also enhances the probability of ubiquitination of Nrf2 through increasing the proximity of Nrf2 to the proteasomal degradation machinery.

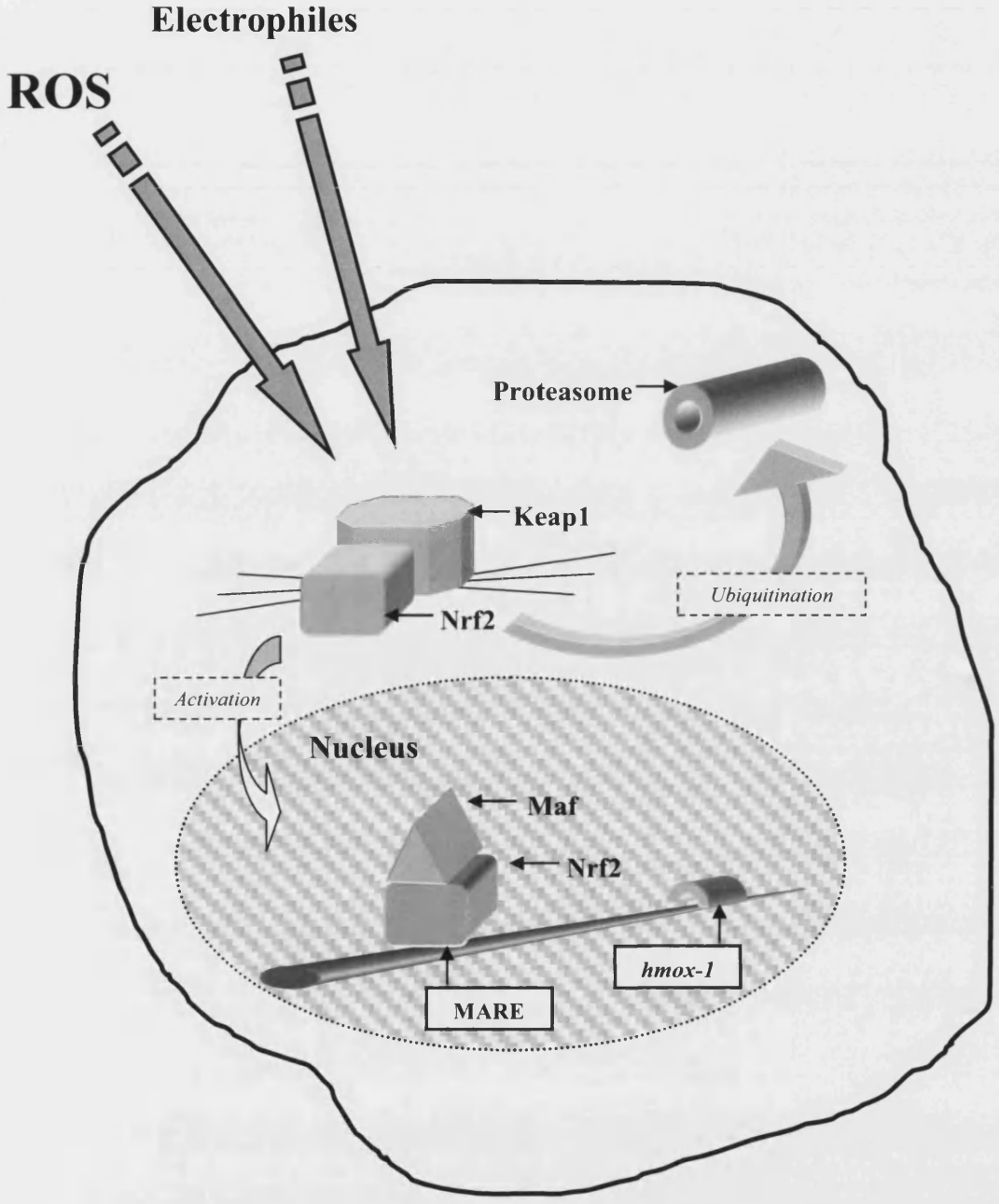
Electrophiles
ROS
Proteasome
Keap1
Nrf2
Ubiquitination
Activation
Nucleus
Maf
Nrf2
hmox-1
MARE

### 1.4.4 Nrf2 activation of *HMOX1*

Using both rodent and human models, Nrf2 has been implicated in HO-1 gene activation by a wealth of inducers. These include: arsenite, cadmium, heme, *tert*-butylhydroquinone (*t*-BHQ) (Alam *et al.*, 1999; Alam *et al.*, 2000), acrolein (Wu *et al.*, 2006), cobalt (Gong *et al.*, 2001; Shan *et al.*, 2006), curcumin (Balogun *et al.*, 2003; Rushworth *et al.*, 2006), 15-deoxy-delta12,14-prostaglandin j2 ($PGJ_2$) (Gong *et al.*, 2002), epigallocatechin-3-gallate (EGCG) (Wu *et al.*, 2005), gold (Kataoka *et al.*, 2001), 1-chloro-2,4-nitrobenzene (CDNB), diethyl maleate (DEM), glucose oxidase (GO), $H_2O_2$ (Ishii *et al.*, 2000), 1,2,3,4,6-penta-O-galloyl-beta-D-glucose (PGG) (Pae *et al.*, 2006), and hypoxia (Cho *et al.*, 2002).

Studies have shown that dissociation of Nrf2 from the cytoplasmic anchor protein Keap1 is the dominant mechanism responsible for Nrf2 phase II gene activation. In relation to this, an abundance of known inducers of *HMOX1* have been shown to augment nuclear accumulation of Nrf2. Moreover, in addition to nuclear localisation, studies have shown that Nrf2 protein accumulation may occur through Nrf2 protein stabilisation. The HO-1 inducing agents cadmium (Stewart *et al.*, 2003) and heme (Alam *et al.*, 2003), have been shown to increase Nrf2 protein half-life from 13 to 100 mins and 13 to 110 mins respectively.

Electromobility shift assays have shown that Nrf2-Maf heterodimers bind to the MARE consensus sequence *in vitro* (Itoh *et al.*, 1997). As stated previously, it is known that a MARE regulatory element exists at approximately 4 kb upstream of the human *HMOX1* transcriptional start site (Takeda *et al.*, 1994). Unpublished searches of the human *HMOX1* upstream region by this laboratory have revealed the presence of a second MARE containing enhancer region approximately 9.1 kb upstream of the *HMOX1* transcriptional start site. As shown in figure 1.4, conservation of the structure, location, and multiplicity of MARE sites between the rodent and human genome defines a clear argument for the analogous conservation of regulation between these two species. A concern of this study is to provide insights into the UVA regulation of *HMOX1* by Nrf2 in human skin cells.

## 1.5 The Oxidising Carcinogen UVA

### 1.5.1 General remarks

In the year 2000, over one million cases of skin cancer were diagnosed in the U.S., 78 % of which were basal cell carcinoma, 20 % squamous cell carcinoma, and 2 % malignant melanoma. UVA wavelengths have been strongly implicated in the aetiology of the most life threatening cutaneous malignancy, malignant melanoma (Moan *et al.*, 1999; Setlow *et al.*, 1993). The incidence of malignant melanoma has increased by a factor of approximately 15 in the past 60 years. This increase has been attributed to an increasing number of fair skinned European and North American citizens travelling to foreign climates, and to the increasing use of sun beds in these societies (Westadahl *et al.*, 2000). The ever-increasing number of individuals presenting with neoplastic related disorders has placed a huge burden on global health resources. Consequently, enormous emphasise has been placed on the elucidation of the aetiology of such pathologies.

### 1.5.2 Apoptosis and carcinogenesis

Cell death can occur by means of two processes, apoptosis or necrosis. The term apoptosis, or programmed cell-death (PCD), refers to a biological cascade of events that result in cell death, and that are therefore fundamental to physiological homeostasis. All apoptotic cells exhibit conserved morphological features that include a reduction in cell volume, membrane blebbing, chromatin condensation, and DNA fragmentation (Kerr *et al.*, 1972, Wyllie, 1980). Necrosis, sometimes referred to as accidental or caspase-independent cell death, is less orderly. Necrosis is morphologically distinct from apoptosis, and although as efficient as apoptosis, necrosis may release harmful chemicals that damage adjacent cells and result in inflammation.

Apoptosis ensures that a suitable equilibrium between cell growth and cell death is maintained, and therefore that cell population and organ size is maintained (Kerr *et al.* 1972). Hence, regulated cell death is as vital for the continued survival as regulated cell growth. Abnormalities in the regulation of cell death have been implicated in the pathogenesis of a wealth of disease states. These include: acquired

immune deficiency syndrome, ischemic injury, neurodegenerative injuries, autoimmune diseases, and cancer (Thompson, 1995). In recent times substantial emphasise has been placed on elucidation of the role of anti-apoptotic genes in carcinogenesis. The anti-apoptotic gene *HMOX1* is one such example. The role of apoptosis in cancer prevention and treatment has recently been reviewed elsewhere (Dlamini *et al.*, 2005; Zhivotovsky and Orrenius, 2006).

### 1.5.3 UVA and apoptosis

Different wavelengths of UVR are known to influence biological systems by different photochemical mechanisms. The method by which different UVR wavelengths induce cell death has been examined previously (Godar *et al.*, 1994; Godar *et al.*, 1999). UVA (320 – 400 nm) was shown to induce both immediate (0 - 4 h) and delayed apoptosis (approximately 20 h); while UVB (280 – 320 nm) and UVC (200 – 280 nm) were shown to only induce delayed apoptosis.

Photo-therapies such as photodynamic therapy (PDT) are one of the few clinical applications of UVA and are used to remedy skin diseases. PDT is a therapeutic modality involving the photo-oxidation of biological material mediated by a localised photosensitiser. When UVA irradiated, the photosensitiser initiates cell death in the diseased tissue. The success of such phototherapies has, at least in part, been attributed to direct killing of diseased cells by apoptosis (Godar *et al.*, 1999b). With regards to the dermatological application of PDT, UVA has been shown to be successful in the treatment of actinic keratoses, basal cell carcinomas, Bowen's disease, morphea, sarcoidosis, warts, and psoriasis (for review see; Gilaberte *et al.*, 2006). It is these therapeutic applications of UVA that have prompted investigations into the mechanism by which UVA causes cell death.

With respect to PDT, it is known that $^1O_2$ is the fundamental mediator of UVA induced cell death (Morita *et al.*, 1997). The role of $^1O_2$ in UVA-induced cell death has also been investigated using transformed human lymphocytes by employing agents with the ability to generate $^1O_2$ and $O^{\bullet}_2^-$ (Godar, 1999). This study concluded that $^1O_2$ was involved in UVA immediate (0 - 4 h) cell death, and that $O^{\bullet}_2^-$ was involved UVA late apoptosis (20 h). An objective of this study is to determine the role of the anti-apoptotic protein HO-1 in UVA-apoptosis.

### 1.5.4 The anti-apoptotic protein HO-1

In excess of 30 % of all mortalities in Western societies can be attributed to neoplastic pathologies. Accumulation of HO-1 has been documented in a variety of cancers. These include: adenocarcinoma, hepatoma, sarcoma, glioblastoma, melanoma, and squamous cell carcinoma (Deininger *et al.*, 2000; Doi *et al.*, 1999; Goodman *et al.*, 1997; Torisu-Itakura *et al.*, 2000; Tsuji *et al.*, 1999). Experimental studies have shown that accumulation of HO-1 results in cellular proliferation, a loss of apoptotic potential, and tumour angiogenesis, factors that are all important for *in vivo* tumour growth (Hellmuth *et al.*, 2002; Sunamura *et al.*, 2003). The anti-apoptotic properties of HO-1 have therefore drawn considerable attention in recent times (for review see; Fang *et al.*, 2004). The HO-1 substrate heme is known to be pro-oxidant and has the ability to generate ROS (Ryter and Tyrrell, 2000). Hence, the anti-apoptotic action of HO-1 has been attributed to the degradation of this pro-oxidant molecule. As well as this, the products of heme degradation, biliverdin and CO, have also been shown to be involved in the anti-apoptotic action of HO-1. Moreover, it has been shown that modulation of labile iron is another factor that may contribute to this anti-apoptotic influence (Ferris *et al.*, 1999).

Iron contributes to the formation of free radicals which subsequently damage DNA, proteins, and lipids (for review see: Meneghini, 1997; Puntarulo *et al.*, 2005). Therefore, accumulation of free $Fe^{2+}$ may ultimately lead to apoptosis. Iron therefore presents a considerable toxicological threat. The concentration of the intracellular iron storage protein ferritin has been shown to reflect cellular labile iron, and is therefore central to intracellular iron homeostasis (Ponka *et al.*, 1998). In relation to this, studies have shown that the level of ferritin increases following up-regulation of HO-1 (Eisenstein *et al.*, 1991; Vile and Tyrrell, 1993). It is therefore likely that the anti-apoptotic action of HO-1 is, at least in part, attributable to sequestration of the pro-oxidant iron. However, a study using human skin cells has shown that UVA, a known inducer of *HMOX1*, results in an immediate release of iron by means of ferritin proteolysis (Pourzand *et al.*, 1999). Therefore, a degree of complexity surrounds the role of iron in apoptosis with regards to UVA up-regulation of *HMOX1*.

Biliverdin is a product of heme degradation, and is rapidly converted to bilirubin by the action of biliverdin reductase. Bilirubin is a lipophilic tetrapyrole and is one of the most abundant endogenous anti-oxidants in humans. This anti-oxidant

action has been attributed to ROS scavenging activity (Minetti *et al.*, 1998). A recent study has shown that physiologically relevant concentrations of bilirubin can protect cells from a 10 000-fold excess of $H_2O_2$ (Baranano *et al.*, 2002). In this study, Baranano and co-workers examined the influence of bilirubin on apoptosis in human keratinocytes. The results of this investigation showed that depletion of bilirubin by RNAi markedly augments ROS concentration and causes apoptotic cell death.

Carbon monoxide is another product of heme degradation and has also been implicated in anti-apoptotic effect of HO-1. Inhibition of apoptosis through the exogenous administration of CO has been shown in a variety of cell lines including, fibroblasts, endothelial cells, and vascular smooth muscle cells (Brouard *et al.*, 2000; Liu *et al.*, 2002). The anti-apoptotic influence of CO has been related to activation of p38 mitogen-activated protein kinase (MAPK) (Brouard *et al.*, 2000; Silva *et al.*, 2006), as well as inhibited expression of the pro-apoptotic protein p53 (Liu *et al.*, 2002). In addition to this, researchers have shown that CO can inhibit apoptotic signalling by suppression of caspase cleavage, as well as inhibited activation of Bcl-2-related proteins (Kim *et al.*, 2006; Wang *et al.*, 2007; Zhang *et al.*, 2003).

A lose of apoptotic potential contributes to the progression of carcinogenesis; therefore, modulation of the anti-apoptotic protein HO-1 is likely to influence the survival of neoplastic lesions. Several recent studies illustrate this point. Zhang *et al.*, (2004) observed an increase in apoptosis using HO-1 RNAi. Results from this laboratory have shown that the inhibition of HO-1 enzymatic activity using a competitive substrate analogue increases apoptosis 2-fold in human skin fibroblasts (unpublished observations). Moreover, inhibition of HO-1 using a competitive substrate analogue has been shown to increase caspase-3 activity (Tanaka *et al.*, 2003). Findings have also been published indicating that *in vitro* application of a pegylated HO-1 competitive substrate analogue can decrease tumour diameter through promoting apoptosis, and furthermore solid tumour apoptosis can be enhanced through HO-1 RNAi (Fang *et al.*, 2003; Sahoo *et al.*, 2002). The literature clearly indicates that inhibition of HO-1 enzymatic activity or gene suppression may have therapeutic value since apoptotic resistance in tumours strongly influences the efficacy of cytotoxic cancer therapies.

Malignant melanoma is the most life-threatening cutaneous malignancy. Clinical oncology studies have indicated that the high probability of mortality associated with this type of cancer can be attributed to the high tendency to aggressive

growth and resistance to apoptosis; yet the cellular mechanisms responsible for melanoma resistance to cytotoxic cancer therapeutics remain to be elucidated. Drug resistance in melanoma is most likely caused by a deregulation of apoptotic pathways (for review see: Rockmann and Schadendorf, 2003; Soengas and Lowe, 2003). Therefore HO-1 may hold significant therapeutic value in the treatment of this cancer. Using a murine model, a single study has evaluated the effect of HO-1 over-expression in melanoma (Was *et al.*, 2006). This study concluded that HO-1 over-expression increased viability, proliferation, and angiogenic potential of melanoma cells, augmented metastasis, and decreased survival of tumour-bearing mice. However, very few studies have evaluated the influence of HO-1 in human melanoma. A recent study has however evaluated the relationship between a microsatellite polymorphism in the *HMOX1* promoter and risk of melanoma (Okamoto *et al.*, 2006). It is known that a (GT)n dinucleotide repeat polymorphism in the *HMOX1* promoter can modulate *HMOX1* gene expression (Yamada *et al.*, 2000). *In vitro* work has revealed that so called 'short *HMOX1* alleles' (fewer than 25 GT repeats), result in increased promoter activation in response to oxidative stimuli when compared to longer alleles (Hirai *et al.*, 2003). Okamoto and co-workers were the first to investigate the role of this polymorphism in relation to melanoma. This study offers findings consistent with the interpretation that individuals with short (GT)n repeats have a greater probability of developing malignant melanoma. The results of this study indicate that individuals homozygous for the short allele have a risk of developing melanoma that is double that of heterozygous individuals. Taken together, all of these data indicate that HO-1, and the proteins involved in *HMOX1* regulation, may hold significant potential in augmentation of current modalities of cancer therapy. An objective of this study is to evaluate the role of HO-1 in human melanoma.

## 1.6 Aims and Objectives

This study will determine the effect of UVA radiation on the transcription factor Nrf2 in primary human skin fibroblasts. Nrf2 is known to be principally regulated by two post-translational mechanisms: cytoplasmic retention (anchoring), and modulation of protein half-life. In this study the effect of UVA on the sub-cellular localisation of Nrf2 will be assessed; and, it will be determined whether UVA-generated reactive oxygen species influence Nrf2 nuclear localisation. In addition to this, this study will establish whether UVA results in Nrf2 protein accumulation. It is known that UVA releases the HO-1 substrate heme from heme-containing proteins, and that heme stabilises Nrf2 in murine cells. This study will address whether exogenous heme treatment results in Nrf2 accumulation in human cells, and whether heme is involved in UVA mediated accumulation of Nrf2. To do this intracellular heme will be depleted prior to UVA treatment. An assay will therefore be developed to allow the amount of intracellular heme to be monitored. Further to this, the effect of UVA on *NRF2* gene activation will also be assessed. Nrf2 is known to activate phase II genes by binding to MARE sites in the 5'-flanking region of these genes. A principal concern of this study is to provide insight into the UVA activation of the anti-apoptotic phase II gene *HMOX1*.

In this study, the hypothesis that HO-1 modulates apoptosis in human melanoma cells will also be investigated. Human melanoma cells often lack apoptotic potential, and therefore prove highly resistant to cytotoxic cancer therapeutics. Studies using human and rodent models have indicated that HO-1 possesses potent anti-apoptotic activity. Employing the oxidising UVA component of solar radiation to induce apoptosis, this study will investigate whether HO-1 over-expression prevents UVA-apoptosis in human melanoma cells. This study aims to provide evidence that HO-1 may prove a suitable therapeutic target for intervention in order to increase the efficacy for cytotoxic cancer therapeutics in human melanoma cells.

# 2. Materials and Methods

# 2. Materials and Methods

## 2.1 Chemicals and Reagents

Unless otherwise stated all biochemicals were of analytical grade and were obtained from Sigma Aldrich (UK). All cell culture constituents were obtained from GIBCO (Invitrogen Life Technologies, UK).

## 2.2 Cell Culture

### 2.2.1 Cell storage and recovery

Cells were stored in liquid nitrogen within ampoules in medium supplemented with 10 % v/v dimethyl sulphoxide (DMSO). For cell recovery, each ampoule was rapidly thawed at 37°C and the contents transferred to a conical centrifuge tube containing 9 ml of warm culture medium. The cell suspension was then centrifuged (1,000 rpm for 5 minutes) and the supernatant discarded. The cell pellet was then re-suspended in an appropriate volume of culture medium and incubated using the cell culture conditions described in section 2.2.2.

### 2.2.2 Cell maintenance

*FEK4 / JUSO / IGR1*

The primary human skin fibroblast cell line FEK4, and the human melanoma cell lines JUSO and IGR1 (refer to table 2.1), were cultured in Earle's modified minimal essential medium (EMEM) supplemented with 10 % v/v heat-inactivated fetal bovine serum (FBS) (15 % FBS was used for FEK4), 2 mM glutamine, 0.2 % sodium hydroxide, 50 U/ml penicillin, and 50 µg/ml streptomycin. Cells were maintained at 37°C in a 5 % $CO_2$ / 95 % air humidified incubator (LEEC Ltd, Nottingham, UK) and were passaged weekly using 0.25 % trypsin (5 minutes, 37°C). FEK4 cells were only employed for experimental procedures between passages 8 and 15.

*TK6*

The human lymphoblastoid cell line TK6 (refer to table 2.1) was routinely cultured in RPMI 1640, supplemented with 10 % v/v heat-inactivated horse serum (HS), 2 mM glutamine, 0.2 % sodium hydroxide, 50 U/ml penicillin, and 50 µg/ml streptomycin. The pH of the culture medium was adjusted to 7.0 by addition of 1.0 ml of 5 M NaOH. Cells were maintained at 37°C in a 5 % $CO_2$ / 95 % air humidified incubator. Using these conditions the cell doubling time was approximately 18 hours. Cells were maintained in exponential growth by splitting 1 in 10 v/v every 3 days.

*NIR (041 and 999)*

The primary human melanocyte cell line NIR (refer to table 2.1), was routinely cultured in Ham's F-10 (PAA Laboratories, UK), supplemented with 5 % v/v heat-inactivated FBS, 2 mM glutamine, 100 U/ml penicillin, 100 µg/ml streptomycin, 200 nM phorbol 12-myristate 13-acetate (PMA), 200 pM cholera toxin (type inaba 569B, azide free) (Merck Biosciences), and 10 ng recombinant human stem cell factor (Fahrenheit Laboratory Supplies, UK). Cells were maintained at 37°C in a 5 % $CO_2$ / 95 % air humidified incubator and were passaged monthly using 0.25 % trypsin (5 minutes, 37°C). NIR cells were only employed for experimental procedures between passages 3 and 5.

*G361*

The human melanoma cell line G361 (refer to table 2.1), was routinely cultured in McCoy's 5A supplemented with 5 % v/v heat-inactivated FBS, 2 mM glutamine, 50 U/ml penicillin, and 50 µg/ml streptomycin. Cells were maintained at 37°C in a 5 % $CO_2$ / 95 % air humidified incubator and were passaged weekly using 0.25 % trypsin (5 minutes, 37°C).

| Cell Line | Description | Reference / Source |
|---|---|---|
| FEK4 | Primary human fore-skin fibroblast cell line | Tyrrell and Pidoux, 1986 |
| IGR1 | Pigmented human melanoma cell line | Dr S. Carrel Ludwig Institute, Lausanne, Switzerland |
| JUSO | Lightly pigmented human melanoma cell line | Dr S. Carrel Ludwig Institute, Lausanne, Switzerland |
| G361 | Lightly pigmented human melanoma cell line | National Radiological Protection Board, Didcot, UK |
| NIR | Primary human melanocyte cell line | National Radiological Protection Board, Didcot, UK |
| TK6 | Human lymphoblastoid cell line | Thilly, 1979 |

**Table 2.1: Summary of cell lines**

The above table summarises the type and source of each of the cell lines used in this study.

## 2.3 Treatments

### 2.3.1 UVA irradiation source and conditions

Cells were irradiated using a broad-spectrum 4 kW UVA lamp (340 – 400 nm) (Sellas, Munich, Germany). The lamp exposure time was calculated using an IL1700 radiometer (International Light, Newbury, USA) with an SEE400 probe. Prior to UVA irradiation, the growth medium was removed from the cells and retained; each dish was then washed twice with phosphate buffered saline (PBS) (Oxoid Ltd, UK). Cells were then covered with PBS supplemented with 0.01 % $Ca^{2+}$ and 0.01 % $Mg^{2+}$ prior to irradiation. In order to maintain a consistent temperature of 25°C throughout the irradiation procedure, irradiation was conducted in an air-conditioned room. Post irradiation the $Ca^{2+}$ / $Mg^{2+}$ supplemented PBS was removed and the dishes were washed twice with PBS. The retained media (referred to as conditioned media) was then added back. Control cells underwent identical treatment, except that they were not irradiated. A dose rate (fluence) of approximately 300 J $m^{-2}$ $sec^{-1}$ was used throughout this study. Therefore, the irradiation time for a dose of 250 $kJ/m^2$ was between 20 and 30 minutes.

### 2.3.2 Actinomycin-D

A stock solution of 5 mg/ml actinomycin-D was prepared in DMSO. This stock solution was diluted by a factor of 1,000 into serum free medium to give a working concentration of 5 μg/ml actinomycin-D (0.1 % DMSO). Before this chemical was added to the cells, the culture medium was removed and the cells were washed twice with PBS. 5 μg/ml actinomycin-D (0.1 % DMSO) was added to the cells one hour post irradiation. The cells were cultured in the presence of this chemical for the time periods indicated at 37°C in a 5 % $CO_2$ / 95 % air humidified incubator.

### 2.3.3 Cadmium chloride

A 100 μM stock solution of cadmium chloride ($CdCl_2$) was prepared in water. This stock solution was diluted by a factor of 10 into serum free medium to give a

final working concentration of 10 μM $CdCl_2$. Cells were exposed to 10 μM $CdCl_2$ or the vehicle control (serum free medium) for the time periods indicated at 37°C in a 5 % $CO_2$ / 95 % air humidified incubator.

2.3.4 Deuterium oxide

PBS was prepared by dissolving one PBS tablet in 100 ml of 99.9 % deuterium oxide ($D_2O$). The $D_2O$-PBS solution was then supplemented with 0.01 % $Ca^{2+}$ and 0.01 % $Mg^{2+}$ and filter sterilised. $D_2O$-PBS was used to cover cells during irradiation in place of $H_2O$-PBS. Control cells were covered with $H_2O$-PBS during irradiation. Cells were covered with the $H_2O$- or $D_2O$-PBS 15 minutes prior to irradiation.

2.3.5 Hemin

A stock solution of 10 mM bovine hemin was prepared in DMSO. This stock solution was diluted by a factor of 10,000 into serum free medium to give a working concentration of 1 μM hemin (0.01 % DMSO). Prior to addition of the chemical to the cells, the culture medium was removed and the cells were washed twice with PBS. Cells were exposed to 1 μM hemin, or the vehicle control (0.01 % DMSO), for the time periods indicated at 37°C in a 5% $CO_2$ / 95% air humidified incubator and under darkened conditions to prevent photodegradation by hemin. Untreated cells remained within the incubator throughout the course of the experiment.

2.3.6 Succinyl acetone

A 1 mM working solution of 4, 6-dioxoheptanoic acid [Succinyl Acetone (SA)] was prepared in serum free medium. The solution was subsequently filter sterilised. Prior to the addition of the chemical to the cells, the culture medium was removed and retained. Cells were then washed twice with PBS. Cells were exposed to 1 mM SA or the vehicle control (serum free medium) for 24 hours at 37°C in a 5 % $CO_2$ / 95 % air humidified incubator. After 24 hours the serum free medium was removed and the conditioned medium returned. Untreated cells remained within the incubator throughout the course of the experiment.

## 2.4 Protein extraction and quantification

### 2.4.1 Whole cell extracts

Following treatment cells were maintained at 37°C in a 5 % $CO_2$ / 95 % air humidified incubator. At the time points stated, the cell culture medium was removed and each dish was washed twice with PBS. Cells were then collected by addition of an appropriate volume of 0.25 % trypsin (37°C for 5 minutes) and / or scraping with a rubber policeman. The detached cells were then pelleted by centrifugation (13,000 rpm for 30 seconds) and the supernatant discarded. The cell pellet was then lysed into an appropriate volume of stabilisation buffer [50 mM tris-HCl pH 7.5, 150 mM NaCl, 10 % Glycerol, 5 mM ethylene-diaminetetraacetic acid (EDTA), 1 % NP40, and 1 mM phenylmethylsulfonyl fluoride (PMSF)]. The cell lysate was then centrifuged at 4°C for 2 minutes at 13,000 rpm. The resultant supernatant containing total cellular free protein was retained and flash-frozen using 100 % ethanol containing dry-ice. Cell extracts were stored at -80°C until required.

### 2.4.2 Nuclear and cytoplasmic cell extracts

Following treatment cells were maintained at 37°C in a 5 % $CO_2$ / 95 % air humidified incubator. At the time points stated, the cell culture medium was removed and each dish was washed twice with PBS. Cells were then collected by addition of an appropriate volume of 0.25 % trypsin (37°C for 5 minutes) and / or scraping with a rubber policeman. The detached cells were then pelleted by centrifugation (13,000 rpm for 30 seconds) and the supernatant was discarded. The cell pellet was then lysed into an appropriate volume of cytosolic extraction buffer [10 mM Hepes pH 7.9, 10 mM KCl, 0.1 M ethylene-glycoltetraacetic acid (EGTA), 0.1 M EDTA, 1.5 mM $MgCl_2$, 1 mM 1,4-dithio-DL-threitol (DTT), and 0.1 x protease inhibitor cocktail (Roche)], and incubated on ice for 15 minutes. NP40 was then added to a final concentration of 0.5 % and the lysate was vigorously vortexed for 10 seconds. The cell lysate was then centrifuged at 13,000 rpm for 30 seconds. The supernatant containing the cytoplasm and RNA was collected and flash-frozen using 100 % ethanol containing dry-ice. The nuclear pellet was then washed in the cytoplasmic extraction buffer before lysis into an appropriate volume of the nuclear extraction

buffer [20 mM Hepes pH 7.9, 400 mM NaCl, 1 mM EGTA, 1 mM EDTA, 1 mM DTT, and 0.1 x protease inhibitor cocktail]. The nuclear lysate was then placed on a rocking platform for 15 minutes at 4°C. The nuclear lysate was the centrifuged at 13,000 rpm for 5 minutes. The supernatant containing the nuclear fraction of the cell was collected and flash-frozen using 100 % ethanol containing dry-ice. Both cytoplasmic and nuclear extracts were stored at -80°C until required.

### 2.4.3 Microsome isolation

Following treatment the cell culture medium was removed and each cell population was washed twice with an appropriate volume of PBS. The cells were then collected by scraping in 1 ml of PBS using a rubber policeman. The cell suspension was then pelleted by centrifugation (1,000 rpm for 5 minutes at 4°C); the supernatant was discarded. The cell pellet was re-suspended into 3 ml of ice cold 0.1 M potassium phosphate buffer (pH 7.0). The cells were then disrupted by 3 cycles of rapid freezing and thawing, and sonication (2 x 10 seconds at the lowest strength). The cell debris and mitochondria were removed by centrifugation at 15,000 g (5 minutes at 4°C). The supernatant was then ultra-centrifuged at 100,000 g (1 hour at 4°C) in order to sediment the microsomal fraction. The resultant firmly packed pellet of microsomes was re-suspended in 100 µl of ice cold 0.1 M potassium phosphate buffer (pH 7.0) and stored at -20°C until required for analysis.

### 2.4.4 Quantification of protein concentration

Protein concentration was calculated using the Bio-Rad protein assay based on the Bradford dye binding procedure (Bradford, 1976). A calibration curve was generated using six concentrations of bovine serum albumin (BSA) (0 – 17 µg/ml) in the same solvent as the cell extract. Each calibration standard was produced in duplicate. For each cell extract the protein concentration was determined in duplicate using 5 µl of extract using a 96-well spectrophotometric microplate reader (VERSAmax, Molecular Devices) and the software package SoftMax Pro.

## 2.5 mRNA extraction and quantification

### 2.5.1 mRNA extraction

Following treatment the cell culture medium was removed and each dish was washed twice with an appropriate volume of PBS. Cells were then collected by scraping with a rubber policeman. The detached cells were then pelleted by centrifugation (13,000 rpm for 30 seconds) and the supernatant was discarded. The cell pellet was then flash-frozen in 100 % ethanol containing dry-ice. Cell extracts were stored at -80°C until RNA extraction. Total RNA isolation was accomplished using Sigma's GenElute™ Mammalian Total RNA Kit according to the manufacturer's instructions. RNA was eluted from the binding column using 50 µl of elution buffer and stored at -80°C until required for experiments.

### 2.5.2 Quantification of mRNA concentration

RNA concentration was determined by spectrophotometric absorbance at 260 nm (GeneQuant II, Pharmacia Biotech). The ratio of absorbance at 260 nm to 280 nm ($A_{260}/A_{280}$) was also determined as a measure of extract purity.

## 2.6 Gel electrophoresis

### 2.6.1 Acrylamide gel electrophoresis

Denaturing gels comprising of either 7.5 % or 10 % acrylamide were used throughout this study. 7.5 % acrylamide gels were prepared as follows: 2.8 ml of 40 % acrylamide (40 %, 29:1, acrylamide: bis-acrylamide) (Fluka, Biochemika), 5.6 ml 1 M Tris pH 8.8, 75 µl of 20 % sodium dodecyl sulphate (SDS), 6.6 ml MilliQ water; total volume approximately 15 ml (enough for two gels). 10 % acrylamide gels were prepared in the same manner but contained 3.8 ml of 40 % acrylamide and 5.6 ml MilliQ water. Both 7.5 % and 10 % acrylamide gels were set by the addition of 100 µl of 10 % ammonium persulphate (APS) and 40 µl of N,N,N',N'-tetramethylethylenediamine (TEMED). The gels were cast between two BioRad glass plates. During setting 20 µl of butanol was poured onto the top of the gel solution in

order to prevent evaporation and to ensure an even surface for a stacking (loading) gel. Stacking gels were prepared as follows: 0.51 ml of 40 % acrylamide (40 %, 29:1, acrylamide: bis-acrylamide), 0.5 ml 1 M Tris pH 6.8, 20 µl of 20 % SDS, 2.86 ml MilliQ water; total volume approximately 4 ml (enough for two gels). Stacking gels were set by the addition of 50 µl of 10 % APS and 20 µl of TEMED. The gels were allowed to set for one hour prior to use.

### 2.6.2 Agarose gel electrophoresis

Agarose gels composed of between 2 and 5 % agarose were used throughout this study. The density of the gel used for each experiment was selected based on the fragment size of the smallest oligonucleotide that was expected to be visualised. 100 ml of agarose gel was prepared as follows: 2 – 5 grams of electrophoresis grade agarose (Invitrogen Life Technologies, UK) was added to 100 ml of either tris-acetate buffer (TAE) (20 mM tris acetate, 1 mM EDTA pH 8.0) or tris-borate buffer (TBE) (45 mM tris base, 45 mM boric acid, 1 mM EDTA pH 8.0) and dissolved using a microwave oven on low power for 2 - 3 minutes. The solution was allowed to cool to approximately 60°C before it was poured into a horizontal casting tray (Danaphor, Grandvaux, Switzerland). The gel was allowed to cool to room temperature for approximately one hour prior to use.

The gel was covered with sufficient TAE or TBE in order to cover the wells. Electrophoresis was performed at 55 volts for an appropriate length of time (usually 60 – 90 minutes) until full band separation had taken place. In order to visualise the bands the gel was bathed in a solution containing 0.7 µg/µl ethidium bromide at room temperature for 20 minutes. Based were visualised under UV light (SynGene, Synoptics Ltd) and analysed using the software package GeneSnap (Synoptics Ltd).

## 2.7 Constructs

### 2.7.1 General remarks

The expression vector pcDNA3.1(+) (Invitrogen Life Technologies, UK) was employed in this study to independently over-express both green fluorescent protein (GFP) and HO-1. pcDNA3.1 is a non-replicative 5.4 kb vector that has been designed for high-level transient expression in mammalian cells. The vector contains a human cytomegalovirus immediate-early (CMV) promoter for high-level gene expression, and ampicillin resistance gene to allow for selection of transformed *E.coli* (refer to figure 2.1). All transient transfection experiments employed the empty pcDNA3.1 vector as a control. The two over-expression vectors used in this study were propagated as described in section 2.8 and were transfected into cultured mammalian cells as described in section 2.9.

### 2.7.2 HO-1 over-expressing construct

pcDNA3.1-HO-1 (a kind gift from Professor Roland Stocker, Medical Foundation Building, The University of Sydney, Australia) was employed throughout this investigation to over-express HO-1. pcDNA3.1-HO-1 contains a 1kb insert of the human *HMOX1* open reading frame. The presence of the 1kb insert was confirmed by restriction digest by this study.

### 2.7.3 Green fluorescent protein over-expressing construct

pcDNA3.1-EGFP was employed throughout this investigation to over-express green fluorescent protein. pcDNA3.1-EGFP was constructed prior to the start of this investigation by Dr Stephen Mitchell, University of Bath.

Green fluorescent protein (GFP) is coded for by the *gfp* gene derived from the jellyfish *Aequorea Victoria.* The gene encodes a protein of 238 residues which produces stable fluorescence with no requirement for exogeneous substrates and that is not destructive to living tissues (Chalfie *et al.*, 1994). The protein absorbs blue light (maximally 395 nm) and emits green light (peak emission at 509 nm). The wild type gene has been engineered to produce mutated forms which have both increased protein stability and enhanced absorption / emission. pcDNA3.1-EGFP contains the GFP mutant F64L / S65T, enhanced (EGFP) (for review see Tsien, 1998). This mutant has an altered emission spectrum allowing visualisation of the protein with a fluorescence microscope using standard FITC filter settings, and also has emission with a magnitude that is in excess of twenty times greater than that of the wild-type.

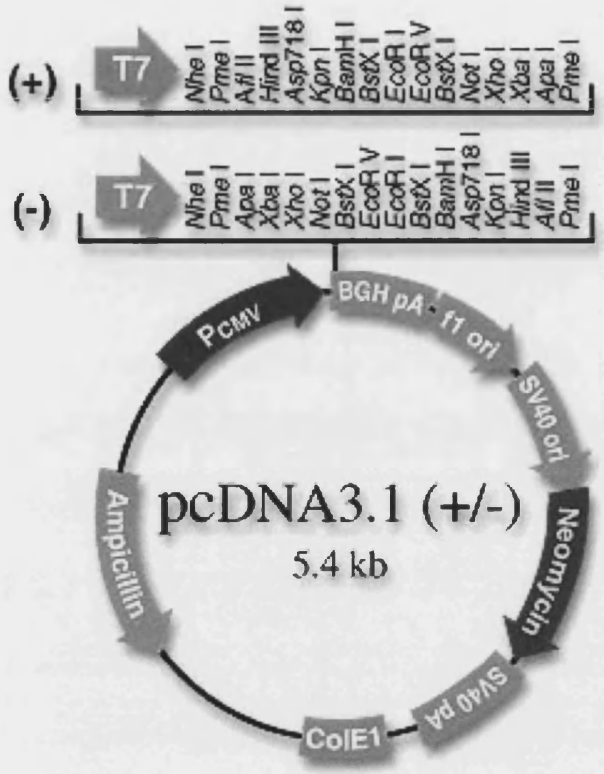


**Figure 2.1:**
**The figure above summarises the features of pcDNA3.1(+ / -)**

Full information relating to this expression vector can be found at:
www.invitrogen.com
(Invitrogen Life Technologies)

## 2.8 Construct propagation and purification

Transformed *Escherichia coli (E. coli)* containing either pcDNA3.1-HO-1 or pcDNA3.1-EGFP (or the empty control vector) were cultured overnight at 37°C in a shaking incubator (New Brunswick Scientific Shaker, UK) in 250 ml of Luria-Betani (LB) broth supplemented with 125 μg/μl ampicillin. The cell suspension was then centrifuged (5000 rpm for 10 minutes at 4°C) and the supernatant discarded. The bacterial pellet was loosened by vortexing and re-suspended into 5 ml of ice cold re-suspension solution (1 % glucose, 25 mM tris-HCl pH 8.0, and 1 mM EDTA pH 8.0). The suspension was then placed on ice and 10 ml of cell lysis solution was added (0.2 M NaOH, 2 % SDS). The solution was then mixed by inversion and placed onto ice for 15 minutes. 7.5 ml of neutralisation solution (0.8 M acetic acid, 0.8 M potassium acetate) was then added. The solution was again mixed by inversion and placed onto ice for 15 minutes. The solution was then centrifuged (10,000 rpm for 15 minutes at 4°C) and the clear DNA containing supernatant retained. 100 μl of RNase A (10 mg/ml) was added and the solution was incubated at 37°C for 30 – 60 minutes. After this incubation period, 10 ml of phenol chloroform was added and the solution vigorously vortexed. The solution was then centrifuged (10,000 rpm for 15 minutes at 4°C). The lower phase containing protein contaminants was discarded, the clear supernatant was retained. Approximately 20 ml of 100 % ethanol was added, and the solution was vortexed vigorously for 1 minute. The solution was then centrifuged (10,000 rpm for 15 minutes at 4°C) and the supernatant again discarded. The pellet was then washed in 70 % ethanol and air-dried for 20 – 30 minutes. Once dried, the pellet was re-suspended into 555 μl of sterile MilliQ water. 106 μl of 5 M NaOH followed by 172 μl of 50 % $PEG_{4000}$ was then added. The solution was vortexed and incubated on ice for 30 minutes. After this incubation period the solution was centrifuged (13,000 rpm for 15 minutes at room temperature) and the supernatant was discarded. The resulting DNA pellet was washed in 70 % ethanol and air dried until clear. The pellet was then re-suspended into 300 μl of TE buffer (10 mM Tris, 1 mM EDTA) and the concentration of DNA determined by spectrophotometry (GeneQuant II, Pharmacia Biotech).

## 2.9 Transient transfection

Cells were seeded into 6-well plates (Nunc, Wiesbaden, Germany) 48 - 72 hours prior to transfection. Cells were maintained according to the conditions described in section 2.2.2. Cells were transfected with either pcDNA3.1-HO-1 or pcDNA3.1-EGFP (refer section 2.7.2 and 2.7.3 respectively), or the empty control vector using the commercially available transfection reagents Lipofectamine™ 2000 (Invitrogen Life Technologies, UK) or GeneJuice® (Novagen, UK) according to the manufacturer's instructions. Cell monolayers were transfected whilst in exponential growth (50 – 80 % confluent). Cells were transfected with the amount of plasmid DNA, and using the ratio of plasmid DNA to transfection reagent indicated. Prior to transfection the cell culture medium was removed and each dish was washed twice with an appropriate volume of PBS. Cells were then bathed in the serum free medium Opti-MEM containing the transfection reagent / DNA complex and incubated for 4 - 5 hours at 37°C in a 5 % $CO_2$ / 95 % air humidified incubator. After this period, the transfection medium was replaced with fresh complete medium and the cells were cultured for the time periods indicated before treatment or harvesting. Cells were collected by addition of 500 µl of 0.25 % trypsin (37°C for 5 minutes).

## 2.10 Spectrophotometric detection of intracellular heme

Spectrophotometry was used to determine the intracellular heme concentration. The assay is based on the work of Kvam *et al.*, (1999). In this assay the nitrogen ligands from the protein-bound heme are replaced by pyridine in alkali. The resultant hemochrome is quantified by the difference spectrum of the reduced versus oxidised compound. Whole cell extracts were harvested and prepared as described in section 2.4.1. The protein concentration of each extract was determined as described in section 2.4.4.

For each sample a 0.84 ml aqueous cell extract of known protein content was produced. 200 µl of reagent grade pyridine was added, and the solution vortexed. 100 µl of 1 M NaOH was then added, and the solution again vortexed. The sample was then split in equal volumes into two disposable cuvettes and a baseline

absorbance spectrum taken from 500 to 600 nm (UVIKON 922 Spectrophotometer). A few crystals of sodium dithionite and 10 µl of water was added to one of the cuvettes in order to reduce the hemochrome. 10 µl of 3 M potassium ferricyanide was added to the other cuvette to oxidise the hemochrome. An absorbance spectrum of the reduced versus oxidised heme was then obtained between 500 and 600 nm. The heme concentration was calculated based on the difference in absorption between the peak at 557 nm and the trough at 575 nm of the reduced sample, and using a millimolar extinction coefficient of 20.7.

### 2.11 Fluorometric detection of intracellular heme

An assay for the fluorometric determination of intracellular heme was developed based on the work of Morrison, (1965) and Sassa, (1976). The assay is based on the conversion of heme to its fluorescent porphyrin derivative by the removal of heme iron under acidic conditions. Either whole cell tissue homogenate or a solution containing total cellular microsomes was used for this assay. Whole cell extracts were harvested and prepared as described in section 2.4.1. Protein concentration was determined as detailed in section 2.4.4. Microsomes were isolated as described in section 2.4.3.

For each sample the amount of protein stated in the figure legend was added to 1 ml of 2 M oxalic acid (the volume of oxalic acid was always at least 20 times greater than the volume of homogenate used). In addition to this, a series of 8 hemin standards were prepared in 0.1 M phosphate buffer pH 7.4 containing 0.05 % BSA, and diluted 1:1 v/v with 2 M oxalic acid. The final concentration of the hemin standards ranged from 100 – 800 nM. Each cell extract sample and standard was produced in duplicate, one of which was boiled at 100°C for 30 minutes (in order to remove the heme iron), the other control sample was incubated at room temperature for the same time period. All samples were covered during this incubation period in order to prevent evaporation. Each cell extract and standard, both boiled and control, was produced in duplicate.

The fluorescence of each sample was read at 600 nm emission using a spectrofluorometer (SFM 25, Kontron Instruments) set at 405 nm excitation. The value of the un-boiled control sample (representing background fluorescence) was subtracted from the boiled sample fluorescence where the heme iron had been

removed. The relative fluorescence of the 8 hemin standards was plotted against concentration on a linear scale in order to produce a standard curve. If the standards were not linear when plotted, the experiment was considered void. The standard curve was used to estimate the heme concentration of the cell extracts.

**2.12 Western blotting**

Total cellular protein or nuclear and cytoplasmic fractions were prepared as described in section 2.4.1 and 2.4.2 respectively. Protein concentration was determined as described in section 2.4.4. Cell extracts were diluted with 3 x Laemmli (loading) buffer [180 mM tris pH 6.8, 3 % SDS, 150 mM DTT, 30 % glycerol, 0.0015 % bromophenol blue] and heated to 95°C for 5 minutes. Protein bands were then separated on 7.5 – 10 % denaturing acrylamide gels at 150 volts for 60 – 90 minutes whist bathed in running buffer (1.5 % w/v tris, 7.2 % w/v glycine, 0.5 % SDS). Acrylamide gels were prepared as described in section 2.6.1. The separated protein bands were then transferred onto nitrocellulose membrane (Amersham Biosciences, UK) using a BioRad eletro-transfer unit at 100 volts for 90 minutes. The cassette holding the acrylamide gel and nitrocellulose membrane was bathed in transblot buffer (3 % w/v tris, 14.4 % w/v glycine, 20 % methanol) and placed on ice during protein electro-transfer.

Following electro-transfer the nitrocellulose membranes were stained with red ponceau in order to visualise successful protein transfer. Membranes were then thoroughly washed with PBS supplemented with 0.5 % tween (Acros Organics, Geel, Belgium). The nitrocellulose membranes were then blocked at 4°C over-night in 5 % w/v milk powder in PBS. After blocking, nitrocellulose membranes were incubated for 60 – 90 minutes at room temperature bathed in a 5 % w/v milk powder-PBS solution containing one of the following primary antibodies: 1:200 anti-Nrf2 rabbit polyclonal antibody (H-300, Santa Cruz Biotechnology); 1:200 anti-HO-1 mouse monoclonal antibody (OSA-110, Stressgen Bioreagents); 1:500 anti-actin mouse monoclonal antibody (A4700, Sigma-Aldrich). After exposure of the primary antibody, nitrocellulose membranes were washed thoroughly in 0.5 % tween-PBS. Membranes were then covered in a 5 % w/v milk powder-PBS solution containing either 1:5000 anti-mouse- or anti-rabbit-HRP conjugated secondary antibody and rocked gently on a 3D rocking platform (Stuart Scientific) for 60 minutes at room

temperature. Immunoreactive bands were visualised using enhanced chemiluminescent plus detection (Amersham Biosciences, UK).

In order to re-probe for other immunoreactive bands, membranes were bathed in stripping solution [62.5 mM tris-HCl pH 6.8, 1 % SDS, 0.1 M b-mercaptoethanol (Acros Organics, Geel, Belgium)] and incubated at 55°C for 20 minutes. Prior to re-probing membranes were thoroughly washed in both 0.5 % tween-PBS and 5 % w/v milk powder in PBS.

## 2.13 Flow cytometry

### 2.13.1 General comments

Flow cytometry was performed using a FACScan (Becton Dickinson, Erembodegon, Belgium). All flow cytometric data was analysed using the software package CellQuest (Becton Dickinson, Erembodegon, Belgium). Unless otherwise stated cells were suspended in PBS during FACScan acquisition; for each sample 10,000 events were recorded. For experiments involving dual colour acquisition, sufficient compensation was employed to resolve any emission spectra overlap.

### 2.13.2 Quantification of apoptosis

Quantification of apoptosis and necrosis was accomplished using the annexin-V-fluos (AV) (Roche, UK) and propidium iodide (PI) staining method. Fine changes in the cell surface, but not loss of membrane integrity, is a morphological feature associated with apoptosis (Andree *et al.*, 1990; Creutz, 1992; Fadok *et al.*, 1992). Phosphatidylserine (PS) is a plasma membrane component that is known to translocate from the inner part of the membrane to the outer surface during apoptosis (Vermes *et al.*, 1995). AV is a $Ca^{2+}$-dependent phospholipid–binding protein with a high affinity for PS (Vermes *et al.*, 1995). Thus, AV can be used as a sensitive probe for apoptotic cells (Homburg *et al.*, 1995; Koopman, *et al.*, 1994; Verhoven *et al.*, 1995). Necrotic cells also exhibit PS on the outer surface of the membrane, however this can be related to a loss of membrane integrity. Thus, the application of a dye exclusion test in the form of PI in combination with AV allows apoptotic cells to be differentiated from necrotic cells.

Following treatment cells were maintained at 37°C in a 5 % $CO_2$ / 95 % air humidified incubator. At the time points stated in the figure legend the cell culture medium was removed and retained, and each dish was washed twice with an appropriate volume of PBS. Cells were then collected by addition of 500 µl of 0.125 % trypsin (37°C for 5 minutes). The retained conditioned medium was then added to the detached cell suspension in order to inactivate the trypsin, and the cells were pelleted by centrifugation (1,000 rpm for 5 minutes). The supernatant was discarded and the cell pellet re-suspended into 1 ml of PBS to wash the cells. The cell suspension was then centrifuged (1,000 rpm for 5 minutes) and the supernatant discarded. The cell pellet was then re-suspended into 100 µl of AV / PI labelling solution. The labelling solution comprised of 98 µl of incubation buffer [19 parts annexin V w/o $Ca^{2+}$ buffer (0.15 M NaCl, 10 mM hepes), 1 part 100 mM $CaCl_2$], 1 µl AV, and 1 µl PI (1 in 20 dilution in PBS). The cells were then incubated in the labelling solution at room temperature for 15 minutes under darkened conditions. A further 400 µl of incubation buffer was then added to each sample prior to FACScan acquisition. All samples were stored on ice under darkened conditions whilst acquisition was taking place. During acquisition and analysis, data was viewed using a two-dimensional log dot plot defined by the FL1 and FL3 fluorescent profiles. Double stained cells were considered necrotic, whereas AV positive PI negative stained cells were deemed to be apoptotic (refer to figure 2.2).

**Figure 2.2: Two dimensional flow cytogram: determination of apoptosis**

*(next page)*

In order to determine the percentage of cells undergoing apoptosis in any given population, cells were treated as described in section 2.13.2 and analysed by flow cytometry. During acquisition and analysis, data was viewed using a two-dimensional log dot plot defined by the FL1 and FL3 fluorescent profiles. The percentage of living, apoptotic, and necrotic cells was determined by superimposing four quadrants over the flow cytogram. The position of these four quadrants remained constant for each experiment. Double stained cells, those that increased in fluorescence on both the FL1 and FL3 axis, were considered necrotic (upper right). Annexin positive / propidium iodide negative stained cells, those that increased in fluorescence on the FL1 axis but not on the FL3 axis, were deemed to be apoptotic (lower right). Figure 2.2(a) shows a typical cytogram of unirradiated cells. Figure 2.2(b) shows a typical cytogram of irradiated cells.

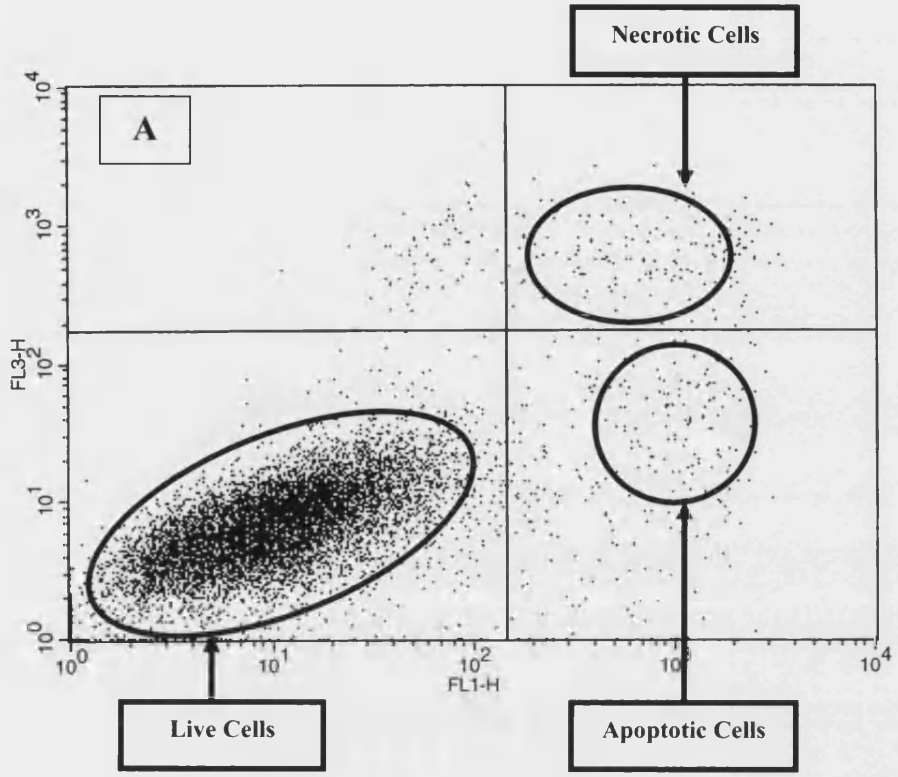
Necrotic Cells
A
FL3-H
FL1-H
Live Cells
Apoptotic Cells

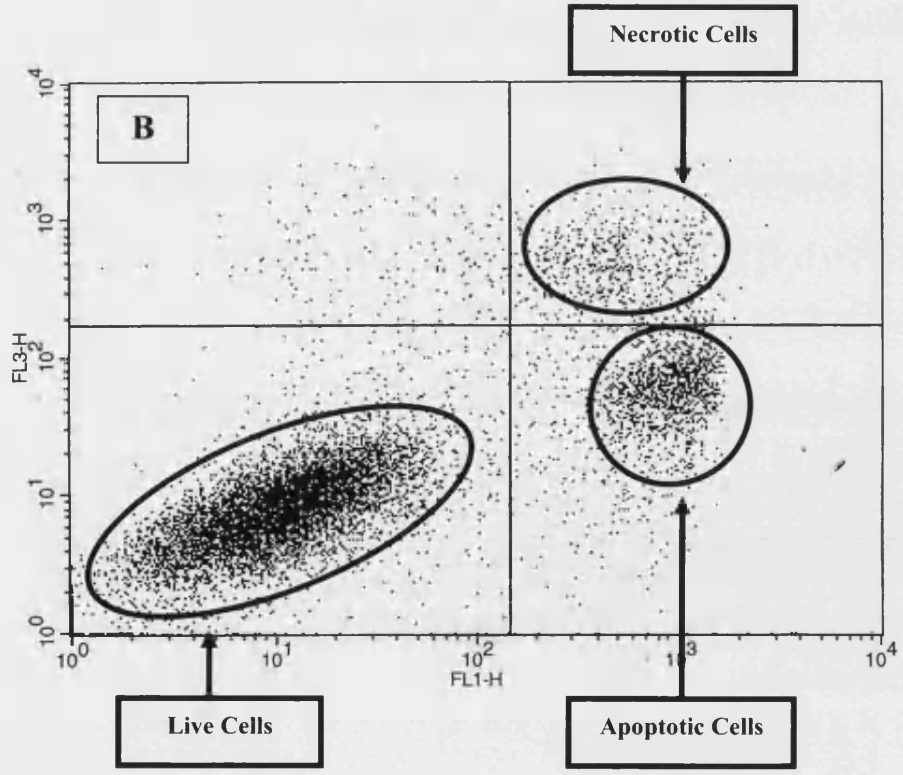
Necrotic Cells
B
FL3-H
FL1-H
Live Cells
Apoptotic Cells

### 2.13.3 Quantification of transient transfection efficiency

In order to quantify transfection efficiency, cells were transfected with the GFP over-expressing construct pcDNA3.1-EGFP as described in section 2.9. At the time points indicated, the cell culture medium was removed and each cell population was washed twice with an appropriate volume of PBS. Cells were then collected by addition of 1 ml of 0.25 % trypsin (37°C for 5 minutes) and / or scraping with a rubber policeman. The detached cells were then pelleted by centrifugation (1,000 rpm for 5 minutes) and the supernatant was discarded. During acquisition and analysis data was viewed using a one-dimensional log histogram plot defined by the FL1 fluorescent profile. The percentage of cells transfected was deemed to be the percentage of cells exhibiting a higher fluorescence than 98 % of the lowest fluorescing cells in the control sample population (refer to figure 2.3).

**Figure 2.3: One dimensional flow cytogram: determination of transfection efficiency**

*(next page)*

In order to determine the percentage of transfected cells in any given population, cells were treated as described in sections 2.9 and 2.13.3 and analysed by flow cytometry. During acquisition and analysis data was viewed using a one-dimensional log histogram plot defined by the FL1 fluorescent profile. The percentage of cells transfected was deemed to be the percentage of cells exhibiting a higher fluorescence than 98 % of the lowest fluorescing cells in the control sample population. Figure 2.3(a) shows a typical histogram of un-transfected control cells (M1 < 2 %). Figure 2.3(b) shows a typical cytogram of cells transfected with the GFP over-expressing construct pcDNA3.1-EGFP (M1 = % of transfected cells).

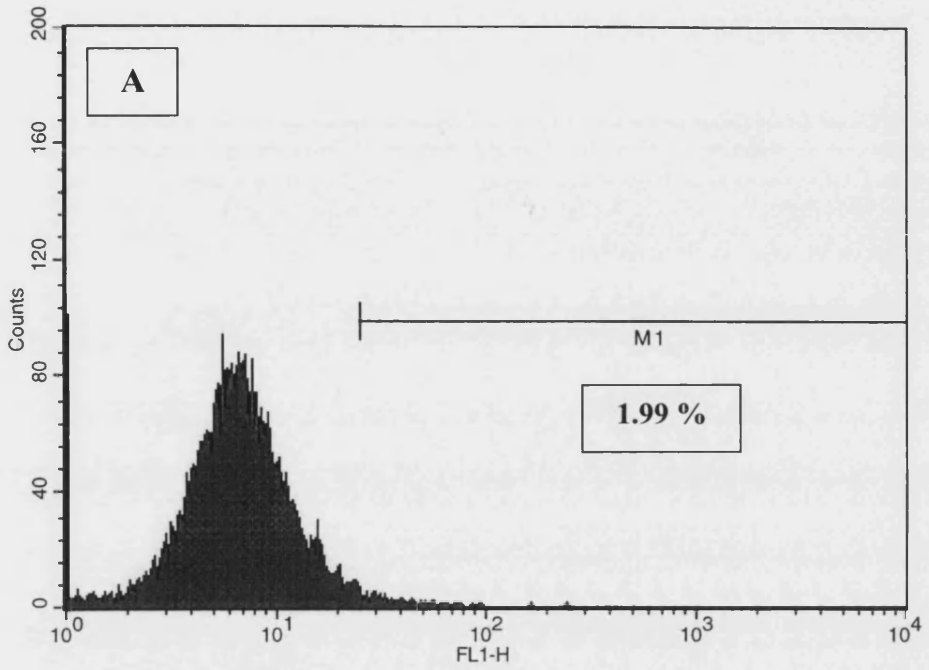
A
Counts
M1
1.99 %
FL1-H

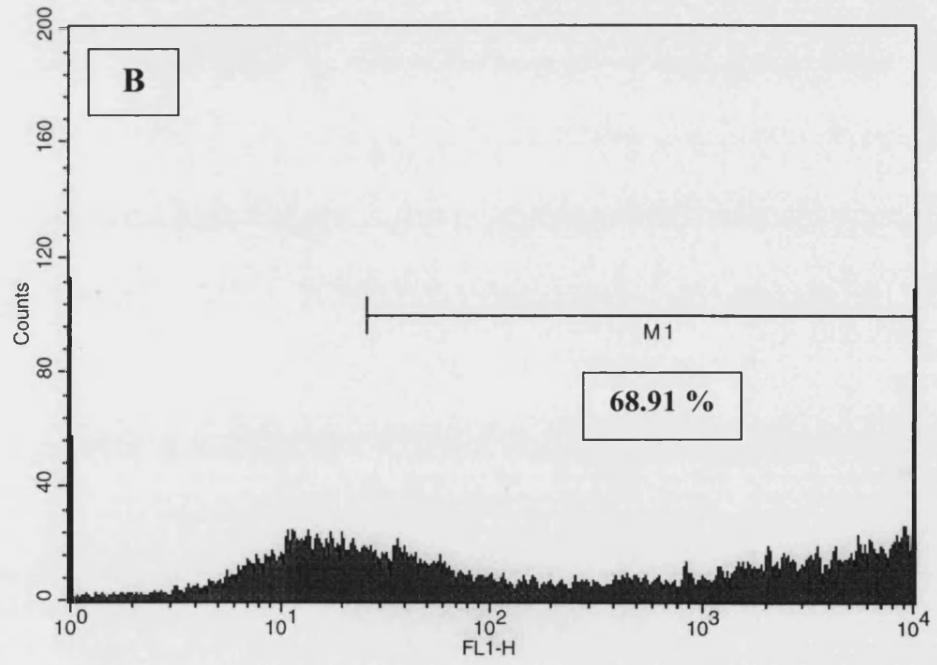
B
Counts
M1
68.91 %
FL1-H

## 2.14 Immunocytochemistry

Cells were grown to 80 % confluency on sterilised glass coverslips (thickness 1, 22 x 22 mm, VWR International) using the cell culture conditions described in section 2.2.2. Following treatment, and at the time points indicated in the figure legend, the cell culture medium was removed and each coverslip was gently washed twice with PBS. Each coverslip was then bathed in 2 ml of a 4 % solution of PFA and incubated at room temperature for 15 minutes on a 3D rocking platform (lowest speed setting). Warmed PBS and PFA were used for these steps to prevent possible temperature shock to the cells and subsequent alteration in protein localisation. The PFA was removed, and the coverlsips were washed twice with PBS. The cells were then permeabilised by bathing the coverslips with -20°C 100 % methanol for 5 minutes. The methanol was removed, and again the coverlsips were washed twice with PBS. Blocking of non-specific sites was accomplished by application of 1 - 2 drops of Image-iT™ Fx signal enhancer according to the manufacturer's instructions (Alexa-Fluor system, Invitrogen Life Technologies). The coverslips were then washed twice in PBS and incubated at room temperature for one hour with the primary antibody [anti-Nrf2 rabbit IgG polyclonal antibody (H-300, Santa Cruz Biotechnology)]. The primary antibody was diluted 1:100 in PBS; a final concentration of approximately 2 μg/μl. The coverslips were then washed twice in PBS for 5 minutes on a 3D rocking platform (intermediate speed setting) and then incubated in the dark for 2 hours with the secondary antibody according to the manufacturer's instructions [Alexa-Fluor goat anti-rabbit (Invitrogen Life Technologies)]. The coverslips were then washed twice in PBS for 5 minutes on a 3D rocking platform (intermediate speed setting). Cells were then incubated in Hoechst stain (1:1000 dilution in PBS) for 5 minutes at room temperature to allow visualisation of nuclei. Coverslips were then washed twice in PBS for 5 minutes and were mounted onto glass microscope slides (1.0 mm thick, BDH) using Dakocytomation fluorescent mounting medium (DakoCytomation, UK). The cells were analysed by oil immersion epifluorescence (Zeiss Immersol, 518N) at 63x magnification on a Nikon Eclipse TE2000-U microscope equipped with a Lambda 10-2 filter unit (Shutter Instrument Co, UK). Alexa-Fluor goat anti-rabbit was excited at 650 nm and emission was collected at 668 nm. Hoechst stain was excited by ultraviolet light at 350 nm and emission collected at 461 nm. Images were recorded

using the software program UltraVIEW. The mean fluorescence of each image was determined using the software package ImageJ. For each cell the fluorescence intensity was determined in both the cytoplasm and the nucleus. A predefined area was chosen and superimposed over the cytoplasm and then the nucleus of each cell. The mean fluorescence of each cell was determined by dividing the fluorescence intensity by the area. The mean fluorescence for each entire image is the mean fluorescence of all of the cells contained in that image. For each experiment the mean fluorescence intensity of each image has been normalised against the mean fluorescence of the untreated control.

## 2.15 Reverse transcription

RNA was extracted and quantified as described in sections 2.5.1 and 2.5.2 respectively. For each sample, reverse transcription was performed using 1 μg of total RNA using the SuperScript™ III system (Invitrogen Life Sciences) for first strand cDNA synthesis according to the manufacturer's instructions. For each sample 1 μl of 50 μM oligo$(dT)_{20}$ was used as primer. Oligo(dT) primers were chosen as this priming method is known to produce a product suitable for real-time polymerase chain reaction (PCR) more consistently than random hexamers or gene-specific primers. Reverse transcription was performed using a FlexiGene (Techne) heating block. Following reverse transcription the remaining RNA template was destroyed by the addition of 1 μl of RNase H to all of the samples in order to increase the sensitivity of subsequent PCR reactions. Samples were stored at -20°C until required for PCR.

## 2.16 Real-time polymerase chain reaction (PCR)

### 2.16.1 General remarks

Real time PCR was performed using the LightCycler system (Roche Applied Science, Germany). The LightCycler instrument provides an extremely powerful tool for real time quantification of gene expression using a cDNA pool generated as described in section 2.15. The LightCycler system functions through the incorporation of the DNA binding dye SYBR Green I (Roche Molecular

Biochemicals, Germany), which exhibits greatly enhanced fluorescence when bound to double stranded DNA. At the end of each elongation phase the SYBR Green I dye binds to the amplified PCR product and can be detected by fluorescence at 530 nm excitation; thus, the level of fluorescence recorded after each elongation phase is proportional to the amount amplicon contained within each sample.

### 2.16.2 Real time PCR – Roche LightCycler system

Throughout this study, gene expression was measured by relative quantification using the software programme LightCycler 4.0 (Roche Applied Science, Germany). For quantification of *HMOX1*, *NRF2*, and *GAPDH* gene expression, calibrator normalised relative quantification monocolour with efficiency correction of 2 was employed throughout this study. Relative quantification allows the comparison of two ratios: the ratio of a target cDNA sequence (*NRF2 / HMOX1*) to a housekeeping reference cDNA sequence (*GAPDH*) in an unknown sample, to the ratio of the same two sequences in a standard sample called a 'calibrator'. The calibrator represents typical proportions of the target and reference sequences against which the unknown sample can be compared. The same calibrator was included in all of the LightCycler experiments throughout this study allowing for inter-experimental comparison. The melting temperature ($T_m$) of all PCR products was also determined at the end of each PCR reaction in order to confirm the product identity and differentiate from non-specific products such as primer-dimers.

For all LightCycler experiments the LightCycler – DNA Master SYBR Green I ready to use PCR reaction mix was used (Roche Applied Science, Germany). This reaction mix contained *Taq* DNA polymerase, dNTPs, SYBR Green I dye, and 10 mM $MgCl_2$; only the addition of the specified gene-specific primers, and an adjustment in the $Mg^{2+}$ concentration, was required for optimal PCR. For analysis of *NRF2, HMOX1,* and glyceraldehyde-3-phosphate dehydrogenase (*GAPDH)* gene expression, a reaction mix was prepared containing a final concentration of 0.5 µM of both the forward and reverse primer. The primer sequences used are represented in table 2.2.

For real time PCR a total volume of 20 µl of reaction mixture was prepared for each sample. The reaction mixture was contained within a 20 µl LightCycler capillary (Roche Applied Science, Germany) during analysis. Samples were analysed

using the LightCycler 1.5 instrument (Roche Molecular Biochemicals, Germany). For analysis of *HMOX1* and *GAPDH* gene expression, PCR conditions determined by this laboratory prior to the start of this study were used (as detailed in table 2.3 and 2.4). A final $Mg^{2+}$ concentration of 3.0 mM was used in all experiments for analysis of both *HMOX1* and *GAPDH* gene expression. For analysis of *NRF2* expression, the conditions required for optimal real time PCR were determined (as discussed in sections 2.16.3 and 2.16.4).

| Gene | Forward Primer (5' to 3') | Reverse Primer (5' to 3') |
|---|---|---|
| *NRF2* | GCGACGGAAAGAGTATGAGC | GTTGGCAGATCCACTGGTTT |
| *HMOX1* | AAGAGGCCAAGACTGCGTTC | GGTGTCATGGGTCAGCAGC |
| *GAPDH* | GACATCAAGAAGGTGGTGAA | TGTCATACCAGGAAATGAGC |

Table 2.2: The primer sequences used for *NRF2*, *HMOX1*, and *GAPDH* RT-PCR
The primers were designed by Dr Stephen Mitchell (*NRF2*) and Dr Sharmila Basu-Modak (*HMOX1* and *GAPDH*) using the software programme Primer 3.

| | Temperature (°C) | Time (seconds) | Ramp Rate (°C/second) | Acquisition Mode | |
|---|---|---|---|---|---|
| **Denaturation** | 95 | 30 | 20 | None | |
| **Amplification** | 95 | 0 | 20 | None | |
| | 55 | 5 | 20 | None | **40 Cycles** |
| | 72 | 4 | 20 | Single | |
| **Melting Curve** | 95 | 0 | 20 | None | |
| | 65 | 15 | 20 | None | **1 Cycle** |
| | 95 | 0 | 0.1 | Continuous | |
| **Cooling** | 40 | 30 | 20 | None | |

Table 2.3: The settings used for real time PCR monitoring of the *HMOX1* gene using the LightCycler system. These conditions were determined by Dr Sharmila Basu-Modak prior to the start of this study.

| | Temperature (°C) | Time (seconds) | Ramp Rate (°C/second) | Acquisition Mode | |
|---|---|---|---|---|---|
| **Denaturation** | 95 | 30 | 20 | None | |
| **Amplification** | 95 | 0 | 20 | None | |
| | 60 | 5 | 20 | None | **40 Cycles** |
| | 72 | 8 | 20 | Single | |
| **Melting Curve** | 95 | 0 | 20 | None | |
| | 65 | 15 | 20 | None | **1 Cycle** |
| | 95 | 0 | 0.1 | Continuous | |
| **Cooling** | 40 | 30 | 20 | None | |

Table 2.4: The settings used for real time PCR monitoring of the *GAPDH* gene using the LightCycler system. These conditions were determined by Dr Sharmila Basu-Modak prior to the start of this study.

### 2.16.3 Optimisation of magnesium concentration for *NRF2* PCR

In order for optimal *NRF2* real time PCR to take place, the $Mg^{2+}$ concentration of the reaction mixture was first optimised. The optimum $Mg^{2+}$ concentration was determined using a calibrator cDNA pool and the *NRF2* primers shown in table 2.2. Nine reaction mixtures were prepared using the LightCycler – DNA Master SYBR Green I PCR reaction mix according to the manufacturer's instructions containing final $Mg^{2+}$ concentrations ranging from 1.0 – 5.0 mM. For each $Mg^{2+}$ concentration duplicate samples were produced. Samples that contained no cDNA were produced at the lowest and highest $Mg^{2+}$ concentrations. Real time PCR was performed on the samples using pre-optimised LightCycler settings including an assumed primer annealing temperature of 55°C.

### 2.16.4 Optimisation of *NRF2* primer annealing temperature

The optimum primer annealing temperature for *NRF2* real-time PCR was determined using non-quantitative gel PCR. A reaction mixture was prepared containing the *NRF2* primers shown in table 2.2 using Sigma's ReadyMix™ *Taq* without $MgCl_2$ according to the manufacturer's instructions. All of the samples contained a final $Mg^{2+}$ concentration of 2.0 mM and a final primer concentration of 0.5 µM. PCR was performed on a FlexiGene (Techne) heating block with variable temperature gradient using the following programme: Denaturation [95°C, 180 seconds]; Amplification [(94°C, 20 seconds) (*50 – 70°C*, 10 seconds) (72°C, 20 seconds)]; Termination [(72°C, 300 seconds) (4°C, ∞)]. The samples were subjected to 30 cycles of amplification. During the primer annealing phase, the temperature of the heating block was set at a gradient ranging from 50 – 70°C at increments of approximately 2°C. For each sample, 10 µl of the reaction product was subjected to agarose gel electrophoresis using a 3 % gel as described in section 2.6.2.

## 2.17 Statistical Analysis

Unless otherwise stated, results are expressed as a mean and error bars represent one standard deviation above and below the mean. A one-way analysis of variance (ANOVA) was used as appropriate to test the significance of data. A $p$ value of less than 0.05 was deemed to be significant.

# 3. Results

# 3. Results

## 3.1 The sub-cellular distribution of Nrf2 following UVA irradiation

FEK4 cells are primary fibroblasts derived from a human foreskin explant (Tyrrell and Pidoux, 1986). Researchers from this laboratory have extensively investigated the response of this cell line to UVA radiation, and it is known that UVA up-regulates the defence enzyme HO-1 in these cells (Keyse and Tyrrell, 1987; Keyse and Tyrrell, 1989). In this study FEK4 primary human fibroblasts have been employed as a model to investigate the effect of UVA on the transcription factor Nrf2. The sub-cellular distribution of Nrf2 was monitored in FEK4 cells following a physiologically relevant dose of UVA radiation (250 $kJ/m^2$). Following treatment, FEK4 cells were incubated in conditioned media for the indicated time periods before fixing. Nrf2 was then visualised by means of immunocytochemistry.

As shown in figure 3.1, the staining system used to monitor Nrf2 resulted in virtually no non-specific binding of the fluorophor conjugated secondary antibody allowing for precise monitoring of Nrf2. Further to this, a low level of fluorescence was observed in unirradiated control cells allowing Nrf2 accumulation to be visualised. As shown in figure 3.1, UVA irradiation resulted in immediate accumulation of Nrf2 in both the cytoplasm and the nucleus of FEK4 primary human fibroblasts. The images show accumulated Nrf2 in the peri-nuclear region of FEK4 cells 1 and 2 hours post UVA treatment. UVA irradiation resulted in Nrf2 protein accumulation in the nucleus of FEK4 cells from 1 to 4 hours post treatment. The mean fluorescence of each image has been determined as described in section 2.14. The fluorescence of each image has been normalised against the fluorescence of the unirradiated controls and is shown as a relative fold change. These data are consistent with the interpretation that UVA enhances Nrf2 accumulation in human skin cells.

To further investigate this effect, Nrf2 was monitored in both the cytoplasmic and nuclear fraction of FEK4 fibroblasts using SDS-PAGE and western blotting. Cells were UVA treated (250 $kJ/m^2$) and subsequently incubated in conditioned media for the indicated time period before cytoplasmic and nuclear extracts were prepared. As shown in figure 3.2 and 3.3, UVA treatment did not enhance the level of Nrf2 residing in the cytoplasm, but did enhance the level of Nrf2 in nucleus when compared to an unirradiated control sample. As determined by western blotting, the

level of Nrf2 residing in the nucleus was substantially enhanced within 1 hour of irradiation. Nrf2 nuclear accumulation continued until 3 or 4 hours after UVA treatment. Both of these experiments were independently repeated with nearly identical results (data not shown). With respect to figure 3.2 and 3.3, cadmium was employed as a positive control. In Hepa cells work has shown that Nrf2 continues to accumulate up to 4 hours following treatment with cadmium (Stewart *et al.*, 2003). As shown in figure 3.3, the physiologically relevant dose of UVA radiation used here resulted in stronger nuclear accumulation of Nrf2 than in response to treatment with 10 μM $CdCl_2$.

Taken together these data show that UVA causes whole cell accumulation of Nrf2 in primary human skin cells; an effect that can possibly be attributed to the release of Nrf2 from the proteasome degradation pathway.

**Figure 3.1: UVA causes Nrf2 protein accumulation in human skin cells: Immunocytochemistry**

(*next page*)

FEK4 primary human fibroblasts were treated with UVA (250 kJ/m$^2$) and incubated in conditioned media at 37°C for the indicated time period. The control samples were treated exactly the same as the UVA irradiated samples, but were not irradiated. Cells were fixed and immunostained with anti-Nrf2 rabbit polyclonal primary antibody followed by Invitrogen's Alexa-Fluor goat anti-rabbit antibody as described in the section 2.14. Blocking of non-specific sites was accomplished by application of Invitrogen's Image-iT™ Fx signal enhancer. Cells were incubated in Hoechst stain to allow visualisation of nuclei. The cells were analysed by oil immersion epifluorescence microscopy at 63x magnification on a Nikon Eclipse TE2000-U microscope and using the software programme UltraVIEW. The images were produced by superimposing the nuclei (BLUE) onto Nrf2 protein (PINK). The mean fluorescence of each image was determined using the software package ImageJ as described in section 2.14.

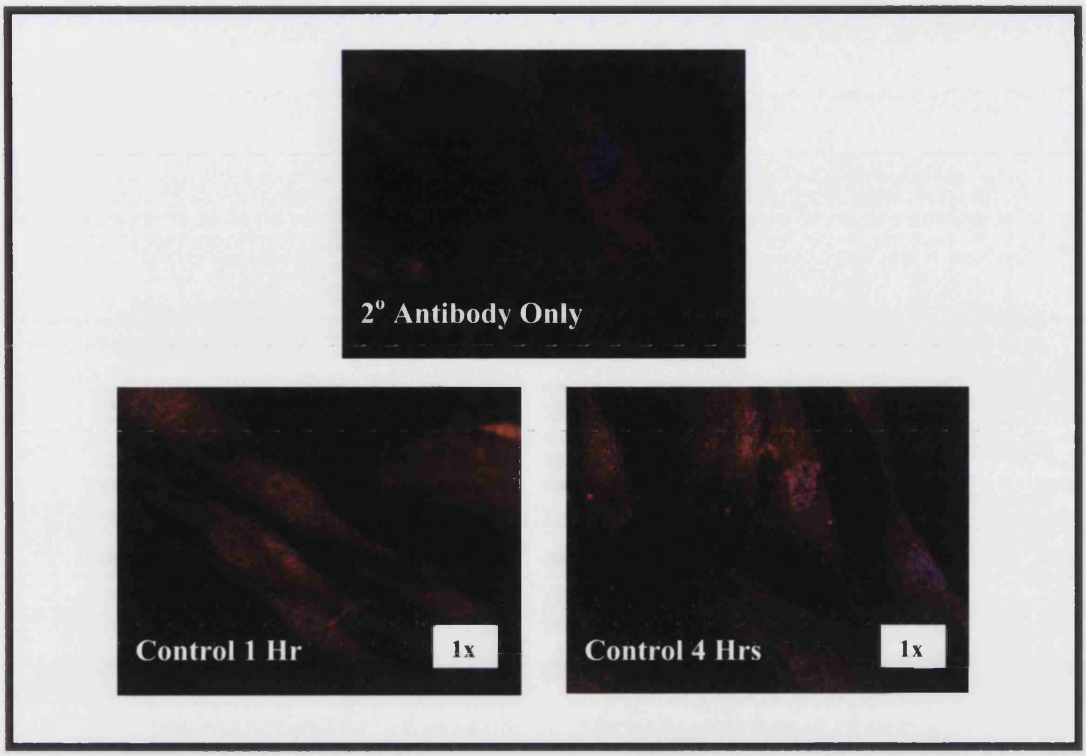
2° Antibody Only
Control 1 Hr
1x
Control 4 Hrs
1x

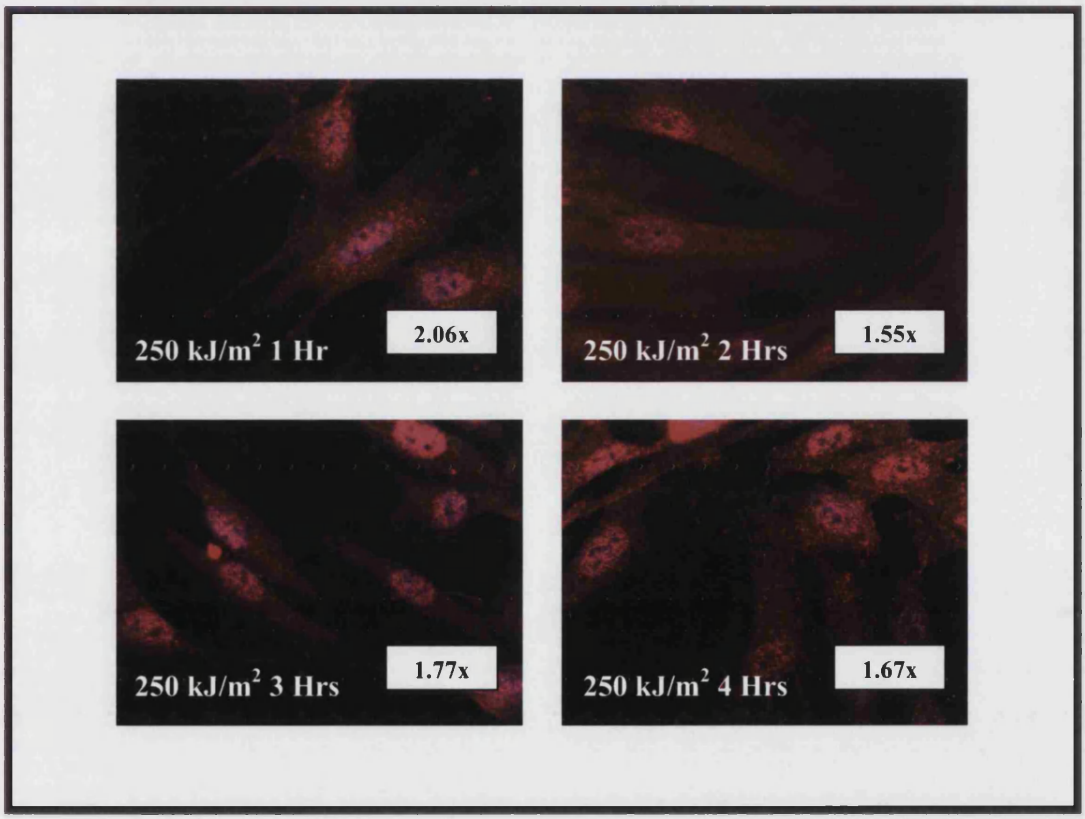
250 kJ/m² 1 Hr
2.06x
250 kJ/m² 2 Hrs
1.55x
250 kJ/m² 3 Hrs
1.77x
250 kJ/m² 4 Hrs
1.67x

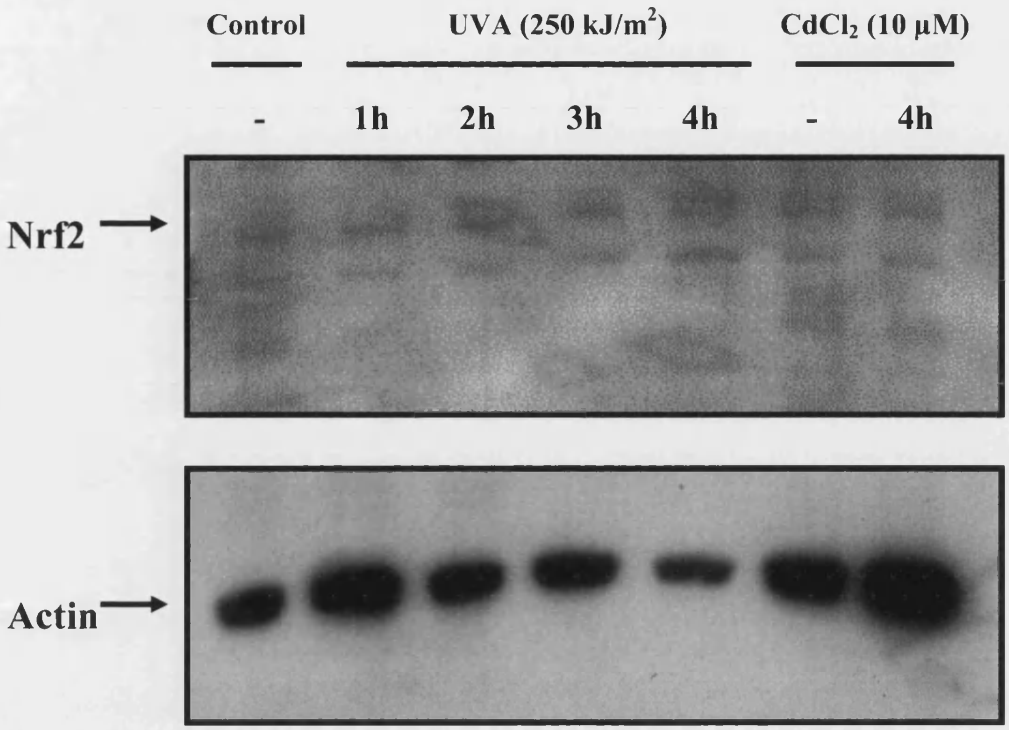


**Figure 3.2: Cytoplasmic Nrf2 is unaffected by UVA radiation**

Freshly confluent FEK4 primary human fibroblasts were treated with either UVA (250 kJ/m$^2$) or a $CdCl_2$ (10 µM) and incubated in conditioned media at 37°C for the indicated time period. Cytoplasmic extracts were prepared as described in section 2.4.2, and protein concentration was determined using the method of Bradford. Equal amounts of cytoplasmic protein (10 µg/lane) were analysed by SDS-PAGE and western blotting as described in section 2.12. After visualisation of Nrf2 protein, the membrane was re-probed for actin to evaluate equal loading. The control sample was treated exactly the same as the UVA irradiated samples, but was not irradiated. This experiment was independently repeated with nearly identical results (data not shown).

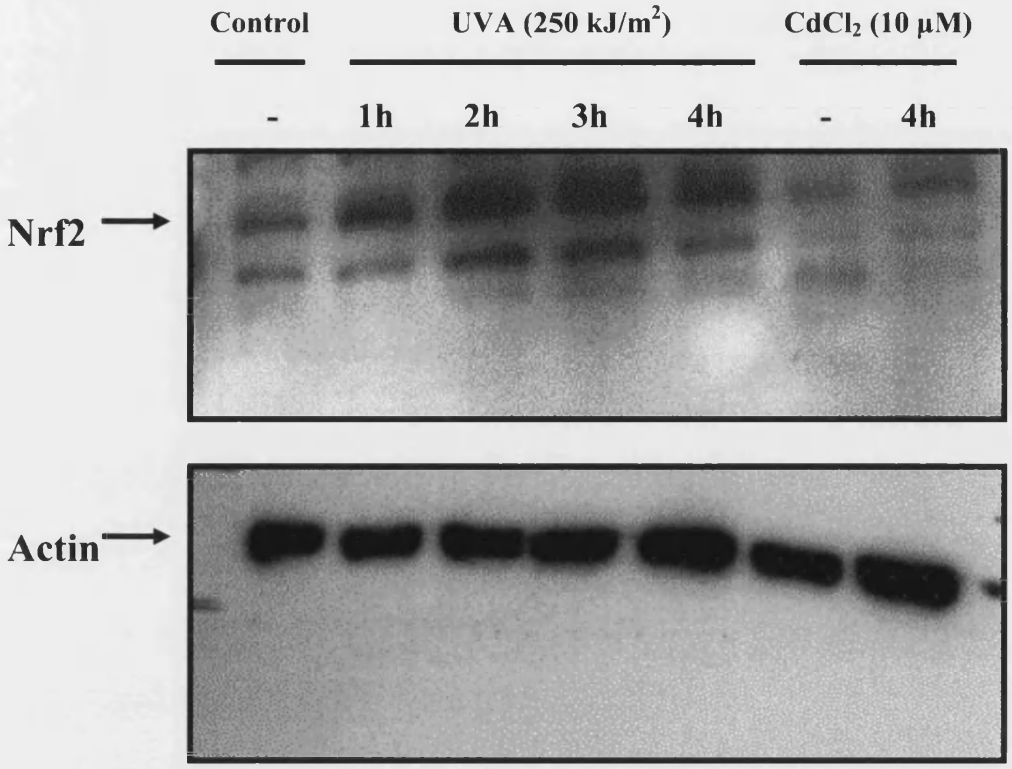


**Figure 3.3: UVA radiation causes nuclear accumulation of Nrf2**

Freshly confluent FEK4 primary human fibroblasts were treated with either UVA (250 kJ/m$^2$) or a $CdCl_2$ (10 µM) and incubated in conditioned media at 37°C for the indicated time period. Nuclear extracts were prepared as described in section 2.4.2, and protein concentration was determined using the method of Bradford. Equal amounts of nuclear protein (10 µg/lane) were analysed by SDS-PAGE and western blotting as described in section 2.12. After visualisation of Nrf2 protein, the membrane was re-probed for actin to evaluate equal loading. The control sample was treated exactly the same as the UVA irradiated samples, but was not irradiated. This experiment was independently repeated with nearly identical results (data not shown).

### 3.2 The effect of UVA irradiation and hemin on Nrf2 accumulation

Following UVA treatment, Nrf2 was monitored in FEK4 primary human fibroblast whole cell extracts using SDS-PAGE and western blotting. FEK4 cells were irradiated with a physiologically relevant dose of UVA (250 $kJ/m^2$) and subsequently incubated in conditioned media. The cells were incubated for the indicated time periods before whole cell extracts were prepared. As shown in figure 3.4 and 3.5, UVA treatment substantially increased the total cellular level of Nrf2 protein when compared to unirradiated control cells. These data show that UVA treatment resulted in immediate accumulation of Nrf2 protein (1 hour post irradiation), and that Nrf2 accumulation continued for up to 12 hours following treatment. These findings are consistent with the idea that UVA stabilises Nrf2.

Previous work from this laboratory has shown that UVA treatment of FEK4 fibroblasts leads to an immediate release of the HO-1 substrate, heme, from heme-containing proteins (Kvam *et al.*, 1999). Furthermore, recent data derived from a murine model has indicated that heme promotes stabilisation of Nrf2 through prevention of ubiquitination (Alam *et al.*, 2003). It was therefore hypothesised that heme may stabilise Nrf2 in human cells, and that the Nrf2 protein accumulation observed in response to UVA treatment may be dependent on the release of heme from heme-containing proteins. The effect of heme on Nrf2 was investigated in primary human fibroblasts using SDS-PAGE and western blotting. FEK4 cells were treated with 1 μM hemin and incubated in conditioned media for the indicated time periods before whole cell extracts were prepared. As shown in figure 3.6, hemin treatment resulted in accumulation of Nrf2. Using 30 μg pf total cellular protein extract for SDS-PAGE and western blotting, the data indicate that Nrf2 accumulation can be detected in FEK4 cells from 1 hour following treatment with 1 μM hemin.

Nrf2 was also monitored following treatment with hemin by means of imaging. FEK4 cells were treated with 1 μM hemin and incubated in conditioned media for the indicated time periods. Nrf2 was visualised by means of immunocytochemistry and epifluorescence microscopy. As shown in figure 3.7, the staining system employed to monitor Nrf2 resulted in virtually no non-specific binding of the fluorophor conjugated secondary antibody allowing for precise monitoring of Nrf2. In agreement with the data depicted in figure 3.6, the imaging data shown in figure 3.7 confirms the accumulation of Nrf2 in response to hemin

treatment. The mean fluorescence of each image has been determined as described in section 2.14. For each image the mean fluorescence has been normalised against the mean fluorescence of the untreated control. The data indicate a moderate fold increase in Nrf2 of between 1.17 and 1.35.

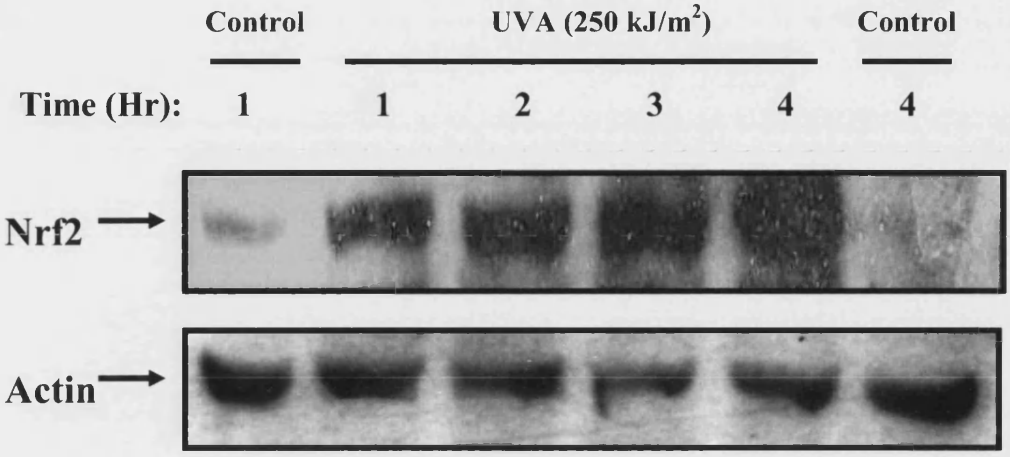


**Figure 3.4: UVA radiation causes immediate whole cell accumulation of Nrf2 protein in human skin fibroblasts**

Freshly confluent FEK4 primary human fibroblasts were treated with UVA (250 kJ/m$^2$) and incubated in conditioned media at 37°C for the indicated time period. The control samples were treated exactly the same as the UVA irradiated samples, but were not irradiated. Whole cell extracts were prepared as described in section 2.4.1. Protein concentration was determined using the method of Bradford. Equal amounts of protein (30 µg/lane) were analysed by SDS-PAGE and western blotting as described in section 2.12. After visualisation of Nrf2 protein, the membrane was re-probed for actin in order to evaluate equal loading.

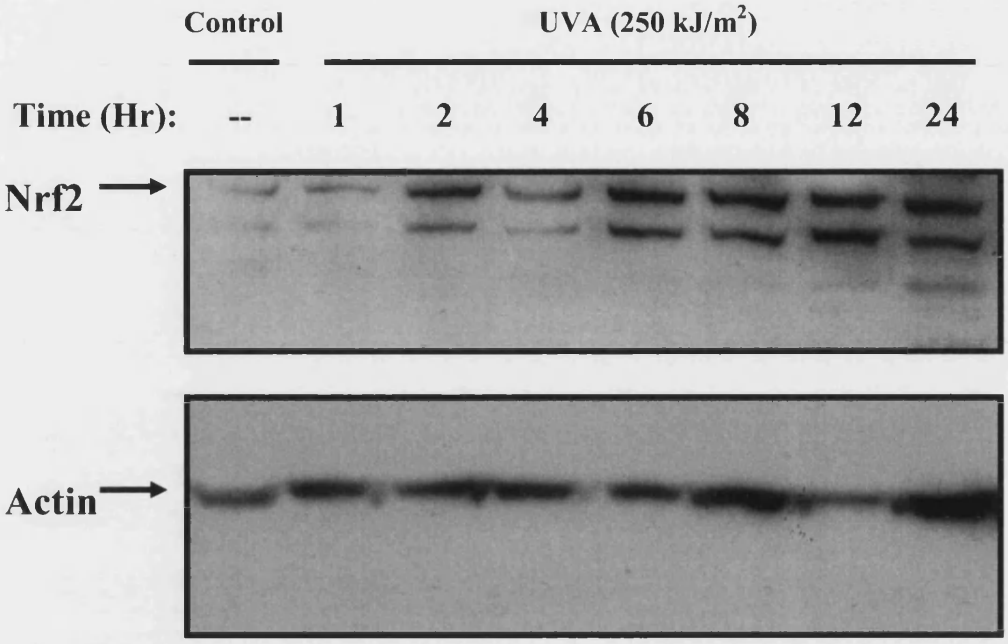


**Figure 3.5: UVA radiation causes whole cell accumulation of Nrf2 protein in human skin fibroblasts up to 12 hours post irradiation**

Freshly confluent FEK4 primary human fibroblasts were treated with UVA (250 kJ/m$^2$) and incubated in conditioned media at 37°C for the indicated time period. The control sample was treated exactly the same as the UVA irradiated sample, but was not irradiated. Whole cell extracts were prepared as described in section 2.4.1. Protein concentration was determined using the method of Bradford. Equal amounts of protein (30 µg/lane) were analysed by SDS-PAGE and western blotting as described in 2.12. After visualisation of Nrf2 protein, the membrane was striped and re-probed for actin in order to evaluate equal loading.

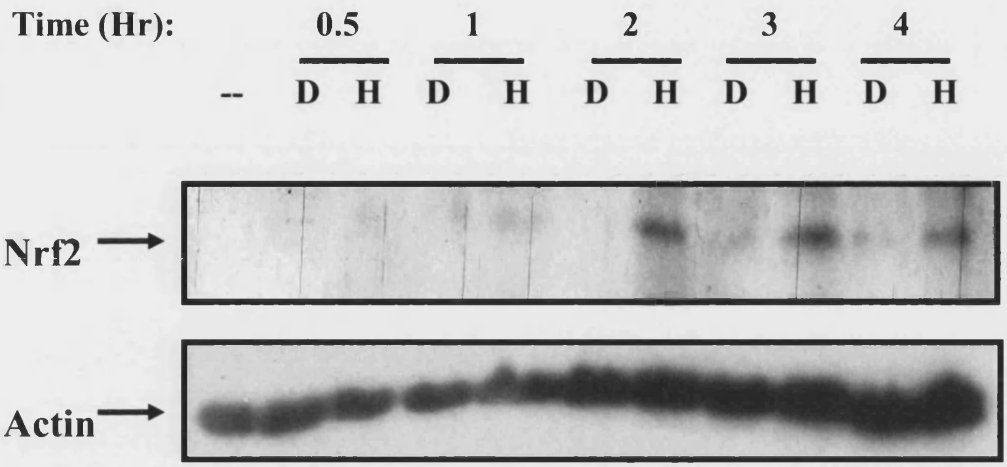


**Figure 3.6: Hemin treatment causes Nrf2 protein accumulation in human skin fibroblasts as determined by western blotting**

Freshly confluent FEK4 primary human fibroblasts were treated with either 1 μM hemin (H) or the vehicle [0.01 % DMSO (D)] and incubated in serum free medium at 37°C for the time period indicated. The control sample (--) was untreated and remained in the incubator for the duration of the experiment. Whole cell extracts were prepared as described in section 2.4.1, and protein concentration was determined using the method of Bradford. Equal amounts of protein (30 μg/lane) were analysed by SDS-PAGE and western blotting as described in section 2.12. After visualisation of Nrf2 protein, the membrane was striped and re-probed for actin in order to evaluate equal loading.

**Figure 3.7: Hemin causes Nrf2 protein accumulation in human skin fibroblasts as determined by epifluorescence microscopy**

(*next page*)

FEK4 primary human fibroblasts were treated with either 1 μM hemin or the vehicle (0.01 % DMSO) and incubated in conditioned media at 37°C for the indicated time period. The untreated sample remained in the incubator for the duration of the experiment. Cells were fixed and immunostained with anti-Nrf2 rabbit polyclonal primary antibody followed by Invitrogen's Alexa-Fluor goat anti-rabbit as described in the Materials and Methods (section 2.14). Blocking of non-specific sites was accomplished by application of Invitrogen's Image-iT™ Fx signal enhancer. Cells were incubated in Hoechst stain to allow visualisation of nuclei. The cells were analysed by oil immersion epifluorescence at 63x magnification on a Nikon Eclipse TE2000-U microscope and using the software programme UltraVIEW. The images were produced by superimposing the visualised nuclei (BLUE) onto Nrf2 protein (PINK). The mean fluorescence of each image was determined using the software package ImageJ as described in section 2.14.

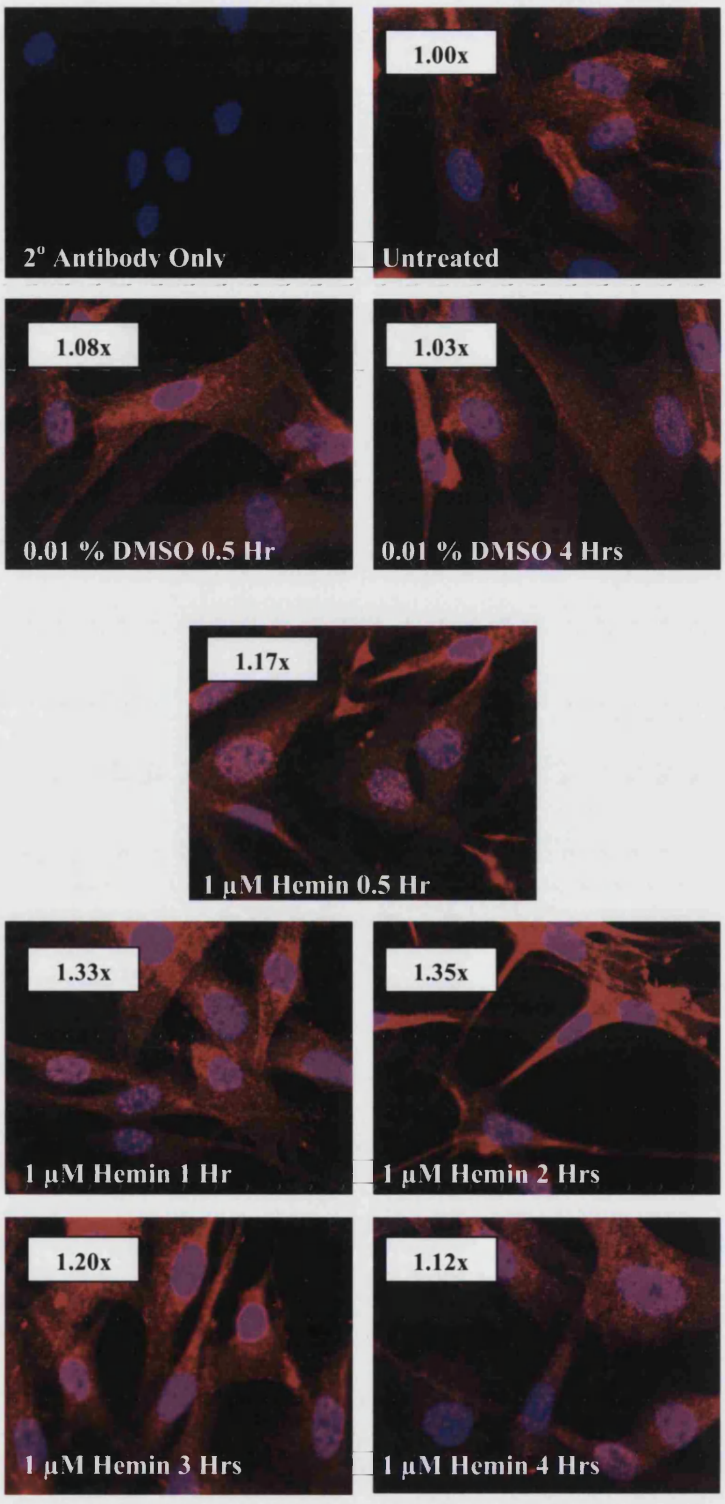
2° Antibody Only
1.00x
Untreated
1.08x
0.01 % DMSO 0.5 Hr
1.03x
0.01 % DMSO 4 Hrs
1.17x
1 µM Hemin 0.5 Hr
1.33x
1 µM Hemin 1 Hr
1.35x
1 µM Hemin 2 Hrs
1.20x
1 µM Hemin 3 Hrs
1.12x
1 µM Hemin 4 Hrs

## 3.3 Monitoring of intracellular heme

### 3.3.1 Spectrophotometric monitoring of intracellular heme

As shown in section 3.2, both UVA and heme treatment resulted in whole cell accumulation of Nrf2 in FEK4 primary human fibroblasts. UVA is known to release heme from heme-containing proteins (Kvam *et al.*, 1999). It was therefore hypothesised that UVA-mediated whole cell accumulation of Nrf2 may be dependent on heme. To fully explore this hypothesis, the effect of depleting intracellular heme prior to UVA treatment was examined.

A spectrophotometric assay was developed to allow the amount of intracellular heme to be monitored. In this assay the nitrogen ligands from protein-bound heme are replaced by pyridine in alkali. The resultant hemochrome is quantified by the difference in absorption between a baseline and reduced sample. As discussed in section 2.10, the baseline absorbance of each sample was obtained from 500 to 600 nm. Each sample was then split into two, one of which was oxidised, the other reduced. An absorbance reading of the reduced and oxidised samples was then obtained between 500 and 600 nm. Using Beer's law and a millimolar extinction coefficient of 20.7, the heme concentration was calculated based on the difference in absorption between the peak at 557 nm and the trough at 575 nm of the reduced sample.

Hemin standards were initially used to assess the sensitivity of this assay. As shown in figure 3.8, oxidation of the hemin standards resulted in virtually no change in absorption when compared to the baseline absorbance. This result was expected, and indicated that complete sample oxidation was occurring without the requirement for the oxidising agent potassium ferricyanide. The accuracy of this assay was assessed using the reduced samples. The actual concentration of the hemin standards was compared to the theoretical concentration calculated using the absorption profile shown in figure 3.8. A discrepancy was observed. The possibility that the hemochrome was incompletely reduced was explored through addition of further reducing agent. No change in absorption was observed. The discrepancy between the actual hemin concentration of the hemin standards, and the value calculated from the spectrophotometric absorption of the hemin standards, suggested that the concentration of heme calculated for tissue extracts would not be accurate. This

discrepancy suggested that a standard curve would be required if this assay was to be employed through-out this investigation. Prior to the generation of a standard curve, it was determined whether or not the assay was sufficiently sensitive to detect endogenous heme in cell extracts.

The sensitivity of this assay, as determined using hemin spiked standards, suggested the need for a large quantity of tissue extract. In order to generate sufficient cell extract the human lymphoblastoid cell line TK6 was employed (Thilly, 1979). As shown in figure 3.9, the sensitivity of this assay was barely sufficient to detect intracellular heme in 1.2 mg total protein of TK6 whole cell tissue extract. What's more, large disparities in absorption were observed between identical tissue extracts (data not shown). The low sensitivity and poor reproducibility of this assay clearly defined the need for the development of a more accurate methodology. Experimental investigations by means of spectrophotometry were terminated.

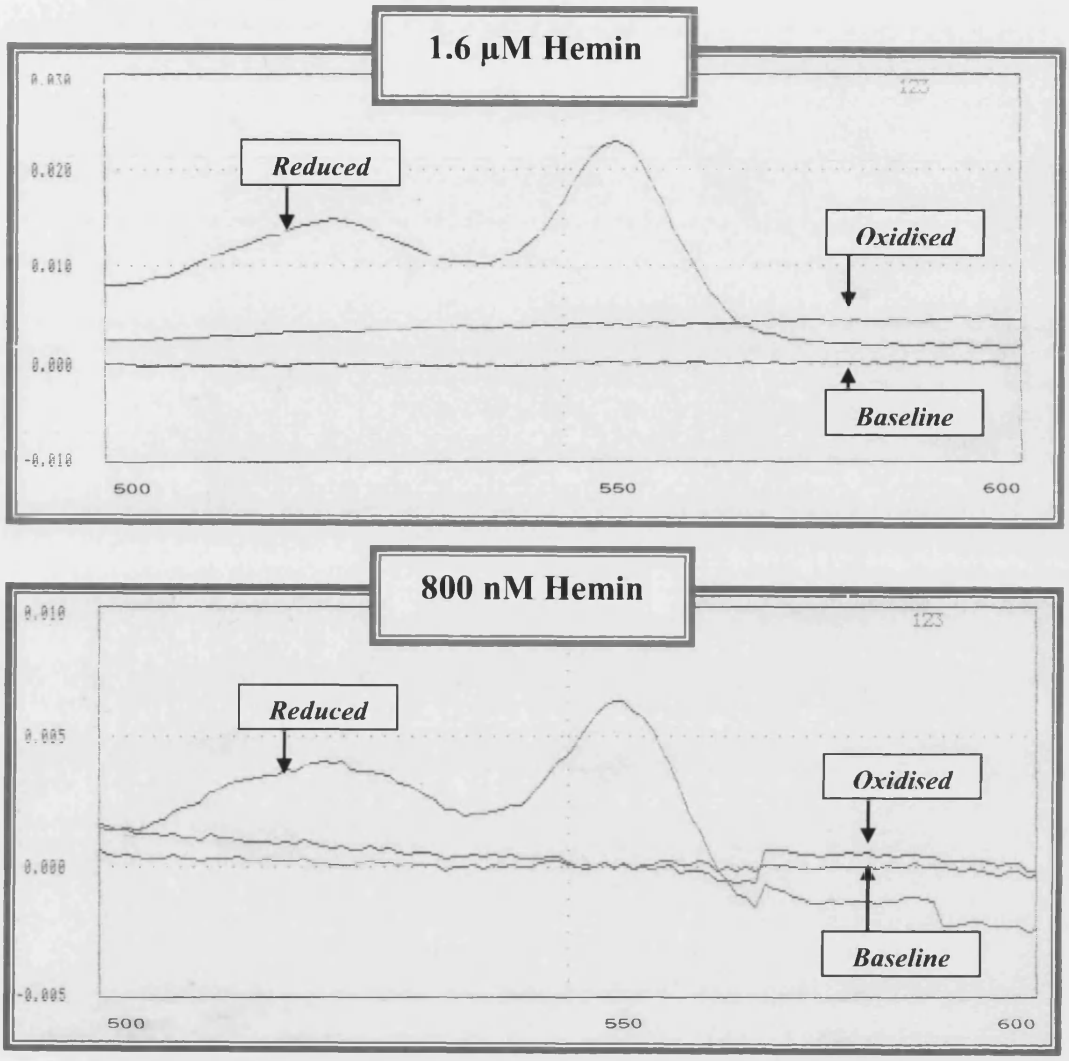


**Figure 3.8: Spectrophotometric quantification of heme concentration: hemin standards**

Hemin standards of 800 nM and 1.6 µM were produced as described in section 2.11. Samples were prepared as detailed in section 2.10 through the addition of pyridine. A baseline absorbance spectrum was taken from 500 to 600 nm. Each sample was then split into two, one of which was oxidised, the other reduced. An absorbance spectrum of the reduced and oxidised sample was then obtained between 500 and 600 nm. Based on the difference in absorption of the reduced sample between the peak at 557 nm and the trough at 575, the actual concentration of the heme standards was compared to the theoretical concentration calculated using Beer's law and a millimolar extinction coefficient of 20.7.

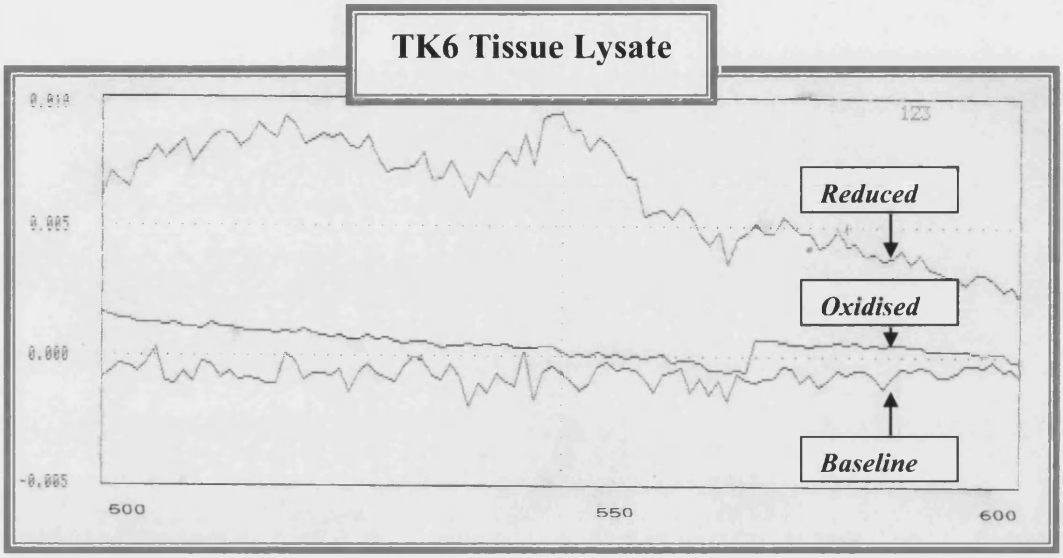


**Figure 3.9: Spectrophotometric quantification of intracellular heme concentration in TK6 cells**

The human lymphoblastoid cell line TK6 was employed to generate a large pool of cell extract. A whole cell tissue extract containing 1.2 mg of total protein was prepared as described in section 2.10. A baseline absorbance spectrum was recorded from 500 to 600 nm. The sample was then split into two, one of which was oxidised, the other reduced. An absorbance spectrum of the reduced and oxidised extract was then obtained between 500 and 600 nm.

### 3.3.2 Spectrofluorometric monitoring of intracellular heme

A spectrofluorometric assay was developed to allow accurate monitoring of intracellular heme. This methodology is based on the work of Morrison, (1965) and Sassa, (1976). The assay involves the conversion of heme to it's fluorescent porphyrin derivative by the removal of heme iron under acidic reducing conditions (as described in section 2.11).

This assay has a linear range that must be established before the concentration of heme in cell extracts can be determined. The linear range of this assay varies between spectrofluorometers and is a function of the sensitivity of each instrument. Using hemin standards, preliminary experiments revealed the non-linear range of this assay to be below 80 nM (data not shown). As shown in figure 3.10, hemin standards ranging from 100 nM to 800 nM produced a linear standard curve. The capacity of this assay to detect heme in whole cell tissue extracts was next examined. FEK4 primary human fibroblasts were treated with 1 mM hemin or the vehicle (0.1 % DMSO) for one hour. Duplicate samples containing 100 μg of total protein were prepared for each treatment. As discussed in section 2.11, one sample from each pair was boiled with 2 M oxalic acid at 100°C for 30 minutes (in order to remove the heme iron); the other sample was incubated at room temperature. The fluorescence of each sample was read at 600 nm emission using a spectrofluorometer set at 405 nm excitation. As shown in figure 3.11, with respect to FEK4 cells treated with DMSO, the fluorescence of the un-boiled samples (representing background fluorescence) was virtually identical to that of the fluorescence of the equivalent boiled sample. The fluorescence of the boiled samples was only greater than the control samples when cells had been pre-treated with 1 mM heme. These results indicated that non-specific fluorescence was preventing detection of endogenous heme in FEK4 cells.

Work from this laboratory has shown that it is microsome localised heme-containing proteins that are destroyed in response to UVA. In an attempt to reduce the level of non-specific background fluorescence observed in the FEK4 whole cell extracts, total cellular microsomes were isolated (as described in section 2.4.3). As shown in figure 3.11, marginally greater fluorescence was observed in some boiled samples when compared to the equivalent control sample. It was hypothesised that a sample containing a greater amount of total cellular protein may allow visualisation of endogenous heme fluorescence above the background fluorescence. The human

lymphoblastoid cell line TK6 (Thilly, 1979) was again used to generate sufficient cell extract. As shown in figure 3.12, the assay of 1 mg of total protein from TK6 cells produced marginally higher fluorescence in the boiled samples when compared to the control samples. However, when this experiment was independently repeated using 2 mg of total protein, heme fluorescence could not be detected (data not shown). Taken altogether, these data indicate that non-specific fluorescence negates the possibility of visualisation of endogenous heme using this methodology. Experimental investigations by means of spectrofluorometry were terminated.

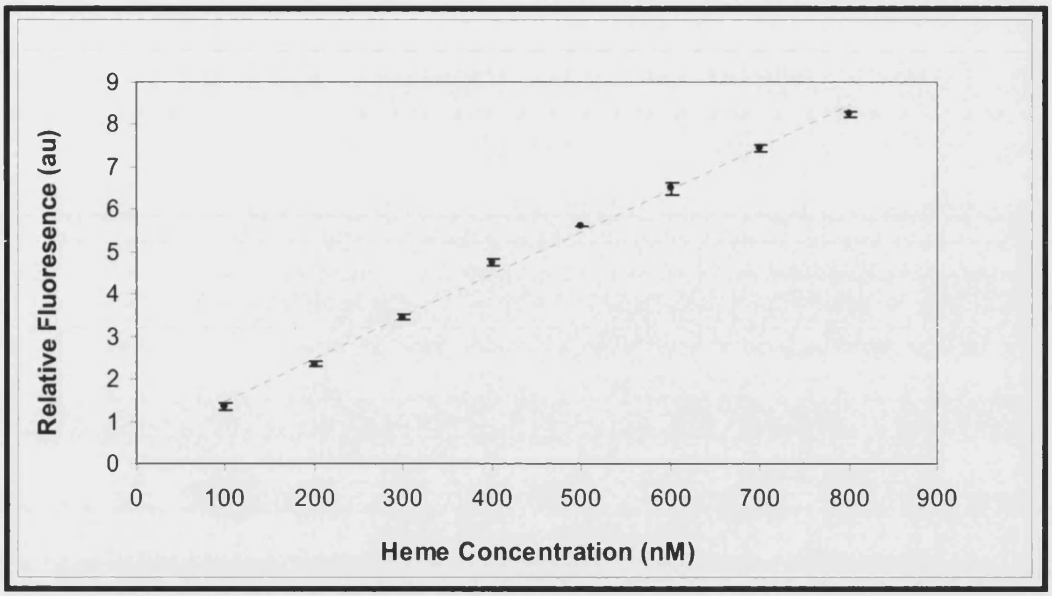


**3.10: Spectrofluorometric determination of heme concentration: standard curve**

A series of 8 heme standards were prepared in a 0.1 M phosphate buffer pH 7.4 containing 0.05 % BSA. Each standard was then diluted 1:1 v/v with 2 M oxalic acid (as described in section 2.10). Each standard was produced in duplicate, one of which was boiled at 100°C for 30 minutes (in order to remove the heme iron), the other control sample was incubated at room temperature for the same period. All samples were covered during this incubation period to prevent evaporation. Each standard, both boiled and control, was produced in duplicate. The fluorescence of each sample was read at 600 nm emission using a spectrofluorometer set at 405 nm excitation. The value of the un-boiled control sample (representing background fluorescence) was subtracted from the boiled sample fluorescence where the heme iron had been removed. The relative fluorescence of the 8 hemin standards has been plotted against concentration on a linear scale in order to produce a standard curve. Each point represents the mean fluorescence of two independent samples. Error bars represent one standard deviation above and below the mean.

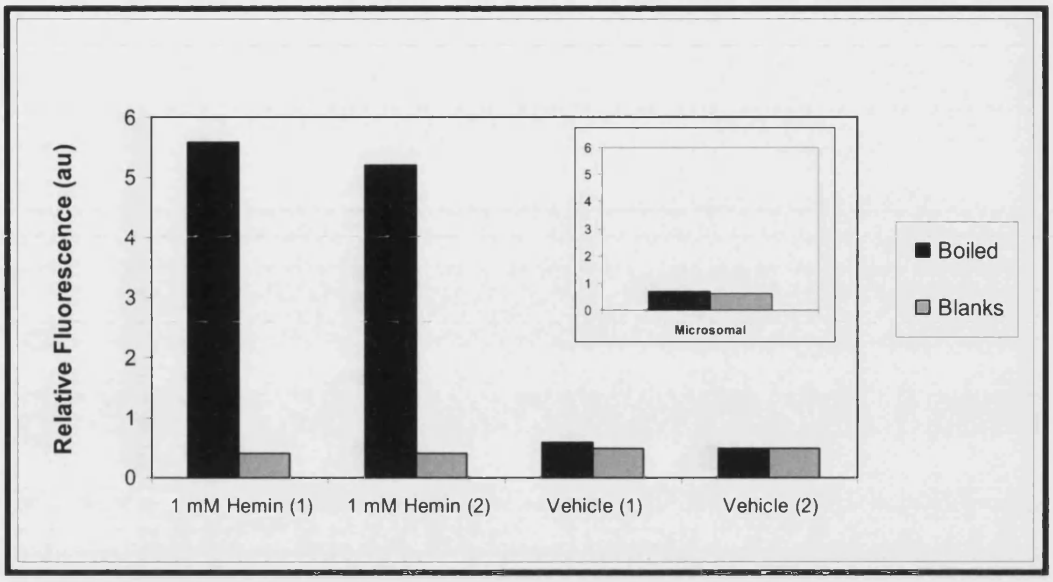


### 3.11: Spectrofluorometric determination of intracellular heme concentration: FEK4

FEK4 primary human fibroblasts were treated with 1 mM hemin or the vehicle (0.1 % DMSO) for one hour. Whole cell extracts were prepared as described in section 2.4.1 and the protein concentration of each extract was determined as described in section 2.4.4. Microsomal cell extracts were untreated, and were prepared as described in section 2.4.3. For each sample (microsomal and whole cell), 100 µg of protein was added to 1 ml of 2 M oxalic acid. Each sample was produced in duplicate, one of which was boiled at 100°C for 30 minutes (in order to remove the heme iron) (BLACK), the other control sample was incubated at room temperature for the same period (GREY). All samples were covered during this incubation period to prevent evaporation. The fluorescence of each sample was read at 600 nm emission using a spectrofluorometer set at 405 nm excitation.

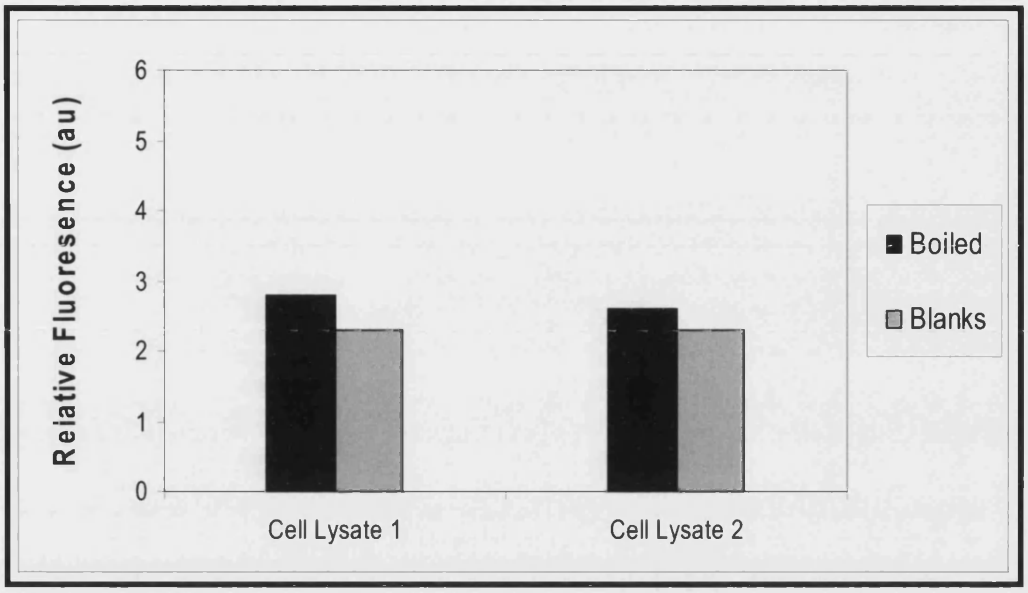


### 3.12: Spectrofluorometric determination of intracellular heme concentration: TK6

The human lymphoblastoid cell line TK6 was used to generate a large pool of cell extract. Whole cell extracts were prepared as described in section 2.4.1 and the protein concentration of each cell extract was determined as described in section 2.4.4. For each sample, 1 mg of protein was added to 1 ml of 2 M oxalic acid. Each sample was produced in duplicate, one of which was boiled at 100°C for 30 minutes (in order to remove the heme iron) (BLACK), the other control sample was incubated at room temperature for the same period (GREY). All samples were covered during this incubation period to prevent evaporation. The fluorescence of each sample was read at 600 nm emission using a spectrofluorometer at 405 nm excitation.

## 3.4 The effect of intracellular heme depletion on UVA-mediated Nrf2 accumulation

Work from this laboratory has shown that UVA treatment of FEK4 primary human fibroblasts results in degradation of microsomal heme-containing proteins in a dose dependant manner (Kvam *et al.*, 1999). Moreover, Kvam *et al.,* (1999) observed no change in the total amount of microsomal heme, or in the total amount of cellular heme. Taken together, these data are consistent with the interpretation that UVA releases heme from microsomal heme-containing proteins. Interestingly, Kvam *et al.,* (1999) demonstrated a clear correlation between the level of heme released and the subsequent accumulation of HO-1 mRNA, therefore indicating that UVA-induced heme release plays a role in up-regulation of *HMOX1* by UVA. In relation to this, recent data derived from a murine model has shown that heme promotes stabilisation of Nrf2 (Alam *et al.*, 2003).

As shown in section 3.2, Nrf2 whole cell accumulation was observed in response to UVA or heme treatment in human skin fibroblasts. The hypothesis that UVA-mediated Nrf2 accumulation is dependent on the UVA-induced release of heme from heme-containing proteins was examined by means of depletion of intracellular heme prior to UVA irradiation. Succinylacetone [(SA) 4,6-dioxoheptanoic acid] was used to deplete intracellular heme. SA is a metabolite of tyrosine, and is a potent irreversible inhibitor of delta-aminolevulinic acid dehydrase, the rate limiting enzyme in heme synthesis (Tschudy *et al.*, 1981). As shown in section 3.3, endogenous heme was below the level of detection by both spectrophotometry and spectrofluorometry in the cell types employed in this study. This prevented monitoring of heme depletion by SA. Previously published data were therefore used to calculate the required SA concentration and treatment time. An SA concentration of 1 mM and treatment time of 24 hours was judged to be sufficient to more than halve the concentration of intracellular heme-containing proteins (Giger and Meyer, 1983).

FEK4 primary human fibroblasts were treated with 1 mM SA or the vehicle (serum free medium) for 24 hours. The cells were then UVA treated (250 $kJ/m^2$) and incubated for the time period indicated before fixing. Immunocytochemistry and epifluorescence microscopy was used to visualise Nrf2. As shown in figure 3.13, the staining methodology employed to visualise Nrf2 resulted in no non-specific binding of the fluorophor conjugated secondary antibody allowing for the precise monitoring

of Nrf2. In agreement with the data shown in section 3.1, the imaging data presented in figure 3.13 shows an immediate accumulation of Nrf2 in response to UVA irradiation of vehicle-treated FEK4 cells; however, this effect was virtually abolished by pre-treatment with the heme synthesis inhibitor SA. The mean fluorescence of each image has been determined and normalised against the fluorescence of the untreated control (as described in section 2.14). The results show between a 1.31 to 1.46 fold increase in fluorescence in irradiated cells pre-treated with the vehicle. Cells treated with the heme synthesis inhibitor prior to irradiation, showed only a 1.10 to 1.13 fold increase in fluorescence. These data therefore validate the hypothesis that, in human skin cells, UVA leads to Nrf2 stabilisation by means of heme.

In this study the effect of intracellular heme depletion on UVA up-regulation of HO-1 was also examined. As determined by western blotting, SA treatment of FEK4 cells prior to UVA treatment was observed to marginally reduce HO-1 accumulation (data not shown). This observation supports the idea that UVA-mediated Nrf2 accumulation by means of heme release, may influence the transcriptional up-regulation of the phase-II gene *HMOX1*.

**Figure 3.13: Heme synthesis inhibition reduces UVA-mediated Nrf2 whole cell protein accumulation in primary human skin cells**

(*next page*)

FEK4 primary human fibroblasts were treated with either 1 mM succinyl acetone or the vehicle (serum free medium) for 24 hours at 37°C. After this time period cells were irradiated at 250 kJ/m$^2$ and incubated in conditioned media for the time periods indicated. The control samples were treated exactly the same as the irradiated samples, but were not irradiated. The untreated sample remained in the incubator for the duration of the experiment. Cells were fixed and immunostained with anti-Nrf2 rabbit polyclonal primary antibody followed by Invitrogen's Alexa-Fluor goat anti-rabbit as described in the Materials and Methods (section 2.14). Blocking of non-specific sites was accomplished by application of Invitrogen's Image-iT™ Fx signal enhancer. Cells were incubated in Hoechst stain to allow visualisation of nuclei. The cells were analysed by oil immersion epifluorescence at 63x magnification on a Nikon Eclipse TE2000-U microscope and using the software programme UltraVIEW. The images were produced by superimposing the visualised nuclei (BLUE) onto Nrf2 protein (PINK). The mean fluorescence of each image was determined using the software package ImageJ as described in section 2.14.

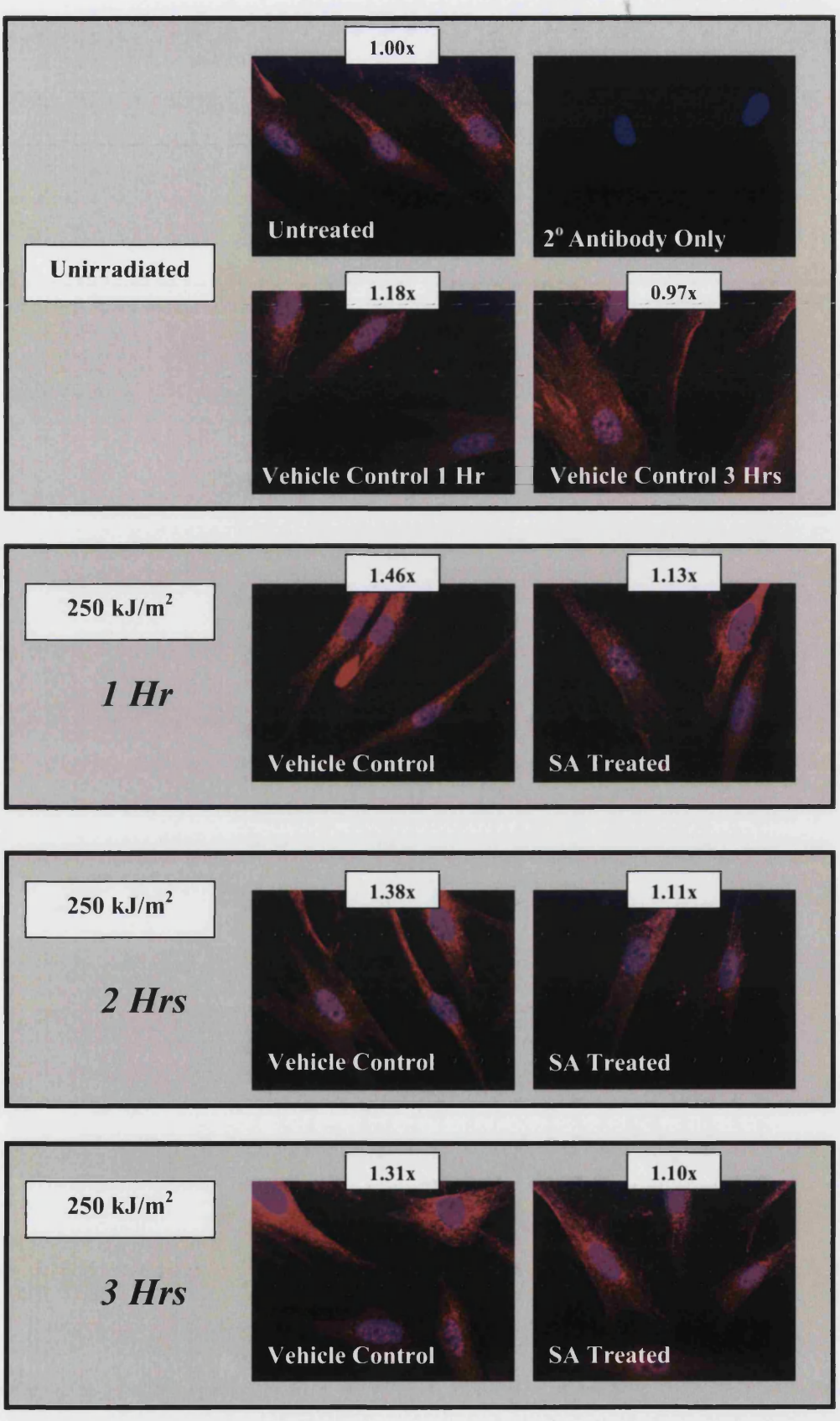
Unirradiated
1.00x
Untreated
2° Antibody Only
1.18x
Vehicle Control 1 Hr
0.97x
Vehicle Control 3 Hrs
250 kJ/m²
1 Hr
1.46x
Vehicle Control
1.13x
SA Treated
250 kJ/m²
2 Hrs
1.38x
Vehicle Control
1.11x
SA Treated
250 kJ/m²
3 Hrs
1.31x
Vehicle Control
1.10x
SA Treated

### 3.5 The role of UVA generated $^1O_2$ in Nrf2 activation

Regulation of Nrf2 is partly achieved through prevention of nuclear availability (Dhakshinamoorthy and Jaiswal, 2001; Itoh *et al.*, 1999). Under reducing conditions Nrf2 is sequestered by Keap1 anchoring the transcription factor within the cytoplasm (Kang *et al.*, 2004), and therefore preventing transcriptional activation of phase II genes. Evidence has been provided to suggest that Keap1 acts as a sensor of oxidative stress; here the influence of UVA-generated ROS on this regulatory system has been investigated in FEK4 primary human fibroblasts.

Singlet oxygen ($^1O_2$) is widely regarded to be the primary effector in UVA gene regulation. In this study the effect of this ROS on Nrf2 sub-cellular localisation has been examined using deuterium oxide ($D_2O$), a strong and reasonably specific $^1O_2$ lifetime enhancer (Lindig *et al.*, 1980). FEK4 primary human fibroblasts were treated with 250 kJ/m$^2$ UVA whilst bathed in PBS prepared using either $H_2O$ or $D_2O$ as a solvent. Following treatment the cells were incubated in conditioned media for the indicated time periods before cytoplasmic and nuclear extracts were prepared. The cytoplasmic and nuclear cell extracts were analysed using SDS-PAGE and western blotting.

As shown in figure 3.14, a moderate increase in the amount of Nrf2 residing in the cytoplasm was observed in FEK4 cells treated with UVA (250 kJ/m$^2$) whilst bathed in $H_2O$-PBS. However no such accumulation was observed in the cytoplasm of cells treated with the same dose of UVA whilst bathed in $D_2O$-PBS. The reduced level of Nrf2 observed in the $D_2O$ treated tissue extracts indicates that UVA-generated ROS communicate some authority over Nrf2 residing in the cytoplasm. As shown in figure 3.15, accumulation of Nrf2 was detected in the nucleus of FEK4 cells treated with UVA whilst bathed in $H_2O$-PBS or $D_2O$-PBS. However, the amount of Nrf2 detected in the nucleus was not affected through treatment with the $^1O_2$ lifetime enhancer $D_2O$.

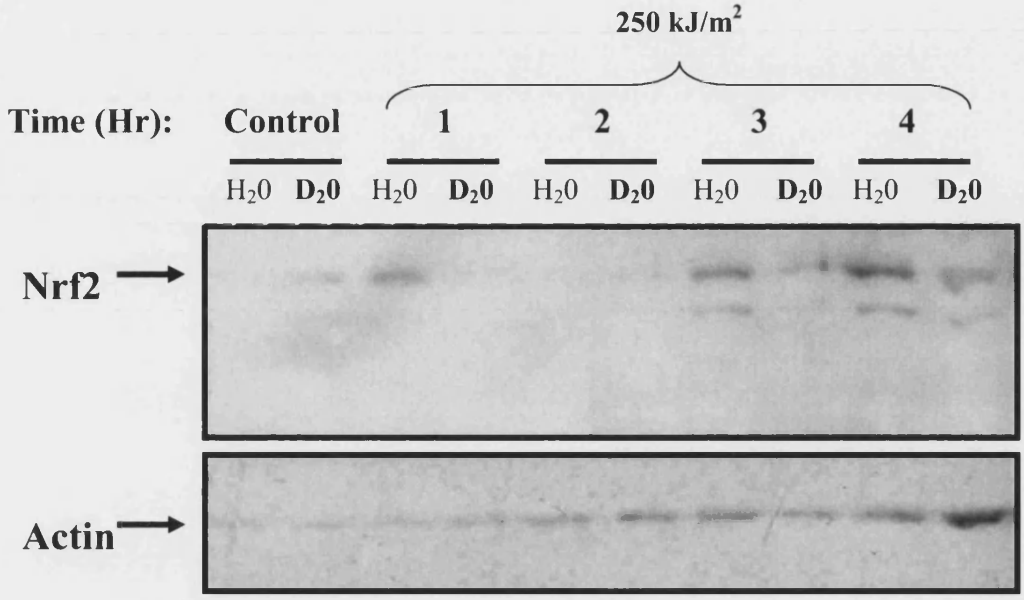


**Figure 3.14: The effect of $D_20$ on cytoplasmic Nrf2**

Freshly confluent FEK4 primary human fibroblasts were UVA treated (250 $kJ/m^2$) as described in section 2.3.1. During irradiation cells were covered with PBS supplemented with 0.01 % $Ca^{2+}$ and 0.01 % $Mg^{2+}$ prepared using either $H_20$ or 99.9 % deuterium oxide ($D_2O$), as detailed in section 2.3.4. The control cells were treated exactly the same as the UVA treated cells, but were not irradiated. Cytoplasmic extracts were prepared as described in the Materials and Methods (section 2.4.2), and protein concentration was determined using the method of Bradford. Equal amounts of cytoplasmic protein (5 µg/lane) were analysed by SDS-PAGE and western blotting as described in the Material and Methods (section 2.12). After visualisation of Nrf2 protein, the membrane was re-probed for actin to evaluate loading. This experiment was repeated with similar results.

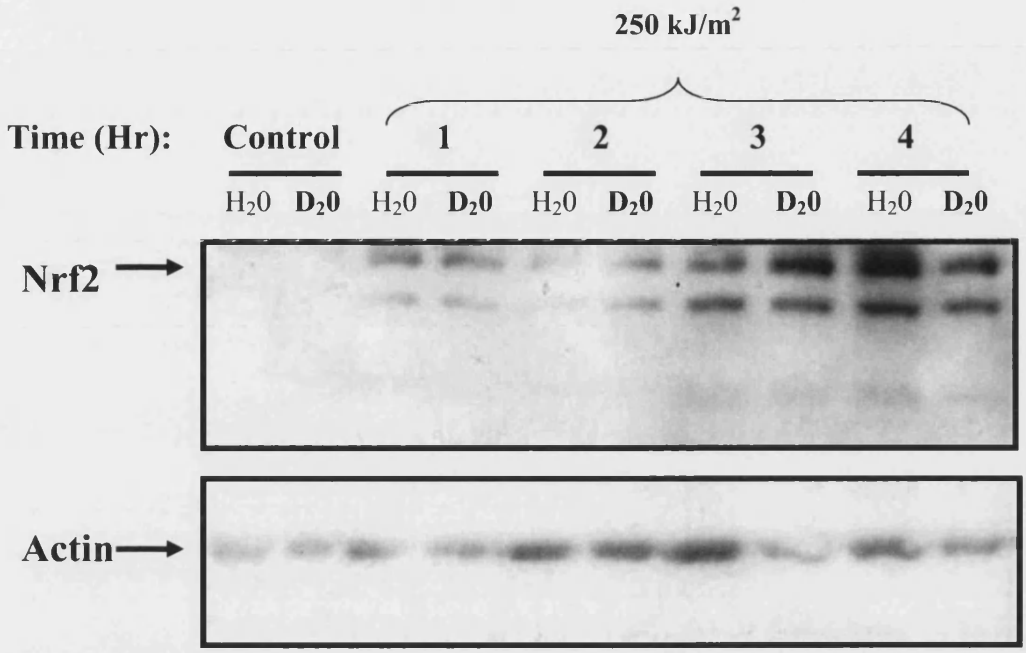


**Figure 3.15: The effect of $D_20$ on nuclear levels of Nrf2**

Freshly confluent FEK4 primary human fibroblasts were UVA treated (250 $kJ/m^2$) as described in section 2.3.1. During irradiation cells were covered with PBS supplemented with 0.01 % $Ca^{2+}$ and 0.01 % $Mg^{2+}$ prepared using either $H_20$ or 99.9 % deuterium oxide ($D_2O$), as detailed in section 2.3.4. The control cells were treated exactly the same as the UVA treated cells, but were not irradiated. Nuclear extracts were prepared as described in the Materials and Methods (section 2.4.2), and protein concentration was determined using the method of Bradford. Equal amounts of nuclear protein (5 µg/lane) were analysed by SDS-PAGE and western blotting as described in Material and Methods (section 2.12). After visualisation of Nrf2 protein, the membrane was re-probed for actin in order to evaluate loading.

## 3.6 The effect of UVA radiation on *NRF2* transcriptional activity

### 3.6.1 General remarks

The LightCycler instrument (Roche Applied Science) provides an extremely powerful tool for real time quantification of gene expression by accurately measuring mRNA levels (refer to section 2.16). In this study, the LightCycler system was used to determine the effect of UVA radiation on the level of *NRF2* gene activation by means of real time RT-PCR. Throughout this study gene expression was measured by calibrator normalised relative quantification. Relative quantification is based upon the comparison of two ratios: the ratio of a target cDNA sequence (*NRF2*) to a housekeeping reference cDNA sequence (*GAPDH*) in an unknown sample, to the ratio of the same two sequences in a standard sample called a 'calibrator'. The calibrator represents typical proportions of the target and reference sequences against which the unknown sample can be compared. Throughout this study the same calibrator was included in all of the LightCycler experiments to allow for inter-experimental comparison. The results of this investigation (figure 3.26 and 3.27) are expressed as the target / reference ratio of each sample normalised by the target / reference ratio of the calibrator (set as 1).

### 3.6.2 Data presentation

LightCycler data has been presented in the form of amplification curves, and as melting curves / peaks. Amplification curves are used to assess the relative cDNA starting concentration of the target (*NRF2*) and reference (*GAPDH*) sequences. The number of PCR amplification cycles is plotted against relative fluorescence at 530 nm after each amplification cycle. The relative cDNA starting concentration is based upon the crossing point (Cp) of each sample; that is the number of PCR cycles that are required for the fluorescence of each sample to be detected above background fluorescence (expressed as a cycle number). Relative quantitative analysis is therefore based on the assumption that the concentration of cDNA at a sample's crossing point is the same for every sample containing the same target cDNA.

The melting temperature ($T_m$) of all PCR products was determined at the end of each PCR reaction to confirm the product identity, and to differentiate the specific

PCR product from non-specific double stranded oligonucleotides such as primer-dimers. The temperature required to separate complementary DNA strands can vary enormously. This melting temperature ($T_m$) is dependent upon the length of the strand, the sequence of the strand, and the GC content of the strand. The unique melting temperature of a PCR product therefore allows identification of non-specific PCR products which may influence the outcome of a PCR reaction. Using the DNA binding dye SYBR Green I (refer to section 2.16), the LightCycler System defines the melting temperature of a PCR product as the point at which half of the SYBR Green I dye has separated from the double strand PCR product. In this study, the melting data has been presented in two forms: a melting curve (fluorescence versus time) and a melting peak (-dF/dT versus temperature). The melting peak is derived from the melting curve and shows the negative derivative of fluorescence with respect to temperature. Integration of the area under a melting peak can be used for quantitative comparisons between samples. Displaying the melting profile of a PCR product as a peak allows for straightforward identification of non-specific PCR products.

### 3.6.3 Optimisation of the conditions required for *NRF2* real time RT-PCR

For accurate real time PCR quantification of gene expression, the conditions of the reaction must first be optimised. The conditions used for *HMOX1* and *GAPDH* real time PCR were determined in this laboratory by Dr. Sharmila Basu-Modak prior to the start of this study. A $Mg^{2+}$ concentration of 3.0 mM and the LightCycler settings displayed in tables 2.3 and 2.4 were used through-out this study for these two genes. The conditions required for *NRF2* real time PCR were determined.

The concentration of $Mg^{2+}$ required for effective primer / template association is unique for each PCR reaction. Therefore, optimisation of the $Mg^{2+}$ concentration is a pre-requisite for effective PCR. The optimal magnesium concentration required for *NRF2* real time RT-PCR was determined as described in section 2.16.3. Identical samples with $Mg^{2+}$ concentrations of between 1.0 – 5.0 mM were analysed using the LightCycler settings shown in table 3.1 and an arbitrary primer annealing temperature of 55°C. For each $Mg^{2+}$ concentration duplicate samples were analysed. No-template-control (NTC) samples were also included. The results are shown in figure 3.16.

The optimal $Mg^{2+}$ concentration for any PCR reaction is defined as the $Mg^{2+}$ concentration that correlates with the greatest amount of PCR product generated per amplification cycle. Using the DNA binding dye SYBR Green I with the LightCycler system, the optimal $Mg^{2+}$ concentration is defined as the sample(s) with the steepest amplification gradient during log-linear PCR amplification; and as the $Mg^{2+}$ concentration that generates the greatest amount of specific PCR product at the end of the reaction. As shown in figure 3.16, both of the samples supplemented with 1 mM $Mg^{2+}$ to the 1 mM of $Mg^{2+}$ already contained in the ready to use PCR reaction mix produced the steepest amplification gradient during log-linear PCR. As determined by the area underneath the PCR melting peak, this concentration of $Mg^{2+}$ also generated the greatest amount of PCR product. Further confirmation that optimal PCR resulted from sample supplementation with 1 mM $Mg^{2+}$ can be found in the samples supplemented with 0.5 mM and 1.5 mM $Mg^{2+}$; all of which showed reduced reaction efficiency, and less PCR product.

The optimum primer annealing temperature for *NRF2* real-time RT-PCR was determined using non-quantitative gel PCR (as described in section 2.16.4). PCR was performed on a heating block with a variable temperature gradient. During the primer annealing phase the temperature of the heating block was set at a gradient ranging from 50 – 70°C using the temperature increments indicated in figure 3.17. As shown in figure 3.17, primer annealing temperatures of 52.4 and 54.1°C produced the greatest amount of PCR product after 30 cycles of amplification. A second experiment was conducted in which a temperature gradient of approximately 40 – 60°C was used during primer annealing (data not shown). The results of this experiment confirmed the data shown in figure 3.17. Based on these data, a primer annealing temperature of 53°C was used for *NRF2* real time PCR.

Serial dilution of cDNA was used to determine the relative cDNA starting dilution required for effective *NRF2* real time PCR. A cDNA pool was generated by a large-scale reverse transcription reaction (as descried in section 2.15) using total RNA extracted from FEK4 cells 3 hours after a dose of 250 $kJ/m^2$ UVA. A serial cDNA dilution ranging from undiluted to a 1 in 100 dilution was analysed using the optimised $Mg^{2+}$ concentration and primer annealing temperature (refer figure 3.16 and 3.17). As shown in figure 3.18, a low *NRF2* cDNA copy number was observed. The data show that only the use of undiluted FEK4 cDNA is sufficient for relative quantification of *NRF2* gene expression using the LightCycler system. The data

shown in figure 3.18 were also used to assess the potential for the generation of a standard efficiency value.

Calibrator normalised relative quantification can be used to determine relative gene expression with or without PCR efficiency correction. In theory, a perfect PCR reaction would generate two daughter strands of DNA per parental strand of DNA per amplification cycle; an efficiency of two. However, no PCR reaction is perfect. Efficiency correction adjusts for this. A standard efficiency value is generated by serial dilution of cDNA. The concentration of the dilution series is plotted against the Cp values of the samples. The slope of this standard curve is equal to the efficiency of the PCR reaction. Efficiency correction influences the relative fold change in gene expression of any reaction, and is generally employed in experiments where a large gene induction is expected. However, the use of a single efficiency value for all PCR reactions can incur inaccuracies if inter-experimental differences in amplification efficiency are observed. In this study, inter-experimental differences in *NRF2* amplification efficiency, and a low *NRF2* copy number, were observed. The determination of a reaction efficiency value therefore proved unfeasible and would only serve to incorporate error. An efficiency value of 2 was therefore employed throughout this study. Using this efficiency value, the LightCycler system automatically generates the ratio of the target cDNA sequence (*NRF2*) to a housekeeping reference cDNA sequence (*GAPDH*) in an unknown sample based on a mathematical model were no calibration curve is needed (Phaffl, 2001).

PCR product size should not exceed 700 base pairs for real time PCR using the LightCycler system. The *NRF2* primers employed throughout this study (shown in table 2.1) correspond to an amplicon size of 142 base pairs. The *Taq* DNA polymerase used throughout this study can incorporate 25 base pairs per second. An elongation time of 7 seconds (n + 1 seconds) was therefore used throughout. The optimised conditions for *NRF2* real time PCR are shown in table 3.1.

**Figure 3.16: Optimisation of the magnesium concentration required for *NRF2* PCR**

(*next page*)

The optimal magnesium concentration required for *NRF2* real time RT-PCR [LightCycler System (Roche Applied Science, Germany)] was determined using a cDNA pool generated by a large-scale reverse transcription reaction (as descried in section 2.15) using total RNA extracted from FEK4 primary human fibroblasts (as described in section 2.5.1). 2 µl of this cDNA pool was added to a PCR master-mix (as described in section 2.16.2) containing 0.5 µM of both the forward and reverse *NRF2* primers (as shown in table 2.1). $Mg^{2+}$ concentrations of between 1.0 and 5.0 mM were analysed. A total reaction mixture volume of 20 µl was prepared for each sample. All of the samples were assayed in duplicate and no-template-control (NTC) samples were included. All of the samples were analysed simultaneous using the settings shown in table 3.1, and using an arbitrary primer annealing temperature of 55°C. Samples were analysed using the LightCycler 1.5 instrument. Gene expression was measured by relative qualification using the software programme LightCycler 4.0. The data is presented in the form of fluorescence history and as a melting peak.

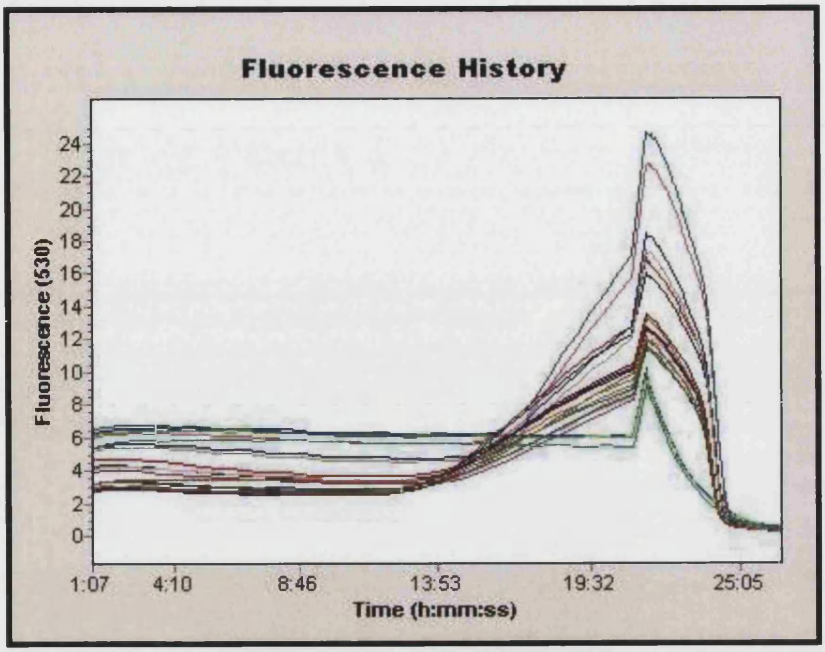
Fluorescence History
Fluorescence (530)
24
22
20
18
16
14
12
10
8
6
4
2
0
1:07
4:10
8:46
13:53
19:32
25:05
Time (h:mm:ss)


1 0.0-Mg
2 0.0-Mg
3 0.5-Mg
4 0.5-Mg
5 1.0-Mg
6 1.0-Mg
7 1.5-Mg
8 1.5-Mg
9 2.0-Mg
10 2.0-Mg
11 2.5-Mg
12 2.5-Mg
13 3.0-Mg
14 3.0-Mg
15 3.5-Mg
16 3.5-Mg
17 4.0-Mg
18 4.0-Mg
19 0.0-Mg-NTC
20 4.0-Mg-NTC

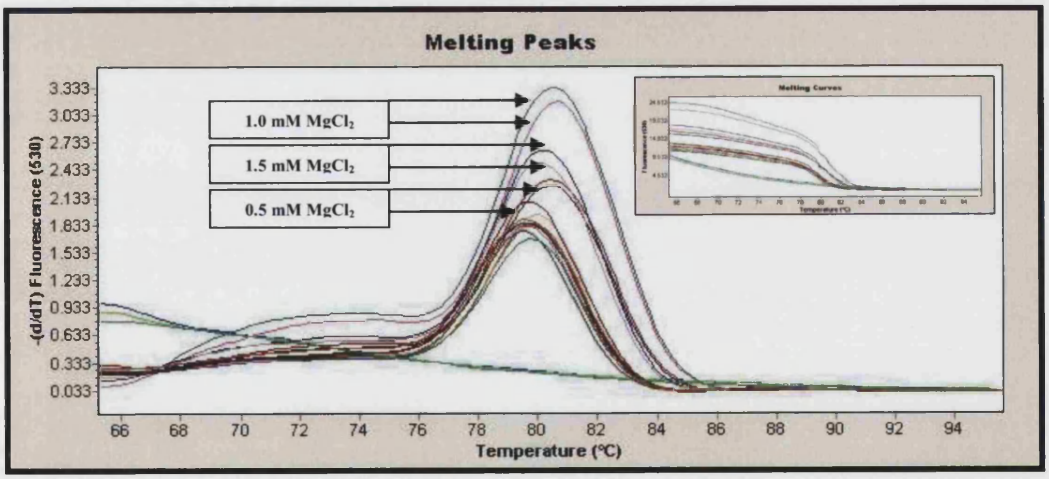
Melting Peaks
1.0 mM MgCl2
1.5 mM MgCl2
0.5 mM MgCl2
-(d/dT) Fluorescence (530)
3.333
3.033
2.733
2.433
2.133
1.833
1.533
1.233
0.933
0.633
0.333
0.033
66
68
70
72
74
76
78
80
82
84
86
88
90
92
94
Temperature (°C)

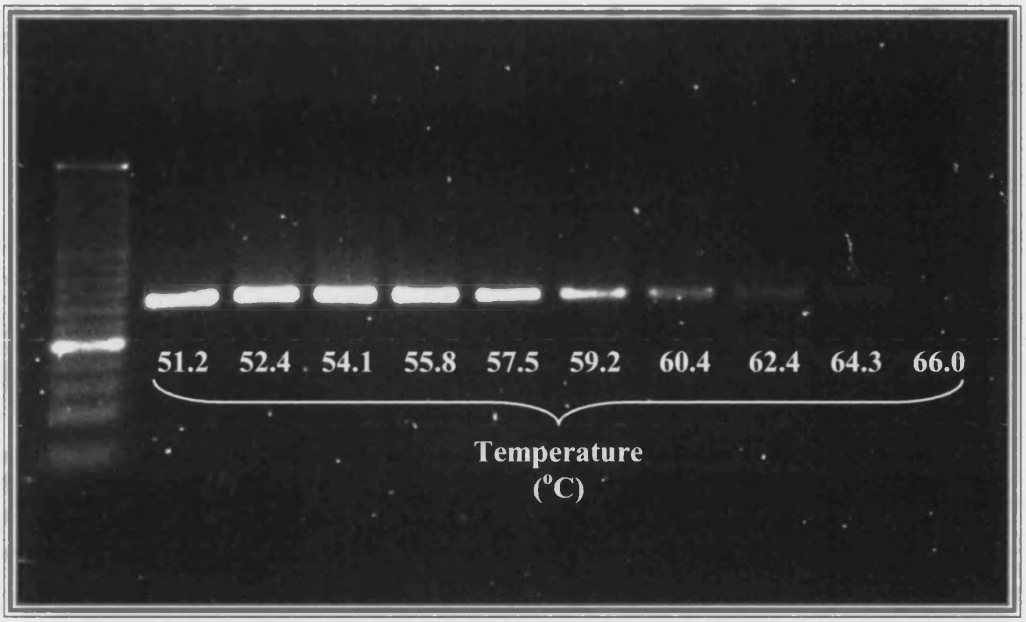


**Figure 3.17: Optimisation of the primer annealing temperature required for *NRF2* PCR**

The optimum primer annealing temperature for *NRF2* real-time RT-PCR was determined using non-quantitative gel PCR. A reaction mixture was prepared using Sigma's Readymix™ *Taq* without $MgCl_2$ according to the manufacturer's instructions. All of the samples contained 0.5 µM of both the forward and reverse *NRF2* primer (shown in table 2.1), and a final $Mg^{2+}$ concentration of 2.0 mM. The calibrator pool was used as a source of cDNA. PCR was performed on a FlexiGene (Techne) heating block with a variable temperature gradient using the following programme: Denaturation [95°C, 180 seconds]; Amplification [(94°C, 20 seconds) (*50 – 70°C*, 10 seconds) (72°C, 20 seconds)]; Termination [(72°C, 300 seconds) (4°C, ∞)]. 30 cycles of PCR amplification were used. During the primer annealing phase, the temperature of the heating block was set at a gradient ranging from 50 – 70°C at the temperature increments indicated above. For each sample, 10 µl of the reaction product was used for agarose gel electrophoresis using a 3 % gel as described in section 2.6.2.

**Figure 3.18: cDNA dilution series**

*(next page)*

A serial dilution of cDNA was analysed to determine an appropriate starting dilution for *NRF2* real time PCR using the LightCycler system; and to assess the potential for the generation of a standard efficiency file. A cDNA pool was used that had been generated by a large-scale reverse transcription reaction using total RNA extracted from FEK4 cells 3 hours after a dose of 250 $kJ/m^2$ UVA. 2 µl of this cDNA pool, ranging from undiluted to a 1 in 100 dilution, was added to a PCR master-mix (as described in section 2.16.2) containing 0.5 µM of both the forward and reverse *NRF2* primers (as described in table 2.1), and a final $Mg^{2+}$ concentration of 2.0 mM. A total reaction mixture volume of 20 µl was prepared for each sample. Each cDNA dilution was analysed four times. A no-template-control (NTC) sample was also included. All of the samples were analysed simultaneous using the settings shown in Table 3.1. Samples were analysed using the LightCycler 1.5 instrument. Gene expression was measured by relative qualification using the software programme LightCycler 4.0. The data is presented in both the form of an amplification curve and as a melting peak / curve.

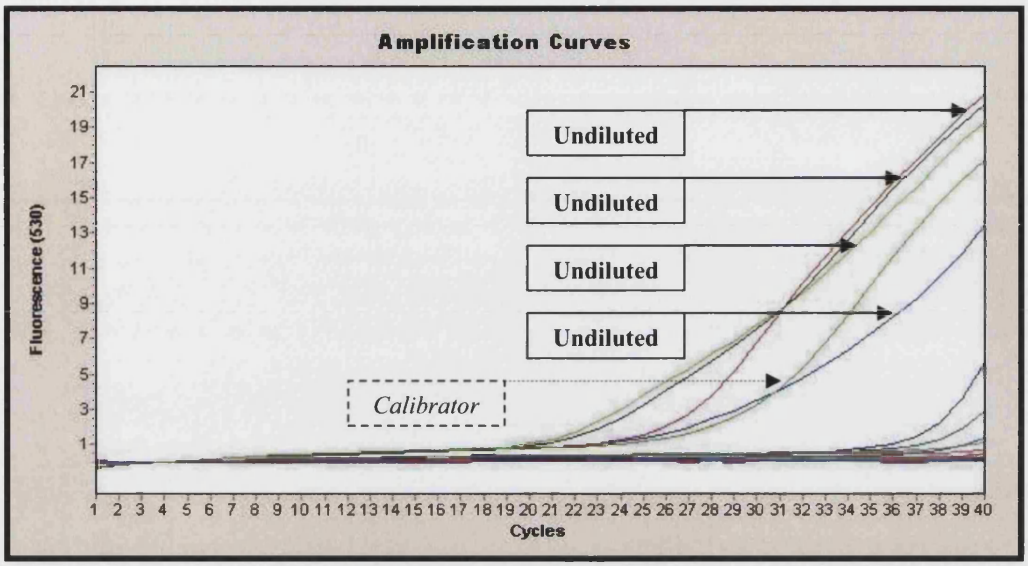
Amplification Curves
Fluorescence (530)
Cycles
Undiluted
Undiluted
Undiluted
Undiluted
Calibrator

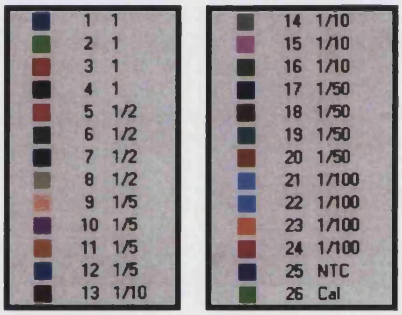
1 1
2 1
3 1
4 1
5 1/2
6 1/2
7 1/2
8 1/2
9 1/5
10 1/5
11 1/5
12 1/5
13 1/10


14 1/10
15 1/10
16 1/10
17 1/50
18 1/50
19 1/50
20 1/50
21 1/100
22 1/100
23 1/100
24 1/100
25 NTC
26 Cal

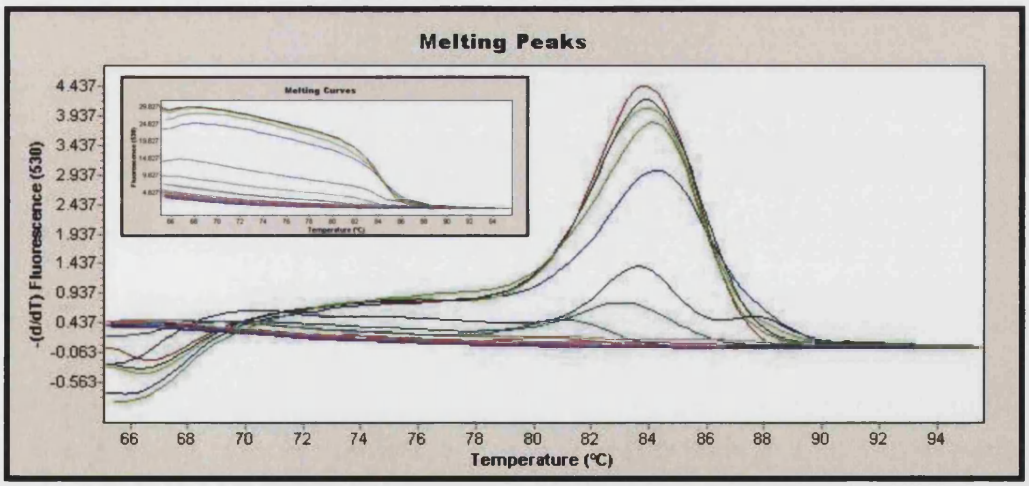
Melting Peaks
-(d/dT) Fluorescence (530)
Temperature (°C)
Melting Curves

| | Temperature (°C) | Time (seconds) | Ramp Rate (°C/second) | Acquisition Mode | |
|---|---|---|---|---|---|
| **Denaturation** | 95 | 30 | 20 | None | |
| **Amplification** | 95 | 0 | 20 | None | |
| | 53 | 5 | 20 | None | **40 Cycles** |
| | 72 | 7 | 20 | Single | |
| **Melting Curve** | 95 | 0 | 20 | None | |
| | 65 | 15 | 20 | None | **1 Cycle** |
| | 95 | 0 | 0.1 | Continuous | |
| **Cooling** | 40 | 30 | 20 | None | |

Table 3.1: The optimised settings used for real time PCR monitoring of the *NRF2* gene using the LightCycler system. A $Mg^{2+}$ concentration of 2 mM was used throughout this study for *NRF2* real time PCR.

### 3.6.4 Determination of *NRF2* mRNA half-life

To determine the time period required to assess the effect of UVA on *NRF2* gene activation, an attempt was made to determine the half-life of *NRF2* mRNA. The half-life of *NRF2* mRNA was measured in FEK4 primary human fibroblasts which were either untreated, control treated, or UVA treated (250 $kJ/m^2$). Cells were incubated for one hour following UVA treatment to allow accumulation of *NRF2* mRNA. The cells were then treated with 5 μg/ml of the transcriptional inhibitor actinomycin-D (as described in section 2.3.2), and cultured for the indicated time periods before harvesting (shown in hours). Total RNA extraction and reverse transcription was performed as described in section 2.5.1 and 2.15 respectively. Previous work this laboratory has shown that *GAPDH* mRNA is not significantly degraded following actinomycin D treatment (Keyse *et al.*, 1990). *GAPDH* was therefore employed as a reference to normalise inter-sample variation in cDNA starting concentration.

As shown in figure 3.20, a single melting temperature was observed at the end of this PCR reaction. This illustrates that only specific PCR product was generated. The amplification curves for this experiment are shown in figure 3.19. The data indicated that treatment with actinomycin-D did not influence the relative amount of *NRF2* mRNA in the untreated, control treated, or UVA treated FEK4 cells treated up to 4 hours. These data therefore indicate that the half-life of *NRF2* mRNA may be in excess of 4 hours. Further experimental investigations are required to determine this.

**Figure 3.19: Determination of *NRF2* mRNA half-life: amplification curves**

(*next page*)

FEK4 primary human fibroblasts were either untreated (Un), control treated (Sm), or UVA treated [(Uv) 250 kJ/m$^2$]. All of the cells were exposed to 5 µg/ml actinomycin-D (as described in section 2.3.2) one hour after the start of the experiment (determined to be the completion of irradiation of the irradiated samples). Cells were then cultured for the indicated time period before harvesting (indicated in hours). Total RNA was extracted as described in section 2.5.1, and reverse transcription was performed as described in section 2.15. 2 µl of this cDNA, either undiluted for *NRF2,* or a 1 in 5 dilution for *GAPDH*, was added to a PCR master-mix (as described in section 2.16.2) containing 0.5 µM of both the forward and reverse primer (shown in table 2.1). A $Mg^{2+}$ concentration of 2.0 mM was used for *NRF2* and 3.0 mM for *GAPDH.* A total reaction mixture volume of 20 µl was prepared for each sample. A no-template-control (NTC) and calibrator (Cal) sample was also included. The samples were analysed independently for either *NRF2* or *GAPDH* using the settings shown in Table 3.1 or Table 2.4 respectively. Samples were analysed using the LightCycler 1.5 instrument. Gene expression was measured by relative qualification using the software programme LightCycler 4.0. The *NRF2* (Target) and *GAPDH* (Reference) data is presented in the form of amplification curves.

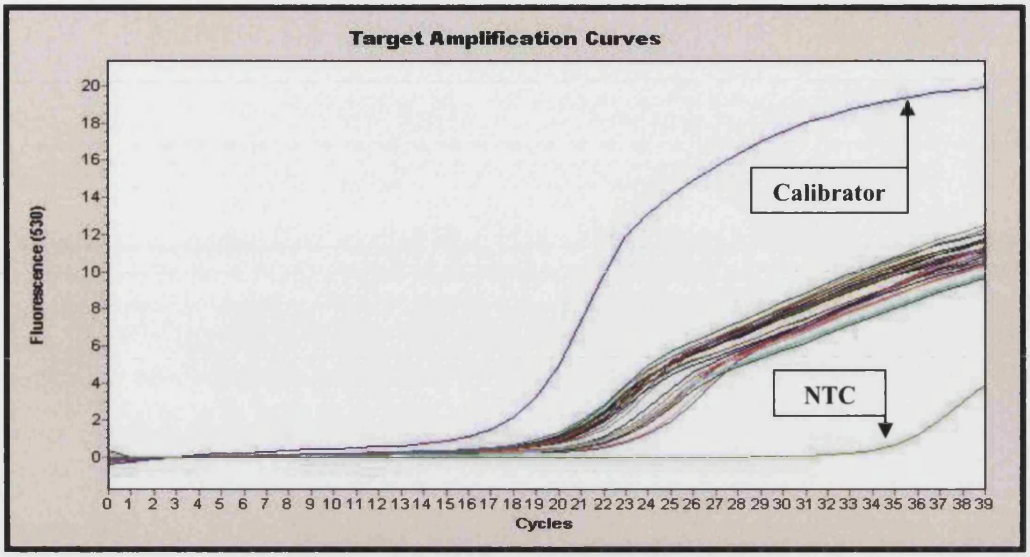
Target Amplification Curves
Fluorescence (530)
Cycles
Calibrator
NTC

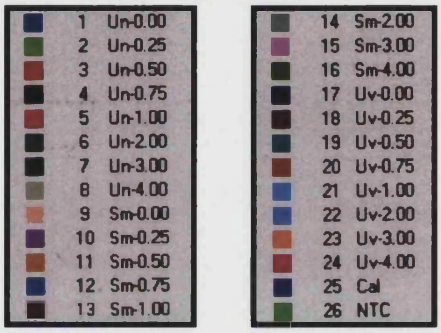
1 Un-0.00
2 Un-0.25
3 Un-0.50
4 Un-0.75
5 Un-1.00
6 Un-2.00
7 Un-3.00
8 Un-4.00
9 Sm-0.00
10 Sm-0.25
11 Sm-0.50
12 Sm-0.75
13 Sm-1.00
14 Sm-2.00
15 Sm-3.00
16 Sm-4.00
17 Uv-0.00
18 Uv-0.25
19 Uv-0.50
20 Uv-0.75
21 Uv-1.00
22 Uv-2.00
23 Uv-3.00
24 Uv-4.00
25 Cal
26 NTC

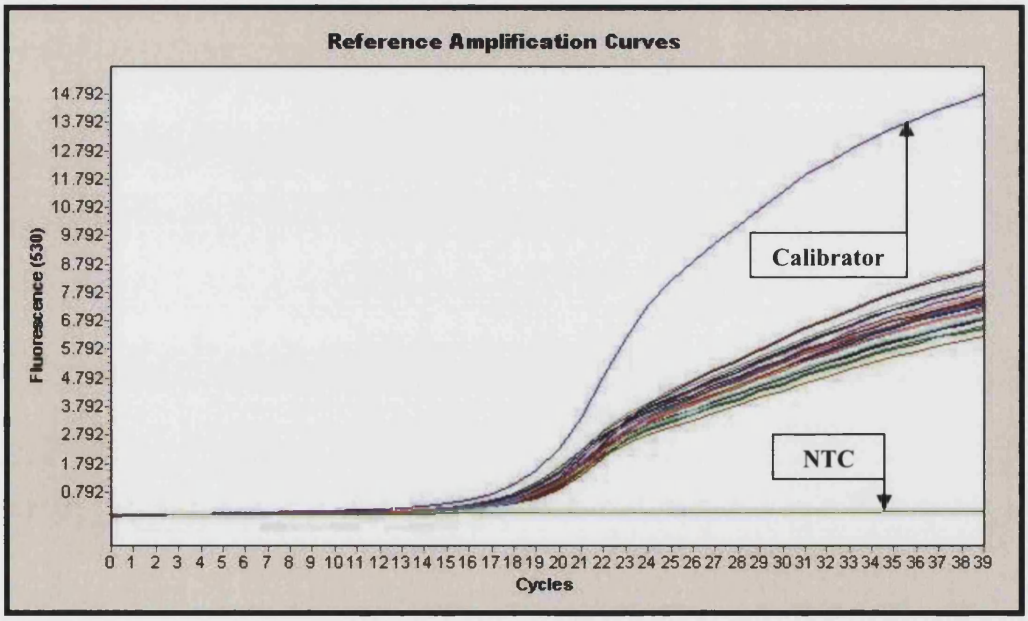
Reference Amplification Curves
Fluorescence (530)
Cycles
Calibrator
NTC

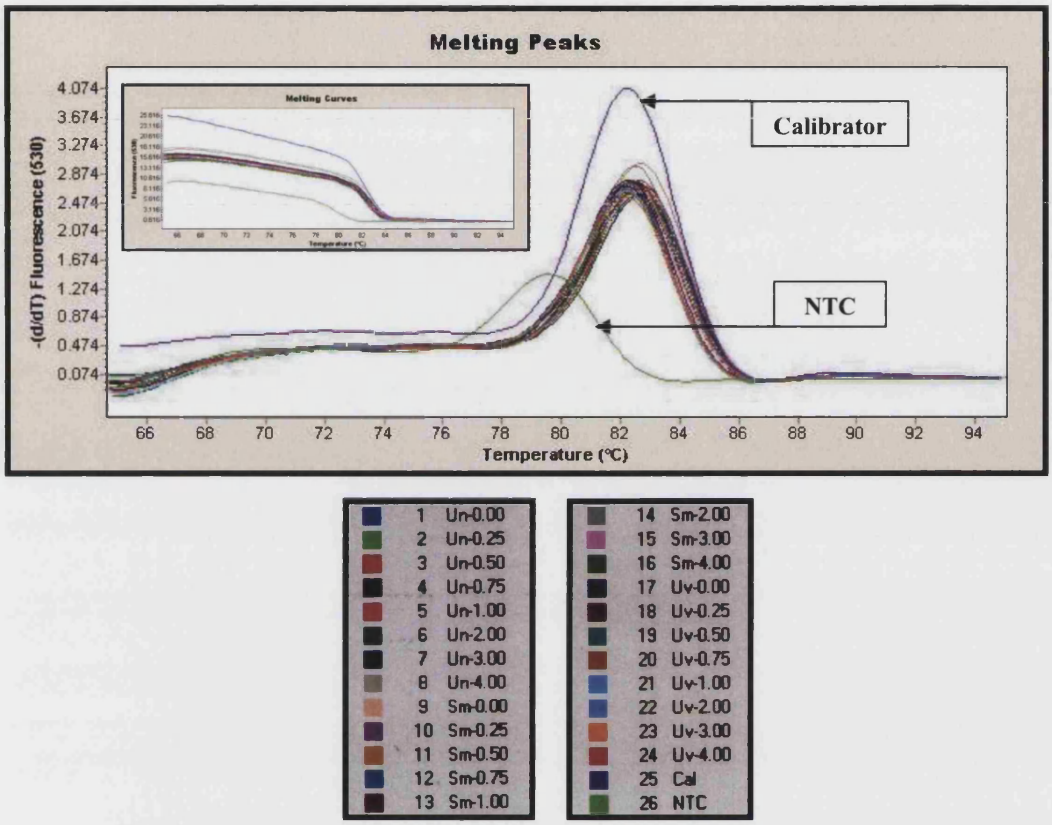


**Figure 3.20: Determination of *NRF2* mRNA half-life: *NRF2* PCR product melting peak / curve**

The melting curve and melting peak relates to the *NRF2* data in figure 3.19. The data is shown as both a melting curve (fluorescence versus time) and meting peak (-dF/dT versus temperature).

### 3.6.5 Real time PCR monitoring of *NRF2* gene expression following UVA treatment

In order to determine the influence of UVA radiation on *NRF2* transcriptional activity, FEK4 primary human fibroblasts were either control treated (Sham), or UVA treated (250 kJ/m$^2$). The time frame required to assess the influence of UVA on *NRF2* gene activity was selected based on previously published data (Kwak *et al.*, 2002). Following treatment, total RNA was extracted at the time points indicated (as described in section 2.5.1). Reverse transcription was performed as described in section 2.15. Two independent time courses (series A and series B) both consisting of irradiated and control samples were produced. The optimised conditions for *NRF2* PCR (shown in table 3.1) were used throughout this study for real time RT-PCR using the LightCycler 1.5 instrument.

UVA is known to transcriptionally up-regulate the HO-1 gene (Keyse *et al.*, 1990). The relative levels of HO-1 mRNA were therefore determined in both series A and B. Virtually no HO-1 gene up-regulation was observed in the unirradiated samples with respect to both of these independent series. With respect to series A, approximately a 40-fold up-regulation of the *HMOX1* locus was observed in the UVA irradiated samples (refer figure 3.21). This experiment was independently repeated using series B with nearly identical results. These data reflect observations previously made by this laboratory and serve as a positive control.

The *NRF2* and *GAPDH* amplification curves relating to series A and series B are shown in figures 3.22 and 3.24 respectively. The data from these amplification curves has been graphed and is presented in figures 3.26 (series A) and 3.27 (series B). These graphs represent the target (*NRF2*) / reference (*GAPDH*) ratio of each sample divided by the target / reference ratio of the calibrator. For ease of understanding the calibrator target concentration divided by the calibrator reference concentration has been set as 1 for both series. This allows these two sets of data to be unequivocally compared. The melting data relating to the *NRF2* PCR products for both series A and B are shown in figure 3.23 and 3.25 respectively. The melting data for both series A and B suggests impeccable PCR priming and reaction parameters resulting in the generation of only specific PCR product.

As shown in figure 3.26 and 3.27, both of the independent sample series analysed for *NRF2* transcriptional activity display low frequency oscillations in the level of *NRF2* mRNA in both the control and UVA treated samples. The UVA

irradiated samples show disruption to these oscillations, and exhibit a lower level of *NRF2* transcriptional activity immediately following UVA treatment when compared to the unirradiated control samples. The data shown in figures 3.26 and 3.27 has been combined in figure 3.28. Here the data have been combined to show the intra-experimental calibrator normalised mean of the irradiated samples divided by the mean of the control (unirradiated) samples for both series. This graph allows visualisation of the relative transcriptional activity of the irradiated samples over the unirradiated samples.

This graph exemplifies a period of reduced *NRF2* transcriptional activity in the irradiated samples when compared to the unirradiated samples for between 2 – 4 hours post-irradiation. This period of reduced transcriptional activity is succeeded by a period of enhanced transcriptional activity lasting in excess of 12 hours. Both series A and series B indicate a transcriptional time peak of 8 hours post treatment in the irradiated samples. A 1.67-fold and 2.02-fold relative fold increase in transcriptional activity in the irradiated samples over the un-irradiated control samples is observed in series A and series B respectively. These data show that UVA radiation exercises an influence over *NRF2* transcriptional activity in these primary human skin cells.

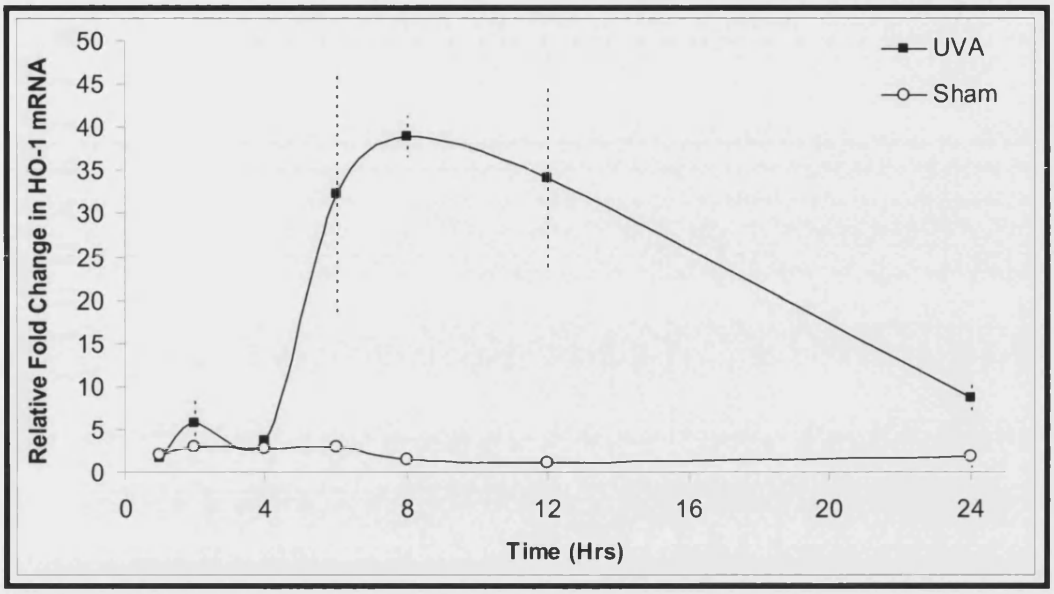


**Figure 3.21: The relative fold change of *HMOX1* transcriptional activity in both control and UVA irradiated FEK4 cells (series A)**

The graph shows HO-1 mRNA levels in both UVA (250 kJ/m$^2$) and control treated FEK4 cells. The samples have been normalised against the same calibrator. The graph shows the target (*HMOX1*) / reference (*GAPDH*) ratio of each sample divided by the target / reference ratio of the calibrator. Here the calibrator target concentration divided by the calibrator reference concentration has been set as 1. Each point represents the mean of two identical intra-experimental samples ran simultaneously. The error bars represent one standard deviation above and below the mean. This experiment was repeated with time course B with similar results.

**Figure 3.22: Determination of the effect of UVA radiation on *NRF2* transcriptional activity: amplification curves (series A)**

(*next page*)

FEK4 primary human fibroblasts were either untreated, control treated (Sham), or UVA treated (250 $kJ/m^2$). Control cells were treated exactly the same as UVA irradiated samples, but were not irradiated. Cells were then cultured for the indicated time period before harvesting. The untreated cells remained in the incubator for the duration of the experiment. Total RNA was extracted as described in section 2.5.1, and reverse transcription was performed as described in section 2.15. 2 µl of this cDNA, either undiluted for *NRF2,* or a 1 in 5 dilution for *GAPDH*, was added to a PCR master-mix (as described in section 2.16.2) containing 0.5 µM of both the forward and reverse primer (shown in table 2.1). A final $Mg^{2+}$ concentration of 2.0 mM was used for *NRF2* and 3.0 mM for GAPDH. A total reaction mixture volume of 20 µl was prepared for each sample. A no-template-control (NTC) and calibrator (Cal) sample was also included. The samples were analysed independently for either *NRF2* or *GAPDH* using the settings shown in table 3.1 and table 2.4 respectively. Samples were analysed using the LightCycler 1.5 instrument. Gene expression was measured by relative qualification using the software programme LightCycler 4.0. The *NRF2* (Target) and *GAPDH* (Reference) data is presented in the form of amplification curves. The melting curve analysis relating to the *NRF2* PCR product is presented in figure 3.23, and the relative fold change in *NRF2* transcriptional activation for both the irradiated and control samples is shown in figure 3.26.

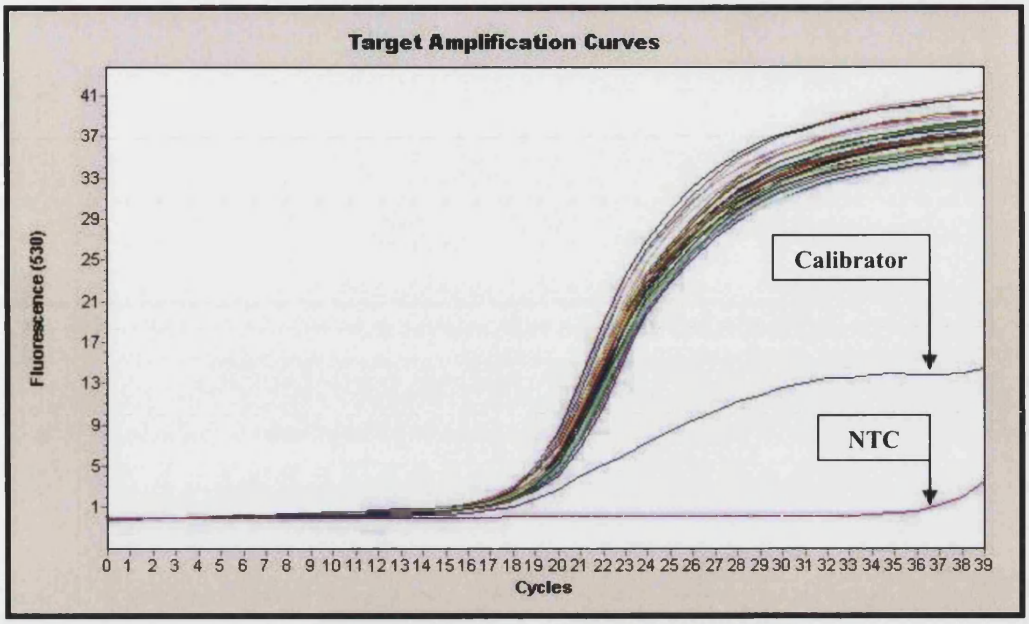
Target Amplification Curves
Fluorescence (530)
Cycles
Calibrator
NTC

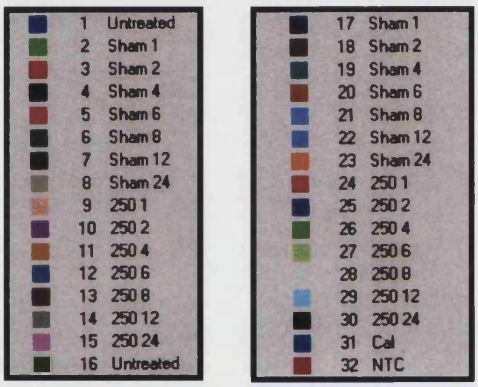
1 Untreated
2 Sham 1
3 Sham 2
4 Sham 4
5 Sham 6
6 Sham 8
7 Sham 12
8 Sham 24
9 250 1
10 250 2
11 250 4
12 250 6
13 250 8
14 250 12
15 250 24
16 Untreated


17 Sham 1
18 Sham 2
19 Sham 4
20 Sham 6
21 Sham 8
22 Sham 12
23 Sham 24
24 250 1
25 250 2
26 250 4
27 250 6
28 250 8
29 250 12
30 250 24
31 Cal
32 NTC

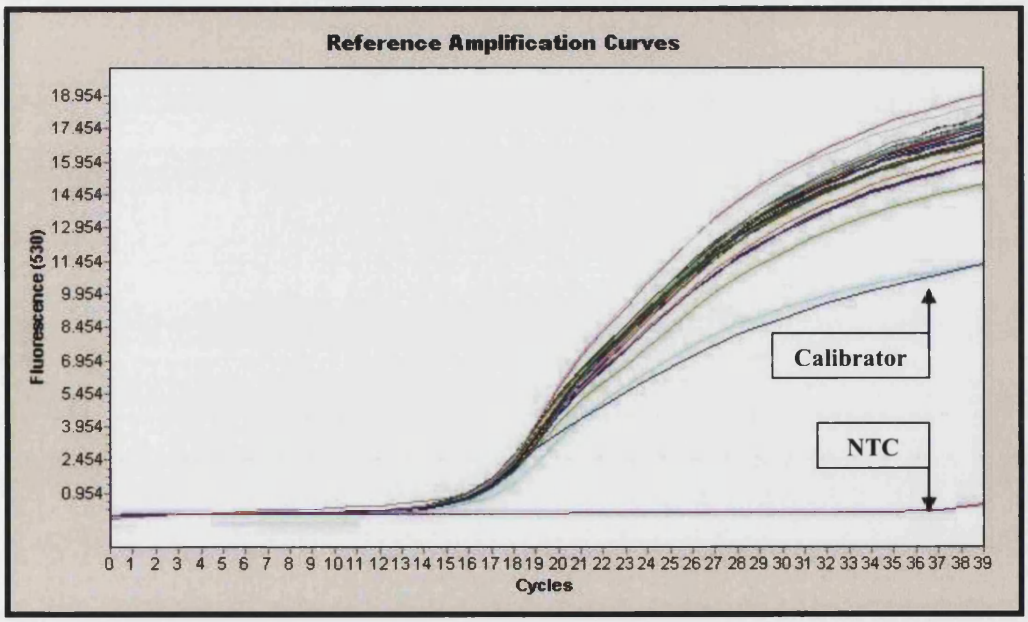
Reference Amplification Curves
Fluorescence (530)
Cycles
Calibrator
NTC

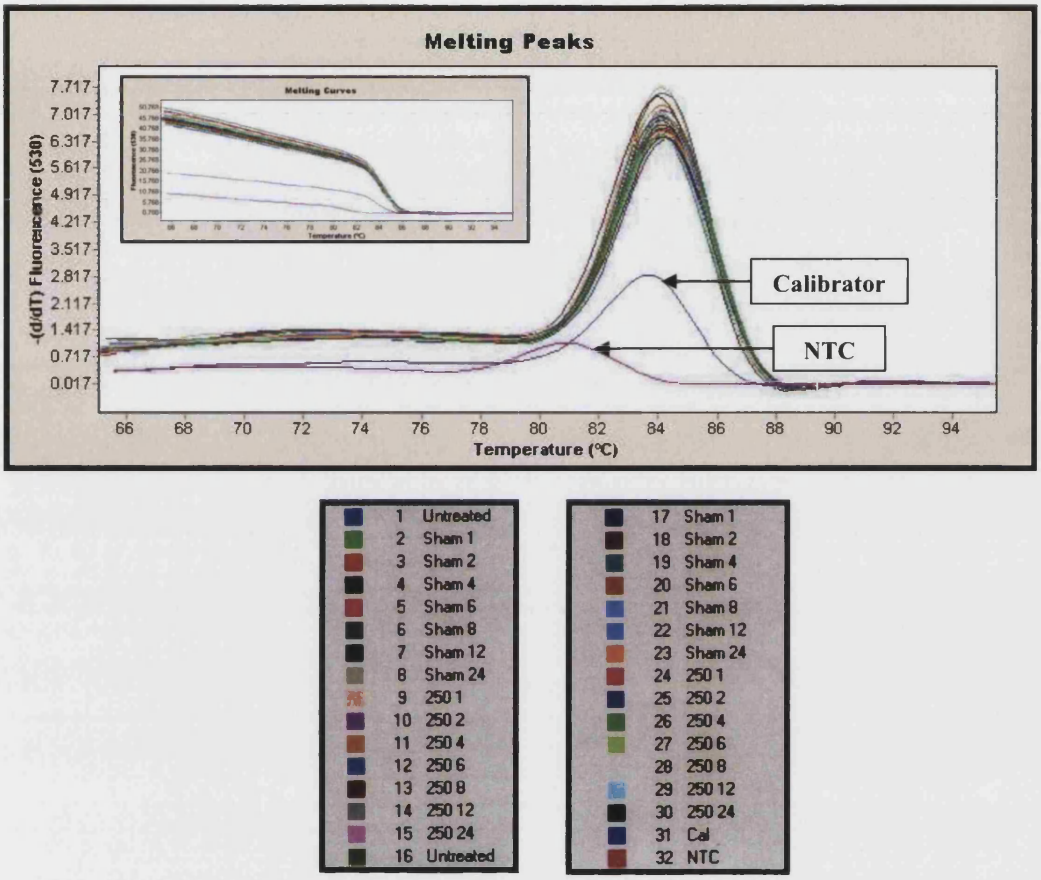


**Figure 3.23: Series A: *NRF2* PCR product melting curve and melting peak**

The melting curve and melting peak relates to the *NRF2* data in figure 3.22. The data is shown as both a melting curve (fluorescence versus time) and meting peak (-dF/dT versus temperature).

**Figure 3.24: Determination of the effect of UVA radiation on *NRF2* transcriptional activity: amplification curves (series B)**

(*next page*)

FEK4 primary human fibroblasts were either control treated (Sham), or UVA treated (250 $kJ/m^2$). Control cells were treated exactly the same as UVA irradiated samples, but were not irradiated. Cells were then cultured for the indicated time period before harvesting. Total RNA was extracted as described in section 2.5.1, and reverse transcription was performed as described in section 2.15. 2 µl of this cDNA, either undiluted for *NRF2,* or a 1 in 5 dilution for *GAPDH,* was added to a PCR master-mix (as described in section 2.16.2) containing 0.5 µM of both the forward and reverse primer (shown in table 2.1). A final $Mg^{2+}$ concentration of 2.0 mM was used for *NRF2* real time PCR and 3.0 mM for *GAPDH* real time PCR. A total reaction mixture volume of 20 µl was prepared for each sample. Several no-template-control (NTC) samples and calibrator (Cal) sample were included. The samples were analysed independently for either *NRF2* or *GAPDH* using the settings shown in table 3.1 and table 2.4 respectively. Samples were analysed using the LightCycler 1.5 instrument. Gene expression was measured by relative qualification using the software programme LightCycler 4.0. The *NRF2* (target) and *GAPDH* (reference) data is presented in the form of amplification curves. The melting curve analysis relating to the *NRF2* PCR product is presented in figure 3.25, and the relative fold change in *NRF2* transcriptional activation for both the irradiated and control samples is shown in figure 3.27.

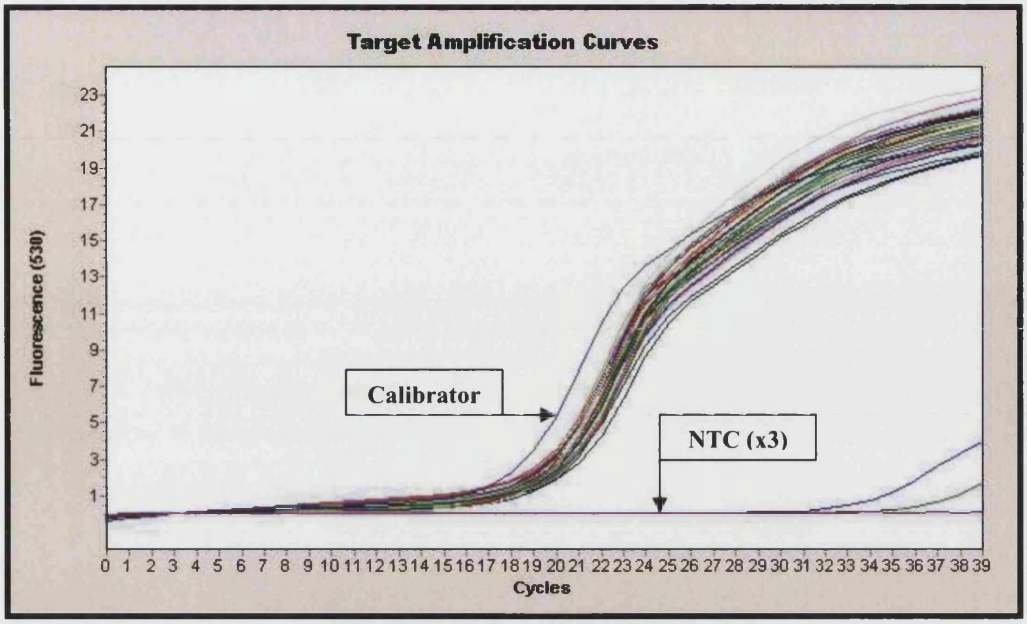
Target Amplification Curves
Fluorescence (530)
Cycles
Calibrator
NTC (x3)

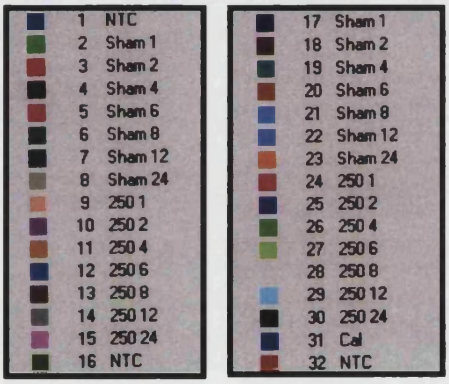
1 NTC
2 Sham 1
3 Sham 2
4 Sham 4
5 Sham 6
6 Sham 8
7 Sham 12
8 Sham 24
9 250 1
10 250 2
11 250 4
12 250 6
13 250 8
14 250 12
15 250 24
16 NTC
17 Sham 1
18 Sham 2
19 Sham 4
20 Sham 6
21 Sham 8
22 Sham 12
23 Sham 24
24 250 1
25 250 2
26 250 4
27 250 6
28 250 8
29 250 12
30 250 24
31 Cal
32 NTC

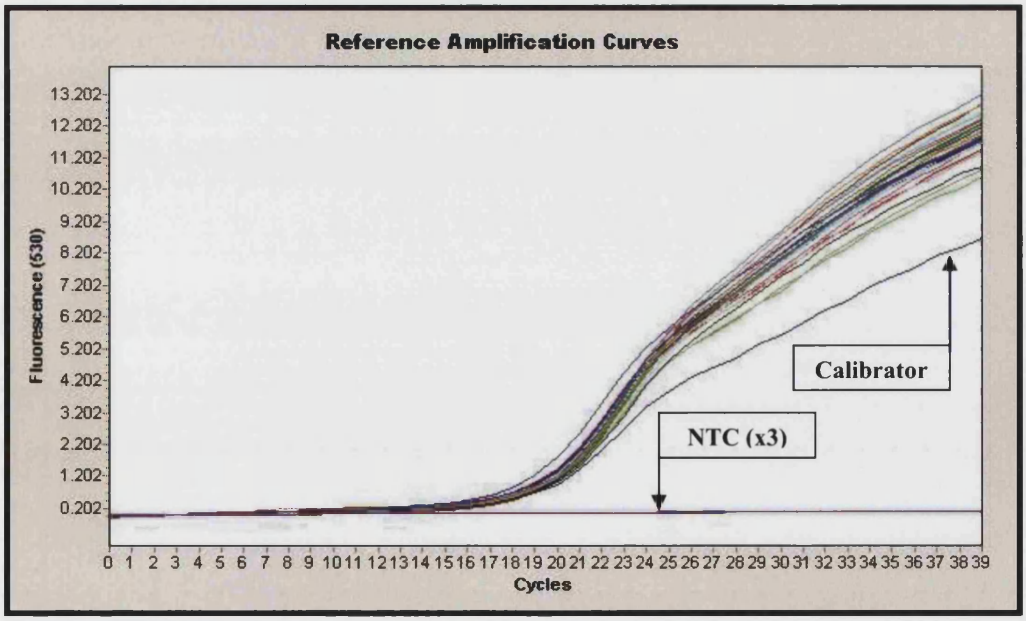
Reference Amplification Curves
Fluorescence (530)
Cycles
Calibrator
NTC (x3)

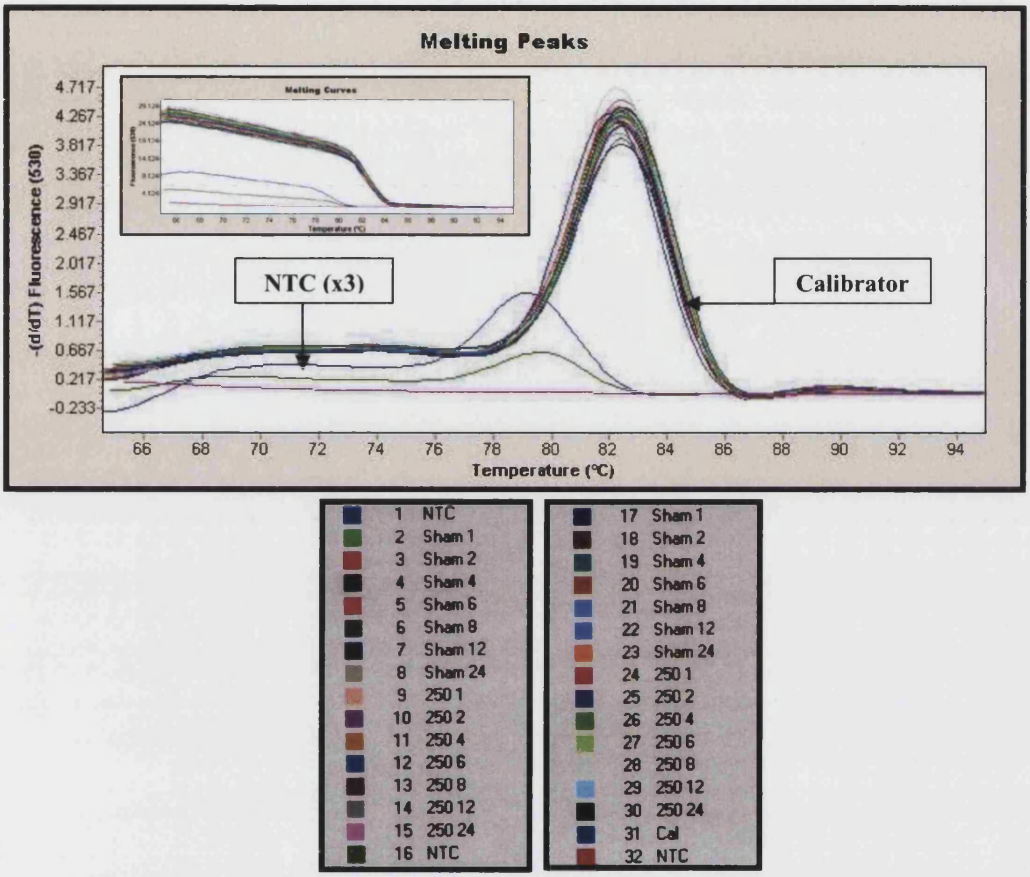


**Figure 3.25: Series A: *NRF2* PCR product melting curve and melting peak**

The melting curve and melting peak relates to the *NRF2* data in figure 3.24. The data is shown as both a melting curve (fluorescence versus time) and meting peak (-dF/dT versus temperature).

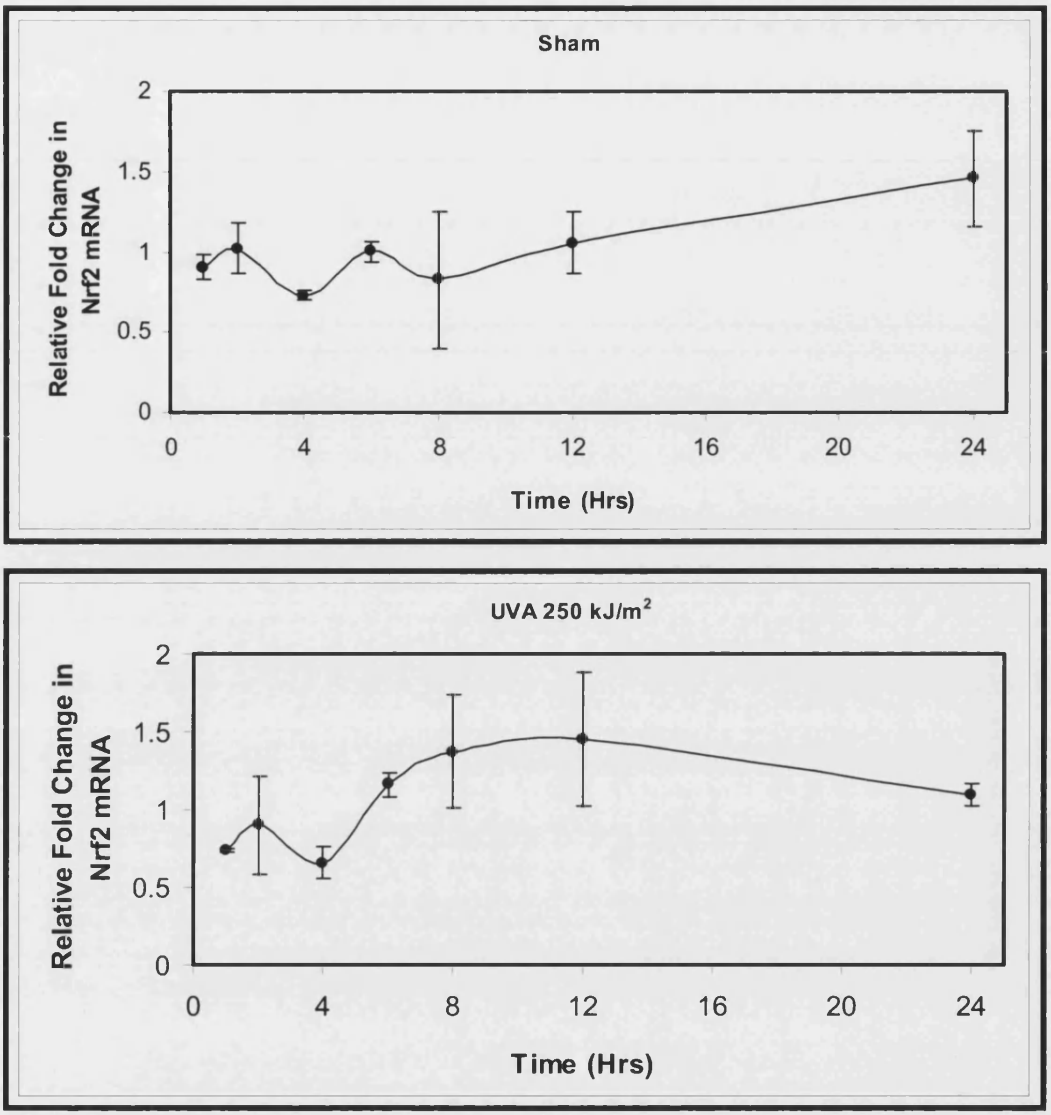


**Figure 3.26: The relative fold change of *NRF2* transcriptional activity in both control and UVA irradiated cells (series A)**

The graphs represent the data shown in figure 3.22. For clarity the control and UVA irradiated samples have been plotted separately. To allow for inter-experimental comparison, all of the LightCycler data has been normalised against the same calibrator. The graph shows the target (*NRF2*) / reference (*GAPDH*) ratio of each sample divided by the target / reference ratio of the calibrator. Here the calibrator target concentration divided by the calibrator reference concentration has been set as 1. Each point represents the mean of two identical intra-experimental samples ran simultaneously. The error bars represent one standard deviation above and below the mean.

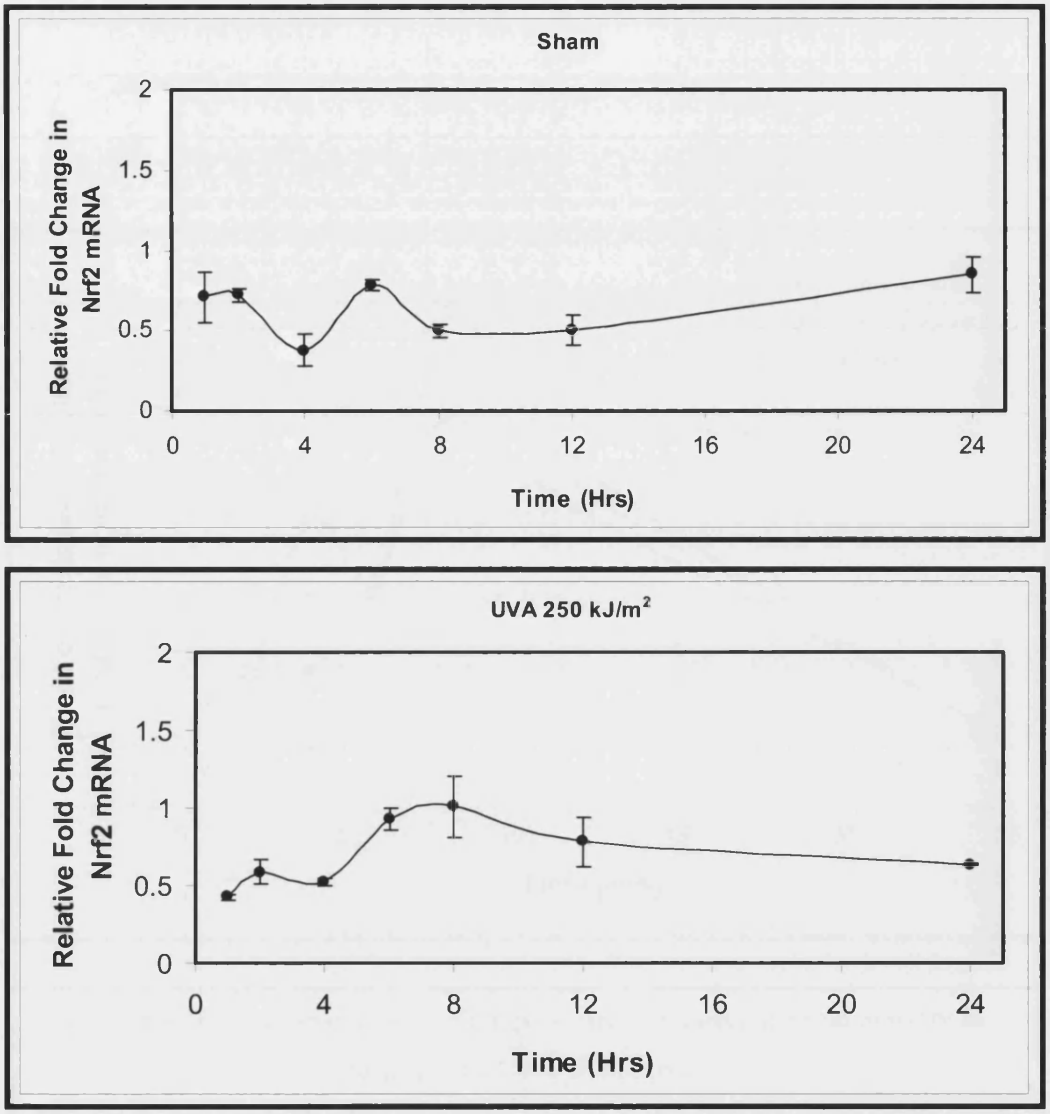


**Figure 3.27: The relative fold change of *NRF2* transcriptional activity in both control and UVA irradiated cells (series B)**

The graphs represent the data shown in figure 3.24. For clarity the control and UVA irradiated samples have been plotted separately. To allow for inter-experimental comparison, all of the LightCycler data has been normalised against the same calibrator. The graph shows the target (*NRF2*) / reference (*GAPDH*) ratio of each sample divided by the target / reference ratio of the calibrator. Here the calibrator target concentration divided by the calibrator reference concentration has been set as 1. Each point represents the mean of two identical intra-experimental samples ran simultaneously. The error bars represent one standard deviation above and below the mean.

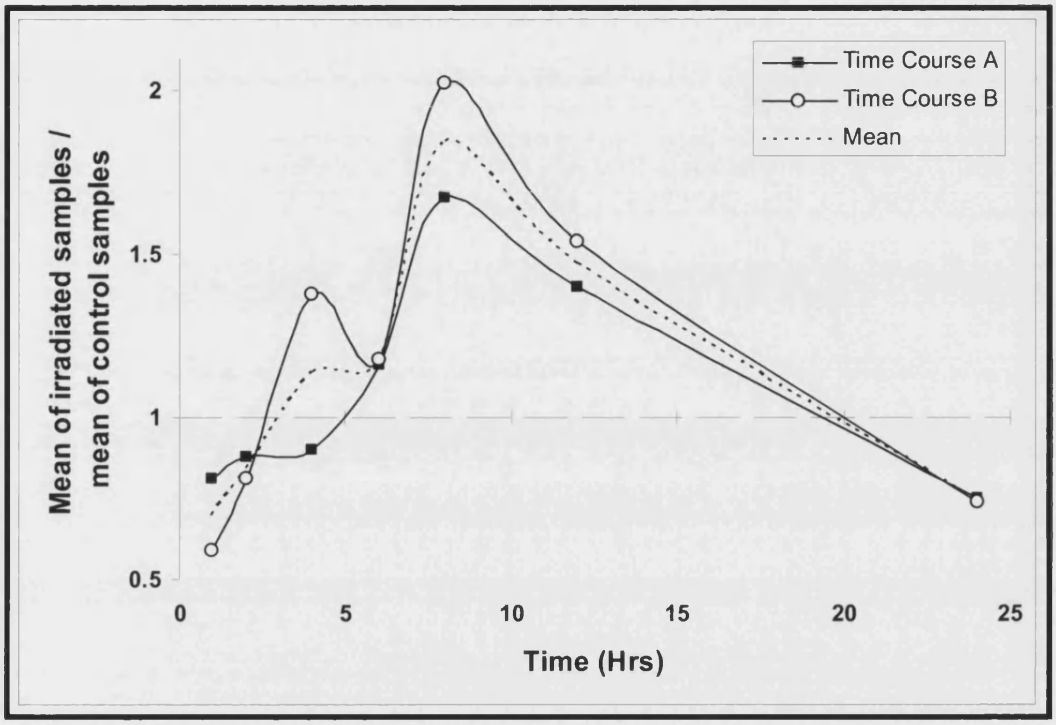


**Figure 3.28: The relative fold change in *NRF2* transcriptional activity in response to UVA irradiation**

The graph represents the data shown in figures 3.26 and 3.27. The graph shows the intra-experimental calibrator normalised mean of the irradiated samples divided by the control (un-irradiated) samples for both independent time courses.

## 3.7 The anti-apoptotic role of HO-1 in human melanoma cells

### 3.7.1 General remarks

Using both murine and human models, studies have shown the transcription factor Nrf2 to be involved in the activation of the phase II enzyme HO-1 (refer to sections 1.3.6 and 1.4.4). HO-1 has been shown to possess potent anti-apoptotic activity and has been implicated in the pathogenesis and proliferation of various neoplastic pathologies (refer to section 1.5.4). This study has examined the anti-apoptotic activity of HO-1 in human skin cells.

Prior to the start of this investigation, work from this laboratory had shown the primary human fibroblast cell line FEK4 to be highly resistant to UVA-induced apoptosis (Proteggente *et al.*, 2003). Furthermore, this cell line is known to exhibit strong up-regulation of the HO-1 gene in response to UVA radiation (Keyse *et al.*, 1989). It was hypothesised that the lack of susceptibility of this cell line to UVA-apoptosis may be attributable to UVA up-regulation of *HMOX1*, and furthermore, that this resistance to apoptosis may ultimately be dependent on UVA-activation of the transcription factor Nrf2. To investigate this hypothesis, it was determined whether or not HO-1 enzymatic activity could modulate apoptosis in FEK4 cells (data not shown).

FEK4 fibroblasts were treated with various doses of UVA. Immediately following irradiation the cells were treated with varying concentrations (0 – 1 mM) of the HO-1 competitive substrate analogue tin-protoporphyrin IX dichloride. To assess whether reduced HO-1 enzymatic activity resulted in increased apoptosis, the cells were assayed for characteristics inherent to apoptosis at various time points. These experiments produced data indicating that treatment with 1 mM of this competitive substrate analogue could mediate a two-fold increase in the percentage of cells undergoing UVA-apoptosis when compared to irradiated vehicle treated cells. However, the HO-1 competitive substrate analogue tin-protoporphyrin IX dichloride is known to be highly photo-reactive and generate ROS in response to exposure to sunlight. Data was obtained that indicated that the increased percentage of FEK4 cells undergoing UVA-apoptosis when treated with tin-protoporphyrin IX dichloride was not entirely specific to reduced HO-1 enzymatic activity. Owing to the

experimental complications associated with this compound, investigations by this methodology were discontinued.

In order to investigate the anti-apoptotic role of HO-1 in human skin cells further, a HO-1 over-expressing construct suitable for eukaryotic transient transfection was employed (refer section 2.7.2). In order, to explore the effect of HO-1 over-expression there was a prerequisite to establish a cell line that satisfied two criteria: firstly, the cell line needed to exhibit sufficient UVA-induced apoptosis to observe resistance to apoptosis conferred by HO-1 over expression; and secondly, the cell line needed to be amenable to transient transfection with this construct. The lack of UVA-apoptosis observed in FEK4 cells prevented the use of this cell line for this investigation.

As discussed in section 1.5.3, malignant melanoma is the most life-threatening cutaneous malignancy. Clinical oncology studies have shown that the high probability of mortality associated with this type of cancer can be attributed to resistance to apoptosis; yet the cellular mechanisms underlying this resistance remain to be elucidated. As such, investigations were conducted into the anti-apoptotic activity of HO-1 in human skin using human melanoma cells. Melanoma cells are phenotypically diverse. A number of human melanoma cell lines were therefore assessed for fulfilment of the afore mentioned criteria.

### 3.7.2 Quantification of UVA-apoptosis and transient transfection efficiency in human melanocytes and melanoma cells

To investigate the potential anti-apoptotic role of HO-1 in human skin there was a requirement to identify a human melanoma cell line that was both amenable to transient transfection with the HO-1 over-expressing construct pcDNA-3.1-HO1, and that exhibited apoptotic potential. The human melanoma cells lines G361, JUSO, and IGR1 (refer to section 2.2.2) were selected for this investigation. Investigations prior to the start of this study had shown these cells lines to be sensitive to UVA induced cell death (unpublished observations). The human melanocyte cell line NIR (refer section 2.2.2) was also employed during this investigation to allow for a degree of comparison between human melanoma cells and melanocytes. As discussed in section 1.5.3, UVA has been shown to induce both immediate (0 - 4 Hrs) and delayed (20 Hrs) apoptosis. Up-regulation of *HMOX1* is likely to pre-dominantly influence

late UVA-apoptosis. UVA-induced late apoptosis and necrosis was therefore quantified in the cell lines G361, JUSO, IGR1, and NIR.

Cells in exponential growth were treated with varying doses of UVA. After 20 hours the cells were collected and incubated in a labelling solution containing annexin V and prodidium iodide (as described in section 2.13.2). The percentage of cells exhibiting characteristics inherent to apoptosis and necrosis was determined by flow cytometry (as described in section 2.13). Figures 3.29 and 3.30 show the percentage of cells undergoing UVA-apoptosis and -necrosis respectively. As expected, necrosis was the predominant form of cell death observed in FEK4 cells. For this reason, FEK4 cells were not employed to investigate the effect of HO-1 over-expression on UVA-apoptosis. Similarly, G361 human melanoma cells proved highly resistant to UVA-apoptosis, and sensitive to UVA-induced necrosis. IGR1 human melanoma cells proved sensitive to both forms of UVA induced cell death, and exhibited virtually identical necrotic and apoptotic profiles. The exceptionally long growth period associated with NIR049 human melanocytes (doubling time > 7 days) dictated a limited investigation into the form of cell death induced by UVA in this cell line. These data identified necrosis to be the sole form of cell death undertaken by this cell line. The necrotic and apoptotic profiles relating to JUSO human melanoma cells proved more favourable to the needs of this study. As shown in figure 3.29 and 3.30, JUSO cells proved sensitive to UVA-induced apoptosis, but not necrosis. The cell survival data relating to JUSO is in agreement with data published previously (Applegate *et al.*, 1996).

The potential for high level transient transfection was determined. G361, JUSO, IGR1, and NIR cells were seeded at various densities 48 - 72 hours prior to transfection. The cells were transfected with 1.5 μg of the green fluorescent protein over-expressing construct pcDNA3.1-EGFP (refer section 2.7.3). Transfection of this construct allowed for rapid determination of transfection efficiency by flow cytometry. Transfection was accomplished using 3 μl of Lipofectamine™ 2000 according to the manufacturer's instructions (as described in section 2.9). Untransfected cells were treated exactly the same as the transfected cells, but were not transfected. The cells were cultured for 40 - 48 hours prior to determination of transfection efficiency (as described in section 2.13.3). The percentage of cells transfected was deemed to be the percentage of cells exhibiting a higher fluorescence than 98 % of the lowest fluorescing cells in the untransfected cell population (refer to

figure 2.3). As shown in figure 3.31, with the exception of G361 cells, all of the cell lines analysed exhibited a transfection efficiency in excess of 40 %. Further to this, separate investigations indicated that a transfection efficiency of approximately 70 % could be expected with respect to JUSO cells. The high transfection efficiency and pro-apoptotic nature of both JUSO and IGR1 human melanoma cells underlined the suitability of these two cells lines for this investigation. HO-1 over-expression by pcDNA3.1-HO-1 transient transfection was next evaluated in JUSO, IGR1, and NIR cells.

pcDNA3.1-HO1 (a kind gift from Professor Roland Stocker, The University of Sydney) was subjected to restriction enzyme digestion. This confirmed the presence of the 1 kb HO-1 insert (data not shown). IGR1 cells were subsequently transfected with 1.5 μg of either pcDNA3.1 or pcDNA3.1-HO1 using the commercially available transfection reagents GeneJuice® and Lipofectamine™ 2000 (as described in section 2.9). As shown in figure 3.32, strong HO-1 over-expression was observed in IGR1 cells transfected using the cationic transfection reagent Lipofectamine™ 2000, but not in cells transfected using GeneJuice®. All subsequent transfections were therefore performed using Lipofectamine™ 2000. As shown in figure 3.33, strong pcDNA3.1-HO1 mediated HO-1 over-expression was observed in the cell lines JUSO and FEK4 using Lipofectamine™ 2000. However, HO-1 over-expression was not observed in NIR049 human melanocytes, a result possibly attributable to the protracted doubling time associated with this cell line.

After consideration, based upon pro-apoptotic and anti-necrotic characteristics, and the strong potential for HO-1 over-expression, the cell line JUSO was selected for further investigations into the potential anti-apoptotic activity of HO-1 in human skin cells.

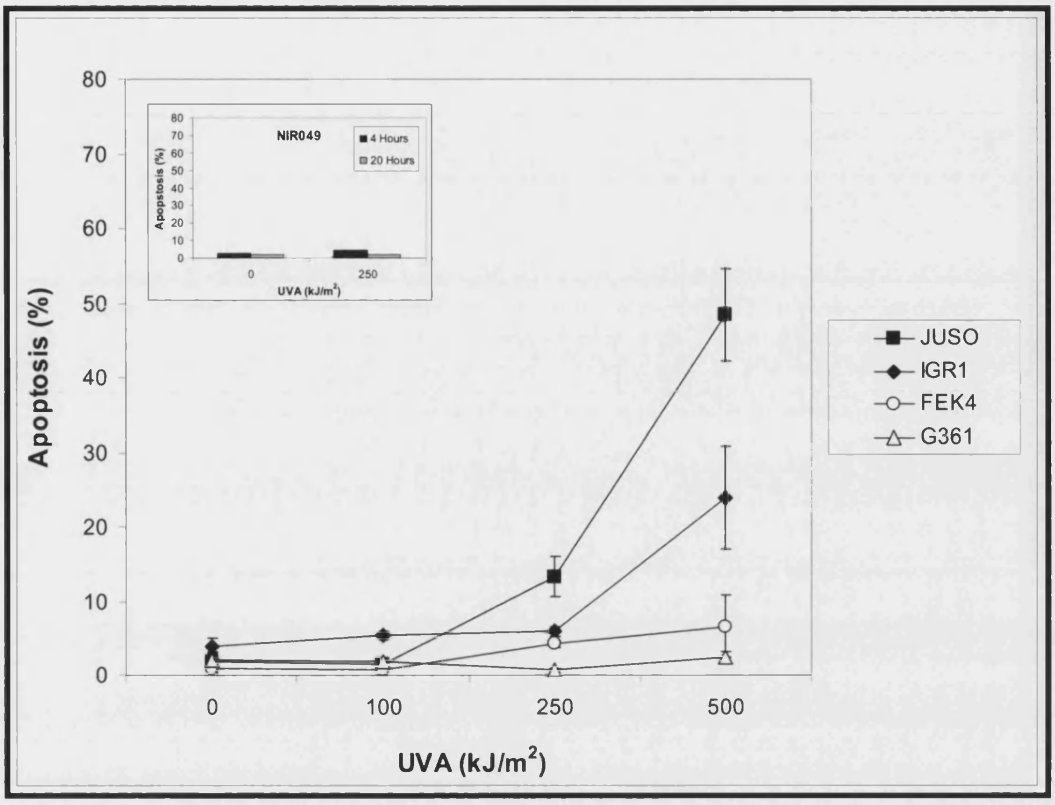


**Figure 3.29: Determination of late UVA-induced apoptosis**

Cells in exponential growth were irradiated with UVA at the stated dose and then incubated in conditioned media at 37°C for 20 hours. The cells were then collected and incubated in a labelling solution containing annexin V and prodidium iodide for 15 minutes (as described in section 2.13.2). The percentage of cells undergoing apoptosis was determined using flow cytometry (as described in section 2.13). During acquisition and analysis, data was viewed using a two-dimensional log dot plot defined by the FL1 and FL3 fluorescent profiles. Annexin V positive propidium iodide negative stained cells were deemed to be apoptotic (refer to figure 2.2). 10000 events were recorded for each sample. The percentage of NIR049 cells undergoing both early and late apoptosis was quantified. For NIR049 the percentages indicated represent one sample. For all of the other cells lines, each point represents the mean of three independent samples. The error bars represent one standard deviation above and below the mean.

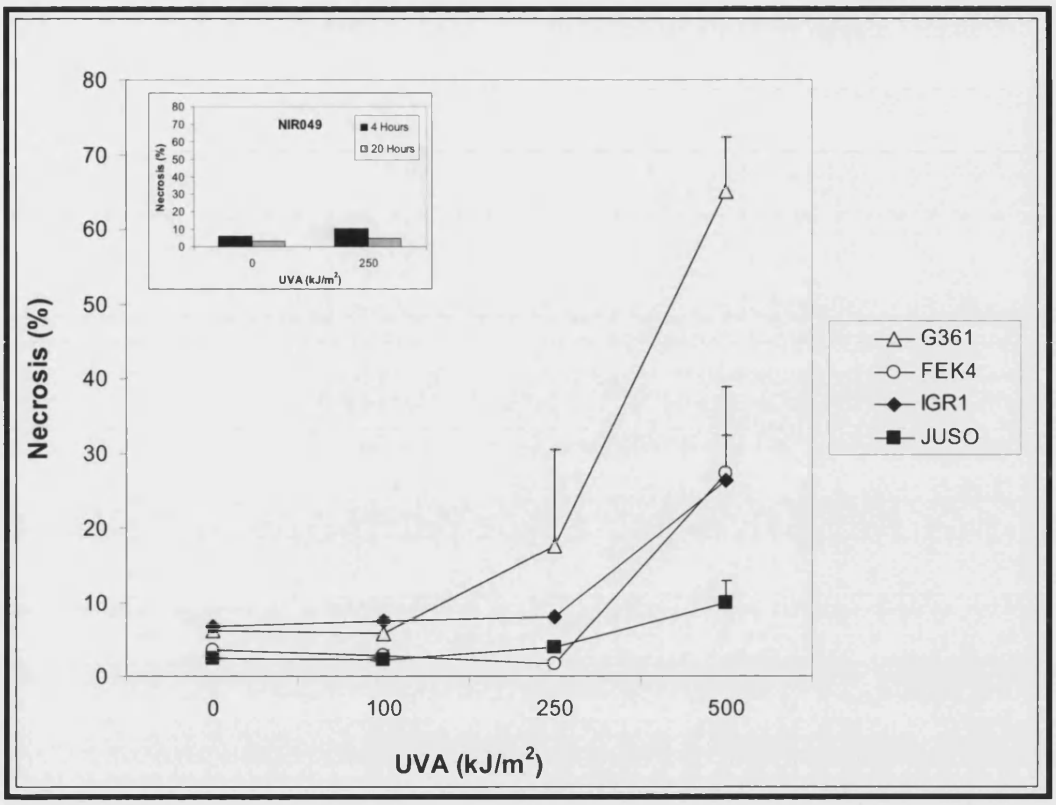


**Figure 3.30: Determination of UVA-induced necrosis**

Cells in exponential growth were irradiated with UVA at the stated dose and then incubated in conditioned media at 37°C for 20 hours. The cells were then collected and incubated in a labelling solution containing annexin V and prodidium iodide for 15 minutes (as described in section 2.13.2). The percentage of cells undergoing necrosis was determined using flow cytometry (as described in section 2.13). During acquisition and analysis, data was viewed using a two-dimensional log dot plot defined by the FL1 and FL3 fluorescent profiles. Double stained cells were considered to be necrotic (refer to figure 2.2). 10000 events were recorded for each sample. The percentage of NIR049 cells undergoing necrosis at both 4 and 20 hours after treatment was quantified. For NIR049 the percentages indicated represent one sample. For all of the other cells lines, each point represents the mean of three independent samples. For clarity only the upper error bars are shown. The error bar represents one standard deviation above mean.

**Figure 3.31: Determination of the transfection efficiency of pcDNA3.1-EGFP using Lipofectamine™ 2000**

*(Next page)*

Cells were seeded at the stated density into 6-well plates 48 - 72 hours prior to transfection. Cells were transfected with 1.5 μg of pcDNA3.1-EGFP (refer to section 2.7.3) using 3 μl of Lipofectamine™ 2000 according to the manufacturer's instructions (as described in section 2.9). The untransfected cells were treated exactly the same as the transfected cells, but were not transfected. Cells were incubated at 37°C in serum free medium containing the transfection reagent / DNA complex for 4 – 5, after which the transfection medium was replaced with fresh complete medium. The cells were then cultured for 40 - 48 hours prior to the determination of transfection efficiency. Transfection efficiency was determined by flow cytometry (as described in section 2.13.3). 10000 events were recorded for each sample. During acquisition and analysis, data was viewed using a one-dimensional log histogram plot defined by the FL1 fluorescent profile. The percentage of cells transfected was deemed to be the percentage of cells exhibiting a higher fluorescence than 98 % of the lowest fluorescing cells in the untransfected sample population (refer to figure 2.3).

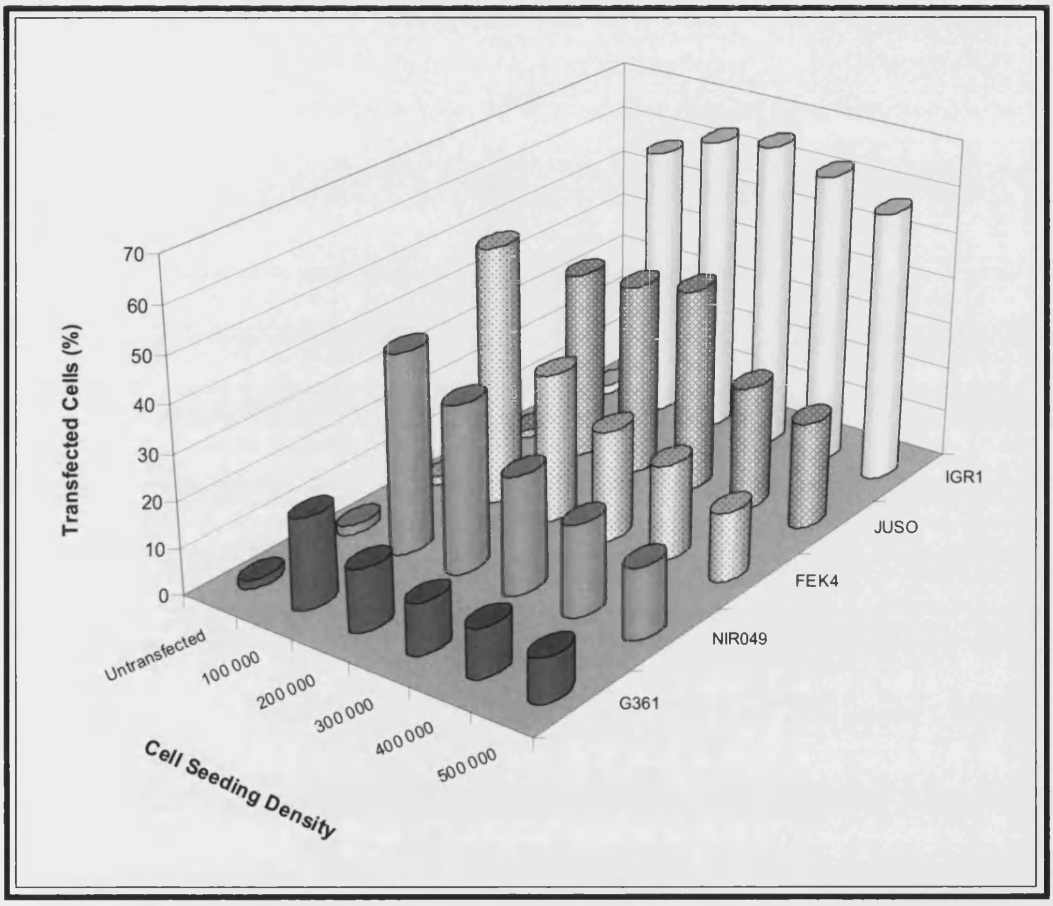
Transfected Cells (%)
70
60
50
40
30
20
10
0
Untransfected
100 000
200 000
300 000
400 000
500 000
Cell Seeding Density
G361
NIR049
FEK4
JUSO
IGR1

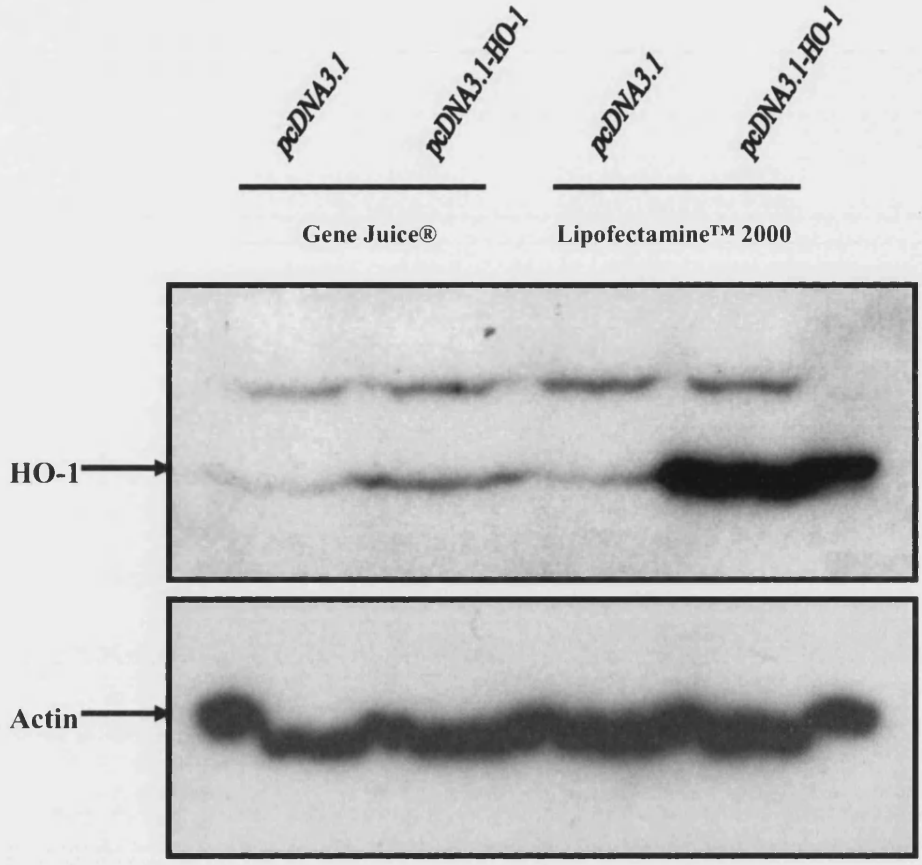


**Figure 3.32: pcDNA3.1-HO-1 mediated HO-1 over-expression in IGR1 human melanoma cells**

IGR1 human melanoma cells were transfected with either 1.5 µg of the HO-1 over-expressing construct pcDNA3.1-HO1, or the empty control vector (pcDNA3.1), using the commercially available transfection reagent GeneJuice® or Lipofectamine™ 2000 according to the manufacturer's instructions (as described in section 2.9). Cells were harvested 48 hours after transfection and whole cell extracts were prepared as described in section 2.4.1. Protein content was determined using the method of Bradford (refer to section 2.4.4). Equal amounts of protein (40 µg/lane) were analysed by SDS-PAGE and western blotting as described in Material and Methods (refer to section 2.12). After visualisation of HO-1 protein, the membrane was re-probed for actin to evaluate loading.

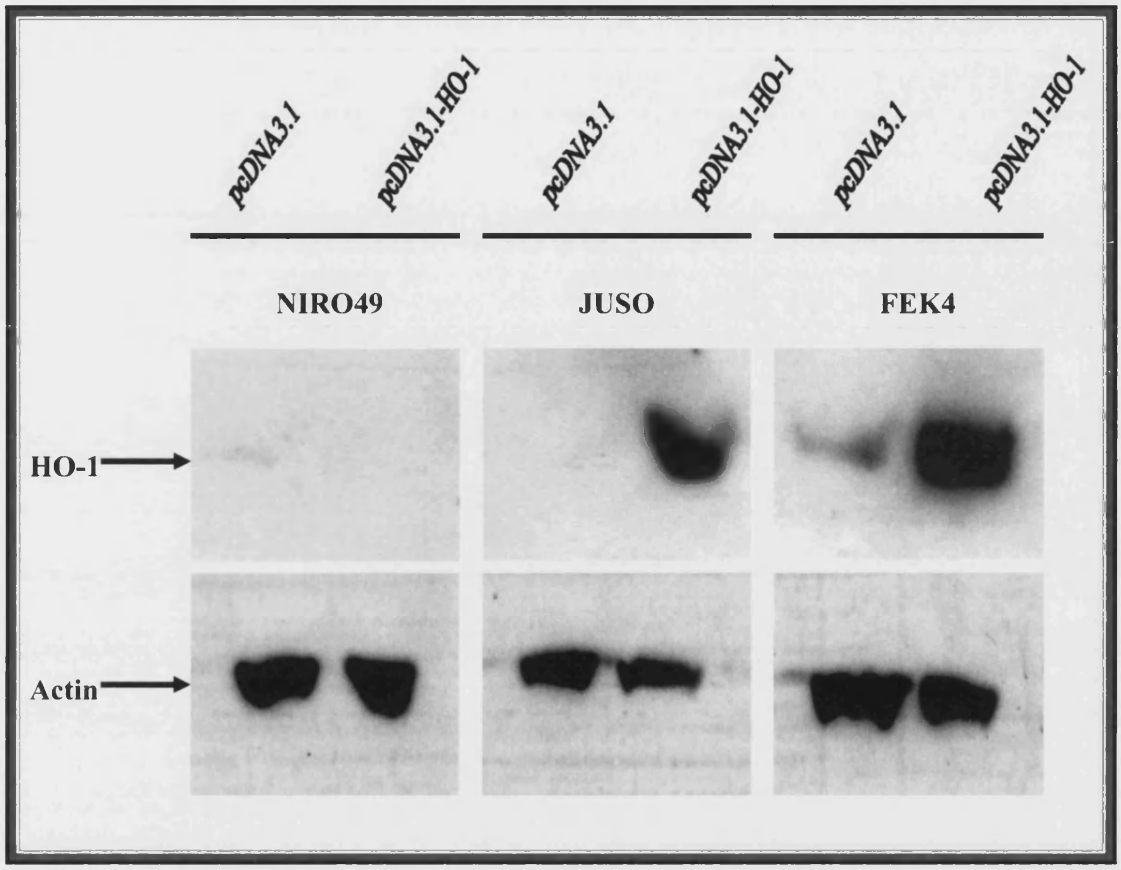


**Figure 3.33: pcDNA3.1-HO1 mediated HO-1 over-expression in NIRO49, JUSO, and FEK4 human skin cells**

Cells were transfected with either 1.0 µg of the HO-1 over-expressing construct pcDNA3.1-HO1, or the empty control vector (pcDNA3.1), using the commercially available transfection reagent Lipofectamine™ 2000 according to the manufacturer's instructions (as described in section 2.9). Cells were harvested 44 - 48 hours after transfection and whole cell extracts were prepared as described in section 2.4.1. Protein content was determined using the method of Bradford (section 2.4.4). Equal amounts of protein (10 µg/lane) were analysed by SDS-PAGE and western blotting as described in Material and Methods (refer section 2.12). After visualisation of HO-1 protein, the membrane was stripped and re-probed for actin to evaluate loading.

### 3.7.3 Determination of UVA up-regulation of HO-1 in human melanocytes and melanoma cells

As shown in section 3.7.2, JUSO human melanoma cells proved sensitive to UVA-induced apoptosis and amenable to transfection with the HO-1 over-expressing construct pcDNA3.1-HO1. This cell line was therefore selected for further investigation into the anti-apoptotic activity of HO-1 in human skin. It was hypothesised that a lack of up-regulation of the anti-apoptotic protein HO-1 may underlie the sensitivity of JUSO cells to UVA-apoptosis. The effect of UVA irradiation on HO-1 protein levels was therefore determined in this cell line. In addition to this, the effect of UVA radiation on HO-1 was also evaluated in NIR049, a cell line shown to be resistant to UVA-apoptosis.

JUSO human melanoma cells and NIR049 human melanocytes were treated with UVA (250 $kJ/m^2$) whilst in exponential growth. Following treatment, the cells were covered with conditioned media and returned to the incubator. At the stated time point, cells were harvested and whole cell extracts were prepared as described in section 2.4.1. Equal amounts of protein were analysed by SDS-PAGE and western blotting as described in section 2.12. As shown in figure 3.34, UVA irradiation (250 $kJ/m^2$) of JUSO cells resulted in a moderate increase in HO-1 protein at 24, 36, and 48 hours following treatment when compared to an unirradiated control sample. As shown in figure 3.35, strong HO-1 up-regulation was observed in human melanocytes. HO-1 protein accumulation was visualised from 4 hours following UVA treatment (250 $kJ/m^2$) of NIR049 cells. Peak HO-1 protein accumulation was observed 12 hours after UVA treatment. This experiment was independently repeated with nearly identical results. The repeat of this experiment included control and irradiated samples for two hours following treatment, both of which did not show HO-1 accumulation (data not shown).

As shown in figure 3.29, JUSO human melanoma were shown to be sensitive to late UVA-apoptosis, NIR049 human melanocytes were not. Only moderate HO-1 protein accumulation was observed in UVA treated JUSO cells, whereas strong HO-1 protein accumulation observed in NIR049 human melanocytes. Taken together, these data support the notion that HO-1 may exert some influence over apoptosis in these human skin cells.

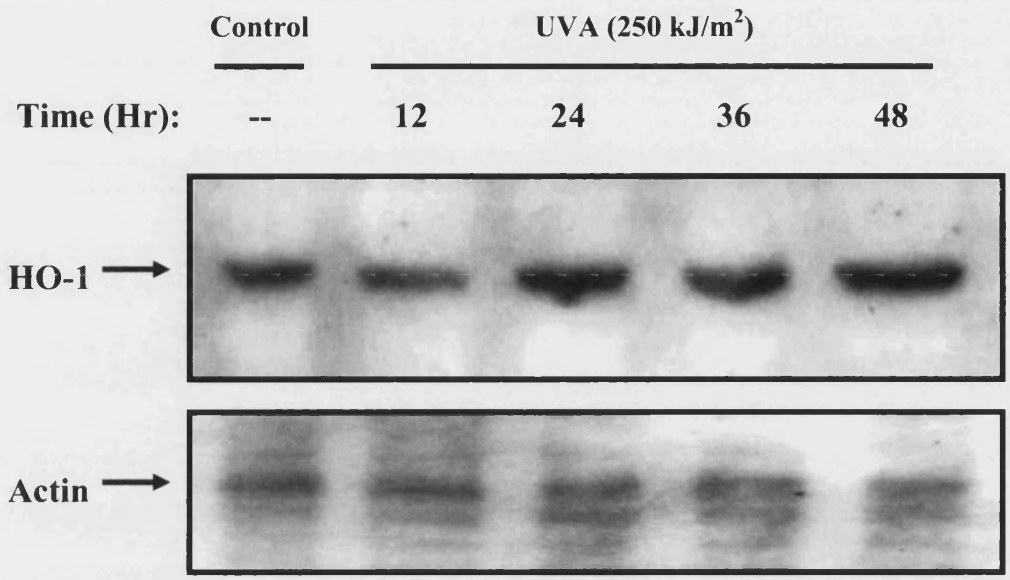


**Figure 3.34: UVA treatment causes whole cell accumulation of HO-1 protein in JUSO human melanoma cells**

JUSO human melanoma cells were treated with UVA (250 kJ/m$^2$). The cells were then incubated in conditioned media at 37°C for the indicated time period. The control sample was treated exactly the same as the UVA irradiated sample, but was not irradiated. Whole cell extracts were prepared as described in the Materials and Methods (refer to section 2.4.1). Protein concentration was determined using the method of Bradford. Equal amounts of protein (30 µg/lane) were analysed by SDS-PAGE and western blotting as described in Material and Methods (refer to section 2.12). After visualisation of HO-1 protein, the membrane was re-probed for actin to evaluate loading.

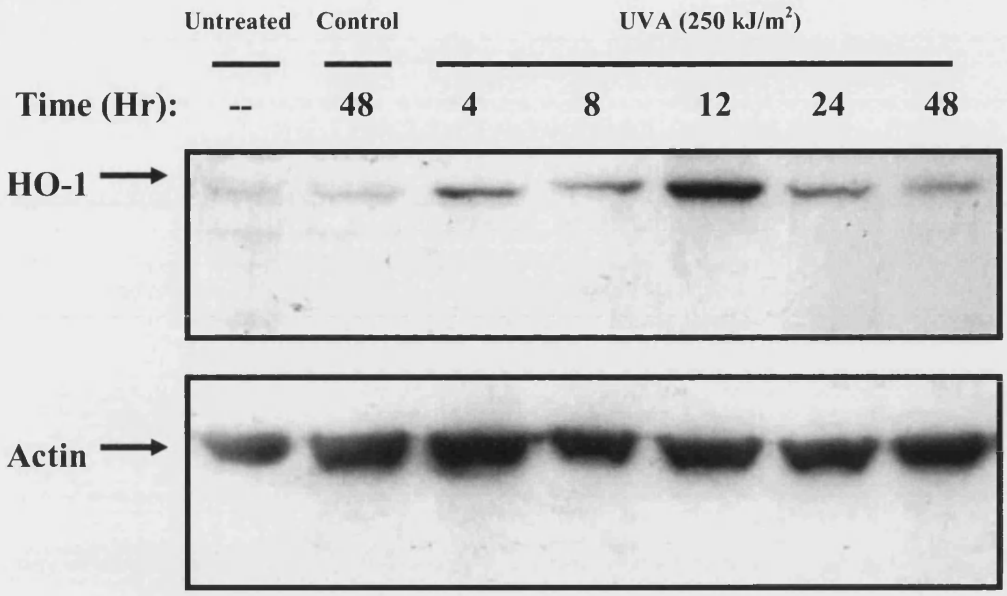


**Figure 3.35: UVA radiation causes whole cell accumulation of HO-1 protein in primary human skin melanocytes**

NIR049 human melanocytes in exponential growth were treated with UVA (250 kJ/m$^2$). The cells were then incubated in conditioned media at 37°C for the indicated time period. The control sample was treated exactly the same as the UVA irradiated sample, but was not irradiated. Whole cell extracts were prepared as described in the Materials and Methods (refer to section 2.4.1). Protein concentration was determined using the method of Bradford. Equal amounts of protein (15 µg/lane) were analysed by SDS-PAGE and western blotting as described in Material and Methods (refer section 2.12). After visualisation of HO-1 protein, the membrane was re-probed for actin to evaluate loading. This experiment was repeated with nearly identical results.

### 3.7.4 The role of HO-1 in UVA-apoptosis in JUSO human melanoma cells

Prior to the optimisation of transfection conditions, preliminary experiments were conducted using JUSO human melanoma cells to assess the involvement of HO-1 in both early and late UVA-apoptosis. JUSO cells were seeded at 1 x $10^5$ into 6-well plates 48 hours prior to transfection. Cells were then transfected with 1.5 μg of either pcDNA3.1-HO1, or the empty control vector pcDNA3.1, using 3 μl of Lipofectamine™ 2000 according to the manufacturer's instructions (as described in section 2.9). Cells were then cultured for the stated time period before UVA treatment. Following UVA treatment the cells were cultured for either 4 or 20 hours. The percentage of cells exhibiting characteristics inherent to necrosis or apoptosis was then determined by flow cytometry (as described in section 2.13). The transfection efficiency of each experiment was estimated by transfection of pcDNA3.1-EGFP into a separate cell population using the transfection conditions described above.

As shown in figure 3.36, with respect to cells transfected with the control vector pcDNA3.1, a marginal increase in early UVA-apoptosis (1.1 % to 1.5 %) was observed between unirradiated cells and UVA treated cells (400 kJ/$m^2$). Crucially, HO-1 over-expression prevented this increase in apoptosis. Virtually no change in the percentage of cells undergoing necrosis was observed in this experiment. These data indicate that HO-1 may mediate protection against early UVA-apoptosis in melanoma cells. The transfection efficiency of this experiment was approximately 36 %.

As shown in figure 3.37, JUSO cells displayed a dose-dependent increase in late UVA-apoptosis (20 hours post treatment). A moderate dose-dependent increase in UVA-necrosis was observed. Transfection of JUSO cells with the HO-1 over-expressing construct pcDNA3.1-HO1 reduced the level of apoptosis in unirradiated and irradiated cells. However, this effect was dose independent. HO-1 over-expression did not influence necrosis in this experiment. These preliminary data indicate that HO-1 may mediate protection against background apoptosis, but it is not clear whether HO-1 influences late UVA-apoptosis. The transfection efficiency of this experiment was approximately 69 %.

**Figure 3.36: Quantification of UVA induced early cell death in JUSO human melanoma cells transfected with pcDNA3.1 or pcDNA3.1-HO1**

*(Next page)*

Cells were seeded at 1 x $10^5$ into 6-well plates 48 hours prior to transfection. Cells were transfected with 1.5 µg of either pcDNA3.1-HO1 or the control vector pcDNA3.1 (refer to section 2.7). Cells were transfected using 3 µl of Lipofectamine™ 2000 according to the manufacturer's instructions (as described in section 2.9). The cells were incubated at 37°C in serum free medium containing the transfection reagent / DNA complex for 4 hours, after which the transfection medium was replaced with fresh complete medium. The cells were then cultured for 38 hours prior to UVA treatment. Following UVA treatment the cells were cultured for 4 hours. The cells were then collected and incubated in a labelling solution containing annexin V and prodidium iodide for 15 minutes (as described in section 2.13.2). The percentage of cells undergoing apoptosis and necrosis was determined using flow cytometry (as described in section 2.13). During acquisition and analysis data was viewed using a two-dimensional log dot plot defined by the FL1 and FL3 fluorescent profiles. Annexin V positive, propidium iodide negative stained cells were considered to be apoptotic, double stained cells were considered to be necrotic (refer to figure 2.2). 10000 events were recorded for each sample. The percentages represent the mean of three independent samples. The error bars represent one standard deviation above and below the mean. The transfection efficiency of this experiment was approximately 36 % as determined by transfection of pcDNA3.1-EGFP (refer to section 2.13.3). pcDNA3.1-EGFP was transfected using the same conditions used for cells transfected with pcDNA3.1 or pcDNA3.1-HO1. This experimental data can be viewed in appendix A.

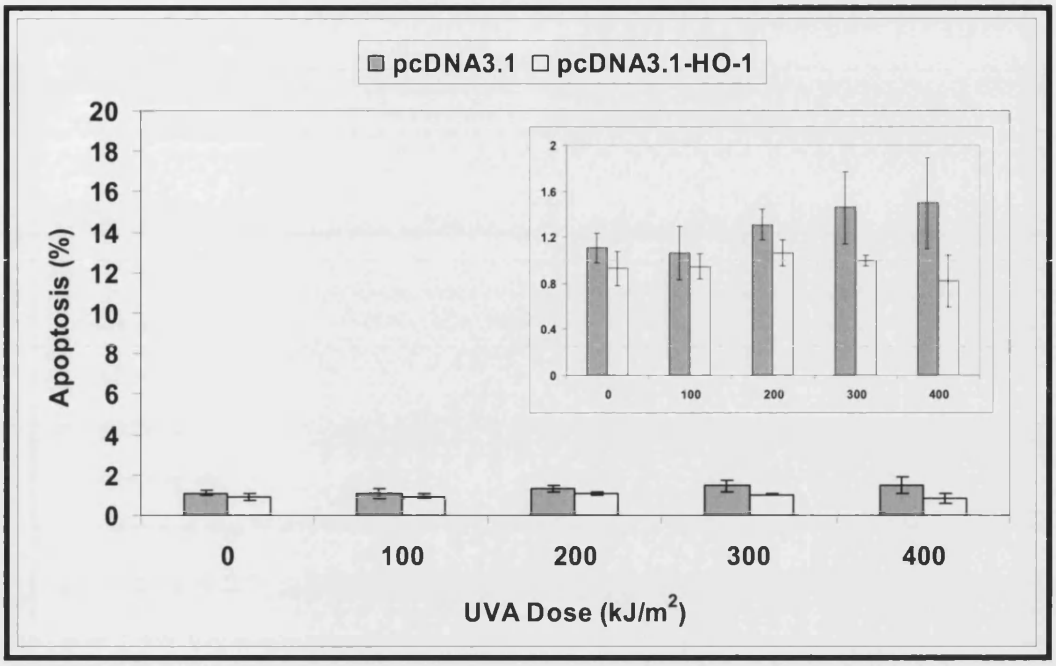
pcDNA3.1
pcDNA3.1-HO-1
Apoptosis (%)
20
18
16
14
12
10
8
6
4
2
0
0
100
200
300
400
UVA Dose (kJ/m2)
2
1.6
1.2
0.8
0.4
0
0
100
200
300
400

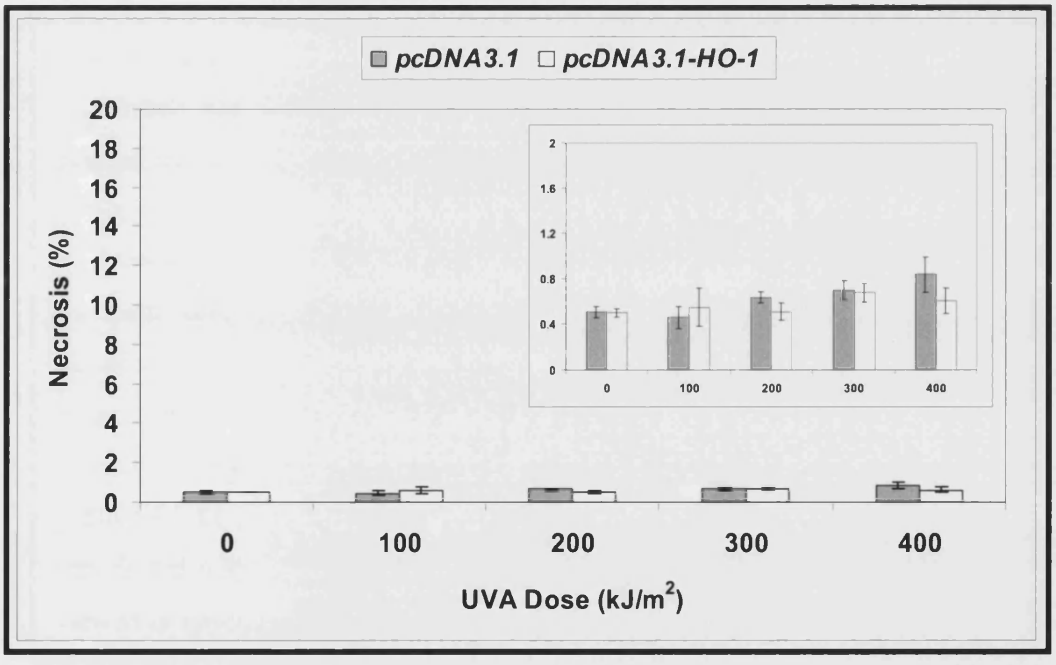
pcDNA3.1
pcDNA3.1-HO-1
Necrosis (%)
20
18
16
14
12
10
8
6
4
2
0
0
100
200
300
400
UVA Dose (kJ/m2)
2
1.6
1.2
0.8
0.4
0
0
100
200
300
400

**Figure 3.37: Quantification of UVA induced late cell death in JUSO human melanoma cells transfected with pcDNA3.1 or pcDNA3.1-HO1**

*(Next page)*

Cells were seeded at 1 x $10^5$ into 6-well plates 48 hours prior to transfection. Cells were transfected with 1.5 μg of either pcDNA3.1-HO1 or the control vector pcDNA3.1 (refer to section 2.7). Cells were transfected using 3 μl of Lipofectamine™ 2000 according to the manufacturer's instructions (as described in section 2.9). The cells were incubated at 37°C in serum free medium containing the transfection reagent / DNA complex for 6 hours, after which the transfection medium was replaced with fresh complete medium. The cells were then cultured for 20 hours prior to UVA treatment. Following UVA treatment the cells were cultured for 20 hours. The cells were then collected and incubated in a labelling solution containing annexin V and prodidium iodide for 15 minutes (as described in section 2.13.2). The percentage of cells undergoing apoptosis was determined using flow cytometry (as described in section 2.13). During acquisition and analysis data was viewed using a two-dimensional log dot plot defined by the FL1 and FL3 fluorescent profiles. Annexin V positive, propidium iodide negative stained cells were considered to be apoptotic, double stained cells were considered to be necrotic (refer to figure 2.2). 10000 events were recorded for each sample. The percentages represent the mean of three independent samples. The error bars represent one standard deviation above and below the mean. The transfection efficiency of this experiment was approximately 69 % as determined by transfection of pcDNA3.1-EGFP (refer to section 2.13.3). pcDNA3.1-EGFP was transfected using the same conditions used for cells transfected with pcDNA3.1 or pcDNA3.1-HO1. This experimental data can be viewed in appendix B.

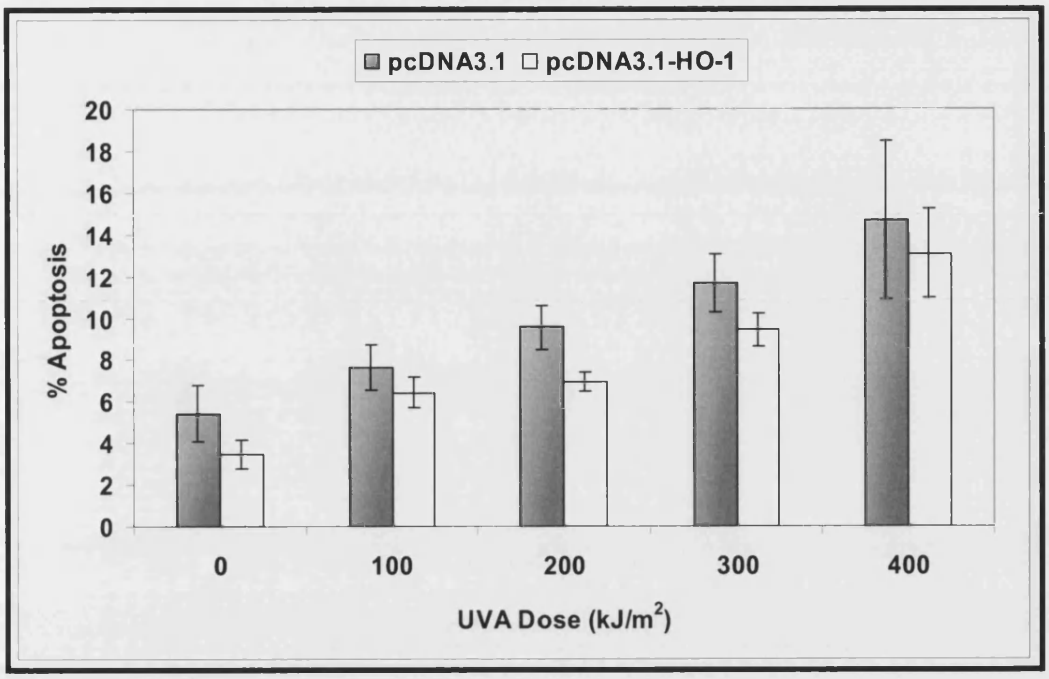
pcDNA3.1
pcDNA3.1-HO-1
% Apoptosis
20
18
16
14
12
10
8
6
4
2
0
0
100
200
300
400
UVA Dose (kJ/m2)

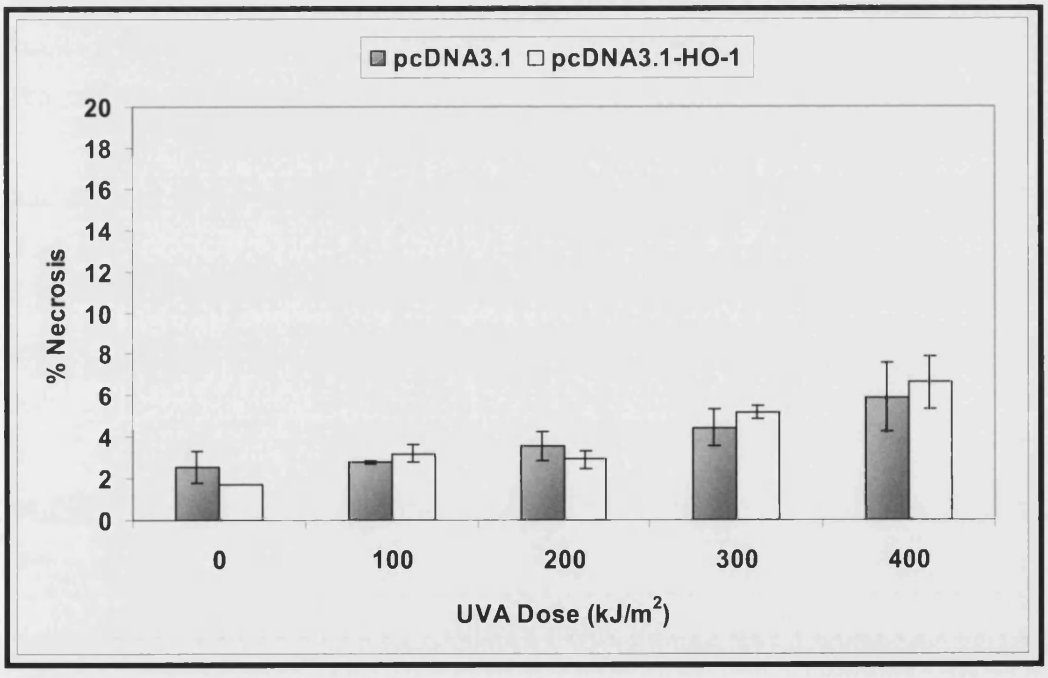
pcDNA3.1
pcDNA3.1-HO-1
% Necrosis
20
18
16
14
12
10
8
6
4
2
0
0
100
200
300
400
UVA Dose (kJ/m2)

### 3.7.5 Transfection condition optimisation

The conditions for JUSO transient transfection were optimised. JUSO cells were seeded at 1 x $10^5$ into 6-well plates. Cells in exponential growth were transfected with the stated amount of pcDNA3.1-EGFP using the commercially available transfection reagent Lipofectamine™ 2000 (as described in section 2.9). In order, to determine the optimal conditions for transfection, both the quantity of DNA, and the ratio of DNA to transfected reagent was varied. For all conditions the transfection efficiency was determined by flow cytometry after 20 hours, and after 44 hours. The percentage of cells transfected was considered to be the percentage of cells exhibiting greater fluorescence than 98 % of the lowest fluorescing cells transfected with 0 μg of DNA (refer to figure 2.3). Prior to analysis by flow cytometry, the percentage of cells attached to the dish was used to estimate the percentage of surviving cells for each transfection condition. The percentage of cells transfected was consistently observed to be greater at 20 hours opposed to 44 hours after transfection. As shown in figure 3.38, 2 μg of DNA transfected using 4 μl of Lipofectamine™ 2000 resulted in the greatest percentage of transfected cells. These conditions resulted in a transfection efficiency of approximately 70 %. Approximately 75 % of cells survived to the point of analysis using these conditions.

The size of a construct is known to influence transfection efficiency, and an increase in transfection efficiency is known to correlate with increased cytotoxicity. Therefore, the possibility of a difference between the transfection efficiency of the control vector pcDNA3.1, and the HO-1 over-expressing vector pcDNA3.1-HO1 was investigated. It was determined whether such a discrepancy could underlie the reduced apoptosis observed in cells transfected with the larger HO-1 over-expressing construct. Cells were co-transfected with the smaller control construct (pcDNA3.1), or with the larger HO-1 over-expressing construct (pcDNA3.1-HO1), in combination with the green fluorescent protein over-expressing construct pcDNA3.1-EGFP.

JUSO cells were seeded at 1 x $10^5$ into 6-well plates 48 hours prior to transfection. Cells in exponential growth were transfected with either pcDNA3.1-EGFP only, or, with 1 μg of pcDNA3.1-EGFP combined with 1 μg of pcDNA3.1 or pcDNA3.1-HO1. Cells were transfected using the commercially available transfection reagent Lipofectamine™ 2000 according to the manufacturer's instructions (as described in section 2.9). The cells were cultured for 20 hours prior to

determination of transfection efficiency. Transfection efficiency was determined by flow cytometry as described previously (refer to figure 2.3). As shown in figure 3.39, the percentage of JUSO cells transfected with the green fluorescent protein over-expressing construct pcDNA3.1-EGFP was not influenced by the presence of either pcDNA3.1 or pcDNA3.1-HO1. These data show that a difference in transfection efficiency resulting from a difference in construct size does not underlie the protection against apoptosis mediated by the HO-1 over-expressing construct pcDNA3.1-HO1.

**Figure 3.38: Optimisation of the conditions required for transient transfection of JUSO human melanoma cells**

*(next page)*

Cells were seeded at 1 x $10^5$ into 6-well plates. Cells in exponential growth were transfected with the stated amount of pcDNA3.1-EGFP (0 – 3 μg) using the commercially available transfection reagent Lipofectamine™ 2000 according to the manufacturer's instructions (as described in section 2.9). To determine the optimal conditions for transfection, both the quantity of DNA, and the ratio of DNA to transfection reagent was varied. The cells were incubated at 37°C in serum free medium containing the transfection reagent / DNA complex for 5 hours, after which the transfection medium was replaced with fresh complete medium. The cells were then cultured for either 20 or 44 hours. Transfection efficiency was determined by flow cytometry (as described in section 2.13.3). 10000 events were recorded for each sample. During acquisition and analysis data was viewed using a one-dimensional log histogram plot defined by the FL1 fluorescent profile. The percentage of cells transfected was considered to be the percentage of cells exhibiting a higher fluorescence than 98 % of the lowest fluorescing cells in the cells transfected with 0 μg of DNA (refer to figure 2.3). The percentage of cells surviving at the point of analysis (20 hours only) was determined by visualisation of the percentage of cells attached to the dish.

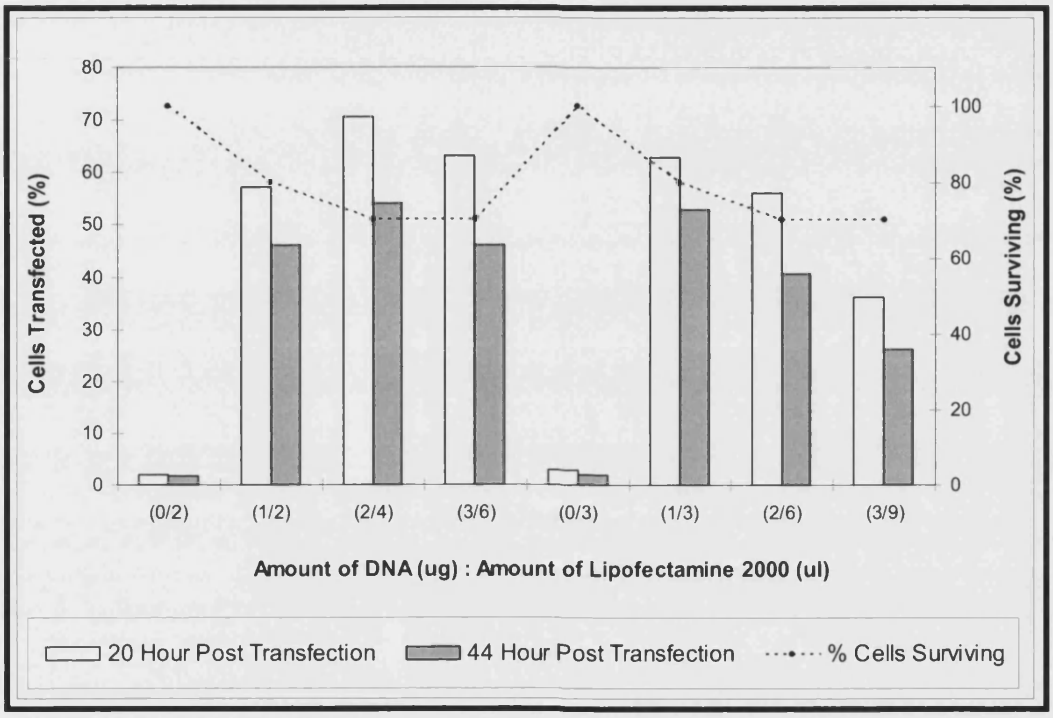
80
70
60
50
40
30
20
10
0
Cells Transfected (%)
100
80
60
40
20
0
Cells Surviving (%)
(0/2)
(1/2)
(2/4)
(3/6)
(0/3)
(1/3)
(2/6)
(3/9)
Amount of DNA (ug) : Amount of Lipofectamine 2000 (ul)
20 Hour Post Transfection
44 Hour Post Transfection
% Cells Surviving

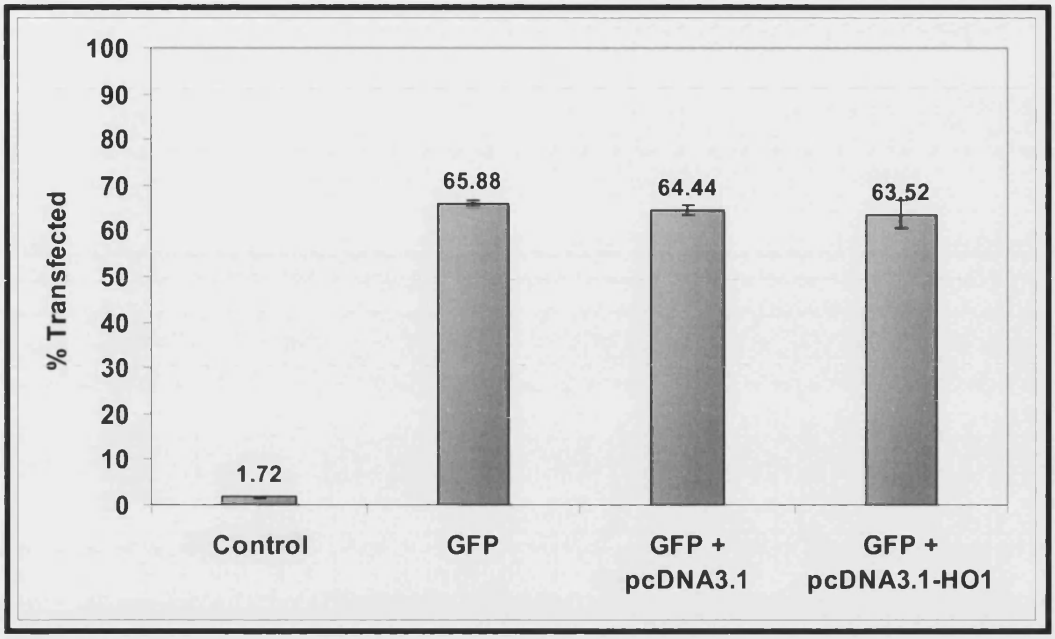


**Figure 3.39: Co-transfection of pcDNA3.1 or pcDNA3.1-HO1 with pcDNA3.1-EGFP**

Cells were seeded at 1 x $10^5$ into 6-well plates 48 hours prior to transfection. Cells in exponential growth were transfected with either 1 µg of pcDNA3.1-EGFP only, or, with 1 µg of pcDNA3.1-EGFP combined with 1 µg of pcDNA3.1 or pcDNA3.1-HO1. Cells were transfected using the commercially available transfection reagent Lipofectamine™ 2000 according to the manufacturer's instructions (as described in section 2.9). The cells were incubated at 37°C in serum free medium containing the transfection reagent / DNA complex for 4 hours, after which the transfection medium was replaced with fresh complete medium. The cells were then cultured for 20 hours prior to determination of transfection efficiency. Transfection efficiency was determined by flow cytometry (as described in section 2.13.3). 10000 events were recorded for each sample. During acquisition and analysis data was viewed using a one-dimensional log histogram plot defined by the FL1 fluorescent profile. The percentage of cells transfected was considered to be the percentage of cells exhibiting a higher fluorescence than 98 % of the lowest fluorescing cells in cells transfected with 0 µg of DNA (refer to figure 2.3). The percentages represent the mean of three independent samples. The error bars represent one standard deviation above and below the mean.

### 3.7.6 The role of HO-1 in late UVA-apoptosis in JUSO melanoma cells

Determination of the time point at which peak UVA-induced apoptosis occurs in JUSO human melanoma cells was attempted by means of nuclear blebbing. However, experimental complications were encountered. Therefore, using optimised transfection conditions (refer figure 3.38), the effect of HO-1 over-expression on late UVA-apoptosis was determined at the time point at which considerable UVA-apoptosis was observed previously (approximately 20 hours). Cells were seeded at 1 x $10^5$ into 6-well plates 48 hours prior to transfection. Cells were transfected with 2.0 µg of either pcDNA3.1-HO1 or the control vector pcDNA3.1. Cells were transfected using 4 µl of Lipofectamine™ 2000 according to the manufacturer's instructions (as described in section 2.9). The cells were then cultured for 20 hours prior to irradiation. Following UVA treatment the cells were cultured for 22 hours. The cells were then collected and incubated in a labelling solution containing annexin V and prodidium iodide for 15 minutes (as described in section 2.13.2). The percentage of cells exhibiting characteristics inherent to apoptosis and necrosis was determined by flow cytometry (as described in section 2.13). Annexin V positive, propidium iodide negative stained cells were considered to be apoptotic, double stained cells were considered to be necrotic (refer to figure 2.2). The transfection efficiency of this experiment was shown to be approximately 69 %.

As shown in figure 3.40, a dose dependent increase in late UVA-apoptosis was not observed in untransfected cells in this experiment. Only transfected cells proved sensitive to UVA irradiation. With respect to cells transfected with the control construct pcDNA3.1, a dose-dependent increase in UVA-apoptosis was observed. Crucially, transfection with the HO-1 over-expressing construct pcDNA3.1-HO1 abolished this dose dependent increase in late UVA-apoptosis. HO-1 over-expression did not influence necrosis. These data indicate that HO-1 over-expression confers protection against apoptosis in JUSO human melanoma cells. However, it is unclear whether HO-1 confers resistance to late UVA-apoptosis, or whether HO-1 confers resistance to the cytotoxicity associated with cationic transfection reagents.

**Figure 3.40: Quantification of late UVA-induced cell death in JUSO human melanoma cells transfected with pcDNA3.1 or pcDNA3.1-HO1 (optimised conditions)**

*(Next page)*

Cells were seeded at 1 x $10^5$ into 6-well plates 48 hours prior to transfection. Cells were transfected with 2.0 µg of pcDNA3.1-HO1 or the empty control vector pcDNA3.1. Cells were transfected using 4 µl of Lipofectamine™ 2000 according to the manufacturer's instructions (as described in section 2.9). The cells were incubated at 37°C in serum free medium containing the transfection reagent / DNA complex for 4 hours, after which the transfection medium was replaced with fresh complete medium. The cells were then cultured for 20 hours prior to irradiation. Following UVA treatment cells were cultured for 22 hours. After 22 hours the cells were collected and incubated in a labelling solution containing annexin V and prodidium iodide for 15 minutes (as described in section 2.13.2). The percentage of cells undergoing apoptosis was determined by flow cytometry (as described in section 2.13). During acquisition and analysis data was viewed using a two-dimensional log dot plot defined by the FL1 and FL3 fluorescent profiles. Annexin V positive, propidium iodide negative stained cells were considered to be apoptotic, double stained cells were considered to be necrotic (refer to figure 2.2). 10000 events were recorded for each sample. The percentages represent the mean of two independent samples. The error bars represent one standard deviation above and below the mean. The transfection efficiency of this experiment was approximately 69 % as determined by transfection of pcDNA3.1-EGFP and quantification by flow cytometry. (refer to section 2.13.3). pcDNA3.1-EGFP was transfected using the conditions used for cells transfected with pcDNA3.1 or pcDNA3.1-HO1. A one-way analysis of variance (ANOVA) was used to test the significance between control transfected (pcDNA3.1) and HO-1 transfected cells (pcDNA3.1-HO-1). A $p$ value of less than 0.05 was considered to be significant [$p < 0.05$ (*), $p < 0.01$ (**), $p = 0.001$ (***)]. This experimental data can be viewed in appendix C.

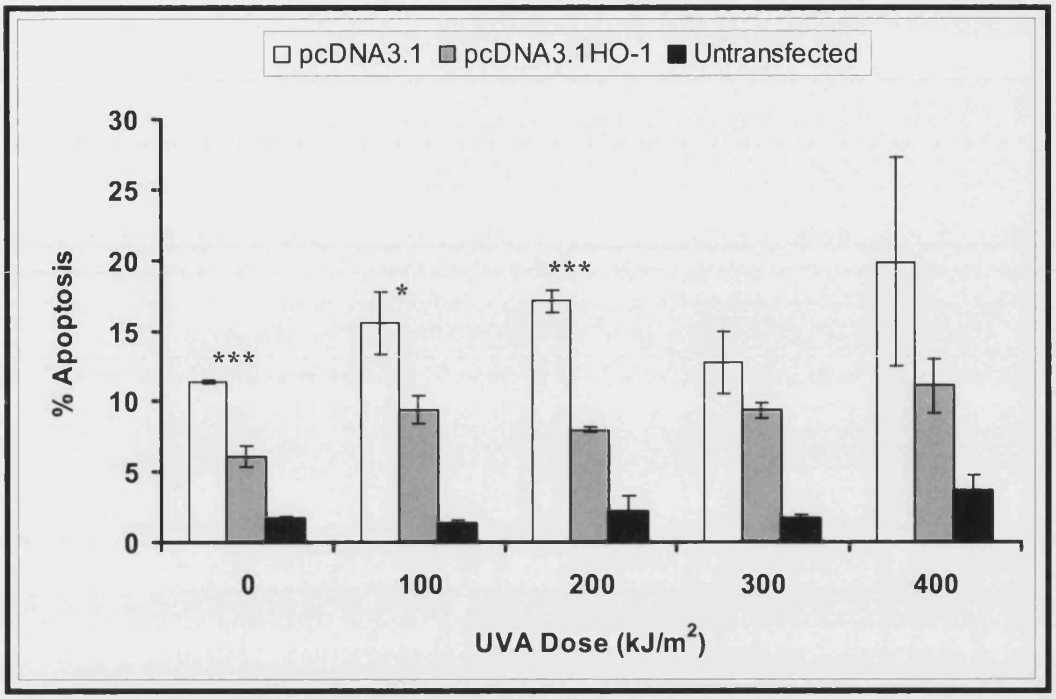
pcDNA3.1
pcDNA3.1HO-1
Untransfected
% Apoptosis
30
25
20
15
10
5
0
***
*
***
0
100
200
300
400
UVA Dose (kJ/m2)

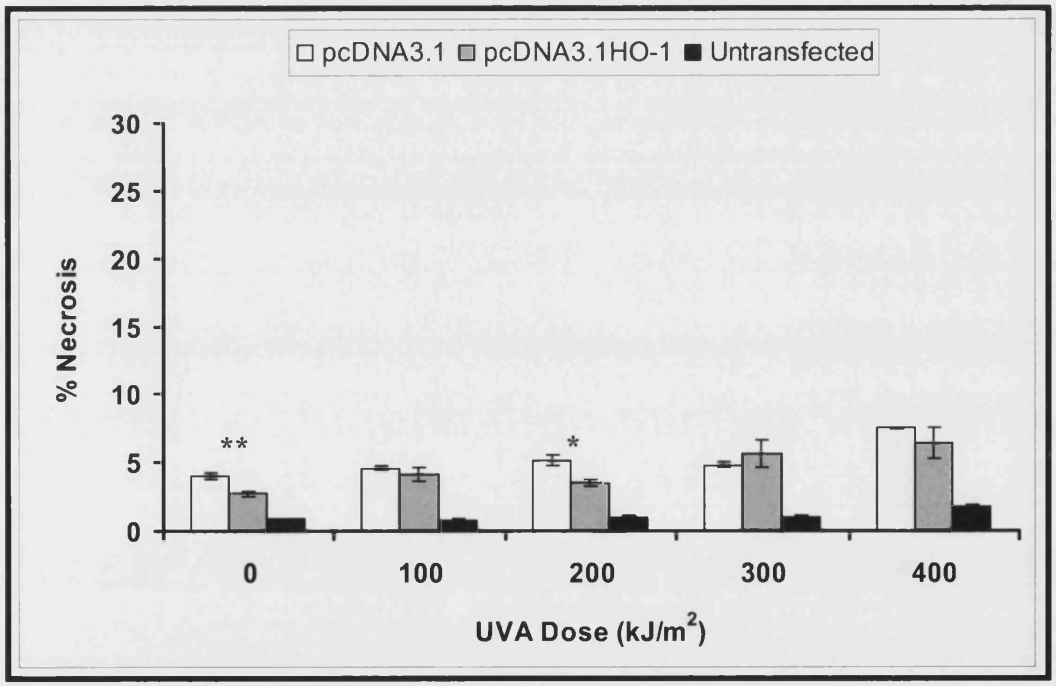
pcDNA3.1
pcDNA3.1HO-1
Untransfected
% Necrosis
30
25
20
15
10
5
0
**
*
0
100
200
300
400
UVA Dose (kJ/m2)

# 4. Discussion

## 4. Discussion

This study has examined the effect of UVA radiation on the transcription factor Nrf2 in human skin fibroblasts. UVA activation of Nrf2 has been shown by this study; this has been attributed to three regulatory mechanisms: enhanced nuclear localisation of Nrf2, accumulation of Nrf2 as a result of UVA-induced heme release, and *NRF2* gene activation. Moreover, in this study the implications of UVA activation of Nrf2 have been investigated. Nrf2 is known to bind to *cis*-acting elements termed MARE (Maf associated recognition elements) within the promoter region of phase II detoxification enzymes and antioxidant proteins. One example is the UVA up-regulated enzyme HO-1. In this study data have been provided indicating that HO-1 modulates apoptosis in human melanoma cells. It is proposed that the anti-apoptotic influence of HO-1 may be dependent on Nrf2 in human skin.

The UVA component of sunlight is considered to be the primary source of oxidative stress to human skin and has been implicated in the pathogenesis of skin aging and cancer. In relation to this, the transcription factor Nrf2 has been shown to be central to the cellular response to oxidative stress. Studies have shown that the cytoplasmic actin-binding protein Keap1 acts as a sensor of oxidative and electrophilic stress, and plays the co-ordinating role in the Nrf2 stress response mechanism. In this study the hypothesis that UVA modulates Nrf2 nuclear availability through the generation of reactive oxygen species (ROS) has been explored.

The ROS singlet oxygen ($^1O_2$) is widely regarded as the primary effector in UVA-regulated gene expression. Here, the effect of UVA-generated $^1O_2$ on the sub-cellular localisation of Nrf2 has been investigated. Results were obtained showing that UVA treatment of primary human skin fibroblasts bathed in $H_2O$ resulted in cytoplasmic accumulation of Nrf2. However, when cells were irradiated whilst bathed in the $^1O_2$ lifetime enhancer $D_2O$, Nrf2 did not accumulate in the cytoplasm. Singlet oxygen is known to activate various protein kinases (for review see: Ryter and Tyrrell, 1998). Moreover, Nrf2 is known to be released from its cytoplasmic anchor protein Keap1 and translocate into the nucleus in response to phosphorylation at $Ser^{40}$ (Bloom and Jaiswal, 2003). Thus, it is conceivable that irradiation of primary human skin fibroblasts whilst bathed in the $^1O_2$ lifetime enhancer $D_2O$ may result in

phosphorylation and nuclear localisation of Nrf2. A study published after the start of this investigation has provided support to the notion that UVA-generated $^1O_2$ augments Nrf2 nuclear localisation. Hirota *et al.*, (2005) documented that UVA, but not UVB, increased nuclear accumulation of Nrf2 in mouse dermal fibroblasts. Hirota and co-workers also demonstrated that UVA-induced nuclear accumulation of Nrf2 was enhanced in a concentration-dependent manner in mouse dermal fibroblasts treated with the $^1O_2$ generating compound hematoporphyrin. In contrast to this, the results of the present study have shown that $D_2O$ treatment does not affect the amount of nuclear Nrf2. Keap1 is known to have 27 reactive cysteine residues. Several studies have shown that oxidation of cysteine residues 151, 273, and 288 prevents Keap1 acting as a substrate adaptor for Cullin3 containing ubiquitin ligases which mark Nrf2 for proteasome attention (for review see: Zhang, 2006). The reduced accumulation of cytoplasmic Nrf2 observed during this investigation contradicts the notion of ROS-mediated enhanced nuclear translocation of Nrf2, and indicates that $^1O_2$ may in fact promote degradation of cytoplasmic Nrf2. However, further work is required to fully elucidate the effect of UVA-generated ROS on Nrf2.

The effect of UVA on Nrf2 accumulation has also been investigated by this study. Recent data from a murine model has shown that heme stabilises Nrf2 (Alam *et al.*, 2003). In relation to this, a study has shown that UVA releases heme from microsomal heme-proteins (Kvam *et al.*, 1999). It has been investigated by the present study whether UVA treatment of FEK4 fibroblasts results in accumulation of Nrf2, and if so, whether this effect is dependent on heme. Here, it has been shown that treatment of primary human fibroblasts with a physiologically relevant dose of UVA (250 kJ/m$^2$) results in whole cell accumulation of Nrf2. It is shown that this effect is immediate (1 hour post irradiation), that the level of total Nrf2 continues to accumulate for at least 4 hours following UVA treatment, and that the level of Nrf2 remains elevated for up to 12 hours following UVA treatment. Treatment of primary human fibroblasts with heme also resulted in Nrf2 whole cell accumulation. Furthermore, treatment with a heme synthesis inhibitor prior to irradiation resulted in decreased UVA-mediated Nrf2 accumulation. These data indicate that UVA stabilises the transcription factor Nrf2, and are consistent with the interpretation that this effect is dependent on the pro-oxidant HO-1 substrate, heme. A concern of this study has been to elucidate the mechanism underlying UVA regulation of *HMOX1*. Kvam *et al.*, (1999) observed a clear correlation between the amount of heme released

in response to UVA treatment of FEK4 cells, and subsequent accumulation of HO-1 mRNA. These data, taken together with the findings of the present study, advocate the hypothesis that UVA up-regulation of *HMOX1* may be the result of UVA-released heme stabilising the transcription factor Nrf2.

Studies have shown that in un-stimulated cells Nrf2 is expressed at a constitutive level but is rapidly degraded by the ubiquitin-proteasome proteolysis system (Itoh *et al.*, 2003; Kobayashi *et al.*, 2006; Nguyen *et al.*, 2003; McMahon *et al.*, 2003; Sekhar *et al.*, 2002; Stewart *et al.*, 2003; Zhang and Hannink, 2003); a pathway that is known to regulate the activity of other transcription factors, such as, p53, c-Fos, c-Jun, NF-κB, and STAT1 (for review see: Hershko and Ciechanover, 1998). Previous studies have proved that it is interference with the Nrf2 degradation pathway that permits Nrf2 accumulation, and furthermore, that the stability of Nrf2 is dependent on its association with the cytoplasmic 'anchor' protein Keap1. It is possible that the stabilisation of Nrf2 by heme observed by this study is an effect that is dependent on ROS-mediated dissociation of Nrf2 from Keap1. The *HMOX1* inducers cadmium, arsenite, and heme have all been shown to promote Nrf2 stability (Alam *et al.*, 2003; Stewart *et al.*, 2003). Crucially, all of these structurally distinct agents have the ability to generate oxidative stress. It is therefore likely that it is ROS generated in the presence of these agents that confers increased stability of Nrf2 by promoting the dissociation of Nrf2 from Keap1 or by preventing Keap1 acting as a substrate adaptor for ubiquitin ligases.

In the present study, enhanced nuclear accumulation of Nrf2 was observed in response to UVA treatment. However, by means of western blotting, cytoplasmic Nrf2 was barely detectable. With respect to murine cells, this is an observation made by another research group (Alam *et al.*, 2003). At present the mechanism by which Nrf2 is transported into the nucleus remains largely uncharacterised. The lack of accumulation of Nrf2 in the cytoplasm observed by the present study is evidence that Nrf2 is constitutively and rapidly transported into the nucleus in response to dissociation from Keap1. Based on the findings of the present study, it is hypothesised that, in response to UVA treatment of human skin fibroblasts, a molecular regulatory system exists where ROS generated by the UVA chromophore heme promote dissociation of Nrf2 from Keap1 and / or prevent Keap1 acting as a substrate adaptor for ubquitin ligases. Keap1 homodimers will therefore become saturated with existing Nrf2 and allow newly synthesised Nrf2 to exist in a free state.

The net result of these processes will be accumulation of Nrf2 within the nucleus and activation phase II genes.

Using real time RT-PCR, the effect of UVA on *NRF2* gene activation was investigated in human skin fibroblasts. Rhythmic low frequency oscillations were observed in the level of Nrf2 mRNA in both control and UVA treated cells. UVA treatment disrupted these oscillations. The amount of accumulated Nrf2 mRNA was lower in UVA treated cells than in control cells for between 1 and 4 hours immediately following irradiation. After 4 hours, the amount of Nrf2 mRNA was increased up to 2-fold in the UVA treated cells compared to the control treated cells. To the best of our knowledge this is the first study to document oscillations in *NRF2* expression and indicates that *NRF2* may autoregulate expression. Evidence of *nrf2* autoregulation was recently published. Treatment of murine keratinocytes with the anti-carcinogen 3*H*-1,2-dithiole-3-thione (D3T) was shown to result in a 2-fold increase in Nrf2 mRNA levels (Kwak *et al.*, 2002). Kwak and co-workers examined the transcriptional activation of *nrf2* by D3T and located two ARE-like sequences in the murine *nrf2* promoter. Using a full-length promoter reporter construct, Kwak and co-workers demonstrated that these ARE-like sequences were required for *nrf2* gene activation by D3T. Moreover, by chromatin immunoprecipitation assay, this study showed direct binding of Nrf2 to its own promoter. A search of the human *NRF2* promoter by the present study has identified that the ARE-like sequences required for D3T activation of *nrf2* are conserved between these two species. With respect to the *NRF2* promoter, these sequences are situated approximately 3.8 and 4.0 kb upstream of the *NRF2* start codon. The present study has also identified sequences in the *NRF2* promoter situated approximately 5.8 and 6.0 kb upstream of the *NRF2* transcriptional start site that closely resemble the MARE consensus sequence. The mechanism of autoregulation of gene expression has been documented in the case of other transcription factors. NF-κB is known to positively regulate its transcription by means of binding to a regulatory element within its promoter (Liptay *et al.*, 1994). Moreover, the transcription factors c-Jun and c-Fos autoregulate expression (Angel *et al.*, 1998; Verma and Sassone-Corsi, 1987). It therefore seems likely that Nrf2 may regulate its expression through *cis*-acting elements in its promoter. Nrf2 accumulation by UVA has been observed in this study. Therefore, the delayed Nrf2 mRNA accumulation following UVA treatment may be symptomatic of UVA stabilisation of Nrf2 which subsequently serves to up-regulate *NRF2* gene activation

through binding to its own promoter. Nrf2 autoregulation may therefore be indicative of a biological mechanism to extend activation of phase II genes. The observation that the level of *NRF2* gene activation is reduced immediately following UVA treatment may be indicative of a separate effect. Sunlight, particularly blue light (420-440 nm), is known to re-set circadian genes (Newman *et al.*, 2003). UVA (320-400 nm) may exert a similar influence. Hence, reduced *NRF2* gene activation immediately following UVA treatment denotes that *NRF2* may exhibit a "circadian trait".

A primary concern of this study has been to provide insight into UVA regulation of *HMOX1*. The observations made by this, and other studies, has now allowed a model for UVA activation of *HMOX1* to be envisaged. As stated, it is known that UVA treatment of primary human skin fibroblasts leads to an immediate release of the HO-1 substrate heme from microsomal heme-proteins (Kvam *et al.*, 1999). Furthermore, Kvam *et al.*, (1999) observed a high degree of correlation between the amount of heme released and the subsequent degree of activation of *HMOX1*. In addition, a study has shown that $^1O_2$ is a major effector in UVA up-regulation of *HMOX1* (Basu-Modak and Tyrrell, 1993). The results of the present study have allowed a regulatory system to be envisaged in human skin where UVA generated ROS and UVA released heme up-regulate *HMOX1* by means of Nrf2.

Searches of human chromosome 22 (Raval and Tyrrell, unpublished observations) have identified two MARE sites upstream of the *HMOX1* transcriptional start site. MARE sites are known to be recognised and bound by heterodimers comprising of a small Maf protein and a CNC-bZIP protein. Heterodimers comprising of a small Maf protein and Nrf2 have been shown to activate the HO-1 gene. Heterodimers comprising of a small Maf protein and Bach1 have been shown to negatively regulate the HO-1 gene. In the present study, findings have been presented consistent with the idea that UVA stabilises Nrf2 through the release of heme. Interestingly, Bach1 is a heme binding protein, and the DNA binding activity of Bach1 has been shown to be negatively regulated by heme binding *in vitro* (Ogawa *et al.*, 2001). Moreover, a more recent investigation has shown that Bach-1 is titrated away from the HO-1 promoter and undergoes nuclear export in the presence of the HO-1 substrate heme (Suzuki *et al.*, 2004). Taken altogether, the findings of this and other studies indicate that heme may act as a signalling molecule for MARE-driven gene expression. Heme may act as a molecular switch for UVA-

regulation of the *HMOX1* locus, modulating activity of both the activator and repressor in an elegant eukaryote regulatory system analogous to the *lac* operon.

In cells that have not been irradiated, a model has been proposed where repressor protein complexes such as Bach1-Maf heterodimers occupy MARE sites in enhancer regions upstream of the HO-1 transcriptional start site in favour of activating protein complexes such as Nrf2-Maf heterodimers. In this model the repressor protein complex activity will be dominant over the activating protein complexes for two reasons. Firstly, a Bach1-Maf heterodimer is likely to be more stable and have a higher affinity for DNA than an Nrf2 containing heterodimer; and secondly, proteins with potent transcriptional activation domains are highly unstable and possess very short half-lives when compared to DNA-binding proteins that lack such domains (Alam *et al.*, 2003; Hershko and Ciechanover, 1998; Stewart *et al.*, 2003). Therefore, it is likely that under basal (reducing) physiological conditions, the HO-1 upstream MARE sites will be occupied by Bach1-Maf heterodimers that either through direct steric blocking, or through the enlistment of co-repressors, will prevent assembly of the pre-transcription complex. In this situation HO-1 transcription will cease completely, or only a very low level of gene expression will be observed. In a stimulated cell system, it is likely that Nrf2-Maf heterodimers will occupy the *HMOX1* upstream MARE sites. In this situation Nrf2 will interact directly and indirectly to increase recruitment of transcription machinery such as co-activators which will ultimately sponsor the recruitment of RNA pol II. In this model for UVA activation of *HMOX1*, heme will play the co-ordinating role in the dynamic exchange between these activating and repressing protein complexes (refer to figure 4.1). Heme released from heme-containing proteins in response to UVA will titrate repressive Bach1-Maf complexes away from MARE within the HO-1 promoter region and promote the nuclear export of Bach1. Concurrently, UVA-released heme will promote stabilisation of Nrf2, therefore enhancing nuclear accumulation of activating Nrf2-Maf heterodimers.

In the present study data have been produced consistent with the interpretation that UVA generated $^1O_2$ modulates the amount of cytoplasmic Nrf2. This effect may be indicative of $^1O_2$ promoting nuclear translocation of Nrf2 which may in itself promote stabilisation of Nrf2 by decreasing the proximity of the transcription factor to proteasome degradation machinery. Accordingly, it is important to state that the role of heme and ROS may not be mutually exclusive. In the same way as heme, ROS

may stabilise Nrf2 through decreasing the probability of ubiquitination; and likewise, the stabilising effect of heme released by UVA may be attributable to heme generated ROS. In relation to this, cadmium and heme, both of which are pro-oxidant and strong inducers of *HMOX1*, have been shown to induce nuclear export of the repressor protein Bach1. Bach1 is redox sensitive owing to the presence of cysteine thiol residues in its DNA binding domain. Hence, it is reasonable to hypothesise that nuclear export of Bach1 is dependent on redox state, and that UVA generated ROS may induce export of this *HMOX1* repressor. Therefore, UVA up-regulation of *HMOX1* may involve a simple feedback loop dependant on intracellular levels of the HO-1 substrate heme; up-regulation that is further enhanced as a result of UVA generated ROS. The net effect of this dynamic protein exchange will be rapid transcriptional up-regulation of the HO-1 gene and accumulation of the enzyme which will then remove the pro-oxidant heme.

**Figure 4.1: Diagrammatic representation of the proposed molecular regulatory system of *HMOX1* by UVA**

*(next page)*

The schematic depicts the regulation of *HMOX1* by UVA. In this model the HO-1 substrate heme plays the co-ordinating role. Under basal physiological conditions, Bach1-MafK heterodimers occupy upstream enhancer elements preventing assembly of the pre-transcription complex. UVA irradiation causes an immediate release of heme from heme containing proteins. In the presence of heme, the heme binding protein Bach1 is titrated away from the *HMOX1* promoter allowing pre-transcription complex assembly. Heme stabilises the transcriptional activator protein Nrf2 simultaneously. This promotes nuclear accumulation of Maf-Nrf2 heterodimers resulting in further up-regulation of *HMOX1*. It is likely that free heme accumulation following UVA treatment plays a crucial role in the dynamic exchange in the occupation of MARE enhancer sites by Bach1 and Nrf2 proteins bound to Maf. Thus, regulation of HO-1 promoter availability involves a simple feedback loop dependant on intracellular levels of the HO-1 substrate heme.

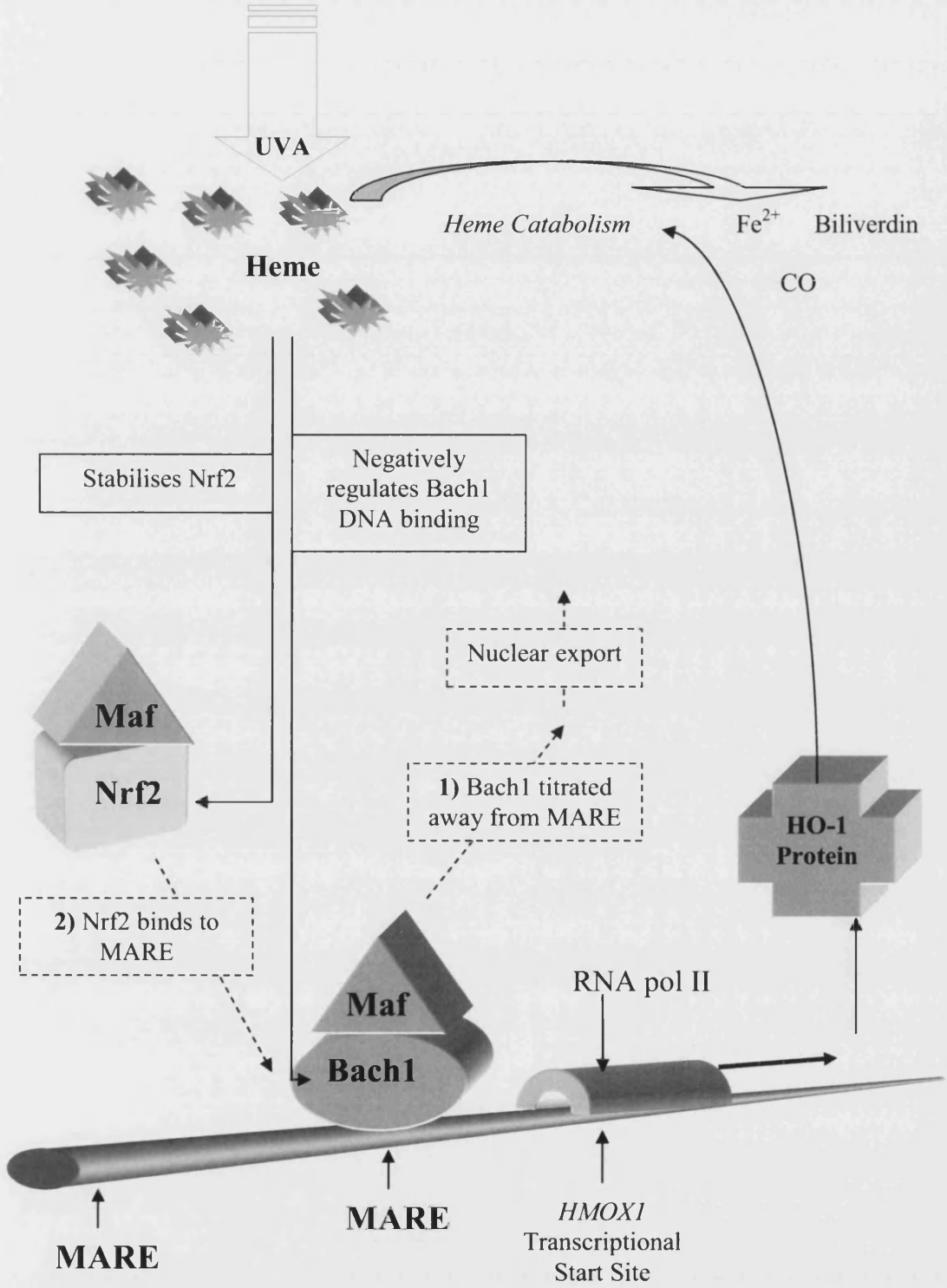
UVA
Heme
Heme Catabolism
$Fe^{2+}$
Biliverdin
CO
Stabilises Nrf2
Negatively regulates Bach1 DNA binding
Nuclear export
Maf
Nrf2
1) Bach1 titrated away from MARE
HO-1 Protein
2) Nrf2 binds to MARE
Maf
Bach1
RNA pol II
MARE
MARE
HMOX1 Transcriptional Start Site

Evidence to support this regulatory system can be found in a recent investigation into the regulation of the phase II gene, NAD(P)H:quinone oxidoreductase 1 (*NQO1*). Dhakshinamoorthy *et al.*, (2005) investigated the involvement of both Nrf2 and Bach1 in the regulation of this gene in human hepatoblastoma cells. Using chromatin immunoprecipitation assay (ChIP), Dhakshinamoorthy and co-workers observed competition between Bach1 and Nrf2 for binding to the NQO1 gene MARE, and furthermore, that MARE-driven gene expression was dependent on a critical balance between Nrf2 and Bach1 within the nucleus. Crucially, this study investigated the role of heme in this human model. The results of this study were consistent with the hypothesis that heme mediates a dynamic exchange between Nrf2 (activating) and Bach1 (repressive) dimeric complexes in MARE-driven gene expression.

Further insight into this model for heme co-ordinated UVA up-regulation of *HMOX1* can be found in three other observations. Firstly, re-irradiation of FEK4 primary human fibroblasts after an initial dose of UVA leads to a much smaller HO-1 mRNA induction response than in a control experiment in which no pre-irradiation is given (Noel *et al.*, 1997). Secondly, as previously stated, micro-molar concentrations of heme are released from microsomal heme-proteins immediately after UVA treatment, and this heme release precedes the induction of HO-1 transcription and enzymatic activity (Kvam *et al.*, 1999). Kvam and co-workers noted however that HO-1 transcriptional up-regulation was not observed for UVA treatments that released an amount of heme below a threshold level of 2 μM. Thirdly, UVA radiation enhances expression of the Bach1 gene several-fold (Raval and Tyrrell, unpublished observations). These three observations indicate a heme-dependent biological mechanism to shut off unwanted and potentially deleterious HO-1 gene activation. It seems likely that the refractoriness to re-induction of the HO-1 gene by UVA is dependent on the total cellular amount of heme-protein, and that a release of heme below a threshold level is not capable of titrating the heme binding repressive protein Bach1 away from the HO-1 promoter, therefore permitting Nrf2-MARE binding. Up-regulation of the Bach1 gene in response to UVA will further augment UVA refractoriness to re-induction of the *HMOX1* locus, and may represent a novel feed-back mechanism resulting from UVA photochemical destruction of existing Bach1 protein bound to heme. These observations indicate that refractoriness to re-induction exists in a situation where the amount of heme-containing proteins has been

substantially reduced, and where free heme has been destroyed by newly synthesised HO-1. In this situation the presence of newly synthesised Bach-1 will prevent Nrf2-MARE binding, and furthermore, a lack of heme-containing proteins will prevent UVA stabilisation of Nrf2. Extremely strong *HMOX1* down-regulation will therefore develop. It has been shown that the development of a complete refractory period to re-induction of the HO-1 gene is limited to UVA and heme, and is not observed in response to other known inducers of the gene (unpublished observations, this laboratory). This refractoriness event therefore emphasises the unique biological mechanism associated with UVA up-regulation of *HMOX1*, further underlining the importance of elucidation of this regulatory mechanism.

In the present study a complete model for UVA activation of Nrf2 has been proposed. This has provided further insights into UVA up-regulation of *HMOX1*. The functional significance of HO-1 protein accumulation in response to UVA has also been investigated by this study. HO-1 accumulation has been documented in a variety of tumours. This accumulation has been linked with cellular proliferation and loss of apoptotic potential, factors that are necessary for *in vivo* tumour growth. This study has therefore investigated the ability of HO-1 to modulate apoptosis. Malignant melanoma is the most life-threatening cutaneous malignancy; this has largely been attributed to the resistance of this form of cancer to apoptosis. However, no studies have addressed the relationship between HO-1 and apoptosis in human melanoma cells. Employing the oxidising UVA component of solar radiation to induce apoptosis, this study has investigated the effect of HO-1 over-expression on apoptosis in human melanoma cells. The results of this investigation have shown that HO-1 prevents UVA-apoptosis in a dose-dependant manner. What's more, the model for UVA activation of *HMOX1* proposed by this study indicates that the anti-apoptotic influence of HO-1 may be dependant on UVA-activation of the transcription factor Nrf2.

In order to investigate the effect of HO-1 over-expression on apoptosis in human melanoma cells, there was a prerequisite to establish a melanoma cell line that was both sensitive to UVA-apoptosis, and that was amenable to transient transfection with the HO-1 over-expressing construct pcDNA3.1-HO1. The human melanoma cell line JUSO satisfied these prerequisites and was selected in this investigation. In preliminary experiments it was observed that HO-1 over-expression protected against 'background' apoptosis. However, negligible protection against UVA-apoptosis was

observed. The conditions for transient transfection were then optimised. Using optimised conditions, it was later observed that transfection with the HO-1 over-expressing construct conferred some protection against UVA-induced late apoptosis when compared to cells transfected with the parental vector. These results were statistically significant with respect to cells treated with 100 and 200 kJ/m$^2$ UVA. In this experiment only a moderate increase in UVA-apoptosis was observed in untransfected cells. This indicates that transfection sensitises JUSO cells to UVA-apoptosis. HO-1 over-expression had no influence on UVA-induced necrosis in JUSO cells. Taken together, these data show that HO-1 over-expression confers protection against apoptosis in JUSO human melanoma cells. However, it remains unclear whether HO-1 confers resistance to UVA-apoptosis, or whether HO-1 confers resistance to the cytotoxicity associated with cationic transfection reagents.

In this study, data consistent with the interpretation that HO-1 possesses anti-apoptotic activity have been provided. These findings are in agreement with studies that have shown that HO-1 down-regulation may have therapeutic value with regards to its ability to augment the efficacy of cytotoxic cancer therapeutics (for review see: Fang *et al.*, 2004; Prawan *et al.*, 2005). To the best of our knowledge, this is the first study to evaluate this therapeutic potential in human melanoma cells. A previous study has however investigated the influence of HO-1 in murine melanoma cells (Was *et al.*, 2006). This study published findings indicating that excess HO-1 protein increased viability, proliferation, and angiogenic potential of melanoma cells, augmented metastasis, and decreased survival of tumour-bearing mice. Recently the relationship between microsatellite polymorphism in the *HMOX1* promoter and risk of melanoma was evaluated (Okamoto *et al.*, 2006). It is known that a (GT)n dinucleotide repeat polymorphism in the *HMOX1* promoter can modulate gene expression through promoting the formation of Z-DNA which suppresses *HMOX1* activation (Yamada *et al.*, 2000). Okamoto *et al.*, (2006) offers findings consistent with the interpretation that individuals homozygous for short (GT)n alleles (fewer than 25 repeats) have a risk of developing melanoma that is double that of heterozygous individuals. Taken together, the findings of the present study, and others, indicate that HO-1 may be a key gene in the pathogenesis of malignant melanoma.

As stated, the transcription factor Nrf2 is known to activate *HMOX1*. The anti-apoptotic activity of HO-1 may therefore be dependent on this activating

transcription factor. Hirota *et al.*, (2005) evaluated the role of Nrf2, and its cytoplasmic anchor protein Keap1, in UVA-apoptosis in murine skin fibroblasts. Using cells derived from knock-out mice, Hirota and co-workers show that disruption of *nrf2* correlates with up to a 1.7-fold increase in UVA-apoptosis, and that a similar effect is observed in response to disrupted Keap1. The anti-apoptotic influence of the Nrf2 / Keap1 regulatory system has been investigated in a variety of other cell types (Kweon *et al.*, 2006; Liu *et al.*, 2007; So *et al.*, 2006; Vargas *et al.*, 2005). These studies produced data consistent with the interpretation that Nrf2 possesses anti-apoptotic activity, and indicated that this anti-apoptotic activity results from HO-1 up-regulation. Similarly to HO-1, excess Nrf2 accumulation has been documented in human tumours (Stacy *et al.*, 2006). It is therefore reasonable to conjecture that Nrf2 may modulate apoptosis by means of HO-1 in human melanoma cells.

Recent scientific literature has advocated Nrf2 inducing agents as potential targets for cancer chemoprevention (for review see: Giudice and Montella, 2006; Jeong *et al.*, 2006; Shen *et al.*, 2005). Up-regulation of Nrf2 resulting in the subsequent induction of phase II detoxifying enzymes presents obvious benefits in the prevention of neoplastic pathologies. However, as indicated by this and other studies, up-regulation of Nrf2 is likely to up-regulate the anti-apoptotic protein HO-1, and this may only serve to exacerbate existing cancerous pathologies. Up-regulation of Nrf2 may therefore offer both beneficial and detrimental effects to patient health, and this indiscriminate approach to phase II gene activation must be viewed with caution.

# 5. References

## 5. References


Agarwal, A., Balla, J., Alam, J., Croatt, A.J., Nath, K.A., (1995), Induction of heme oxygenase in toxic renal injury: a protective role in cisplatin nephrotoxicity in the rat, *Kidney. Int.*, **48**, 1298 – 1307

Agarwal, A., Nick, H., (2000), Renal response to tissue injury: lessons from heme oxygenase-1 Gene Ablation and expression, *J. Am. Soc. Nephrol.*, **11**, 965 – 973

Akagi, R., Takahashi, T., Sassa, S., (2005), Cytoprotective effects of heme oxygenase in acute renal failure, *Contrib. Nephrol.*, **148**, 70 – 85

Alam, J., Shibahara, S., Smith A., (1989), Transcriptional activation of the heme oxygenase gene by heme and cadmium in mouse hepatoma cells, *J. Biol. Chem.*, **264**, 6371 – 6375

Alam, J., Cai, J., Smith, A., (1994), Isolation and characterization of the mouse heme oxygenase-1 gene, *J. Biol. Chem.*, **169**, 1001 – 1009

Alam, J., Camhi, S., Choi, A.M.K., (1995), Identification of a second region upstream of the mouse HO-1 gene that functions as a basal level and inducer-dependent transcription enhancer, *J. Bio. Chem.*, **270**, 11977 – 11984

Alam, J., Stewart, D., Touchard, C., Boinapally, S., Choi, A.M., Cook, J.L., (1999), Nrf2, a Cap'n'Collar Transcription Factor, Regulates Induction of the Heme Oxygenase-1 Gene, *J. Biol. Chem.*, **274**, 26071 – 26078

Alam, J., Wicks, C., Stewart, D., Gong, P., Touchard, C., Otterbein, S., Choi, A.M., Burow, M.E., Tou, J., (2000), Mechanism of heme oxygenase-1 gene activation by cadmium in MCF-7 mammary epithelial cells. Role of p38 kinase and Nrf2 transcription factor, *J. Biol. Chem.*, **275**, 27694 – 27702

Alam, J., Killeen, E., Gong, P., Naquin, R., Hu, B., Stewart, D., Ingelfinger, J.R., Nath, K.A., (2003), Heme activates the heme oxygenase-1 gene in renal epithelial cells by stabilizing Nrf2, *Am. J. Physiol. Renal. Physiol.*, **284**, 743 – 752

Alcaraz, M.J., Fernandez, P., Guillen, M.I., (2003), Anti-inflammatory actions of the heme oxygenase-1 pathway, *Curr. Pharm. Des.*, **9**, 2541 – 2551

Andree, H.A., Reutelingsperger, C.P., Hauptmann, R., Hemker, H.C., Hermens, W.T., Willems, G.M., (1990), Binding of vascular anticoagulant alpha (VAC alpha) to planar phospholipid bilayers, *J. Biol. Chem.*, **265**, 4923 – 4928

Angel, P., Hattori, K., Smeal, T., Karin, M., (1988), The jun proto-oncogene is positively autoregulated by its product, Jun/AP-1, *Cell*, **55**, 875 – 885

Aoki, Y., Sato, H., Nishimura, N., Takahashi, S., Itoh, K., Yamamoto, M., (2001), Accelerated DNA adduct formation in the lung of the Nrf2 knockout mouse exposed to diesel exhaust, *Toxicol. Appl. Pharmacol.*, **173**, 154 – 160

Applegate, L.A., Luscher, P., Tyrrell, R.M., (1991), Induction of heme oxygenase: a general response to oxidant stress in cultured mammalian cells, *Cancer. Res.*, **51**, 974 – 978

Applegate, L.A., Noel, A., Vile, G., Frenk, E., Tyrrell, R.M., (1995), Two genes contribute to different extents to the heme oxygenase enzyme activity measured in cultured human skin fibroblasts and keratinocytes: implications for protection against oxidant stress, *Photochem Photobiol.*, **61**, 285 – 291

Applegate, L.A., Scaletta, C., Labidi, F., Vile, G.F., Frenk, E., (1996), Susceptibility of human melanoma cells to oxidative stress including UVA radiation, *Int. J. Cancer.*, **67**, 430 – 434

Applegate, L.A., Scaletta, C., Panizzon, R., Niggli, H., Frenk, E., (1999), *In vivo* induction of pyrimidine dimers in human skin by UVA radiation: initiation of cell damage and/or intercellular communication, *Int. J. Mol. Med.*, **3**, 467 – 472

auf dem Keller, U., Huber, M., Beyer, T.A., Kumin, A., Siemes, C., Braun, S., Bugnon, P., Mitropoulos, V., Johnson, D.A., Johnson, J.A., Hohl, D., Werner, S., (2006), Nrf transcription factors in keratinocytes are essential for skin tumor prevention but not for wound healing, *Mol. Cell. Biol.*, **26**, 3773 – 3784

Bach, F.H., (2006), Heme oxygenase-1 and transplantation tolerance, *Hum. Immunol.*, **67**, 430 – 432

Balla, J., Nath, K.A., Balla, G., Juckett, M.B., Jacob, H.S., Vercellotti, G.M., (1995), Endothelial cell heme oxygenase and ferritin induction in rat lung by hemoglobin *in vivo, Am. J. Physiol. Lung Cell. Mol. Physiol.* **12**, 321 – 327

Balogun, E., Hoque, M., Gong, P., Killeen, E., Green, C.J., Foresti, R., Alam, J., Motterlini, R., (2003), Curcumin activates the haem oxygenase-1 gene via regulation of Nrf2 and the antioxidant-responsive element, *Biochem. J.*, **371**, 887 – 895

Baranano, D.E., Rao, M., Ferris, C.D., Snyder, S.H., (2002), Biliverdin reductase: a major physiologic cytoprotectant, *Proc. Natl. Acad. Sci. USA*, **99**, 16093 – 16098

Basu-Modak, S., and Tyrrell, R.M., (1993), Singlet oxygen: A primary effector in the ultraviolet A / near-visible light induction of the human heme oxygenase gene, *Cancer. Res.*, **53**, 4505 – 4510

Blazek, E.R., Peak, J.G., Peak, M.J., (1989), Singlet oxygen induces frank strand breaks as well as alkali- and piperidine-labile sites in supercoiled plasmid DNA, *Photochem. Photobiol.*, **49**, 607 – 613

Bloom D.A., Jaiswal. A.K., (2003), Phosphorylation of Nrf2 at Ser40 by protein kinase C in response to antioxidants leads to the release of Nrf2 from INrf2, but is not required for Nrf2 stabilization/accumulation in the nucleus and transcriptional activation of antioxidant response element-mediated NAD(P)H:quinone oxidoreductase-1 gene expression, *J. Biol. Chem.*, **278**, 44675 – 44682

Bode, A.M., Dong, Z., (2003), Mitogen-activated protein kinase activation in UV-induced signal transduction., *Sci STKE.*, **167**, RE2

Bose, B., Soriani, M., Tyrrell, R.M., (1999), Activation of expression of the c-fos oncogene by UVA irradiation in cultured human skin fibroblasts, *Photochem. Photobiol.*, **69**, 489 – 493

Bradford, M.M., (1976), A rapid and sensitive method for the quantitation of microgram quantities of protein utilizing the principle of protein-dye binding, *Anal. Biochem.*, **72**, 248 – 254

Brouard, S., Otterbein, L.E., Anrather, J., Tobiasch, E., Bach, F.H., Choi, A.M., Soares, M.P., (2000), Carbon monoxide generated by heme oxygenase 1 suppresses endothelial cell apoptosis, *J. Exp. Med.*, **192**, 1015 – 1026

Cadet, J., Anselmino, C., Douki, T., Voituriez, L., (1992), Photochemistry of nucleic acids in cells, *J. Photochem. Photobiol.*, **15**, 277 – 298

Calabrese, V., Boyd-Kimball, D., Scapagnini, G., Butterfield, D.A., (2004), Nitric oxide and cellular stress response in brain aging and neurodegenerative disorders: the role of vitagenes, *In. Vivo.*, **18**, 245 – 267

Carraro, C., Pathak, M.A., (1988), Studies on the nature of in vitro and in vivo photosensitization reactions by psoralens and porphyrins, *J. Invest. Dermatol.*, **90**, 267 – 275

Carter, E.P., Garat, C., Imamura, M., (2004), Continual emerging roles of HO-1: protection against airway inflammation, *Am. J. Physiol. Lung. Cell. Mol. Physiol.*, **287**, 24 – 5

Chalfie, M., Tu, Y., Euskirchen, G., Ward, W.W., Prasher, D.C., (1994), Green fluorescent protein as a marker for gene expression, *Science.*, **263**, 802 – 805

Chan, K., Kan, Y.W., (1999), Nrf2 is essential for protection against acute pulmonary injury in mice., *Proc. Natl. Acad. Sci. USA.*, **96**, 12731 – 12736

Chen, W., Hunt, D.M., Lu, H., Hunt, R.C., (1999), Expression of antioxidant protective proteins in the rat retina during prenatal and postnatal development, *Invest. Ophthalmol. Vis. Sci.*, **40**, 744 – 751

Cho, H.Y., Jedlicka, A.E., Reddy, S.P., Kensler, T.W., Yamamoto, M., Zhang, L.Y., Kleeberger, S.R., (2002), Role of NRF2 in protection against hyperoxic lung injury in mice, *Am. J. Respir. Cell. Mol. Biol.*, **26**, 175 – 182

Chouinard, N., Valerie, K., Rouabhia, M., Huot, J., (2002), UVB-mediated activation of p38 mitogen-activated protein kinase enhances resistance of normal human keratinocytes to apoptosis by stabilizing cytoplasmic p53, *Biochem. J.*, **365**, 133 – 145

Christova, T., Diankova, Z., Setchenska, M., (2000), Heme oxygenase - carbon monoxide signalling pathway as a physiological regulator of vascular smooth muscle cells, *Acta. Physiol. Pharmacol. Bulg.*, **25**, 9 – 17

Coohill, T.P., Peak, M.J., Peak, J.G., (1987), The effects of the ultraviolet wavelengths of radiation present in sunlight on human cells *in vitro*, *Photochem. Photobiol.*, **46**, 1043 – 50

Cornelius, L.A., Sepp, N., Li, L.J., Degitz, K., Swerlick, R.A., Lawley, T.J., Caughman, S.W., (1994), Selective upregulation of intercellular adhesion molecule (ICAM-1) by ultraviolet B in human dermal microvascular endothelial cells, *J. Invest. Dermatol.*, **103**, 23 – 28

Creutz, C.E., (1992), The annexins and exocytosis, *Science.*, **258**, 924 – 931

Cullinan, S.B., Gordan, J.D., Jin, J., Harper, J.W., Diehl, J.A., (2004), The Keap1-BTB protein is an adaptor that bridges Nrf2 to a Cul3-based E3 ligase: oxidative stress sensing by a Cul3-Keap1 ligase, *Mol. Cell. Biol.*, **24**, 8477 – 8486

Cunningham, M.L., Johnson, J.S., Giovanazzi, S.M., Peak, M.J., (1985), Photosensitized production of superoxide anion by monochromatic (290 - 405 nm) ultraviolet irradiation of NADH and NADPH coenzymes, *Photochem. Photobiol.*, **42**, 125 – 128

Czochralska, B., Kawcznski, W., Bartosz, G., Shugar, D., (1984), Oxidation of excited-state NADH and NAD dimmer in aqueous medium involved in $O^{2-}$ as a mediator in the presence of oxygen, *Biochim. Biophys. Acta.*, **801**, 404 – 409

Danpure, H.J., Tyrrell, R.M., (1976), Oxygen-dependence of near UV (365 nm) lethality and the interaction of near UV and X-rays in two mammalian cell lines, *Photochem. Photobiol.*, **23**, 171 – 177

Deininger, M.H., Meyermann, R., Trautmann, K., Duffner, E., Grote, F., Wickboldt, J., Schluesener, H.J., (2000), Heme oxygenase (HO)-1 expressing macrophages/microglial cells accumulate during oligodendroglioma progression, *Brain Res.*, **882**, 1 – 8

Devasagayam, T.P., Steenken, S., Obendorf, M.S., Schulz, W.A., Sies, H., (1991), Formation of 8-hydroxy(deoxy)guanosine and generation of strand breaks at guanine residues in DNA by singlet oxygen, *Biochemistry.*, **30**, 6283 – 6289

Devling, T.W., Lindsay, C.D., McLellan, L.I., McMahon, M., Hayes, J.D., (2005), Utility of siRNA against Keap1 as a strategy to stimulate a cancer chemopreventive phenotype, *Proc. Natl. Acad. Sci. USA.*, **102**, 7280 – 7285

Dhakshinamoorthy, S., Jaiswal A.K., (2001), Functional characterization and role of INrf2 in antioxidant response element-mediated expression and antioxidant induction of NAD(P)H:quinone oxidoreductase1 gene, *Oncogene*, **20**, 3906 – 3917

Dhakshinamoorthy, S., Jain, A.K., Bloom, D.A., Jaiswal, A.K., (2005), Bach1 competes with Nrf2 leading to negative regulation of the antioxidant response element (ARE)-mediated NAD(P)H:quinone oxidoreductase 1 gene expression and induction in response to antioxidants, *J. Biol. Chem.*, **280**, 16891 – 16900

Dinkova-Kostova, A.T., Holtzclaw, W.D., Cole, R.N., Itoh, K., Wakabayashi, N., Katoh, Y., Yamamoto, M., Talalay, P., (2002), Direct evidence that sulfhydryl groups of Keap1 are the sensors regulating induction of phase 2 enzymes that protect against carcinogens and oxidants, *Proc. Natl. Acad. Sci. USA.*, **99**, 11908 – 11913

Dlamini, Z., Mbita, Z., Ledwaba, T., (2005), Can targeting apoptosis resolve the cancer saga, *Future. Oncol.*, 1, 339 – 349

Doi, K., Akaike, T., Fujii, S. Tanaka, S., Ikebe, N., Beppu, T., Shibahara, S., Ogawa, M., Maeda, H., (1999), Induction of haem oxygenase-1 by nitric oxide and ischaemia in experimental solid tumours and implications for tumour growth, *Br. J. Cancer.*, **80**, 1945 – 1954

Douki, T., Perdiz, D., Grof, P., Kuluncsics, Z., Moustacchi, E., Cadet, J., Sage, E., (1999), Oxidation of guanine in cellular DNA by solar UV radiation: biological role, *Photochem. Photobiol.*, **70**, 184 – 190

Durante, W., (2003), Heme oxygenase-1 in growth control and its clinical application to vascular disease, *J. Cell. Physiol.*, **195**, 373 – 82

Durchdewald, M., Beyer, T.A., Johnson, D.A., Johnson, J.A., Werner, S., Auf dem Keller, U., (2006), Electrophilic Chemicals but not UV Irradiation or Reactive Oxygen Species Activate Nrf2 in Keratinocytes In Vitro and In Vivo, *J. Invest. Dermatol.*, **127**, 646 – 53

Eggler, A.L., Liu, G., Pezzuto, J.M., van Breemen, R.B., Mesecar, A.D., (2005), Modifying specific cysteines of the electrophile-sensing human Keap1 protein is insufficient to disrupt binding to the Nrf2 domain Neh2, *Proc. Natl. Acad. Sci. USA.*, **102**, 10070 – 10075

Eisenstein, R.S., Garcia-Mayol, D., Pettingell, W., Munro, H.N., (1991), Regulation of ferritin and heme oxygenase synthesis in rat fibroblasts by different forms of iron, *Proc. Natl. Acad. Sci. USA.*, **88**, 688 – 692

Enomoto, A., Itoh, K., Nagayoshi, E., Haruta, J., Kimura, T., O'Connor, T., Harada, T., Yamamoto, M., (2001), High sensitivity of Nrf2 knockout mice to acetaminophen hepatotoxicity associated with decreased expression of ARE-regulated drug metabolizing enzymes and antioxidant genes, *Toxicol. Sci.*, **59**, 169 – 177

Ewing, J.F., Maines, M.D., (1991), Rapid induction of heme oxygenase 1 mRNA and protein by hyperthermia in rat brain: heme oxygenase 2 is not a heat shock protein, *Proc. Natl. Acad. Sci. USA.*, **88**, 5364 – 5368

Fadok, V.A., Savill, J.S., Haslett, C., Bratton, D.L., Doherty, D.E., Campbell, P.A., Henson, P.M., (1992), Different populations of macrophages use either the vitronectin receptor or the phosphatidylserine receptor to recognize and remove apoptotic cells, *J. mmunol.*, **149**, 4029 – 4035

Fang, J., Sawa, T., Akaike, T., Akuta, T., Sahoo, S.K., Khaled, G., Hamada, A., Maeda, H., (2003), In vivo antitumor activity of pegylated zinc protoporphyrin: targeted inhibition of heme oxygenase in solid tumor, *Cancer. Res.*, **63**, 3567 – 3574

Fang, J., Akaike, T., Maeda, H., (2004), Antipoptotic role of heme oxygenase (HO) and the potential as a target in anticancer treatment, *Apoptosis*, **9**, 27 – 35

Ferris, C.D., Jaffrey, S.R., Sawa, A., Takahashi, M., Brady, S.D., Barrow, R.K., Tysoe, S.A., Wolosker, H., Baranano, D.E., Dore., S., Poss, K.D., Snyder, S.H., (1999), Haem oxygenase-1 prevents cell death by regulating cellular iron, *Nat. Cell. Biol.*, **1**, 152-7

Fisher, G.J., Talwar, H.S., Lin, J., Lin, P., McPhillips, F., Wang, Z., Li, X., Wan, Y., Kang, S., Voorhees, J.J., (1998), Retinoic acid inhibits induction of c-Jun protein by ultraviolet radiation that occurs subsequent to activation of mitogen-activated protein kinase pathways in human skin in vivo, *J. Clin. Invest.*, **101**, 1432 – 1240

Fridovich, I., (1978), Superoxide radicals, superoxide dismutases and the aerobic lifestyle, *Photochem. Photobiol.*, **28**, 733 – 741

Furchgott, R.F., Jothianandam, D., (1991), Endothelium-dependant and independent vasodiltaion involving cyclic group gmp; relaxation induced by nitric oxide, carbon monoxide, and light, *Blood Vessels*, **28**, 52 – 61

Garner, P.R., Raineri, I., Epstein, L.B., White, C.W., (1995), Superoxide radical and iron modulate aconitase activity in mammalian cells, *J. Biol. Chem.*, **270**, 13399 – 13405

Giger, U., Meyer, U.A., (1983), Effect of succinylacetone on heme and cytochrome P450 synthesis in hepatocyte culture, *FEBS Lett.*, **21**, 335 – 338

Gilaberte, Y., Serra-Guillen, C., de las Heras, M.E., Ruiz-Rodriguez, R., Fernandez-Lorente, M., Benvenuto-Andrade, C., Gonzalez-Rodriguez, S., Guillen-Barona, C., (2006), Photodynamic therapy in dermatology, *Atas Dermosifiliogr.*, **97**, 83 – 102

Giudice, A., Montella, M., (2006), Activation of the Nrf2-ARE signaling pathway: a promising strategy in cancer prevention, *Bioessays.*, **28**, 169 – 81

Godar, D.E., Miller, S.A., Thomas, D.P., (1994), Immediate and delayed apoptotic cell death mechanisms: UVA versus UVB and UVC radiation, *Cell. Death. Differ.*, **1**, 59 – 66

Godar, D.E., (1999), UVA1 radiation triggers two different final apoptotic pathways, *J. Invest. Dermatol.*, **112**, 3 – 12

Godar, D.E., (1999b), Light and death: photons and apoptosis, *J. Investig. Dermatol. Symp. Proc.*, **4**, 17 – 23

Goldring, C.E., Kitteringham, N.R., Elsby, R., Randle, L.E., Clement, Y.N., Williams, D.P., McMahon, M., Hayes, J.D., Itoh, K., Yamamoto, M., Park, B.K., (2004), Activation of hepatic Nrf2 in vivo by acetaminophen in CD-1 mice. *Hepatology.*, **39**, 1267 – 1276

Goncalves, G.M., Cenedeze, M.A., Feitoza, C.Q., Wang, P.M., Bertocchi, A.P., Damiao, M.J., Pinheiro, H.S., Antunes Teixeira, V.P., dos Reis, M.A., Pacheco-Silva, A., Camara, N.O., (2006), The role of heme oxygenase 1 in rapamycin-induced renal dysfunction after ischemia and reperfusion injury, *Kidney Int.*, **70**, 1742 – 1749

Gong, P., Hu, B., Stewart, D., Ellerbe, M., Figueroa, Y.G., Blank, V., Beckman, B.S., Alam, J., (2001), Cobalt induces heme oxygenase-1 expression by a hypoxia-inducible factor-independent mechanism in Chinese hamster ovary cells: regulation by Nrf2 and MafG transcription factors, *J. Biol. Chem.*, **276**, 27018 – 27025

Gong, P., Stewart, D., Hu, B., Li, N., Cook, J., Nel, A., Alam, J., (2002), Activation of the mouse heme oxygenase-1 gene by 15-deoxy-Delta(12,14)-prostaglandin J(2) is mediated by the stress response elements and transcription factor Nrf2, *Antioxid. Redox. Signal.*, **4**, 249 – 57

Goodman, A.I., Choudhury, M., da Silve, J.L., Scwartzman, M.L., Abraham, N.G., (1997), Overexpression of the heme oxygenase gene in renal cell carcinoma, *Proc. Soc. Exp. Biol. Med.* **214**, 54 – 61

Guo, X., Shin, V.Y., Cho, C.H., (2001), Modulation of heme oxygenase in tissue injury and its implication in protection against gastrointestinal diseases, *Life. Sci.*, **69**, 3113 – 3119

Halliwell, B., and Gutteridge, J., (1990), The chemistry of oxygen radicals and other oxygen derived species. In: *Free radicals in biology and medicine*, New York: Oxford University Press, 22 – 85

Hancock, W.W., Buelow, R., Sayegh, M.H., Turka, L.A., (1998), Antibody-induced transplant arteriosclerosis is prevented by graft expression of anti-oxidant and anti-apoptotic genes, *Nat. Med.*, **4**, 1392 – 1396

Hart, R.W., Setlow, R.B., Woodhead, A.D., (1977), Evidence that pyrimidine dimers in DNA can give rise to tumors, *Proc. Natl. Acad. Sci. USA.*, **74**, 5574 – 5578

Hayes, J.D., Chanas, S.A., Henderson, C.J., McMahon, M., Sun, C., Moffat, G.J., Wolf, C.R., Yamamoto, M., (2000), The Nrf2 transcription factor contributes both to the basal expression of glutathione S-transferases in mouse liver and to their induction by the chemopreventive synthetic antioxidants, butylated hydroxyanisole and ethoxyquin, *Biochem. Soc. Trans.*, **28**, 33 – 41

Heiman, J., Delbro, D., (2005), Carbon monoxide - a toxic gas and a signal molecule with therapeutic potential, *Lakartidningen.*, **102**, 645 – 647

Hellmuth, M., Wetzler, C., Nold, M., Chang, J.H., Frank, S., Pfeilschifter, J., Muhl, H., (2002), Expression of interleukin-8, heme oxygenase-1 and vascular endothelial growth factor in DLD-1 colon carcinoma cells exposed to pyrrolidine dithiocarbamate, *Carcinogenesis*, **23**, 1273 – 1279

Herman, Z.S., (1997), Carbon monoxide: a novel neural messenger or putative neurotransmitter, *Pol. J. Pharmacol.*, **49**, 1 – 4

Herrmann, G., Wlaschek, M., Lange, T.S., Prenzel, K., Goerz, G., Scharffetter-Kochanek, K., (1993), UVA irradiation stimulates the synthesis of various matrix-metalloproteinases (MMPs) in cultured human fibroblasts, *Exp. Dermatol.*, **2**, 92 – 97

Hershko, A., Ciechanover, A., (1998), The ubiquitin system, *Annu. Rev. Biochem.*, **67**, 425 – 479

Hirai, H., Kubo, H., Yamaya, M., Nakayama, K., Numasaki, M., Kobayashi, S., Suzuki, S., Shibahara, S., Sasaki, H., (2003), Microsatellite polymorphism in heme oxygenase-1 gene promoter is associated with susceptibility to oxidant-induced apoptosis in lymphoblastoid cell lines, *Blood*, **102**, 1619 – 1621

Hirota, A., Kawachi, Y., Itoh, K., Nakamura, Y., Xu, X., Banno, T., Takahashi, T., Yamamoto, M., Otsuka, F., (2005), Ultraviolet A irradiation induces NF-E2-related factor 2 activation in dermal fibroblasts: protective role in UVA-induced apoptosis, *J. Invest. Dermatol.*, **124**, 825 – 832

Homburg, C.H., de Haas, M., von dem Borne, A.E., Verhoeven, A.J., Reutelingsperger, C.P., Roos, D., (1995), Human neutrophils lose their surface Fc gamma RIII and acquire Annexin V binding sites during apoptosis in vitro, *Blood.*, **85**, 532 – 540

Horikawa, S., Ito, K., Ikeda, S., Shibata, T., Ishizuka, S., Yano, T., Hagiwara, K., Ozasa, H., Katsuyama, I., (1998), Induction of heme oxygenase-1 in toxic renal injury: mercuric chloride-induced acute renal failure in rat, *Toxicol Lett.*, **94**, 57 - 64

Horvath, I., Donnelly, L.E., Kiss, A., Paredi, P., Kharitonov, S.A., Barnes, P.J., (1998), Raised levels of exhaled carbon monoxide are associated with an increased expression of heme oxygenase-1 in airway macrophages in asthma: a new marker of oxidative stress, *Thorax.*, **53**, 668 – 672

Hunt, D.W., Boivin, W.A., Fairley, L.A., Jovanovic, M.M., King, D.E., Salmon, R.A., Utting, O.B., (2006), Ultraviolet B Light Stimulates Interleukin-20 Expression by Human Epithelial Keratinocytes, *Photochem. Photobiol.*, **82**, 1292 – 1300

Igarashi, K., Hoshino, H., Muto, A., Suwabe, N., Nishikawa, S., Nakauchi, H., Yamamoto, M., (1998), Multivalent DNA binding complex generated by small Maf and Bach1 as a possible biochemical basis for beta-globin locus control region complex, *J. Biol. Chem.*, **273**, 11783 – 11790

Iizuka, T., Ishii, Y., Itoh, K., Kiwamoto, T., Kimura, T., Matsuno, Y., Morishima, Y., Hegab, A.E., Homma, S., Nomura, A., Sakamoto, T., Shimura, M., Yoshida, A., Yamamoto, M., Sekizawa, K., (2005), Nrf2-deficient mice are highly susceptible to cigarette smoke-induced emphysema, *Genes. Cells.*, **10**, 1113 – 1125

Immenschuh, S., Ramadori, G., (2000), Gene regulation of heme oxygenase-1 as a therapeutic target, *Biochem. Pharmacol.*, **60**, 1121 – 1128

Immenschuh, S., Schroder, H., (2006), Heme oxygenase-1 and cardiovascular disease, *Histol. Histopathol.*, **21**, 679 – 85

Inamdar, N.M., Ahn, Y.I., Alam, J., (1996), The heme-responsive element of the mouse heme oxygenase-1 gene is an extended AP-1 binding site that resembles the recognition sequences for MAF and NF-E2 transcription factors, *Biochem. Biophys. Res. Commun.* **221**, 570 – 576

Ishii, T., Itoh, K., Takahashi, S., Sato, H., Yanagawa, T., Katoh, Y., Bannai, S., Yamamoto, M., (2000), Transcription factor Nrf2 coordinately regulates a group of oxidative stress-inducible genes in macrophages, *J. Biol. Chem.*, **275**, 16023 – 16029

Ishikawa, K., Navab, M., Leitinger, N., Fogelman, A.M., Lusis, A.J., (1997), Induction of heme oxygenase-1 inhibits the monocyte transmigration induced by mildly oxidized LDL, *J. Clin. Invest.*, **100**, 1209 – 16

Ishikawa, M., Numazawa, S., Yoshida, T., (2005), Redox regulation of the transcriptional repressor Bach1, *Free. Rad. Biol. Med.*, **38**, 1344 – 1352

Ishizaka, N., de Leon, H., Laursen, J.B., Fukui, T., Wilcox, J.N., De Keulenaer, G., Griendling, K.K., Alexander, R.W., (1997), Angiotensin II-induced hypertension increases heme oxygenase-1 expression in rat aorta, *Circulation*, **96**, 1923 – 1929

Ishizuka, K., Kimura, T.,Yoshitake, J., Akaike, T., Shono, M.,Takamatsu, J., Kats uragi, S., Kitamura, T., Miyakawa, T., (2002), Possible assessment for antioxidant capacity in Alzheimer's disease by measuring lymphocyte heme oxygenase-1 expression with real-time RT-PCR, *Ann. N. Y. Acad. Sci.*, **977**, 173 – 178

Itoh, K., Chiba, T., Takahashi, S., Ishii, T., Igarashi, K., Katoh, Y., Oyake, T., Hayashi, N., Satoh, K., Hatayama, I., Yamamoto, M., Nabeshima, Y., (1997), An Nrf2/small Maf heterodimer mediates the induction of phase II detoxifying enzyme genes through antioxidant response elements, *Biochem. Biophys. Res. Commun.*, **236**, 313 – 322

Itoh, K., Wakabayashi, N., Katoh, Y., Ishii, T., Igarishi, K., Engel, J.D., Yamamoto, M., (1999), Keap1 represses nuclear activation of antioxidant responsive elements by Nrf2 through binding to the amino-terminal Neh2 domain, *Genes Dev.*, **13**, 76 – 86

Itoh, K., Wakabayashi, N., Katoh, Y., Ishii, T., O'Connor, T., Yamamoto, M., (2003), Keap1 regulates both cytoplasmic-nuclear shuttling and degradation of Nrf2 in response to electrophiles, *Genes Cells*, **8**, 379 – 91

Itoh, K., Tong, K.I., Yamamoto, M., (2004), Molecular mechanism activating Nrf2-Keap1 pathway in regulation of adaptive response to electrophiles, *Free. Radic. Biol. Med.,* **36**, 1208 – 1213

Jaiswal, AK., (2004), Nrf2 signalling in coordinated activation of antioxidant gene expression, *Free. Radic. Biol. Med.*, **36**, 1199 – 1207

Jeong, W.S., Jun, M., Kong, A.N., (2006), Nrf2: a potential molecular target for cancer chemoprevention by natural compounds, *Antioxid. Redox. Signal.*, **8**, 99 – 106

Jiang, X., Wang, G.X., Zhou, M.Y., Feng, Y., Wu, Q., Ran, Y.P., (2005), The effect of ultraviolet B on interleukin-8 secretion in human keratinocyte cell line, *Sichuan. Da. Xue. Xue. Bao. Yi. Xue. Ban.*, **36**, 237 – 239

Kang, M.I., Kobayashi, A., Wakabayashi, N., Kim, S.G., Yamamoto, M.., (2004), Scaffolding of Keap1 to the actin cytoskeleton controls the function of Nrf2 as key regulator of cytoprotective phase 2 genes, *Proc. Natl. Acad. Sci. USA.*, **101**, 2046 – 2051

Kataoka, K., Noda, M., Nishizawa, M., (1994), Maf nuclear oncoprotein recognizes sequences related to an AP-1 site and forms heterodimers with both Fos and Jun, *Mol. Cell. Biol.*, **14**, 700 – 712

Kataoka, K., Handa, H., Nishizawa, M., (2001), Induction of cellular antioxidative stress genes through heterodimeric transcription factor Nrf2/small Maf by antirheumatic gold(I) compounds, *J. Biol. Chem.*, **276**, 34074 – 32081

Katoh, Y., Itoh, K., Yoshida, E., Miyagishi, M., Fukamizu, A., Yamamoto, M., (2001), Two domains of Nrf2 cooperatively bind CBP, a CREB binding protein, and synergistically activate transcription, *Genes Cells*, **6**, 857 – 68

Kawashima, A., Oda, Y., Yachie, A., Koizumi, S., Nakanishi, I., (2002), Heme oxygenase-1 deficiency: the first autopsy case, *Human. Pathol.*, **33**, 125 – 30

Kerr, J.F., Wyllie, A.H., Currie, A.R., (1972), Apoptosis: a basic biological phenomenon with wide-ranging implications in tissue kinetics, *Br. J. Cancer.*, **26**, 239 – 257

Keyse, S.M., Tyrrell, R.M., (1987), Both near ultraviolet radiation and the oxidizing agent hydrogen peroxide induce a 32-kDa stress protein in normal human skin fibroblasts. *J. Biol. Chem.*, **262**, 14821 – 14825

Keyse, S.M., Tyrrell, R.M., (1989), Heme oxygenase is the major 32-kDa stress protein induced in human skin fibroblasts by UVA radiation, hydrogen peroxide, and sodium arsenite., *Proc. Natl. Acad. Sci. USA.*, **86**, 99 – 103

Keyse, S.M., Applegate, L.A., Tromvoukis, Y., Tyrrell, R.M., (1990), Oxidant stress leads to transcriptional activation of the human heme oxygenase gene in cultured skin fibroblasts, *Mol. Cell. Biol.*, **10**, 4967 – 4969

Khor, T.O., Huang, M.T., Kwon, K.H., Chan, J.Y., Reddy, B.S., Kong, A.N., (2006), Nrf2-deficient mice have an increased susceptibility to dextran sulfate sodium-induced colitis, *Cancer. Res.*, **66**, 11580 – 11584

Kielbassa, C., Roza, L., Epe, B., (1997), Wavelength dependence of oxidative DNA damage induced by UV and visible light, *Carcinogenesis*, **18**, 811 – 816

Kim, H.S., Loughran, P.A., Kim, P.K., Billiar, T.R., Zuckerbraun, B.S., (2006), Carbon monoxide protects hepatocytes from TNF-alpha/Actinomycin D by inhibition of the caspase-8-mediated apoptotic pathway, *Biochem. Biophys. Res. Commun.*, **344**, 1172 – 1178

Kirkby, K.A., Adin, C.A., (2006), Products of heme oxygenase and their potential therapeutic applications, *Am. J. Physiol. Renal. Physiol.*, **290**, 563 – 571

Kirnbauer, R., Charvat, B., Schauer, E., Kock, A., Urbanski, A., Forster, E., Neuner, P., Assmann, I., Luger, T.A., Schwarz, T., (1992), Modulation of intercellular adhesion molecule-1 expression on human melanocytes and melanoma cells: evidence for a regulatory role of IL-6, IL-7, TNF beta, and UVB light, *J. Invest. Dermatol.*, **98**, 320 – 326

Kobayashi, A., Kang, M.I., Okawa, H., Ohtsuji, M., Zenke, Y., Chiba, T., Igarashi, K., Yamamoto, M., (2004), Oxidative stress sensor Keap1 functions as an adaptor for Cul3-based E3 ligase to regulate proteasomal degradation of Nrf2, *Mol. Cell. Biol.*, **24**, 7130 – 7139

Kobayashi, A., Kang, M.I., Watai, Y., Tong, K.I., Shibata, T., Uchida, K., Yamamoto, M., (2006), Oxidative and electrophilic stresses activate Nrf2 through inhibition of ubiquitination activity of Keap1, *Mol. Cell. Biol.*, **26**, 221 – 229

Koopman, G., Reutelingsperger, C.P., Kuijten, G.A., Keehnen, R.M., Pals, S.T., van Oers, M.H., (1994), Annexin V for flow cytometric detection of phosphatidylserine expression on B cells undergoing apoptosis, *Blood.*, **84**, 1415 – 1420

Krishna, C.M., Uppuluri, S., Riesz, P., Zigler, J.S. Jr, Balasubramanian, D., (1991), A study of the photodynamic efficiencies of some eye lens constituents, *Photochem. Photobiol.*, **54**, 51 – 8

Kuluncsics, Z., Perdiz, D., Brulay, E., Muel, B., Sage, E., (1999), Wavelength dependence of ultraviolet-induced DNA damage distribution: involvement of direct or indirect mechanisms and possible artefacts, *J. Photochem. Photobiol. B.*, **49**, 71 – 80

Kvam, E., Tyrrell, R.M., (1997), Induction of oxidative DNA base damage in human skin cells by UV and near visible radiation, *Carcinogenesis.*, **18**, 2379 – 2384

Kvam, E., Noel, A., Basu-Modak, S., Tyrrell, R.M., (1999), Cyclooxygenase dependent release of heme from microsomal hemeproteins correlates with induction of heme oxygenase 1 transcription in human fibroblasts, *Free. Radic. Biol. Med.*, **26**, 511 – 517

Kwak, M.K., Itoh, K., Yamamoto, M., Kensler, T.W., (2002), Enhanced expression of the transcription factor Nrf2 by cancer chemopreventive agents: role of antioxidant response element-like sequences in the nrf2 promoter, *Mol. Cell. Biol.*, **22**, 2883 – 2892

Kweon, M.H., Adhami, V.M., Lee, J.S., Mukhtar, H., (2006), Constitutive overexpression of Nrf2-dependent heme oxygenase-1 in A549 cells contributes to resistance to apoptosis induced by epigallocatechin 3-gallate, *J. Biol. Chem.*, **281**, 33761 – 33772

Lee, T.S., Chau, L.Y., (2002), Heme oxygenase-1 mediates the anti-inflammatory effect of interleukin-10 in mice, *Nat. Med.*, **8**, 240 – 246

Levere, R.D., Staudinger, R., Loewy, G., Kappas, A., Shibahara, S., Abraham, N.G., (1993), Elevated levels of heme oxygenase-1 activity and mRNA in peripheral blood adherent cells of acquired immunodeficiency syndrome patients, *Am. J. Hematol.*, **43**, 19 – 23

Ley, R.D., Applegate, L.A., Fry, R.J., Sanchez, A.B., (1991), Photoreactivation of ultraviolet radiation-induced skin and eye tumors of Monodelphis domestica, *Cancer. Res.*, **51**, 6539 – 6542

Lindig, B.A., Rodgers, M.A.J., Schaap, A.P., (1980), Determination of the lifetime of singlet oxygen in $D_2O$ using 9,10-Anthracenedipropionic acid, a water-soluble probe, *J. Am. Chem. Soc.*, **102**, 5590 – 5593

Liptay, S., Schmid, R.M., Nabel, E.G., Nabel, G.J., (1994), Transcriptional regulation of NF-kappa B2: evidence for kappa B-mediated positive and negative autoregulation, *Mol Cell Biol.*, **14**, 7695 – 7703

Liu, X.M., Chapman, G.B., Peyton, K.J., Schafer, A.I., Durante, W., (2002), Carbon monoxide inhibits apoptosis in vascular smooth muscle cells, *Cardiovasc. Res.*, **55**, 396 – 405

Liu, X.M., Peyton, K.J., Ensenat, D., Wang, H., Hannink, M., Alam, J., Durante, W., (2007), Nitric oxide stimulates heme oxygenase-1 gene transcription via the Nrf2/ARE complex to promote vascular smooth muscle cell survival, *Cardiovasc. Res.* [Epub ahead of print]

Maines, M.D., (1988), Heme oxygenase: function, multiplicity, regulatory mechanisms, and clinical applications, *FASEB J,* **2**, 2557 – 2568

Maines, M.D., (1997), The heme oxygenase system: a regulator of second messenger gases, *Ann. Rev. Pharmacol. Toxicol.*, **37**, 517 – 554

McCormick, J.P., Fischer, J.R., Pachlatko, J.P., Eisenstark, A., (1976), Characterization of a cell-lethal product from the photooxidation of tryptophan: hydrogen peroxide, *Science.*, **191**, 468 – 469

McCoubrey, W.K., Huang, T.J., Maines, M.D., (1997), Isolation and characterization of a cDNA from the rat brain that encodes hemoprotein heme oxygenase-3, *Eur. J. Biochem.,* **247**, 725 – 732

McMahon, M., Itoh, K., Yamamoto, M., Hayes, J.D., (2003), Keap1-dependent proteasomal degradation of transcription factor Nrf2 contributes to the negative regulation of antioxidant response element-driven gene expression, *J. Biol. Chem.*, **278**, 21592 – 21600

McMahon, M., Thomas, N., Itoh, K., Yamamoto, M., Hayes, J.D., (2004), Redox-regulated turnover of Nrf2 is determined by at least two separate protein domains, the redox-sensitive Neh2 degron and the redox-insensitive Neh6 degron, *J. Biol. Chem.,* **279**, 31556 – 31567

Meneghini, R., (1997), Iron homeostasis, oxidative stress, and DNA damage, *Free. Radic. Biol. Med.*, **23**, 783 – 792

Minetti, M., Mallozzi, C., Di Stasi, A.M., Pietraforte, D., (1998), Bilirubin is an effective antioxidant of peroxynitrite-mediated protein oxidation in human blood plasma, *Arch. Biochem. Biophys.*, **352**, 165 – 174

Mitani, K., Fujita, H., Fukuda, Y., Kappas, A., Sassa, S., (1993), The role of inorganic metals and metalloporphyrins in the induction of haem oxygenase and heat-shock protein 70 in human hepatoma cells. *Biochem. J.*, **290**, 819 – 825

Moan, J., Dahlback, A., Setlow, R.B., (1999), Epidemiological support for an hypothesis for melanoma induction indicating a role for UVA radiation, *Photochem. Photobiol.*, **70**, 243 – 247

Mori, T., Matsunaga, T., Hirose, T., Nikaido, O., (1988), Establishment of a monoclonal antibody recognizing ultraviolet light-induced (6-4) photoproducts, *Mutat. Res.*, **194**, 263 – 270

Morita, A., Werfel, T., Stege, H., Ahrens, C., Karmann, K., Grewe, M., Grether-Beck, S., Ruzicka, T., Kapp, A., Klotz, L.O., Sies, H., Krutmann, J., (1997), Evidence that singlet oxygen-induced human T helper cell apoptosis is the basic mechanism of ultraviolet-A radiation phototherapy, *J. Exp. Med.*, **186**, 1763 – 1768

Morita, T., (2005), Heme Oxygenase and Atherosclerosis, *Athero. Throm. Vasc. Biol.*, **25**, 1786

Morrison, G.R., (1965), Flourometric microdetermination of heme protein, *Anal. Chem.*, **37**, 1124 – 1126

Morse, D., Choi, A.M., (2002), Heme oxygenase-1: the "emerging molecule" has arrived, *Am. J. Respir. Cell. Mol. Biol.*, **27**, 8 – 16

Motohashi, H., O'Connor, T., Katsuoka, F., Engel, J.D., Yamamoto, M., (2002), Integration and diversity of the regulatory network composed of Maf and CNC families of transcription factors, *Gene*, **294**, 1 – 12

Motterlini, R., Foresti, R., Bassi, R., Calabrese, V., Clark J.E., Green, C.J., (2000), Endothelial heme oxygenase-1 induction by hypoxia. Modulation by inducible nitric-oxide synthase and S-nitrosothiols, *J. Biol. Chem.*, **275**, 13613 – 13620

Murata-Kamiya, N., Kamiya, H., Iwamoto, N., Kasai, H., (1995), Formation of a mutagen, glyoxal, from DNA treated with oxygen free radicals, *Carcinogenesis.*, **16**, 2251 – 2253

Murphy, G.M., (1998), The acute effects of ultraviolet radiation on the skin, *Photodermatology*, 44 – 52

Nath, K.A., Balla, G., Vercellotti, G.M., Balla, J., Jacob, H.S., Levitt, M.D., Rosenberg, M.E., (1992), Induction of heme oxygenase is a rapid, protective response in rhabdomyolysis in the rat, *J. Clin. Invest.*, **90**, 267 – 70

Neuzil, J., Stocker, J., (1997), Free and albumin-bound bilirubin are efficient co-antioxidants for alpha-tocopherol, inhibiting plasma and low density lipoprotein lipid peroxidation, *J Biol Chem.*, **269**, 16712 – 16719

Newman, L.A., Walker, M.T., Brown, R.L., Cronin, T.W., Robinson, P.R., (2003), Melanopsin forms a functional short-wavelength photopigment, *Biochemistry.*, **42**, 12734 – 12738

Nguyen, T., Sherratt, P.J., Huang, H.C., Yang, C.S., Pickett, C.B., (2003), Increased protein stability as a mechanism that enhances Nrf2-mediated transcriptional activation of the antioxidant response element. Degradation of Nrf2 by the 26 S proteasome, *J. Biol. Chem.*, **278**, 4536 – 4541

Nguyen, T., Yang, C.S., Pickett, C.B., (2004), The pathways and molecular mechanisms regulating Nrf2 activation in response to chemical stress, *Free. Radic. Biol. Med.*, **37**, 433 – 441

Noël, A., Tyrrell, R.M., (1997), Development of a refractoriness of induced human heme oxygenase-1 gene expression to reinduction of UVA irradiation and hemin, *Photochem. Photobiol.*, **66**, 456 – 462

O'Carra, P., and Colleran, E., (1971), Properties and kinetics of biliverdin reductase, *Biohem. J.*, **125**, 110

Ogawa, K., Sun, J., Taketani, S., Nakajima, O., Nishitani, C., Sassa, S., Hayashi, N., Yamamoto, M., Shibahara, S., Fujita, H., Igarashi, K., (2001), Heme mediates derepression of Maf recognition element through direct binding to transcription repressor Bach1, *EMBO J.*, **20**, 2835 – 2843

Okamoto, I., Krogler, J., Endler, G., Kaufmann, S., Mustafa, S., Exner, M., Mannhalter, C., Wagner, O., Pehamberger, H., (2006), A microsatellite polymorphism in the heme oxygenase-1 gene promoter is associated with risk for melanoma, *Int. J. Cancer.*, **119**, 1312 – 1315

Otterbein, L.E., Kolls, J.K., Mantell, L.L., Cook, J.L., Alam, J., Choi, A.M., (1999), Exogenous administration of heme oxygenase-1 by gene transfer provides protection against hyperoxia-induced lung injury, *J. Clin. Invest.*, **103**, 1047 – 1054

Otterbein, L.E., Choi, A.M.K., (2000), Heme oxygenase: colors of defense against cellular stress, *Am. J. Physiol. Lung. Cell. Mol. Physiol.*, **279**, 1029 – 1037

Otterbein, L.E., Soares, M.P., Yamashita, K., Bach, F.H., (2003), Heme oxygenase-1: unleashing the protective properties of heme, *Trends. Immunol.*, **24**, 449 – 455

Oyake, T., Itoh, K., Motohashi, H., Hayashi, N., Hoshino, H., Nishizawa, M., Yamamoto, M., Igarashi, K., (1996), Bach proteins belong to a novel family of BTB-basic leucine zipper transcription factors that interact with MafK and regulate transcription through the NF-E2 site, *Mol. Cell. Biol.*, **16**, p6083 – 6095

Pae, H.O., Oh, G.S., Jeong, S.O., Jeong, G.S., Lee, B.S., Choi, B.M., Lee, H.S., Chung, H.T., (2006), 1,2,3,4,6-penta-O-galloyl-beta-D-glucose up-regulates heme oxygenase-1 expression by stimulating Nrf2 nuclear translocation in an extracellular signal-regulated kinase-dependent manner in HepG2 cells, *World. J. Gastroenterol.*, **12**, 214 – 221

Peak, M.J., Peak, J.G., Carnes, B.A., (1987), Induction of direct and indirect single-strand breaks in human cell DNA by far- and near-ultraviolet radiations: action spectrum and mechanisms, *Photochem. Photobiol.*, **45**, 381 – 387

Peak, J.G., Peak, M.J., (1990), Ultraviolet light induces double-strand breaks in DNA of cultured human P3 cells as measured by neutral filter elution, *Photochem. Photobiol.*, **52**, 387 – 393

Pederson, A.O., Shonheydor, F., Broderson, R., (1977), Photooxidation of human serum albumin and its complex with bilirubin. *Eur. J. Biochem.*, **72**, 213 – 221

Pfaffl, M., (2001), A new mathematical model for relative quantification in real-time RT-PCR, *Nucleic. Acids. Res.*, **29**, 45

Pflaum, M., Boiteux, S., Epe, B., (1994), Visible light generates oxidative DNA base modifications in high excess of strand breaks in mammalian cells, *Carcinogenesis.*, **15**, 297 – 300

Ponka, P., Beaumont, C., Richardson, D.R., (1998), Function and regulation of transferrin and ferritin, *Semin. Hematol.*, **35**, 35 – 54

Poss, K.D., Tonegawa, S., (1997), Reduced stress defense in heme oxygenase 1-deficient cells, *Proc. Natl. Acad. Sci. USA.*, **94**, 10925 – 10930

Pourzand, C., Watkin, R.D., Brown, J.E., Tyrrell, R.M., (1999), Ultraviolet A radiation induces immediate release of iron in human primary skin fibroblasts: the role of ferritin, *Proc. Natl. Acad. Sci. USA.*, **96**, 6751 – 6756

Prawan, A., Kundu, J.K., Surh, Y.J., (2005), Molecular basis of heme oxygenase-1 induction: implications for chemoprevention and chemoprotection, *Antioxid. Redox. Signal.*, **7**, 1688 – 1703

Proteggente, A.R., Basu-Modak, S., Kuhnle, G., Gordon, M.J., Youdim, K., Tyrrell, R.M., Rice-Evans C.A., (2003), Hesperetin glucuronide, a photoprotective agent arising from flavonoid metabolism in human skin fibroblasts, *Photochem Photobiol.*, **78**, 256 – 261

Puntarulo, S., (2005), Iron, oxidative stress and human health, *Mol. Aspects. Med.*, **26**, 299 – 312

Ramos-Gomez, M., Kwak, M.K., Dolan, P.M., Itoh, K., Yamamoto, M., Talalay, P., Kensler, T.W., (2001), Sensitivity to carcinogenesis is increased and chemoprotective efficacy of enzyme inducers is lost in nrf2 transcription factor-deficient mice, *Proc. Natl. Acad. Sci. USA.*, **98**, 3410 – 3415

Reeve, V.E., Tyrrell, R.M., (1999), Heme oxygenase induction mediates the photoimmunoprotective activity of UVA radiation in the mouse, *Proc. Natl. Acad. Sci. USA.*, **96**, 9317 – 9321

Rockmann, H., Schadendorf, D., (2003), Drug resistance in human melanoma: mechanisms and therapeutic opportunities, *Onkologie.*, **26**, 581 – 587

Ryter, S.W., Tyrrell, R.M., (1998), Singlet molecular oxygen: a possible effector of eukaryotic gene expression, *Free. Radic. Biol. Med.*, **24**, 1520 – 1534

Ryter, S.W., Tyrrell, R.M., (2000), The heme synthesis and degradation pathways: role in oxidant sensitivity:Heme oxygenase has both pro- and antioxidant properties, *Free. Radic. Biol. Med.*, **28**, 289 – 309

Rushmore, T.H., Morton, M.R., Pickett, C.B., (1991), The antioxidant responsive element. Activation by oxidative stress and identification of the DNA consensus sequence required for functional activity, *J. Biol. Chem.*, **266**, 11632 – 11639

Rushworth, S.A., Ogborne, R.M., Charalambos, C.A., O'Connell, M.A., (2006), Role of protein kinase C delta in curcumin-induced antioxidant response element-mediated gene expression in human monocytes, *Biochem. Biophys. Res. Commun.*, **341**, 1007 – 1016

Sahoo, S.K., Sawa, T., Fang, J., Tanaka, S., Miyamoto, Y., Akaike, T., Maeda, H., (2002), Pegylated zinc protoporphyrin: a water-soluble heme oxygenase inhibitor with tumor-targeting capacity, *Bioconjug. Chem.*, **13**, 1031 – 1038

Saikawa, Y., Kaneda, H., Yue, L., Shimura, S., Toma, T., Kasahara, Y., Yachie, A., Koizumi, S., (2000), Structural evidence of genomic exon-deletion mediated by Alu-Alu recombination in a human case with heme oxygenase-1 deficiency, *Hum. Mutat.*, **6**, 178 – 9

Sassa, S., (1976), Sequential induction of heme pathway enzymes during erythroid differentiation of mouse Friend leukemia virus-infected cells, *J. Exp. Med.*, **143**, 305 – 315

Schuller, D.J., Wilks, A., Ortiz de Montelliano, P.R., Poulos, T.L., (1999), Crystal structure of human heme oxygenase-1, *Nat. Struc. Biol.*, **6**, 860 – 867

Sekhar, K.R., Yan, X.X., Freeman, M.L., (2002), Nrf2 degradation by the ubiquitin proteasome pathway is inhibited by KIAA0132, the human homolog to INrf2, *Oncogene*, **21**, 6829 – 6834

Setlow, R.B., Grist, E., Thompson, K., Woodhead, A.D., (1993), Wavelengths effective in induction of malignant melanoma, *Proc. Natl. Acad. Sci. USA.*, **90**, 6666 – 6670

Shan, Y., Lambrecht, R.W., Donohue, S.E., Bonkovsky, H.L., (2006), Role of Bach1 and Nrf2 in up-regulation of the heme oxygenase-1 gene by cobalt protoporphyrin, FASEB J., **20**, 2651 – 2653

She, Q.B., Chen, N., Dong, Z., (2000), ERKs and p38 kinase phosphorylate p53 protein at serine 15 in response to UV radiation, *J. Biol. Chem.*, **275**, 20444 – 20449

Shen, G., Jeong, W.S., Hu, R., Kong, A.N., (2005), Regulation of Nrf2, NF-kappaB, and AP-1 signaling pathways by chemopreventive agents, *Antioxid. Redox. Signal.*, **7**, 1648 – 1663

Shibahara, S., Muller, R.M., Taguchi, H., (1987), Transcriptional control of rat heme oxygenase by heat shock, *J. Biol. Chem.*, **262**, 12889 – 12892

Shibahara, S., (1988), Regulation of heme oxygenase gene expression, *Semin. Hematol.*, **25**, 370 – 376

Silva, G., Cunha, A., Gregoire, I.P., Seldon, M.P., Soares, M.P., (2006), The antiapoptotic effect of heme oxygenase-1 in endothelial cells involves the degradation of p38 alpha MAPK isoform, *J. Immunol.*, **177**, 1894 – 1903

Singh, A., (1982), Chemical and biochemical aspects of superoxide radicals and related species of activated oxygen, *Can. J. Physiol. Pharmacol.*, **60**, 1330 – 1345

Singleton, J.W., Laster, L., (1965), Biliverdin reductase of guinea pig liver, *J. Biol. Chem.*, **240**, 4780 – 4789

Siow, R.C., Sato, H., Mann, G.E., (1999), Heme oxygenase-carbon monoxide signalling pathway in atherosclerosis: anti-atherogenic actions of bilirubin and carbon monoxide, *Cardiovasc. Res.*, **41**, 385 – 394

Smith, M.A., Kutty, R.K., Richey, P.L., Yan, S.D., Stern, D., Chader, G.J., Wiggert, B., Petersen, R.B., Perry, G., (1994), Heme oxygenase-1 is associated with the neurofibrillary pathology of Alzheimer's disease, *Am. J. Pathol.*, **145**, 42 – 47

So, H.S., Kim, H.J., Lee, J.H., Lee, J.H., Park, S.Y., Park, C., Kim, Y.H., Kim, J.K., Lee, K.M., Kim, K.S., Chung, S.Y., Jang, W.C., Moon, S.K., Chung, H.T., Park, R.K., (2006), Flunarizine induces Nrf2-mediated transcriptional activation of heme oxygenase-1 in protection of auditory cells from cisplatin, *Cell. Death. Differ.*, **13**, 1763 – 1775

Soares, M.P., Lin, Y., Anrather, J., Csizmadia, E., Takigami, K., Sato, K., Grey, S.T., Colvin, R.B., Choi, A.M., Poss, K.D., Bach, F.H., (1998), Expression of heme oxygenase-1 can determine cardiac xenograft survival, *Nat. Med.*, **4,** 1073 – 1077

Soengas, M.S., Lowe, S.W., (2003), Apoptosis and melanoma chemoresistance. *Oncogene.*, **22**, 3138 – 3151

Soriani, M., Hejmadi, V., Tyrrell, R.M., (2000), Modulation of c-jun and c-fos transcription by UVB and UVA radiations in human dermal fibroblasts and KB cells, *Photochem. Photobiol.*, **71**, 551 – 558

Soter, N.A., (1990), Acute effects of ultraviolet radiation on the skin, *Semin. Dermatol.*, **9**, 11 – 5

Srivastava, K.K., Cable, E.E., Donohue, S.E., Morisawa, S., (1993), Molecular basis for heme-dependent induction of heme oxygenase in primary cultures of chich embryo hepatocytes. Demonstration of acquired refractoriness to heme, *Eur. J. Biochem.*, **213**, 909 – 917

Stacy, D.R., Ely, K., Massion, P.P., Yarbrough, W.G., Hallahan, D.E., Sekhar, K.R., Freeman, M.L., (2006), Increased expression of nuclear factor E2 p45-related factor 2 (NRF2) in head and neck squamous cell carcinomas, *Head. Neck.*, **28**, 813 – 818

Stewart, D., Killeen, E., Naquin, R., Alam, S., Alam, J., (2003), Degradation of transcription factor Nrf2 via the ubiquitin-proteasome pathway and stabilization by cadmium, *J. Biol. Chem.*, **278**, 2396 – 2402

Stevens, B., Small, R.D., (1976), The photoperoxidation of unsaturated organic molecules-XV.$O_2{}^1\Delta_g$ quenching by bilirubin and biliverdin, *Photochem. Photobiol*, **23**, 33 – 36

Stocker, R., Ames, B.N., (1987), Potential role of conjugated bilirubin and copper in the metabolism of lipid peroxides in bile, *Proc. Natl. Acad. Sc.i USA.*, **84**, 8130 – 8134

Stocker, R., Yamamoto, Y., McDonagh, A.F., Glazer, A.N., Ames, B.N., (1987), Bilirubin is an anti-oxidant of possible physiological importance, *Science*, **235**, 1043 – 1046

Sun, J., Hoshino, H., Takaku, K., Nakajima, O., Muto, A., Suzuki, H., Tahsiro, S., Takahashi, S., Shibahara, S., Alam, J., Taketo, M.M., Yamamoto, M., Igarishi, K., (2002), Hemoprotein Bach1 regulates enhancer availability of heme oxygenase-1 gene, *EMBO,* **21**, 5216 – 5224

Sunamura, M., Duda, D.G., Ghattas, M.H., Lozonschi, L., Motoi, F., Yamauchi, J., Matsuno, S., Shibahara, S., Abraham, N.G., (2003), Heme oxygenase-1 accelerates tumor angiogenesis of human pancreatic cancer, *Angiogenesis*, **6**, 15 – 24

Sutherland, B.M., Cimino, J.S., Delihas, N., Shih, A.G., Oliver, R.P., (1985), Ultraviolet light-induced transformation of human cells to anchorage-independent growth, *Cancer. Res.*, **40**, 1934 – 1939

Suzuki, H., Tashiro, S., Sun, J., Doi, H., Satomi, S., Igarishi, K., (2003), Cadmium induces nuclear export of Bach1, a transcriptional repressor of heme oxygenase-1 gene, *J. Biol. Chem.*, **278**, 49246 – 49253

Suzuki, H., Tashiro, S., Hira, S., Sun, J., Yamazaki, C., Zenke, Y., Ikeda-Saito, M., Yoshida, M., Igarashi. K., (2004), Heme regulates gene expression by triggering Crm1-dependent nuclear export of Bach1, *EMBO*, **23**, 2544 – 2453

Takeda, K., Ishizawa, S., Sato, M., Yoshida, T., Shibahara, S., (1994), Identification of a *cis*-acting element that is responsible for cadmium-mediated induction of the human heme oxygenase gene, *J. Biol. Chem.*, **269**, 22858 – 22867

Taketani, S., (2005), Aquisition, mobilization and utilization of cellular iron and heme: endless findings and growing evidence of tight regulation, *Tohoku. J. Exp. Med.*, **4**, 297 – 318

Tanaka, S., Akaike, T., Fang, J., Beppu, T., Ogawa, M., Tamura, F., Miyamoto, Y., Maeda, H., (2003), Antiapoptotic effect of haem oxygenase-1 induced by nitric oxide in experimental solid tumour, *Br. J. Cancer.*, **88**, 902 – 909

Tenhunen, R., Marver, H.S., Schmid, R., (1968), The enzymatic conversion of heme to bilirubin by microsomal heme oxygenase, *Proc. Natl. Acad. Sci. USA.*, **61**, 748 – 755

Tenhunen, R., Marver, H.S., Schmid, R., (1969), Microsomal heme oxygenase, characterization of the enzyme, *J. Biol. Chem.*, **244**, 6388 – 6394

Thilly, W.G., (1979), Study of mutagenesis in diploid fibroblasts. In: Mammalian Cell Mutagenesis: The Maturation of Test Systems, *Cold Spring Harbour Laboratory Press*, 341 – 350

Thompson, C.B., (1995), Apoptosis in the pathogenesis and treatment of disease, *Science*, **267**, 1456 – 1462

Thompson, D., Basu-Modak, S., Gordon, M., Poore, S., Markovitch, D., Tyrrell, R.M., (2005), Exercise-induced expression of heme oxygenase-1 in human lymphocytes, *Free. Radic. Res.*, **39**, 63 – 69

Torisu-Itakura, H., Furue, M., Kuwano, M., Ono, M., (2000), Co-expression of thymidine phosphorylase and heme oxygenase-1 in macrophages in human malignant vertical growth melanomas, *Jpn. J. Cancer. Res,* **91**, 906 – 910

Torti, F.M., Torti, S.V., (2002), Regulation of ferritin genes and protein, *Blood*, **99**, 3505 – 3516

Trekli, M.C., Riss, G., Goralczyk, R., Tyrrell, R.M., (2003), Beta-carotene suppresses UVA-induced HO-1 gene expression in cultured FEK4, *Free. Radic. Biol. Med.,* **34**, 456 – 464

Tschudy, D.P., Hess, R.A., Frykholm, B.C., (1981), Inhibition of delta-aminolevulinic acid dehydrase by 4,6-dioxoheptanoic acid, *J. Biol. Chem.*, **19**, 9915 – 9923

Tsien, R.Y., (1998), The green fluorescent protein, *Annu. Rev. Biochem.*, **67**, 509 – 544

Tsuji, M.H., Yanagawa, T., Iwasa, S., (1999), Heme oxygenase-1 expression in oral squamous cell carcinoma as involved in lymph node metastasis, *Cancer Lett.*, **138**, 53 – 59

Tyrrell, R.M., (1973), Induction of pyrimidine dimmers in bacterial DNA by 365 nm radiation, *Photochem. Photobiol.*, **17**, 69 – 73

Tyrrell, R.M., (1979), Lethal cellular changes induced by near ultraviolet radiation, *Acta. Biol. Med. Ger.*, **38**, 1259 – 1269

Tyrrell, R.M., Pidoux, M., (1986), Quantitative differences in host cell reactivation of ultraviolet-damaged virus in human skin fibroblasts and epidermal keratinocytes cultured from the same foreskin biopsy, *Cancer. Res.*, **46**, 2665 – 2669

Tyrrell, R.M., Pidoux, M., (1989), Singlet oxygen involvement in the inactivation of cultured human fibroblasts by UVA (334 nm, 365 nm) and near-visible (405 nm) radiations, *Photochem. Photobiol.*, **49**, 407 – 412

Tyrrell, R.M., Keyse, S.M., (1990), New trends in photobiology. The interaction of UVA radiation with cultured cells, *J. Photochem. Photobiol. B.*, **4**, 349 – 361

Tyrrell, R.M., (1991), UVA (320 – 380 nm) radiation as an oxidative stress, *In: Oxidative Stress: Oxidants and Antioxidants*, Academic Press, London, 57 – 83

Tyrrell, R.M., Keyse, S.M., Moraes, E.C., (1991), Cellular defence against UVA (320 – 380 nm) and UVB (290 – 320 nm) radiations, *In: Photobiology: The Science and its Application,* 861 – 871

Tyrrell, R.M., (1994), The molecular and cellular pathology of solar ultraviolet radiation, *Mol. Aspects. Med.*, **15**, 1 – 77

Tyrrell, R.M., (1996), Activation of mammalian gene expression by the UV component of sunlight--from models to reality, *Bioessays.*, **18**, 139 – 148

Umlas, M.E., Franklin, W.A., Chan, G.L., Haseltine, W.A., (1985), Ultraviolet light irradiation of defined-sequence DNA under conditions of chemical photosensitization, *Photochem. Photobiol.*, **42**, 265 – 273

VandeBerg, J.L., Williams-Blangero, S., Hubbard, G.B., Ley, R.D., Robinson, E.S., (1994), Genetic analysis of ultraviolet radiation-induced skin hyperplasia and neoplasia in a laboratory marsupial model (Monodelphis domestica), *Arch. Dermatol. Res.*, **286**, 12 – 17

Vargas, M.R., Pehar, M., Cassina, P., Martinez-Palma, L., Thompson, J.A., Beckman, J.S., Barbeito, L., (2005), Fibroblast growth factor-1 induces heme oxygenase-1 via nuclear factor erythroid 2-related factor 2 (Nrf2) in spinal cord astrocytes: consequences for motor neuron survival, *J. Biol. Chem.*, **280**, 25571 – 25579

Vera, T., Kelsen, S., Yanes, L.L., Reckelhoff, J.F., Stec, D.E., (2006), HO-1 induction lowers blood pressure and superoxide production in the renal medulla of angiotensin II hypertensive mice, *Am. J. Physiol. Regul. Integr. Comp. Physiol.*, 292, 1472 – 1478

Verhoven, B., Schlegel, R.A., Williamson, P., (1995), Mechanisms of phosphatidylserine exposure, a phagocyte recognition signal, on apoptotic T lymphocytes, *J. Exp. Med.*, **182**, 1597 – 1601

Vermes, I., Haanen, C., Steffens-Nakken, H., Reutelingsperger, C., (1995), A novel assay for apoptosis. Flow cytometric detection of phosphatidylserine expression on early apoptotic cells using fluorescein labelled Annexin V, *J. Immunol. Methods.*, **84**, 39 – 51

Verma, I.M., Sassone-Corsi, P., (1987), Proto-oncogene fos: complex but versatile regulation, *Cell*, **51**, 513 – 514

Verna, A., Hirsch, D.J., Glatt, C.E., Ronnett, G.V., Snyder, S.H., (1993), Carbon monoxide: aputative neural messenger, *Science,* **259**, 381 – 384

Vile, G.F., Tyrrell, R.M., (1993), Oxidative stress resulting from ultraviolet A irradiation of human skin fibroblasts leads to a heme oxygenase-dependent increase in ferritin, *J. Biol. Chem.*, **268**, 14678 – 14681

Wakabayashi, N., Itoh, K., Wakabayashi, J., Motohashi, H., Noda, S., Takahashi, S., Imakado, S., Kotsuji, T., Otsuka, F., Roop, D.R., Harada, T., Engel, J.D., Yamamoto, M., (2003), Keap1-null mutation leads to postnatal lethality due to constitutive Nrf2 activation, *Nat. Genet.*, **35**, 238 – 245

Walling, C., (1975), Fenton's reagent revisited, *Act. Chem. Res.*, **8**, 125 – 131

Wang, L.J., Lee, T.S., Lee, F.Y., Pai, R.C., Chau, L.Y., (1998), Expression of heme oxygenase-1 in atherosclerotic lesions, *Am. J. Pathol.*, **152**, 711 – 720

Wang, X., Wang, Y., Kim, H.P., Nakahira, K., Ryter, S.W., Choi, A.M., (2007), Carbon monoxide protects against hyperoxia-induced endothelial cell apoptosis by inhibiting reactive oxygen species formation, *J. Biol. Chem.*, **282**, 1718 – 1726

Was, H., Cichon, T., Smolarczyk, R., Rudnicka, D., Stopa, M., Chevalier, C., Leger, J.J., Lackowska, B., Grochot, A., Bojkowska, K., Ratajska, A., Kieda, C., Szala, S., Dulak, J., Jozkowicz, A., (2006), Overexpression of heme oxygenase-1 in murine melanoma: increased proliferation and viability of tumor cells, decreased survival of mice, *Am. J. Pathol.*, **169**, 2181 – 2198

Webb, R.B., and Lorenz, J.R., (1970), Oxygen dependence and repair of lethal effects of near ultraviolet and visible light, *Photochem. Photobiol.*, **12**, 283 – 289

Webb, R.B., (1977), Lethal and mutagenic effects of near-ultraviolet radiarion, *Photochem. Photobiol.*, **2**, 169 – 262

Westerdahl, J., Ingvar, C., Masback, A., Jonsson, N., Olsson, H., (2000), Risk of cutaneous malignant melanoma in relation to use of sunbeds: further evidence for UV-A carcinogenicity, *Br. J. Cancer.*, **82**, 1593 – 1599

Wilkinson, F.J., (1983), Recommended UV exposure limits for tanning equipment, and spectral irradiances of solarium lamps, sunlamps and daylight, *Australas. Phys. Eng. Sci. Med.*, **6**, 26 – 34

Woo, J., Iyer, S., Mori, N., Buelow, R., (2000), Alleviation of graft-versus-host disease after conditioning with cobalt-protoporphyrin, an inducer of heme oxygenase-1, *Transplantation*, **69**, 623 – 633

Wu, C.C., Hsu, M.C., Hsieh, C.W., Lin, J.B., Lai, P.H., Wung, B.S., (2005), Upregulation of heme oxygenase-1 by Epigallocatechin-3-gallate via the phosphatidylinositol 3-kinase/Akt and ERK pathways, *Life. Sci.*, **78**, 2889 – 2897

Wu, C.C., Hsieh, C.W., Lai, P.H., Lin, J.B., Liu, Y.C., Wung, B.S., (2006), Upregulation of endothelial heme oxygenase-1 expression through the activation of the JNK pathway by sublethal concentrations of acrolein, *Toxicol. Appl. Pharmacol.*, **214**, 244 – 252

Wyllie, A.H., (1980), Glucocorticoid-induced thymocyte apoptosis is associated with endogenous endonuclease activation, *Nature.*, **284**, 555 – 556

Xia, Z.W., Zhong, W.W., Xu, L.Q., Sun, J.L., Shen, Q.X., Wang, J.G., Shao, J., Li, Y.Z., Yu, S.C., (2006), Heme oxygenase-1-mediated CD4+CD25high regulatory T cells suppress allergic airway inflammation, *J. Immunol.*, **177**, 5936 – 5945

Yachie, A., Niida, Y., Wata, T., Igarashi, N., Kaneda, H., Toma, T., Ohta, K., Kasahara, Y., Koizumi, S., (1999), Oxidative stress causes enhanced endothelial cell injury in human heme oxygenase-1 deficiency. *J. Clinical Inv.*, **103**, 129 – 135

Yamada, N., Yamaya, M., Okinaga, S., Nakayama, K., Sekizawa, K., Shibahara, S, Sasaki, H., (2000), Microsatellite polymorphism in the heme oxygenase-1 gene promoter is associated with susceptibility to emphysema, *Am. J. Hum. Genet.*, **66**, 187 – 195

Yates, M.S., Kwak, M.K., Egner, P.A., Groopman, J.D., Bodreddigari, S., Sutter, T.R., Baumgartner, K.J., Roebuck, B.D., Liby, K.T., Yore, M.M., Honda, T., Gribble, G.W., Sporn, M.B., Kensler, T.W., (2006), Potent protection against

aflatoxin-induced tumorigenesis through induction of Nrf2-regulated pathways by the triterpenoid 1-[2-cyano-3-,12-dioxooleana-1,9(11)-dien-28-oyl]imidazole, *Cancer Res.*, **66**, 2488 – 2494

Yoshida, T., Biro, P., Cohen, T., Muller, R.M., Shibahara, S., (1988), Human heme oxygenase cDNA and induction of its mRNA by hemin, *Eur. J. Biochem.* **171**, 457 – 461

Yoshida, T., Sato, M., (1989), Posttranslational and direct integration of heme oxygenase into microsomes, *Biochem Biophys. Res. Commun,* **163**, 1086 – 1092

Zhang, X., Rosenstein, B.S., Wang, Y., Lebwohl, M., Mitchell, D.M., Wei, H., (1997), Induction of 8-oxo-7,8-dihydro-2'-deoxyguanosine by ultraviolet radiation in calf thymus DNA and HeLa cells, *Photochem. Photobiol.*, **65**, 119 – 124

Zhang, D.D., Hannink, M., (2003), Distinct cysteine residues in Keap1 are required for Keap1-dependent ubiquitination of Nrf2 and for stabilization of Nrf2 by chemopreventive agents and oxidative stress, *Mol. Cell. Biol.*, **23**, 8137 – 8151

Zhang, X., Shan, P., Otterbein, L.E., Alam, J., Flavell, R.A., Davis, R.J., Choi, A.M., Lee, P.J., (2003), Carbon monoxide inhibition of apoptosis during ischemia-reperfusion lung injury is dependent on the p38 mitogen-activated protein kinase pathway and involves caspase 3, *J. Biol. Chem.*, **278**, 1248 – 1258

Zhang, X., Shan, P., Jiang, D., Noble, P.W., Abraham, N.G., Kappas, A., Lee, P.J., (2004), Small interfering RNA targeting heme oxygenase-1 enhances ischemia-reperfusion-induced lung apoptosis, *J. Biol. Chem.*, **279**, 10677 – 10684

Zhang, D.D., (2006), Mechanistic studies of the Nrf2-Keap1 signaling pathway, *Drug. Metab. Rev.*, **38**, 769 - 789

Zhivotovsky, B., Orrenius, S., (2006), Carcinogenesis and apoptosis: paradigms and paradoxes, *Carcinogenesis.*, **27**, 1939 – 1945

# 6. Appendix

## Appendix A

| Sample ID | UVA Treatment ($kJ/m^2$) | Transfection Treatment |
|---|---|---|
| **A** | 0 | pcDNA3.1 |
| **B** | 0 | pcDNA3.1-HO1 |
| **C** | 100 | pcDNA3.1 |
| **D** | 100 | pcDNA3.1-HO1 |
| **E** | 200 | pcDNA3.1 |
| **F** | 200 | pcDNA3.1-HO1 |
| **G** | 300 | pcDNA3.1 |
| **H** | 300 | pcDNA3.1-HO1 |
| **J** | 400 | pcDNA3.1 |
| **K** | 400 | pcDNA3.1-HO1 |
| **N** | -- | pcDNA3.1-EGFP |
| **P** | -- | -- |

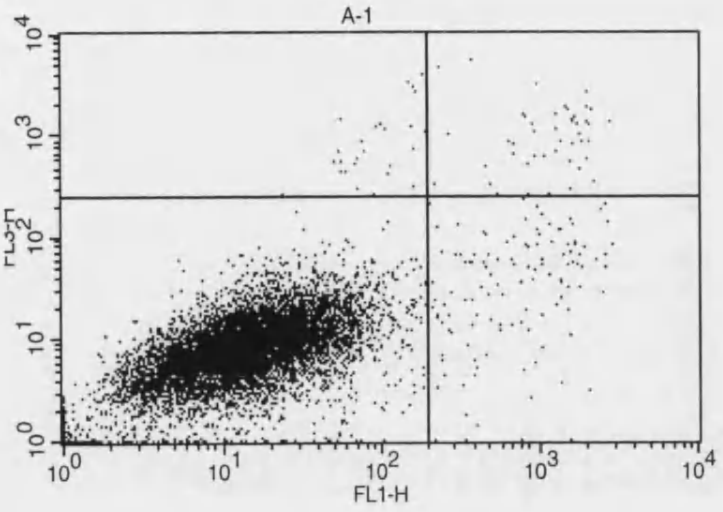


Sample ID: A-1

| Quad | % Total |
|---|---|
| UL | 0.28 |
| UR | 0.45 |
| LL | 98.06 |
| LR | 1.21 |

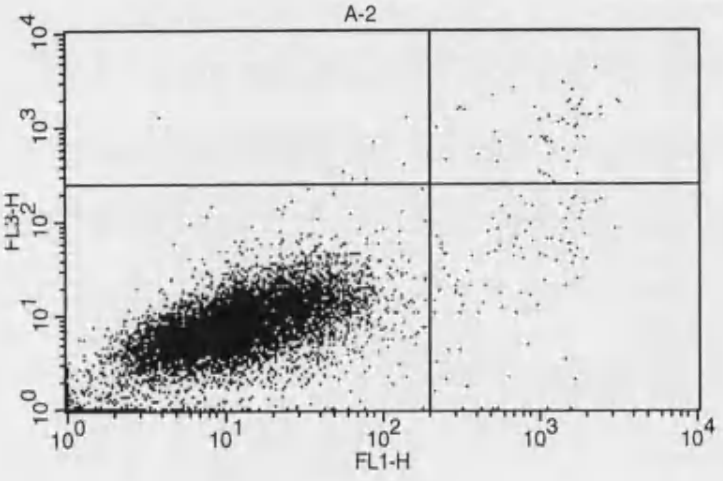


Sample ID: A-2

| Quad | % Total |
|---|---|
| UL | 0.07 |
| UR | 0.54 |
| LL | 98.43 |
| LR | 0.96 |

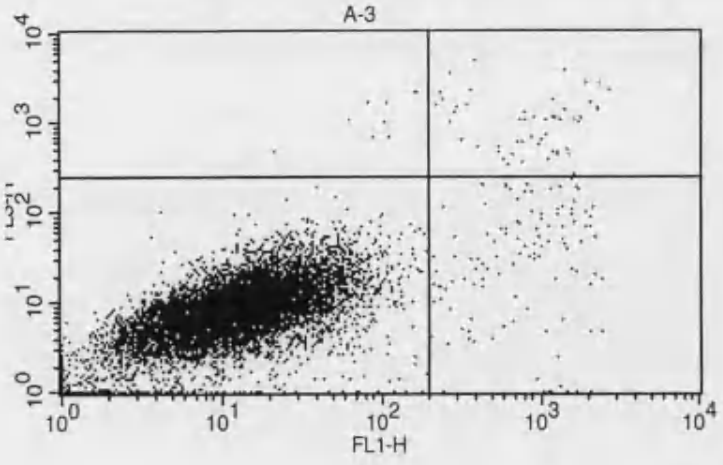


Sample ID: A-3

| Quad | % Total |
|---|---|
| UL | 0.09 |
| UR | 0.53 |
| LL | 98.23 |
| LR | 1.15 |

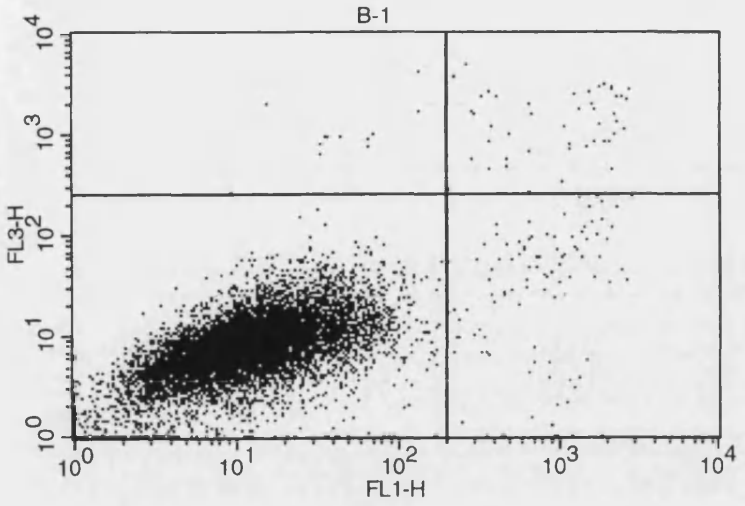


Sample ID: B-1

| Quad | % Total |
|---|---|
| UL | 0.13 |
| UR | 0.46 |
| LL | 98.38 |
| LR | 1.03 |

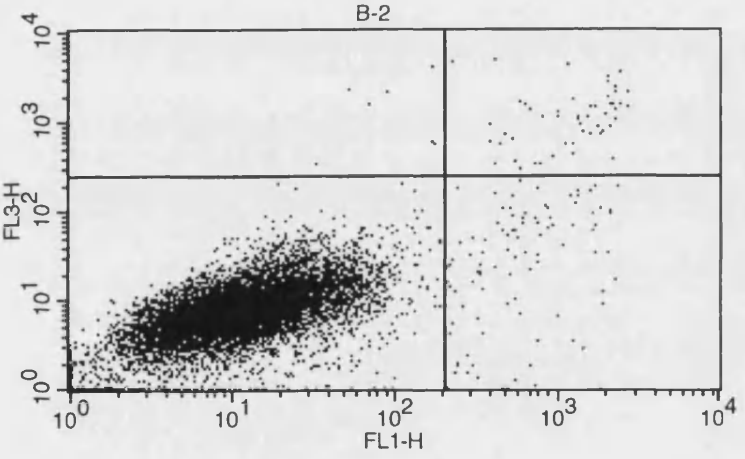


Sample ID: B-2

| Quad | % Total |
|---|---|
| UL | 0.07 |
| UR | 0.53 |
| LL | 98.40 |
| LR | 1.00 |

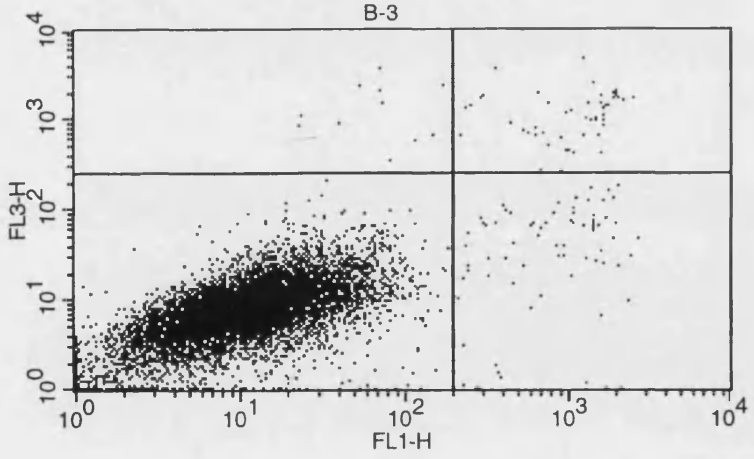


Sample ID: B-3

| Quad | % Total |
|---|---|
| UL | 0.11 |
| UR | 0.51 |
| LL | 98.62 |
| LR | 0.76 |

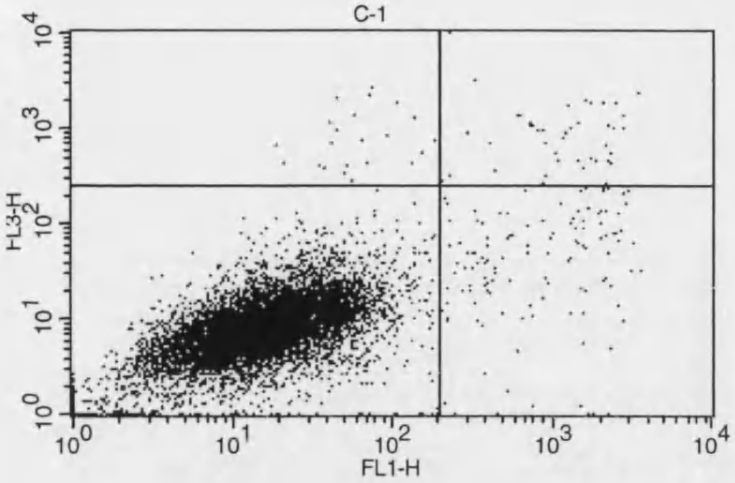


Sample ID: C-1

| Quad | % Total |
|---|---|
| UL | 0.23 |
| UR | 0.42 |
| LL | 98.12 |
| LR | 1.23 |

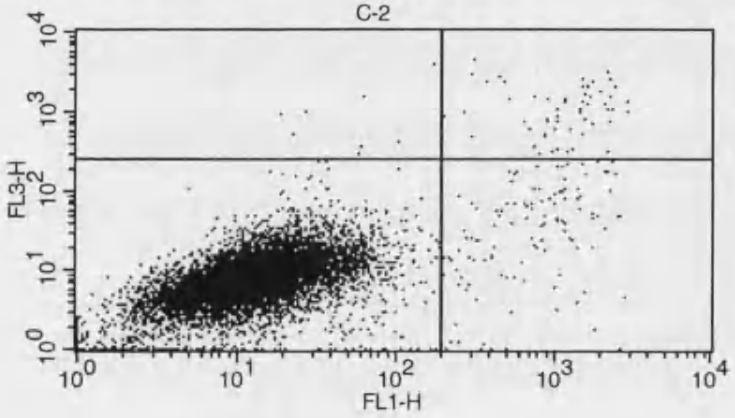


Sample ID: C-2

| Quad | % Total |
|---|---|
| UL | 0.10 |
| UR | 0.57 |
| LL | 98.17 |
| LR | 1.16 |

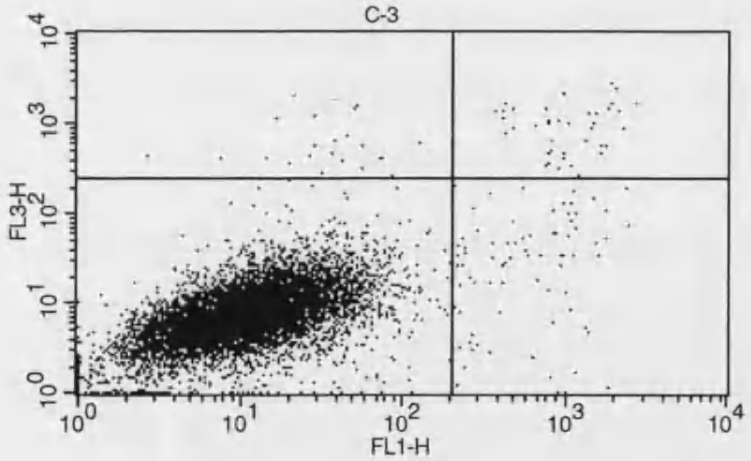


Sample ID: C-3

| Quad | % Total |
|---|---|
| UL | 0.22 |
| UR | 0.39 |
| LL | 98.59 |
| LR | 0.80 |

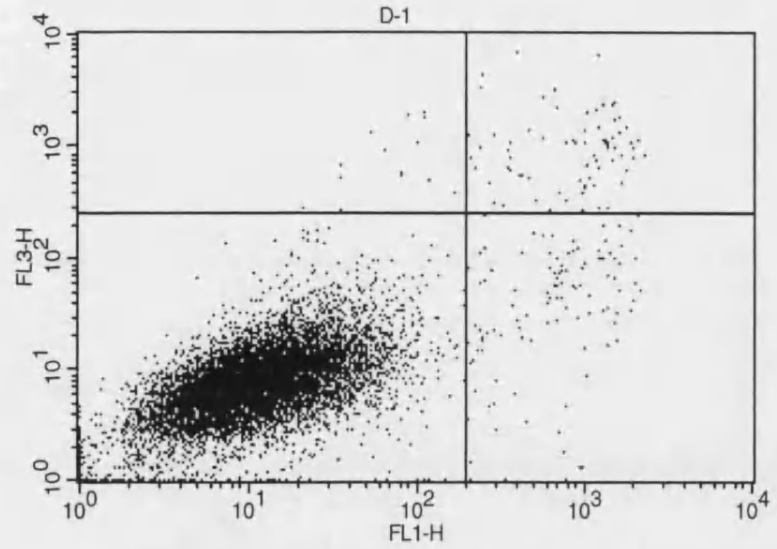


Sample ID: D-1

| Quad | % Total |
|---|---|
| UL | 0.16 |
| UR | 0.73 |
| LL | 98.04 |
| LR | 1.07 |

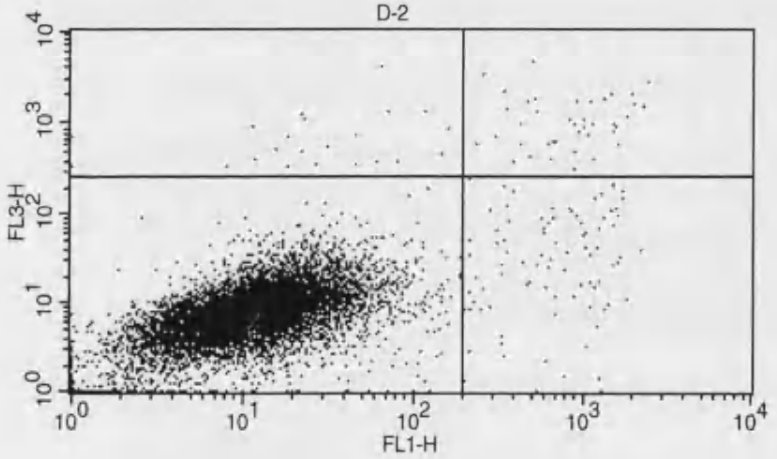


Sample ID: D-2

| Quad | % Total |
|---|---|
| UL | 0.22 |
| UR | 0.40 |
| LL | 98.50 |
| LR | 0.88 |

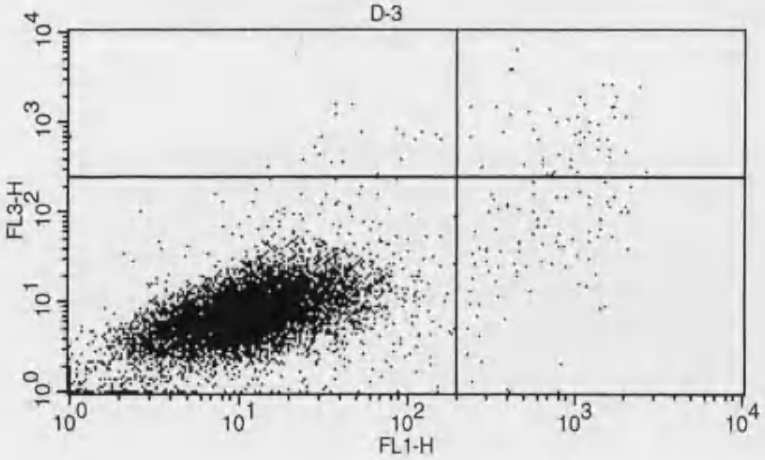


Sample ID: D-3

| Quad | % Total |
|---|---|
| UL | 0.21 |
| UR | 0.52 |
| LL | 98.38 |
| LR | 0.89 |

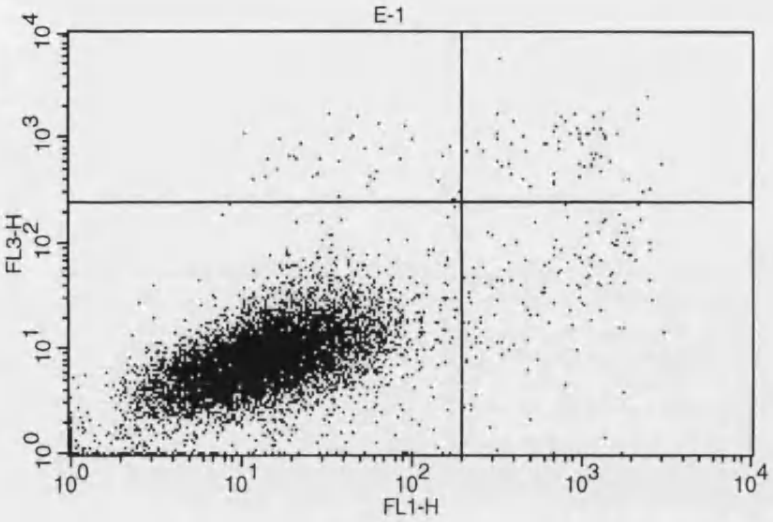


Sample ID: E-1

| Quad | % Total |
|---|---|
| UL | 0.36 |
| UR | 0.63 |
| LL | 97.67 |
| LR | 1.34 |

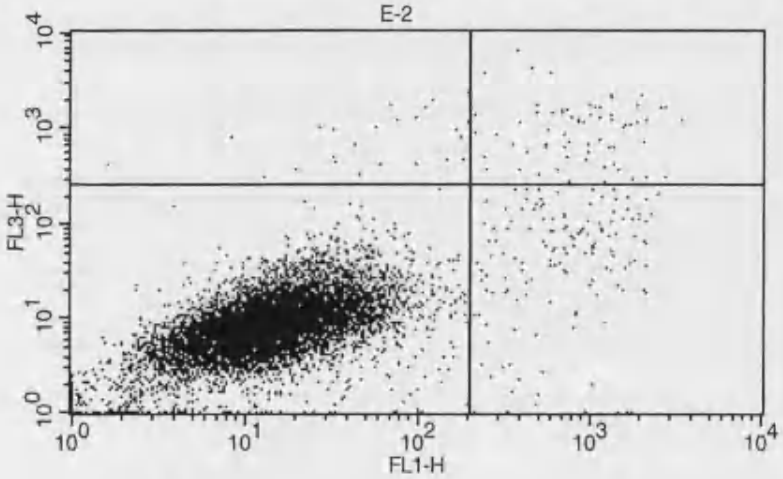


Sample ID: E-2

| Quad | % Total |
|---|---|
| UL | 0.24 |
| UR | 0.69 |
| LL | 97.64 |
| LR | 1.43 |

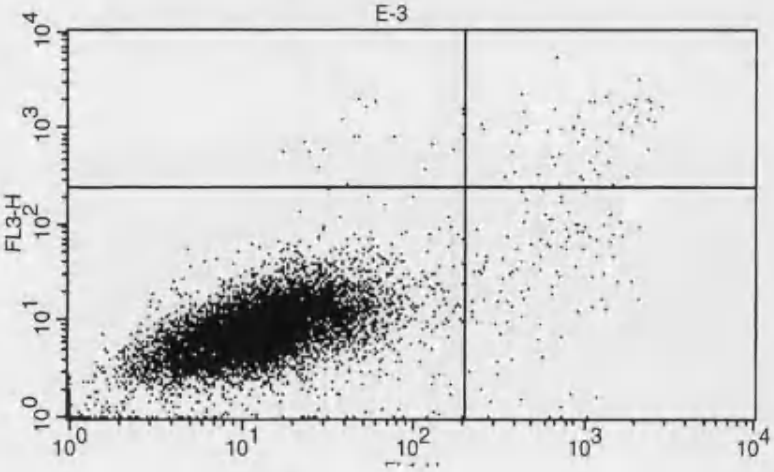


Sample ID: E-3

| Quad | % Total |
|---|---|
| UL | 0.19 |
| UR | 0.59 |
| LL | 98.06 |
| LR | 1.16 |

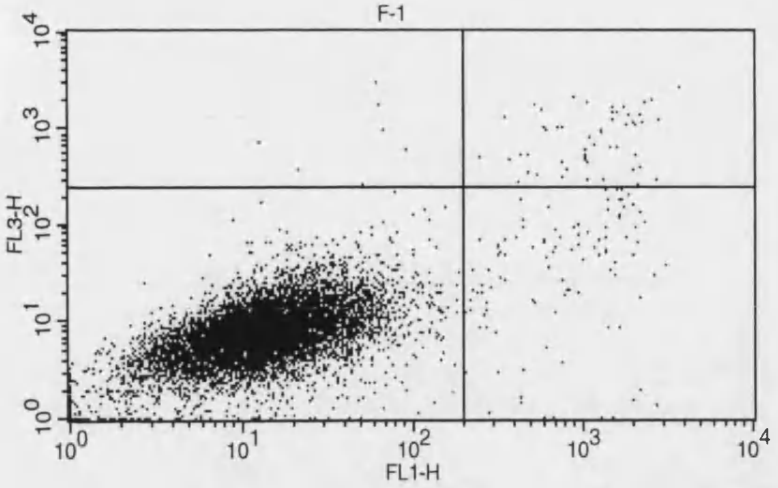


Sample ID: F-1

| Quad | % Total |
|---|---|
| UL | 0.08 |
| UR | 0.52 |
| LL | 98.33 |
| LR | 1.07 |

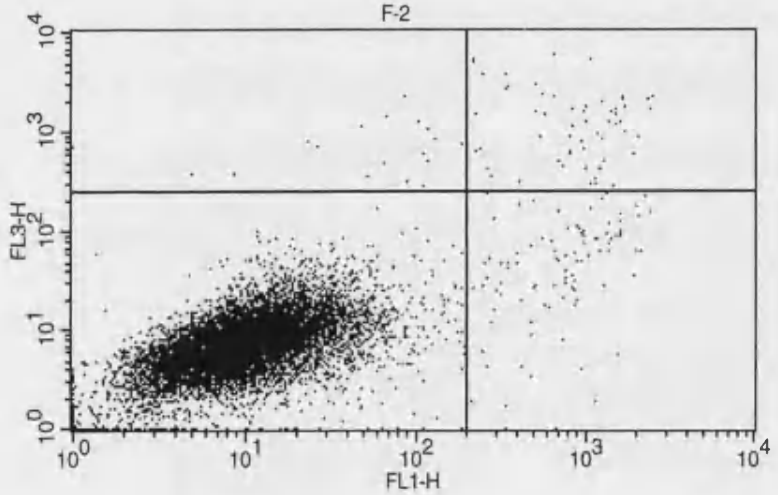


Sample ID: F-2

| Quad | % Total |
|---|---|
| UL | 0.18 |
| UR | 0.58 |
| LL | 98.29 |
| LR | 0.95 |

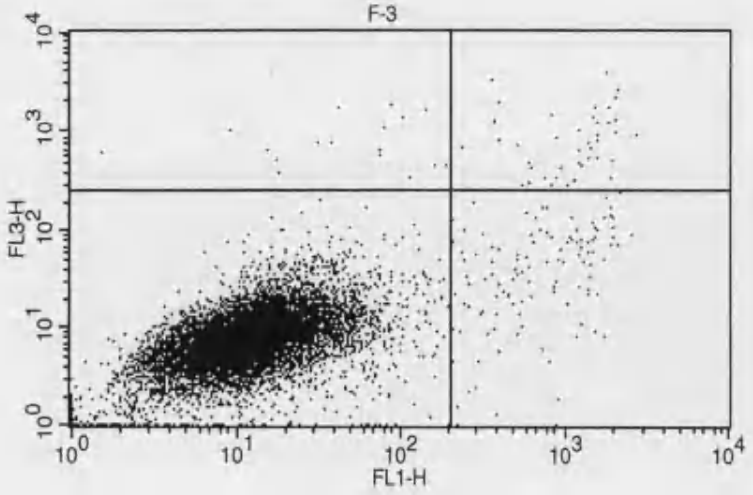


Sample ID: F-3

| Quad | % Total |
|---|---|
| UL | 0.17 |
| UR | 0.43 |
| LL | 98.23 |
| LR | 1.17 |

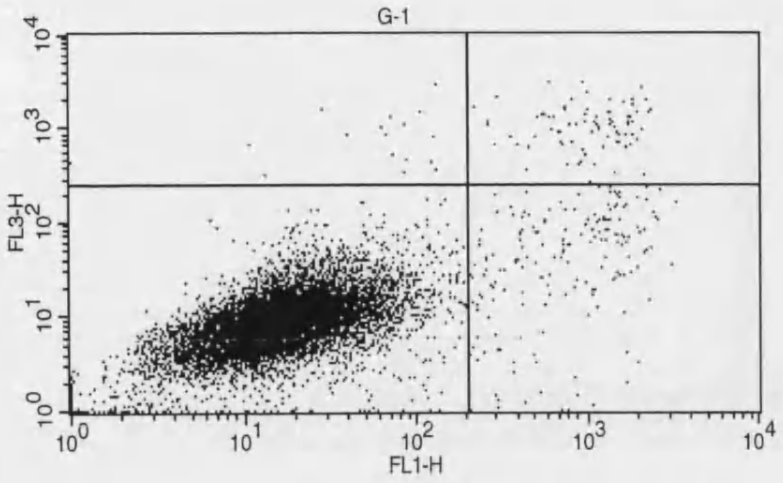


Sample ID: G-1

| Quad | % Total |
|---|---|
| UL | 0.20 |
| UR | 0.80 |
| LL | 97.21 |
| LR | 1.79 |

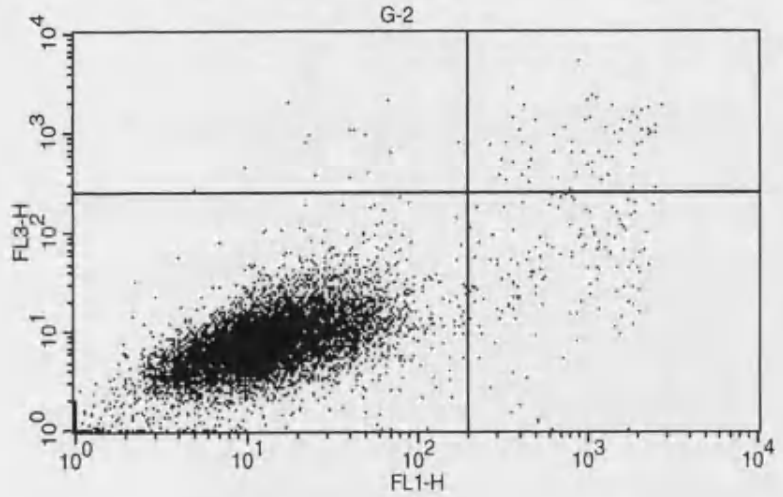


Sample ID: G-2

| Quad | % Total |
|---|---|
| UL | 0.14 |
| UR | 0.64 |
| LL | 97.81 |
| LR | 1.41 |

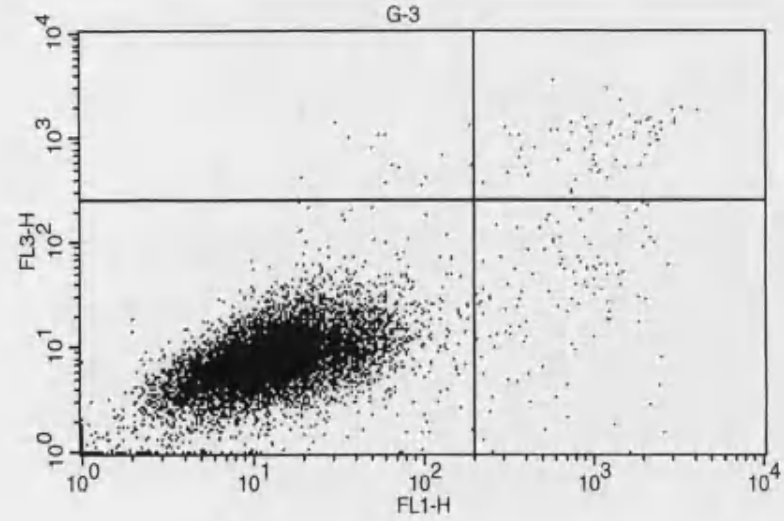


Sample ID: G-3

| Quad | % Total |
|---|---|
| UL | 0.16 |
| UR | 0.66 |
| LL | 98.01 |
| LR | 1.17 |

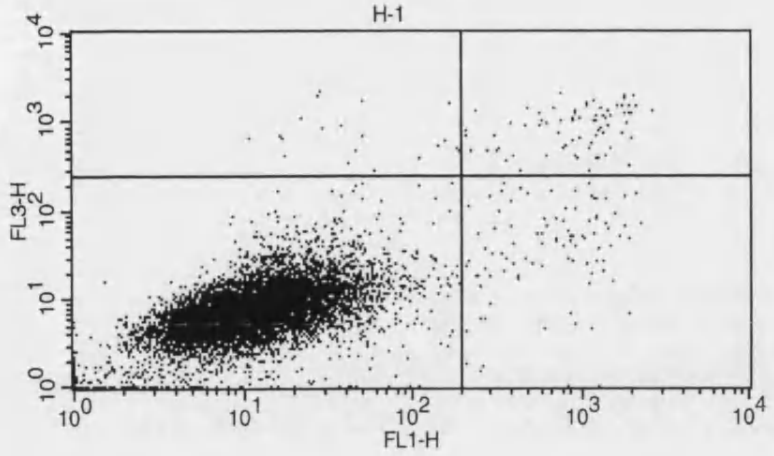


Sample ID: H-1

| Quad | % Total |
|---|---|
| UL | 0.20 |
| UR | 0.77 |
| LL | 98.06 |
| LR | 0.97 |

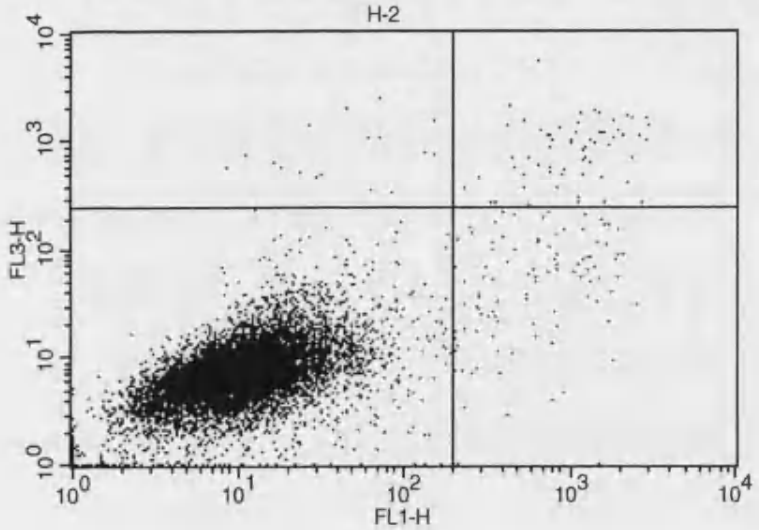


Sample ID: H-2

| Quad | % Total |
|---|---|
| UL | 0.17 |
| UR | 0.64 |
| LL | 98.22 |
| LR | 0.97 |

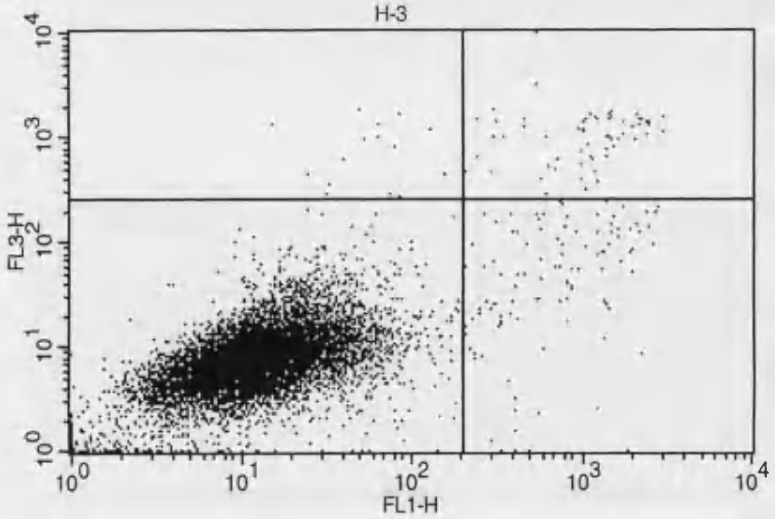


Sample ID: H-3

| Quad | % Total |
|---|---|
| UL | 0.16 |
| UR | 0.62 |
| LL | 98.17 |
| LR | 1.05 |

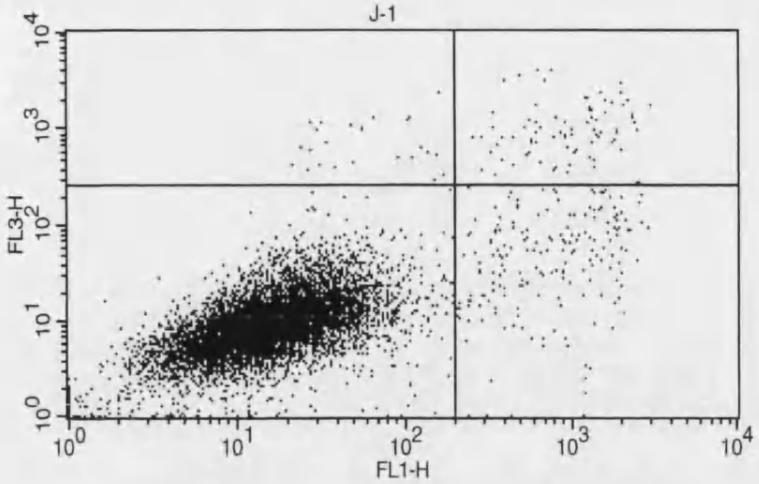


Sample ID: J-1

| Quad | % Total |
|---|---|
| UL | 0.25 |
| UR | 0.84 |
| LL | 96.99 |
| LR | 1.92 |

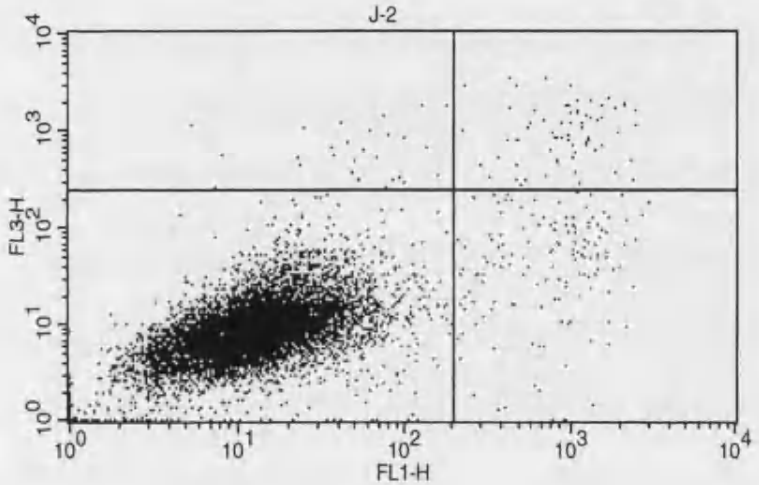


Sample ID: J-2

| Quad | % Total |
|---|---|
| UL | 0.29 |
| UR | 0.68 |
| LL | 97.60 |
| LR | 1.43 |

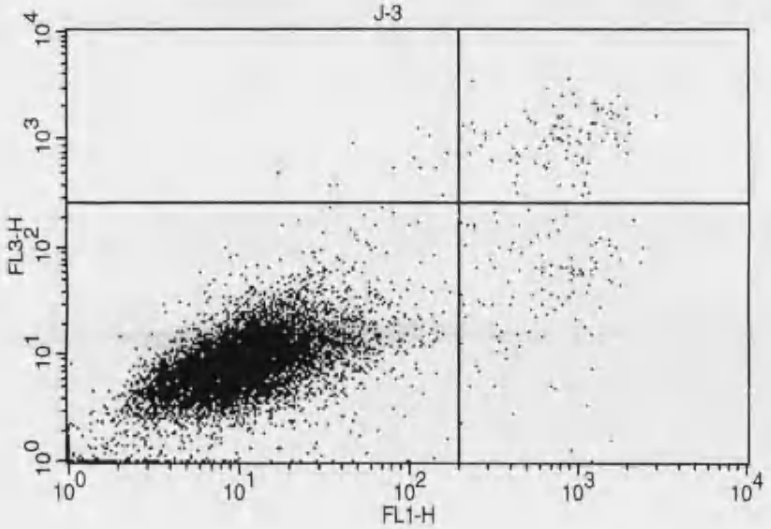


Sample ID: J-3

| Quad | % Total |
|---|---|
| UL | 0.12 |
| UR | 0.99 |
| LL | 97.75 |
| LR | 1.14 |

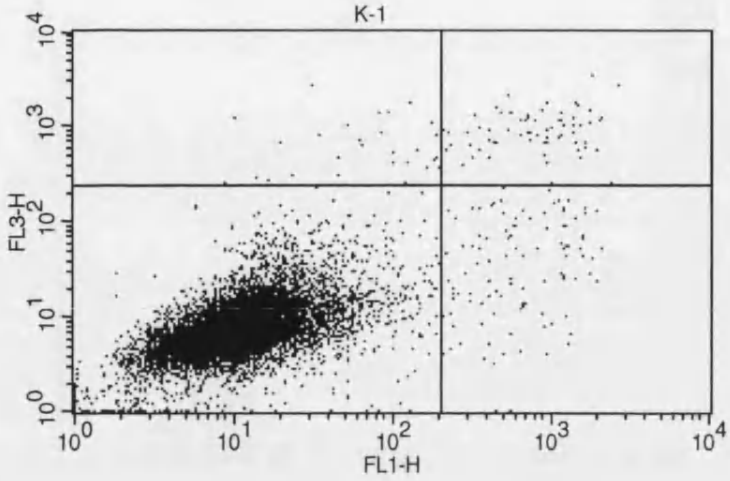


Sample ID: K-1

| Quad | % Total |
|---|---|
| UL | 0.28 |
| UR | 0.67 |
| LL | 97.97 |
| LR | 1.08 |

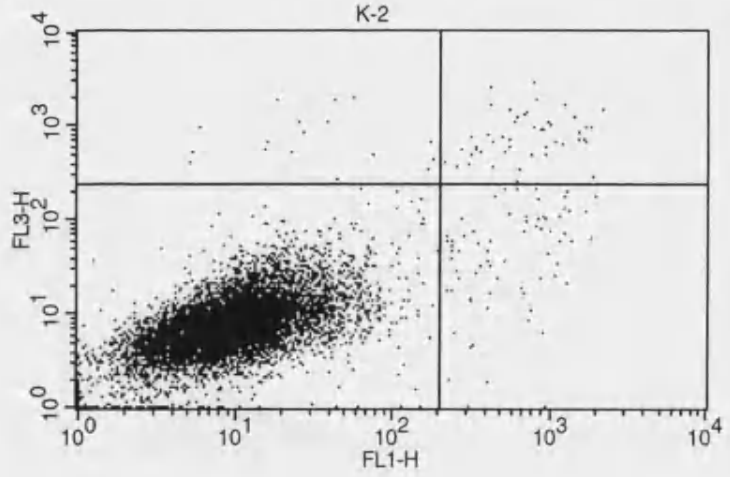


Sample ID: K-2

| Quad | % Total |
|---|---|
| UL | 0.17 |
| UR | 0.48 |
| LL | 98.64 |
| LR | 0.71 |

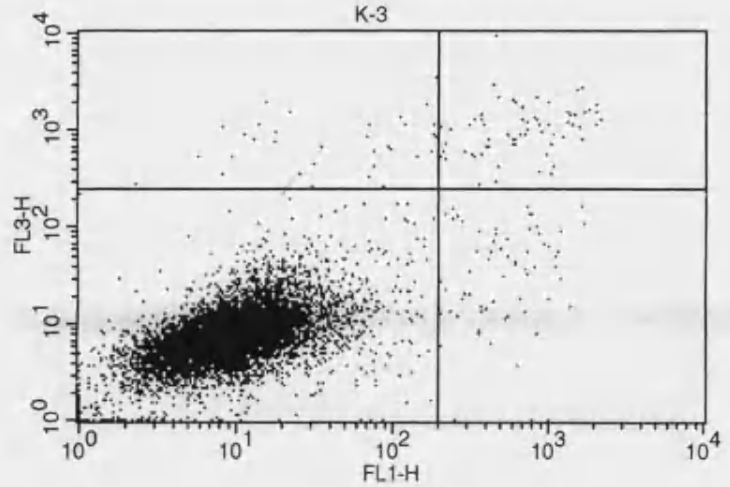


Sample ID: K-3

| Quad | % Total |
|---|---|
| UL | 0.34 |
| UR | 0.68 |
| LL | 98.31 |
| LR | 0.67 |

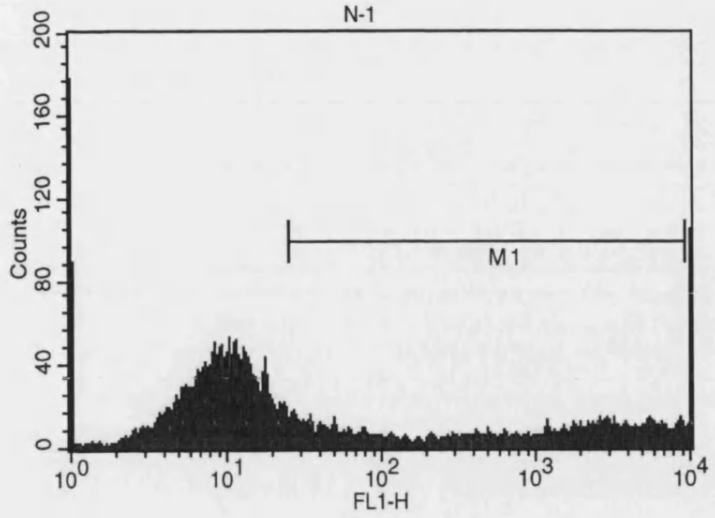


Sample ID: N-1

| Marker | % Total |
|---|---|
| All | 100.00 |
| M1 | 34.18 |

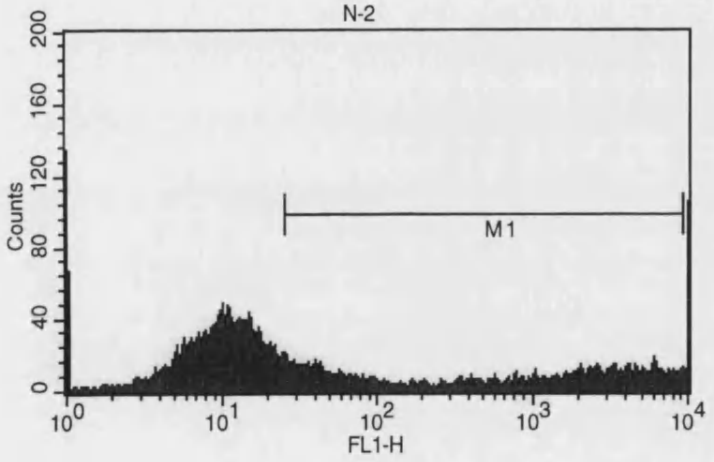


Sample ID: N-2

| Marker | % Total |
|---|---|
| All | 100.00 |
| M1 | 37.95 |

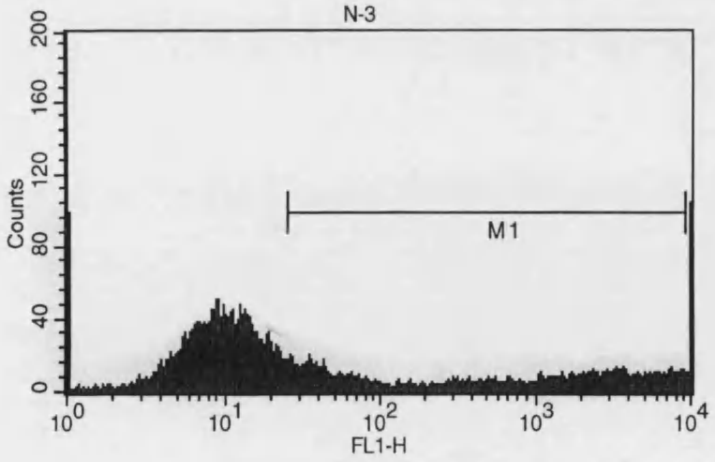


Sample ID: N-3

| Marker | % Total |
|---|---|
| All | 100.00 |
| M1 | 35.02 |

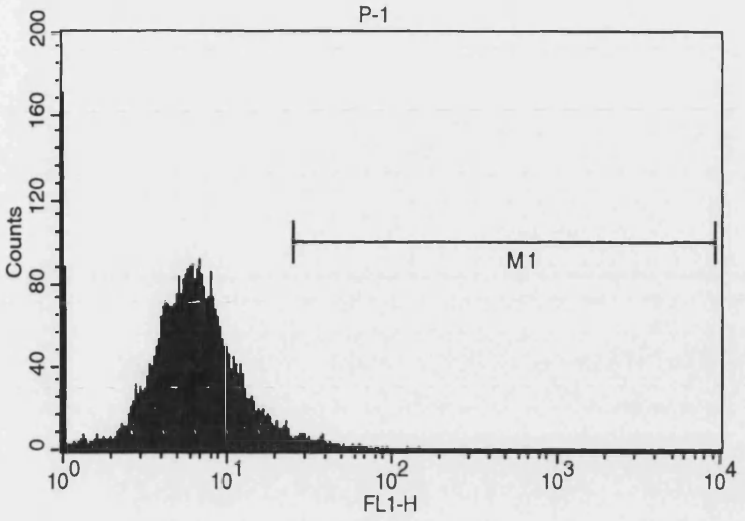


Sample ID: P-1

| Marker | % Total |
|---|---|
| All | 100.00 |
| M1 | 1.83 |

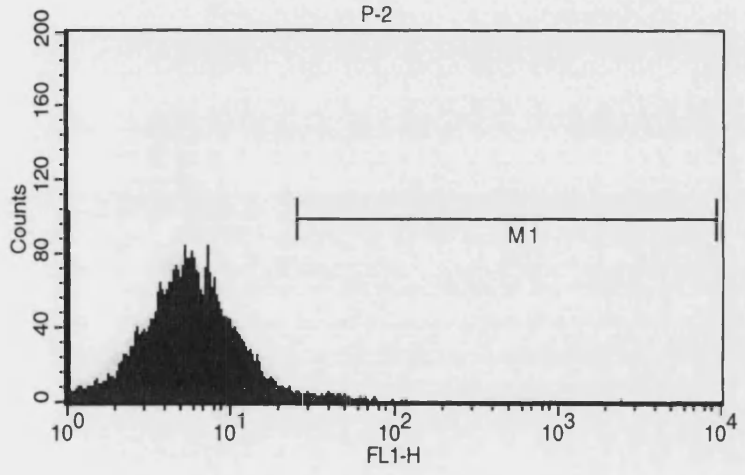


Sample ID: P-2

| Marker | % Total |
|---|---|
| All | 100.00 |
| M1 | 1.82 |

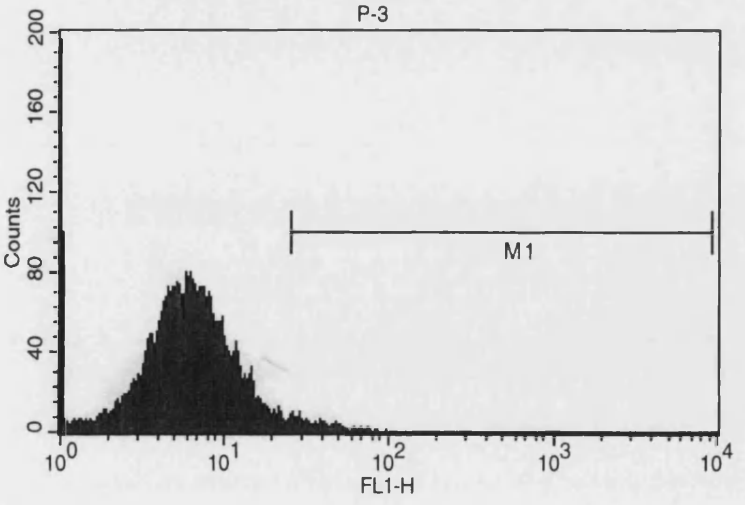


Sample ID: P-3

| Marker | % Total |
|---|---|
| All | 100.00 |
| M1 | 1.97 |

## Appendix B

| Sample ID | UVA Treatment ($kJ/m^2$) | Transfection Treatment |
|---|---|---|
| **A** | 0 | pcDNA3.1 |
| **B** | 0 | pcDNA3.1-HO1 |
| **C** | 100 | pcDNA3.1 |
| **D** | 100 | pcDNA3.1-HO1 |
| **E** | 200 | pcDNA3.1 |
| **F** | 200 | pcDNA3.1-HO1 |
| **G** | 300 | pcDNA3.1 |
| **H** | 300 | pcDNA3.1-HO1 |
| **J** | 400 | pcDNA3.1 |
| **K** | 400 | pcDNA3.1-HO1 |
| **L** | -- | pcDNA3.1-EGFP |
| **M** | -- | -- |

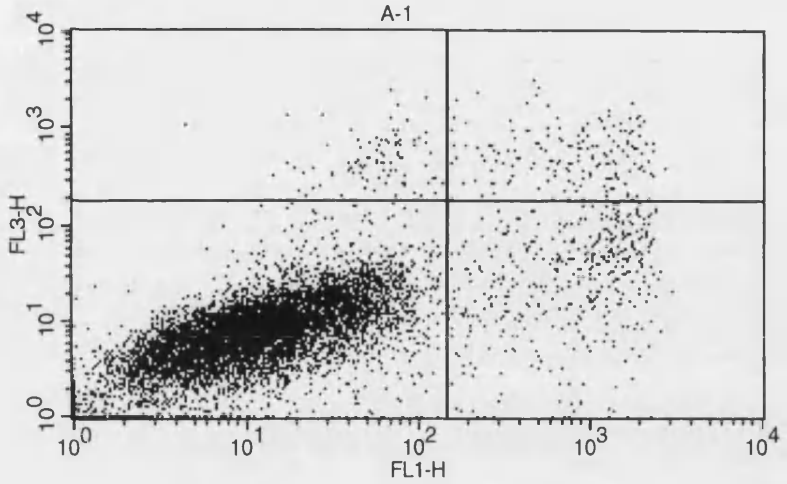


Sample ID: A-1

| Quad | % Total |
|---|---|
| UL | 0.94 |
| UR | 1.73 |
| LL | 92.89 |
| LR | 4.44 |

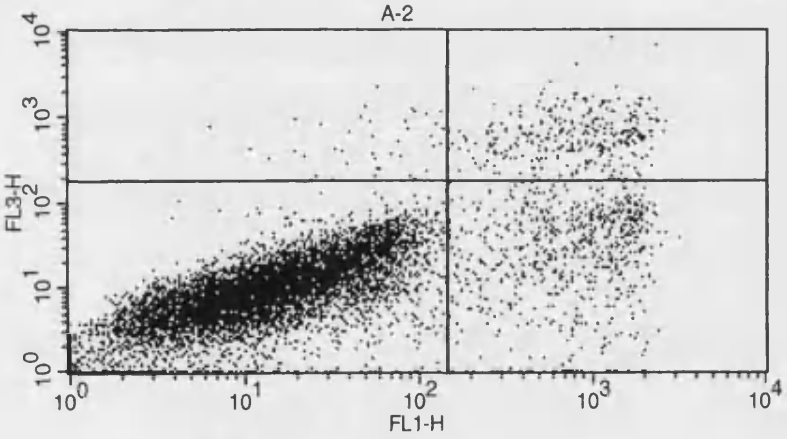


Sample ID: A-2

| Quad | % Total |
|---|---|
| UL | 0.41 |
| UR | 3.30 |
| LL | 89.32 |
| LR | 6.97 |

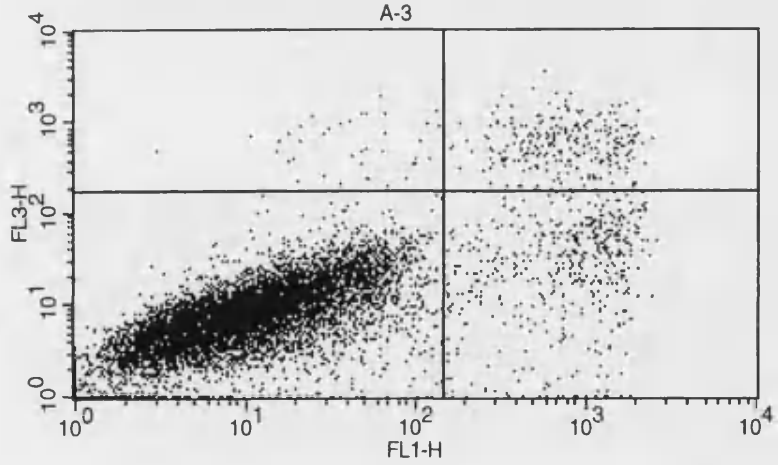


Sample ID: A-3

| Quad | % Total |
|---|---|
| UL | 0.40 |
| UR | 2.58 |
| LL | 92.10 |
| LR | 4.92 |

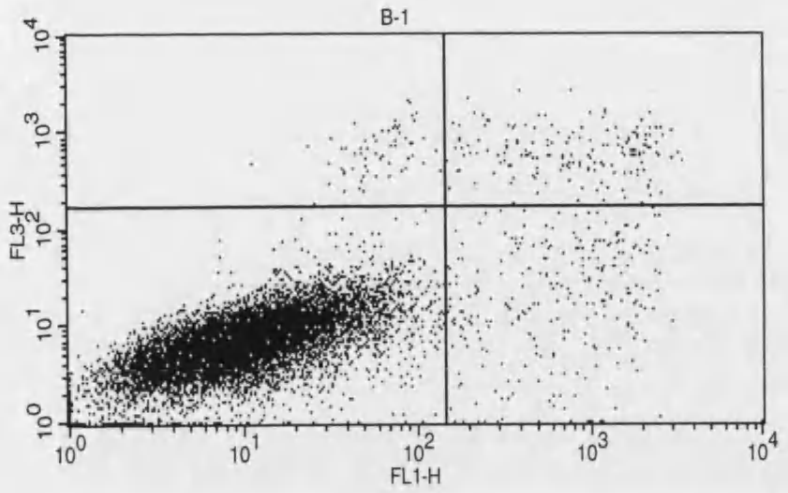


Sample ID: B-1

| Quad | % Total |
|---|---|
| UL | 0.63 |
| UR | 1.72 |
| LL | 94.96 |
| LR | 2.69 |

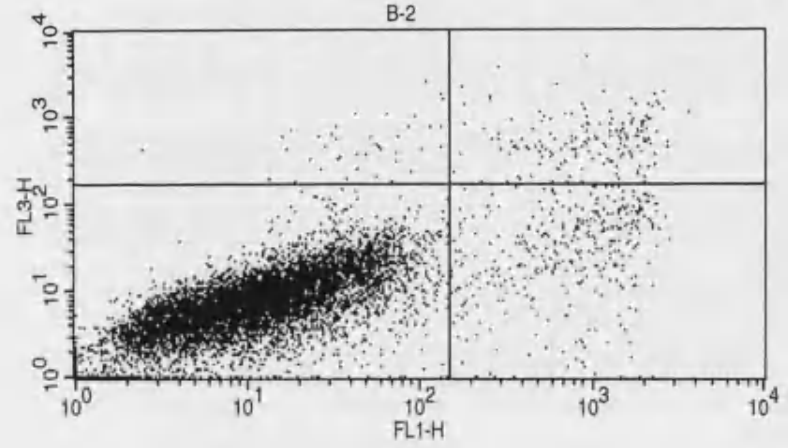


Sample ID: B-2

| Quad | % Total |
|---|---|
| UL | 0.42 |
| UR | 1.70 |
| LL | 94.21 |
| LR | 3.67 |

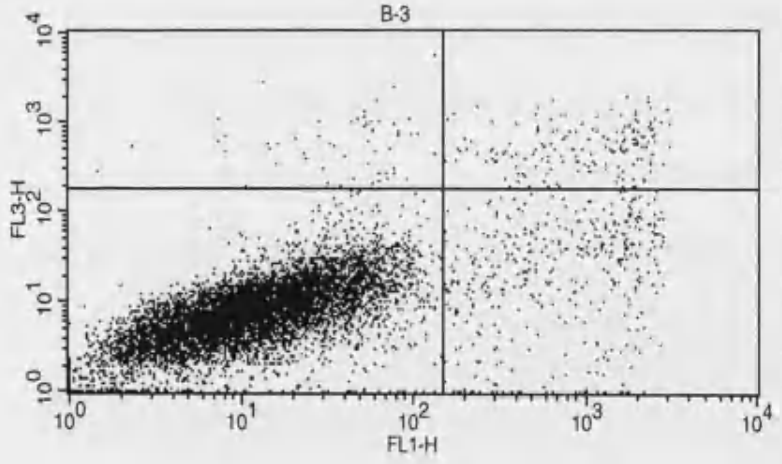


Sample ID: B-3

| Quad | % Total |
|---|---|
| UL | 0.58 |
| UR | 1.71 |
| LL | 93.63 |
| LR | 4.08 |

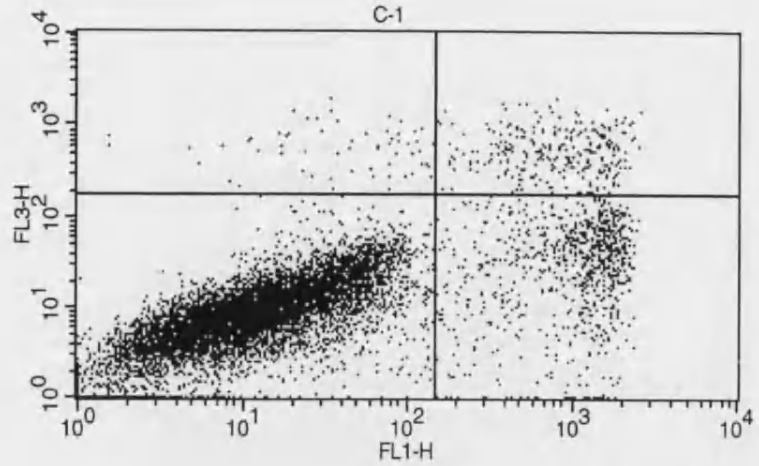


Sample ID: C-1

| Quad | % Total |
|---|---|
| UL | 0.63 |
| UR | 2.74 |
| LL | 88.41 |
| LR | 8.22 |

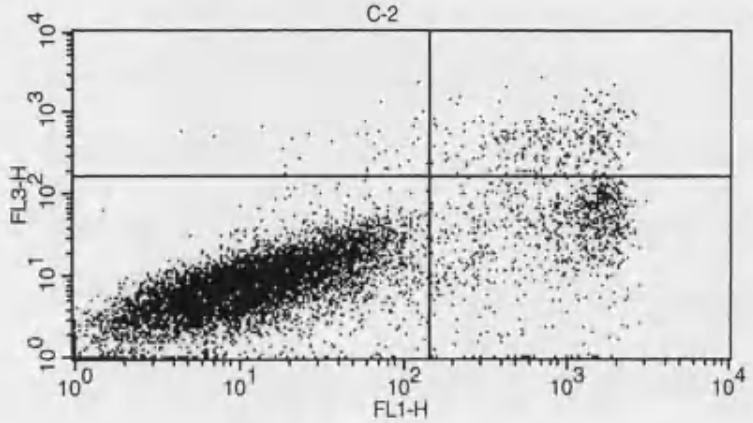


Sample ID: C-2

| Quad | % Total |
|---|---|
| UL | 0.33 |
| UR | 2.85 |
| LL | 88.49 |
| LR | 8.33 |

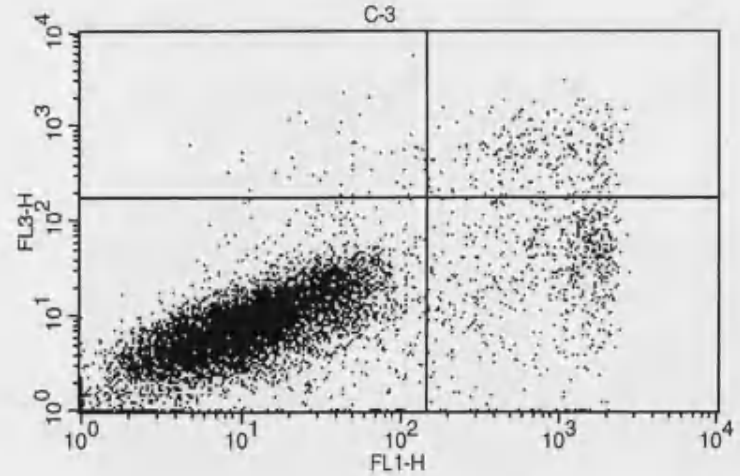


Sample ID: C-3

| Quad | % Total |
|---|---|
| UL | 0.49 |
| UR | 2.76 |
| LL | 90.39 |
| LR | 6.36 |

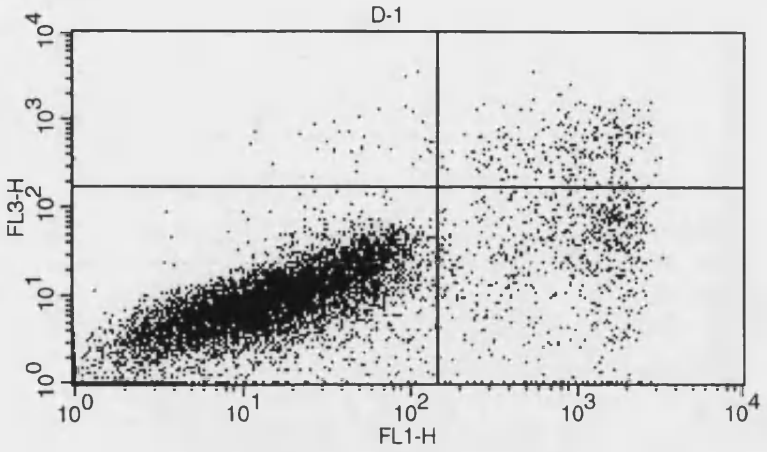


Sample ID: D-1

| Quad | % Total |
|---|---|
| UL | 0.37 |
| UR | 2.89 |
| LL | 89.45 |
| LR | 7.29 |

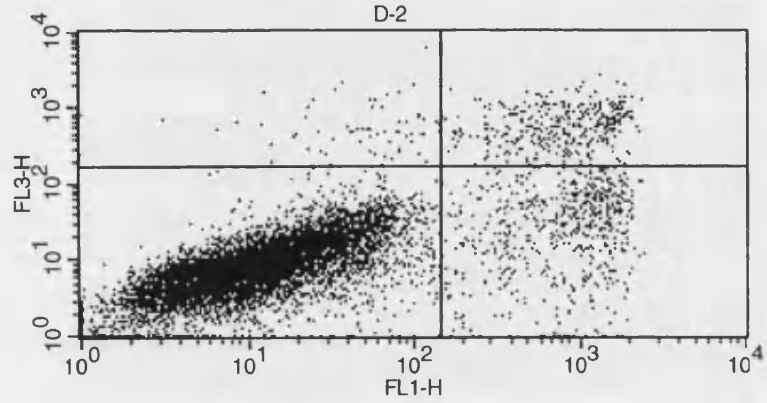


Sample ID: D-2

| Quad | % Total |
|---|---|
| UL | 0.67 |
| UR | 3.67 |
| LL | 89.59 |
| LR | 6.07 |

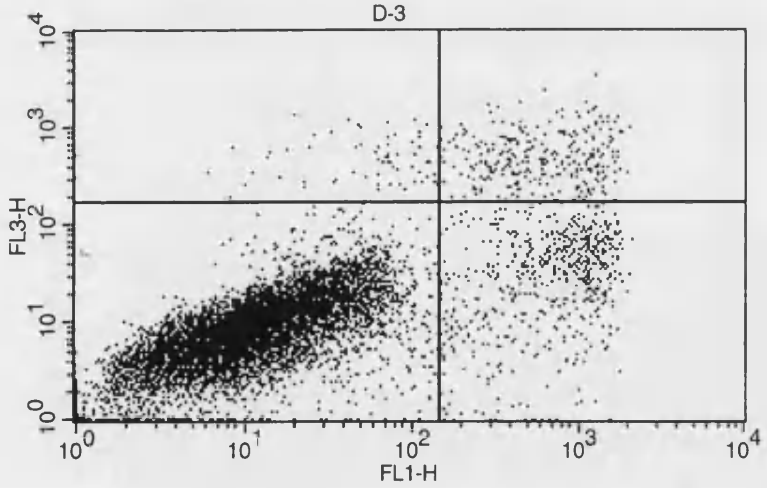


Sample ID: D-3

| Quad | % Total |
|---|---|
| UL | 0.67 |
| UR | 3.05 |
| LL | 90.35 |
| LR | 5.93 |

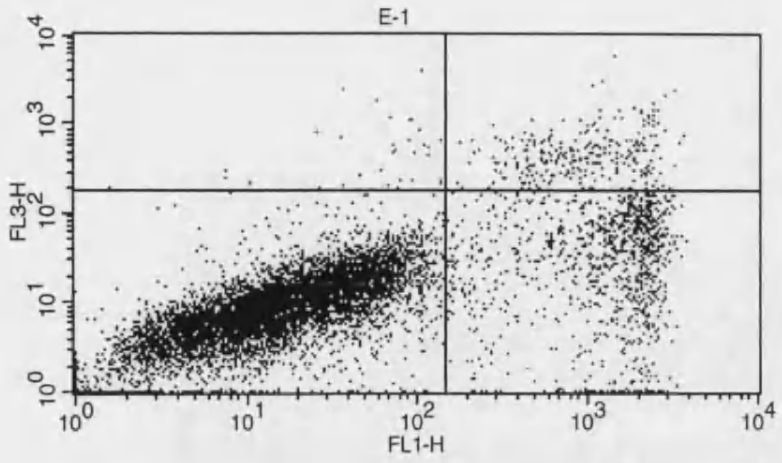


Sample ID: E-1

| Quad | % Total |
|---|---|
| UL | 0.32 |
| UR | 2.81 |
| LL | 86.41 |
| LR | 10.46 |

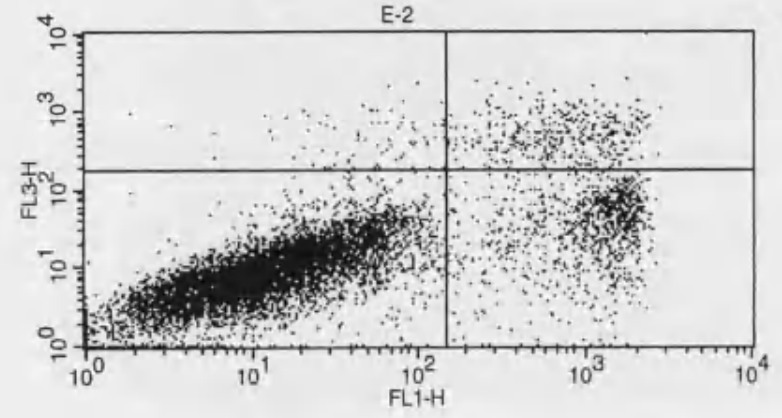


Sample ID: E-2

| Quad | % Total |
|---|---|
| UL | 0.83 |
| UR | 3.80 |
| LL | 85.63 |
| LR | 9.74 |

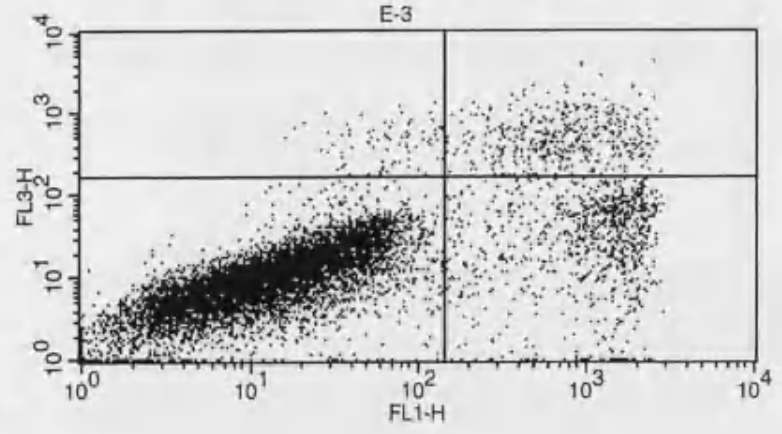


Sample ID: E-3

| Quad | % Total |
|---|---|
| UL | 0.79 |
| UR | 4.09 |
| LL | 86.67 |
| LR | 8.45 |

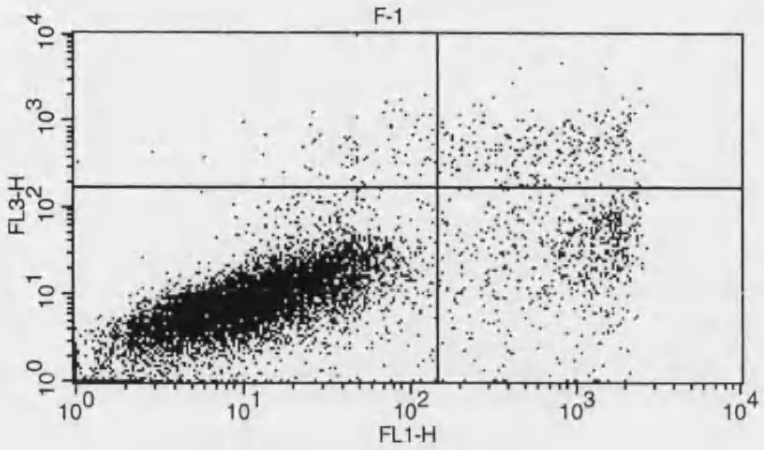


Sample ID: F-1

| Quad | % Total |
|---|---|
| UL | 0.80 |
| UR | 2.68 |
| LL | 90.06 |
| LR | 6.46 |

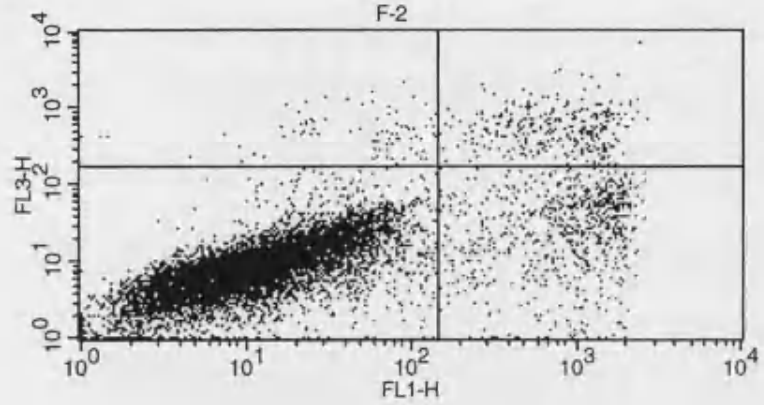


Sample ID: F-2

| Quad | % Total |
|---|---|
| UL | 0.88 |
| UR | 3.12 |
| LL | 88.63 |
| LR | 7.37 |

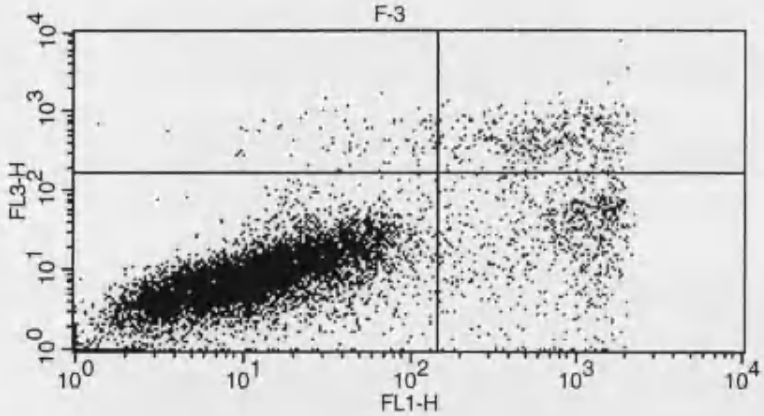


Sample ID: F-3

| Quad | % Total |
|---|---|
| UL | 0.82 |
| UR | 3.59 |
| LL | 88.50 |
| LR | 7.09 |

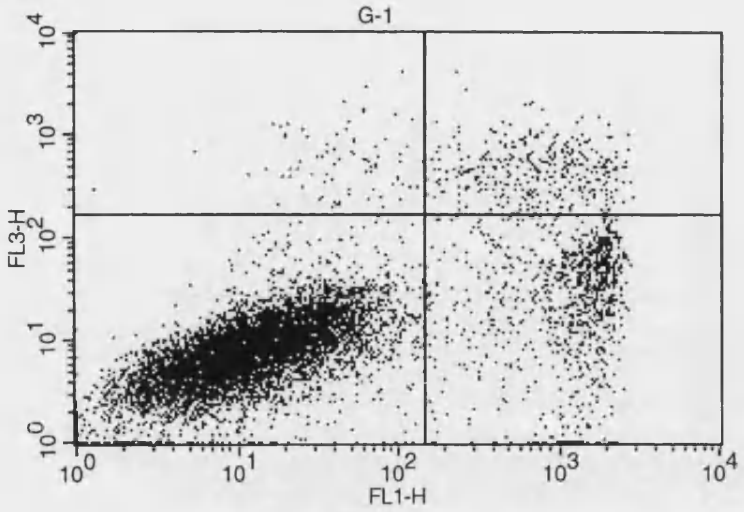


Sample ID: G-1

| Quad | % Total |
|---|---|
| UL | 0.80 |
| UR | 3.43 |
| LL | 85.55 |
| LR | 10.22 |

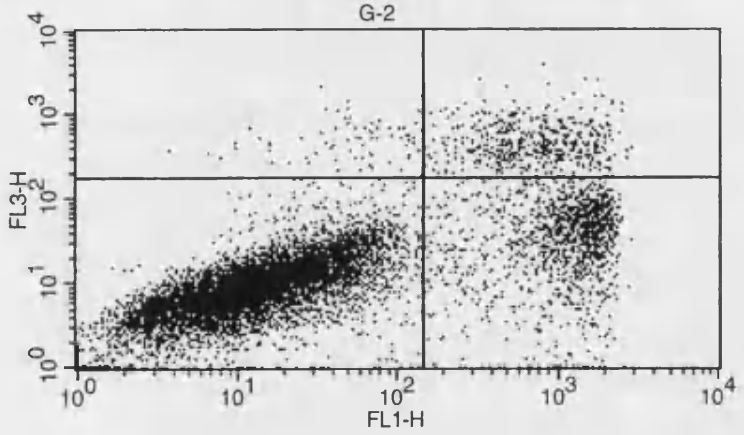


Sample ID: G-2

| Quad | % Total |
|---|---|
| UL | 0.81 |
| UR | 4.95 |
| LL | 81.23 |
| LR | 13.01 |

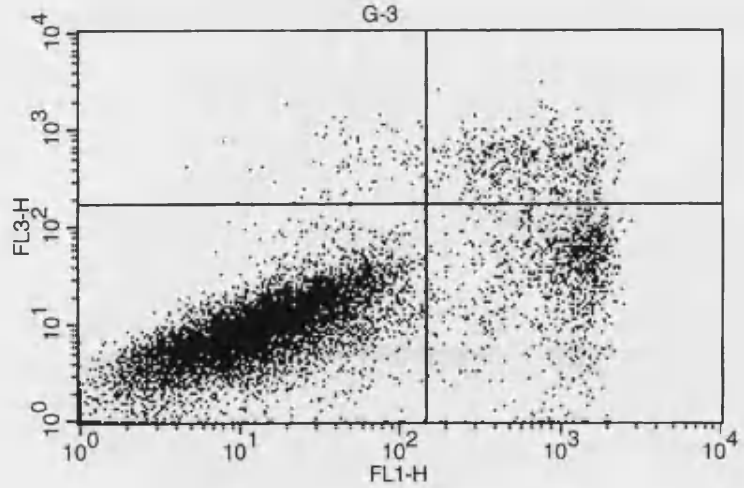


Sample ID: G-3

| Quad | % Total |
|---|---|
| UL | 0.89 |
| UR | 4.91 |
| LL | 82.50 |
| LR | 11.70 |

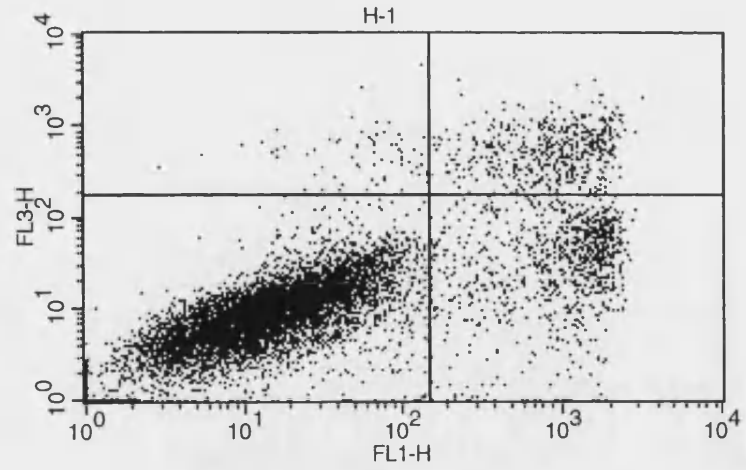


Sample ID: H-1

| Quad | % Total |
|---|---|
| UL | 0.73 |
| UR | 5.41 |
| LL | 84.29 |
| LR | 9.57 |

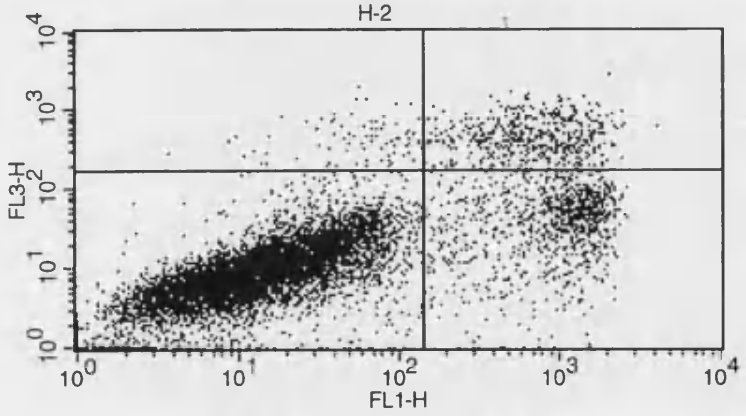


Sample ID: H-2

| Quad | % Total |
|---|---|
| UL | 0.82 |
| UR | 5.25 |
| LL | 83.79 |
| LR | 10.14 |

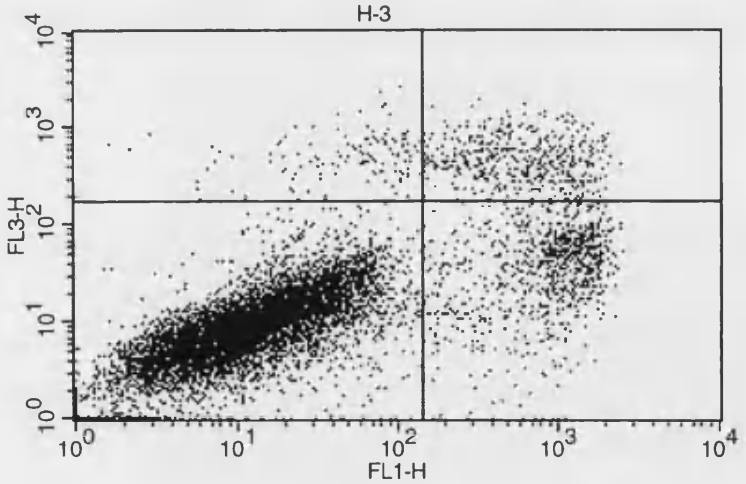


Sample ID: H-3

| Quad | % Total |
|---|---|
| UL | 1.37 |
| UR | 4.80 |
| LL | 85.22 |
| LR | 8.61 |

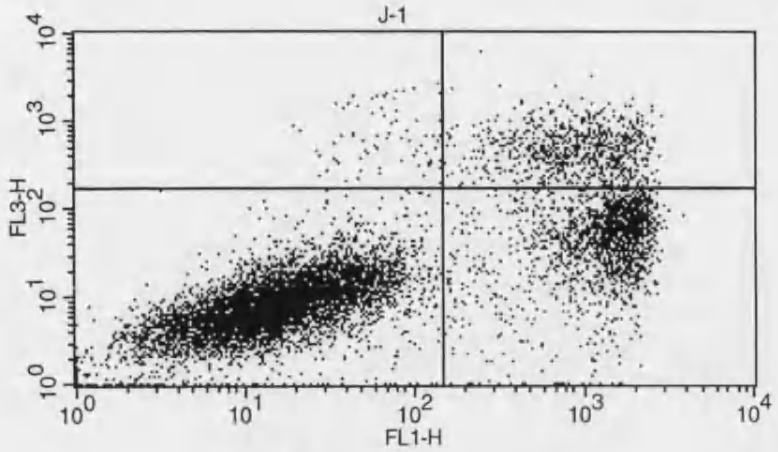


Sample ID: J-1

| Quad | % Total |
|---|---|
| UL | 0.76 |
| UR | 7.60 |
| LL | 73.07 |
| LR | 18.57 |

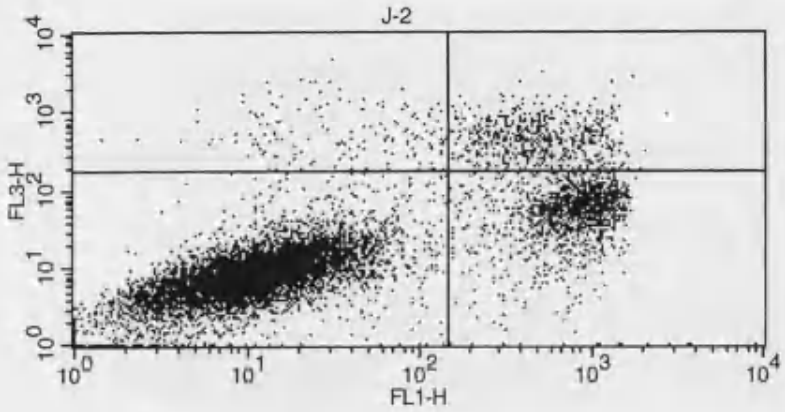


Sample ID: J-2

| Quad | % Total |
|---|---|
| UL | 1.67 |
| UR | 5.81 |
| LL | 78.18 |
| LR | 14.34 |

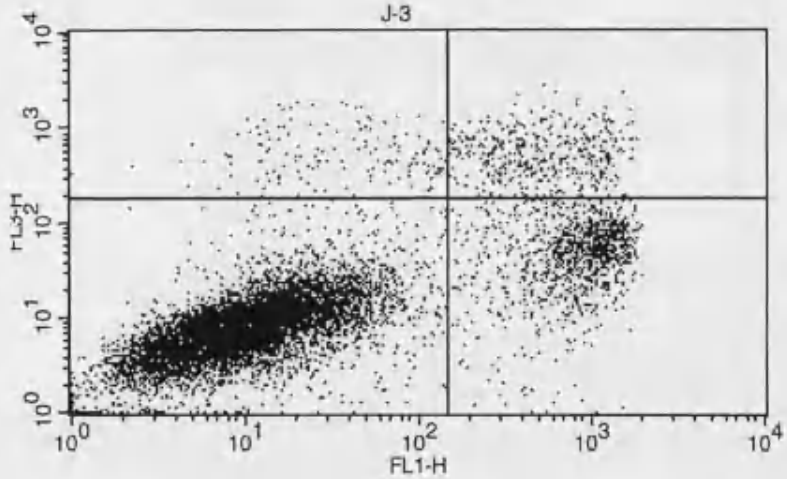


Sample ID: J-3

| Quad | % Total |
|---|---|
| UL | 1.52 |
| UR | 4.30 |
| LL | 83.14 |
| LR | 11.04 |

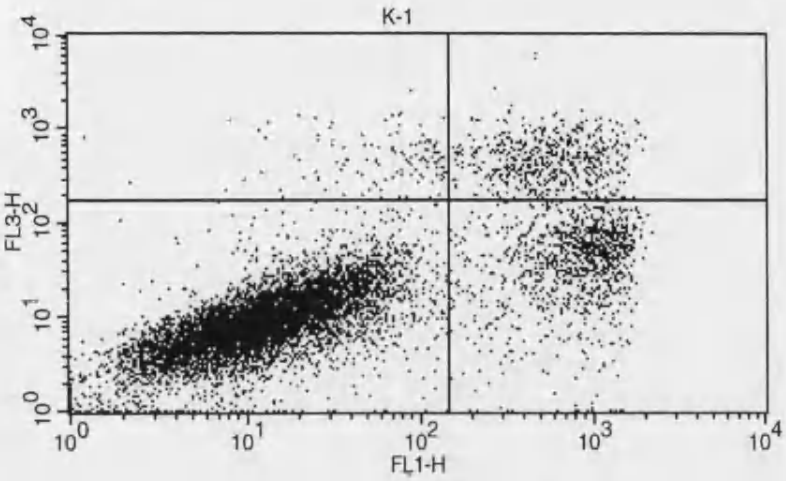


Sample ID: K-1

| Quad | % Total |
|---|---|
| UL | 1.24 |
| UR | 5.39 |
| LL | 82.52 |
| LR | 10.85 |

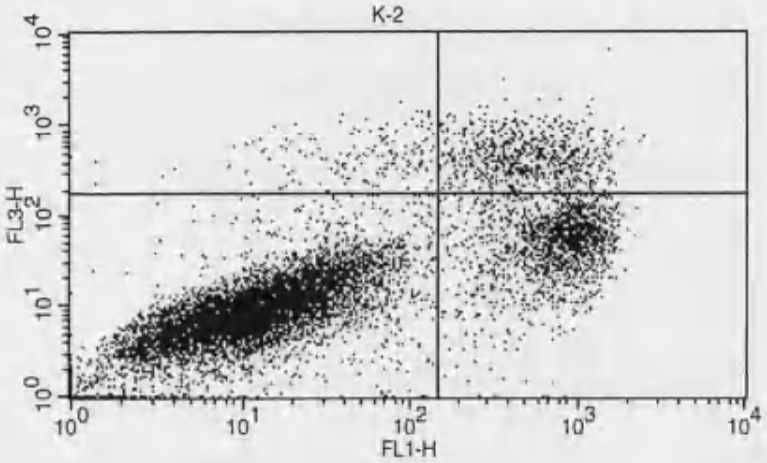


Sample ID: K-2

| Quad | % Total |
|---|---|
| UL | 1.71 |
| UR | 6.55 |
| LL | 76.68 |
| LR | 15.06 |

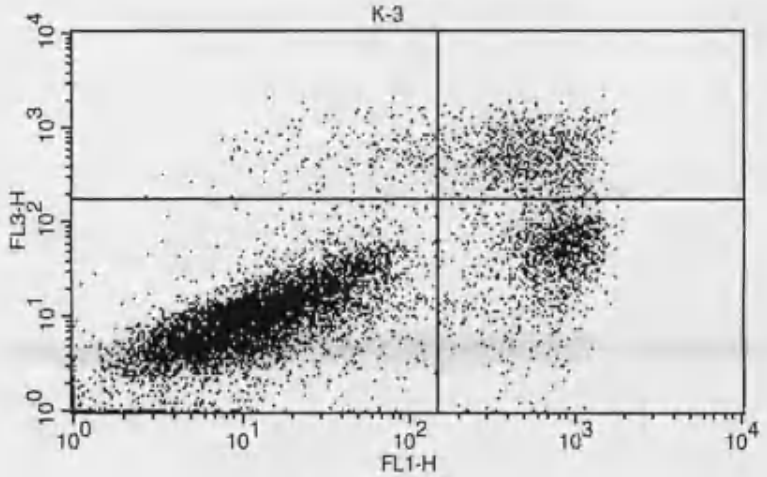


Sample ID: K-3

| Quad | % Total |
|---|---|
| UL | 2.16 |
| UR | 7.95 |
| LL | 76.55 |
| LR | 13.34 |

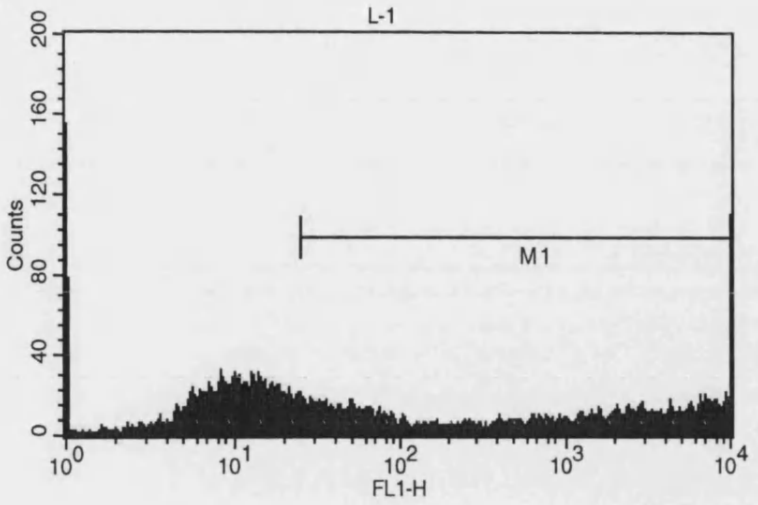


Sample ID: L-1

| Marker | % Total |
|---|---|
| All | 100.00 |
| M1 | 62.37 |

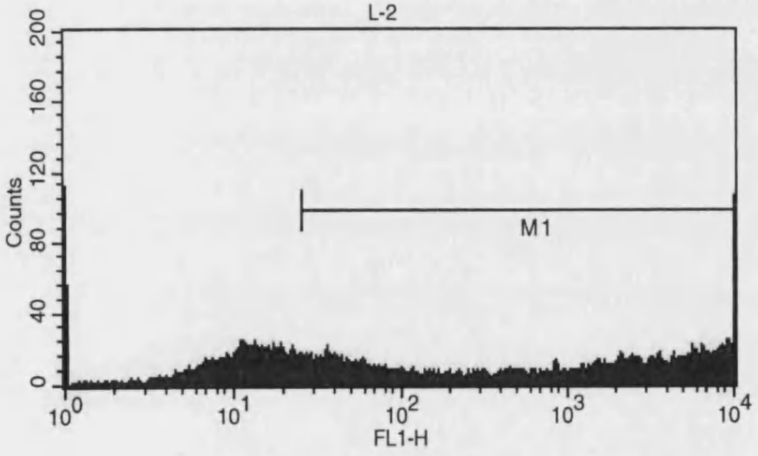


Sample ID: L-2

| Marker | % Total |
|---|---|
| All | 100.00 |
| M1 | 73.84 |

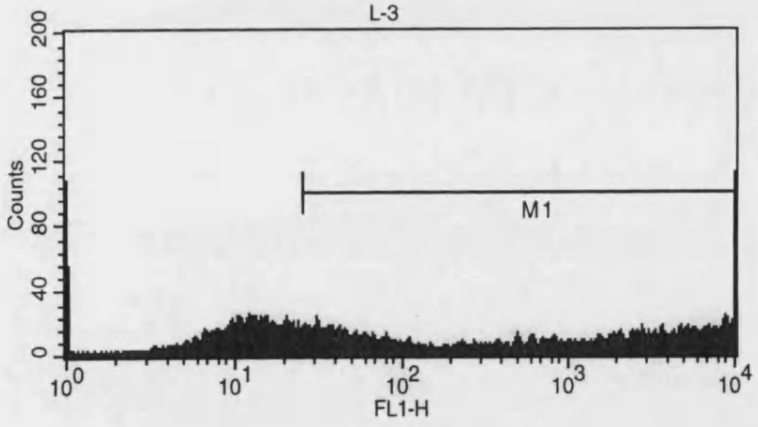


Sample ID: L-3

| Marker | % Total |
|---|---|
| All | 100.00 |
| M1 | 70.84 |

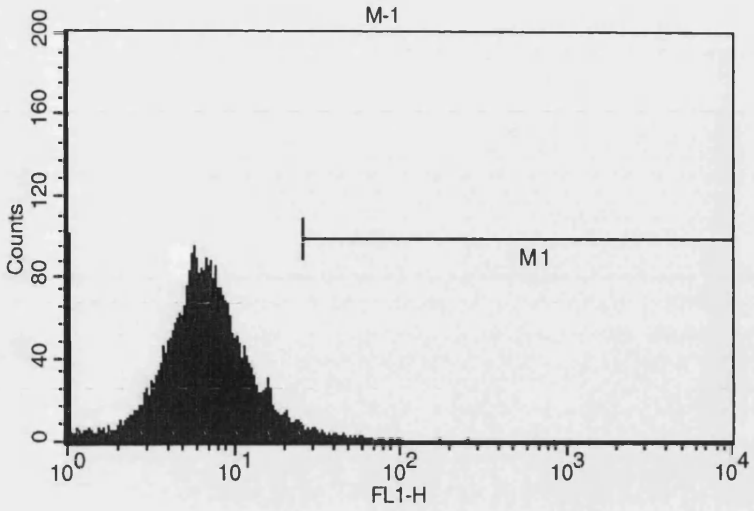


Sample ID: M-1

| Marker | % Total |
|---|---|
| All | 100.00 |
| M1 | 1.44 |

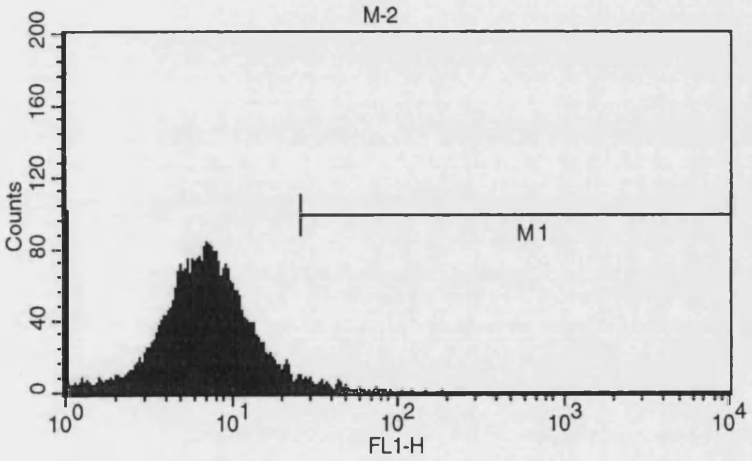


Sample ID: M-2

| Marker | % Total |
|---|---|
| All | 100.00 |
| M1 | 1.91 |

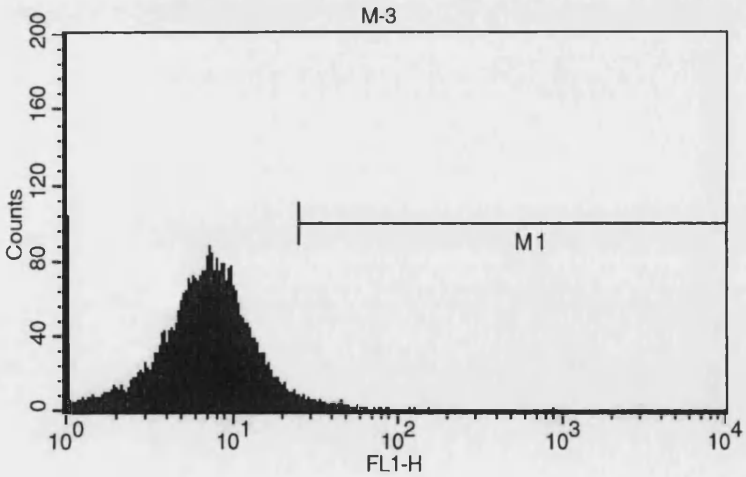


Sample ID: M-3

| Marker | % Total |
|---|---|
| All | 100.00 |
| M1 | 1.96 |

## Appendix C

| Sample ID | UVA Treatment ($kJ/m^2$) | Transfection Treatment |
|---|---|---|
| **A** | 0 | -- |
| **B** | 0 | pcDNA3.1 |
| **C** | 0 | pcDNA3.1-HO1 |
| **D** | 100 | -- |
| **E** | 100 | pcDNA3.1 |
| **F** | 100 | pcDNA3.1-HO1 |
| **G** | 200 | -- |
| **H** | 200 | pcDNA3.1 |
| **J** | 200 | pcDNA3.1-HO1 |
| **K** | 300 | -- |
| **L** | 300 | pcDNA3.1 |
| **M** | 300 | pcDNA3.1-HO1 |
| **N** | 400 | -- |
| **P** | 400 | pcDNA3.1 |
| **Q** | 400 | pcDNA3.1-HO1 |
| **R** | -- | pcDNA3.1-EGFP |
| **S** | -- | -- |

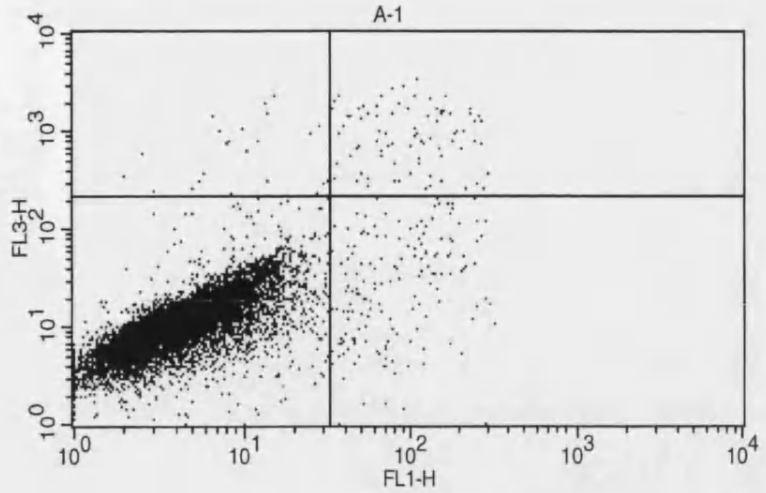


Sample ID: A-1

| Quad | % Gated |
|---|---|
| UL | 0.26 |
| UR | 0.83 |
| LL | 97.24 |
| LR | 1.67 |

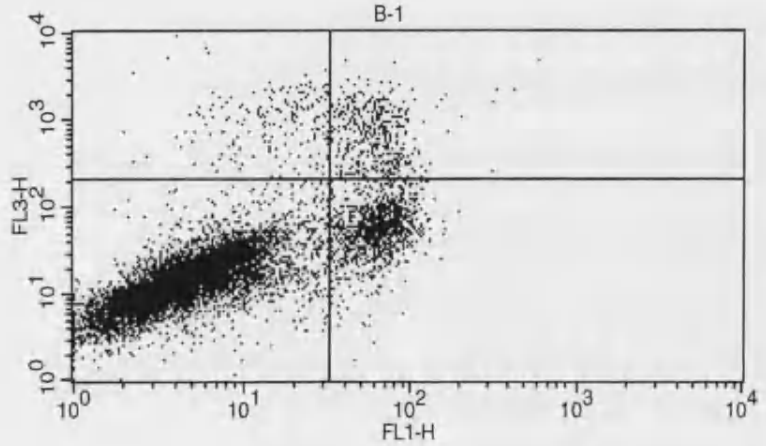


Sample ID: B-1

| Quad | % Gated |
|---|---|
| UL | 1.95 |
| UR | 4.15 |
| LL | 82.45 |
| LR | 11.45 |

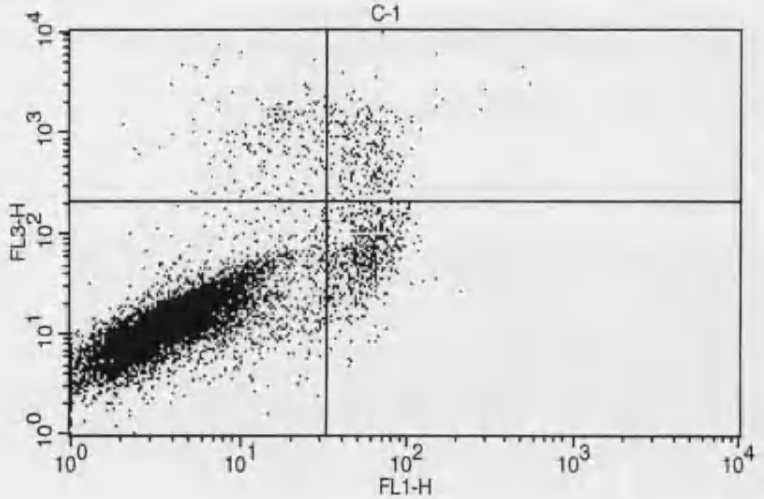


Sample ID: C-1

| Quad | % Gated |
|---|---|
| UL | 1.88 |
| UR | 2.61 |
| LL | 89.89 |
| LR | 5.62 |

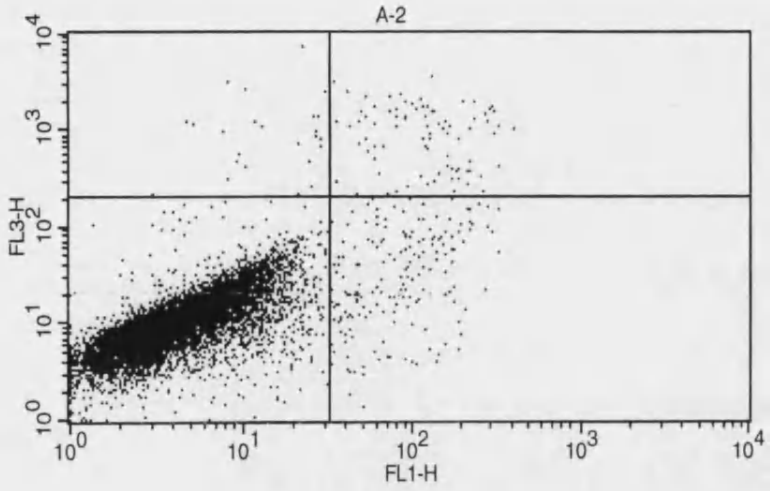


Sample ID: A-2

| Quad | % Gated |
|---|---|
| UL | 0.25 |
| UR | 0.84 |
| LL | 97.07 |
| LR | 1.84 |

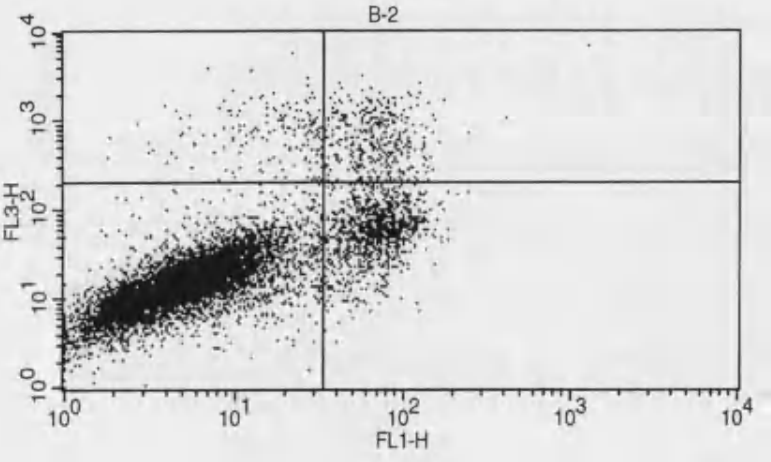


Sample ID: B-2

| Quad | % Gated |
|---|---|
| UL | 1.67 |
| UR | 3.81 |
| LL | 83.21 |
| LR | 11.31 |

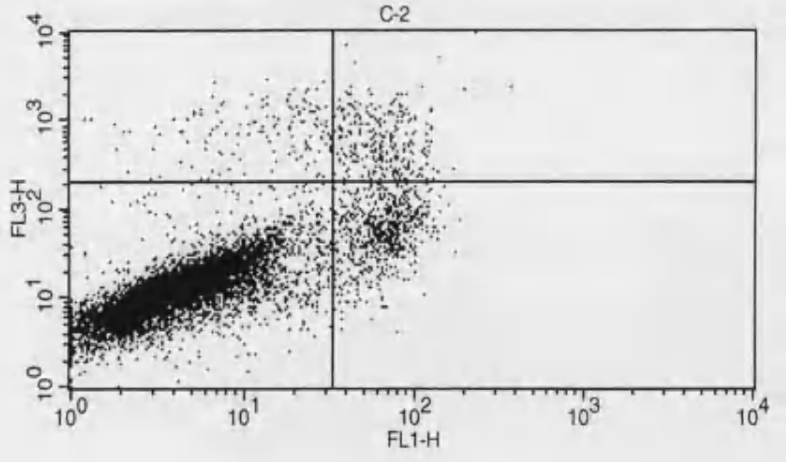


Sample ID: C-2

| Quad | % Gated |
|---|---|
| UL | 1.46 |
| UR | 2.84 |
| LL | 89.10 |
| LR | 6.60 |

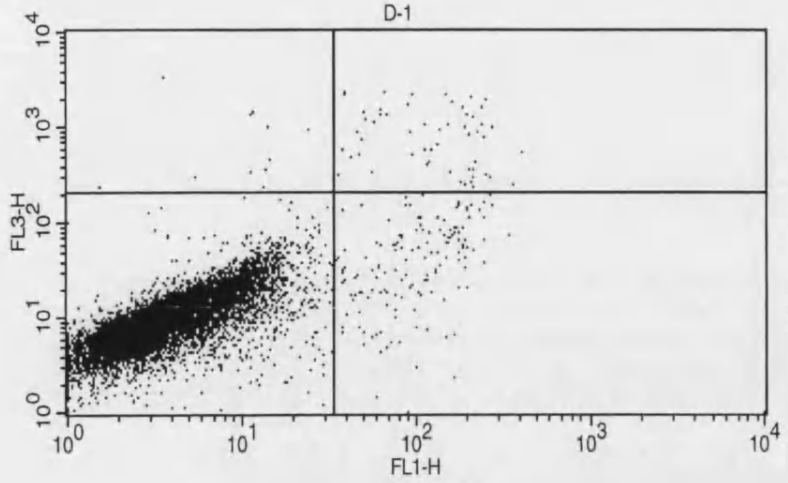


Sample ID: D-1

| Quad | % Gated |
|---|---|
| UL | 0.11 |
| UR | 0.55 |
| LL | 97.84 |
| LR | 1.50 |

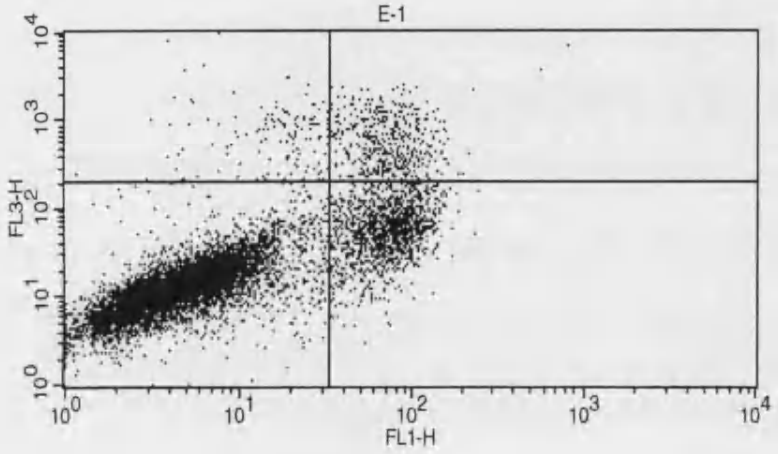


Sample ID: E-1

| Quad | % Gated |
|---|---|
| UL | 1.37 |
| UR | 4.47 |
| LL | 80.20 |
| LR | 13.96 |

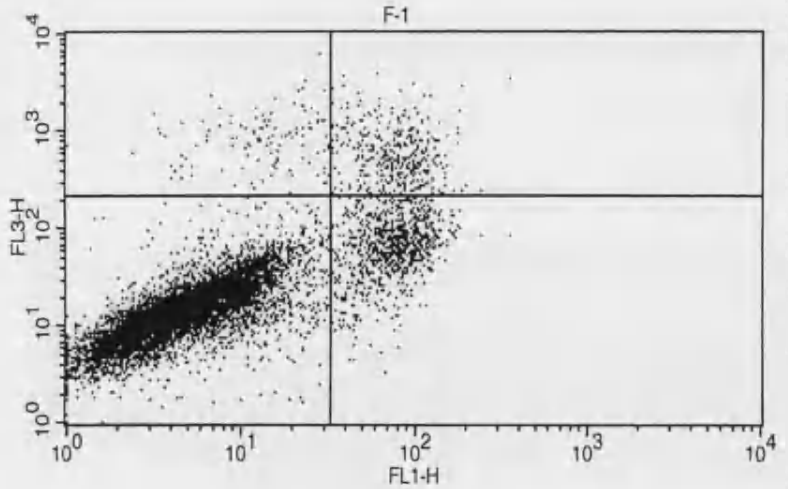


Sample ID: F-1

| Quad | % Gated |
|---|---|
| UL | 1.24 |
| UR | 3.77 |
| LL | 86.25 |
| LR | 8.74 |

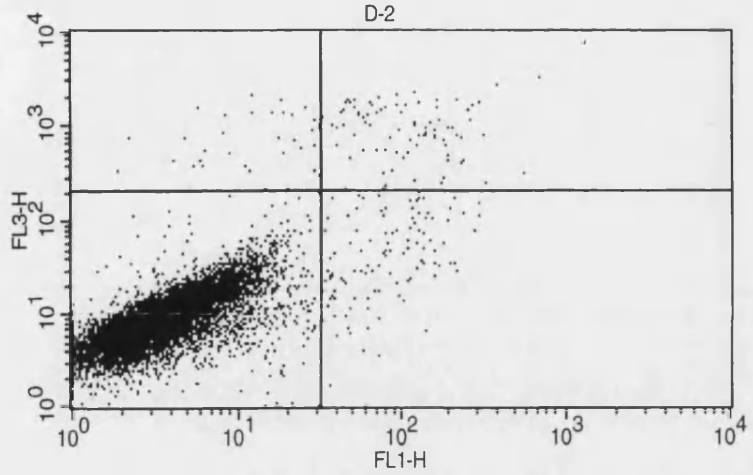


Sample ID: D-2

| Quad | % Gated |
|---|---|
| UL | 0.34 |
| UR | 0.87 |
| LL | 97.68 |
| LR | 1.11 |

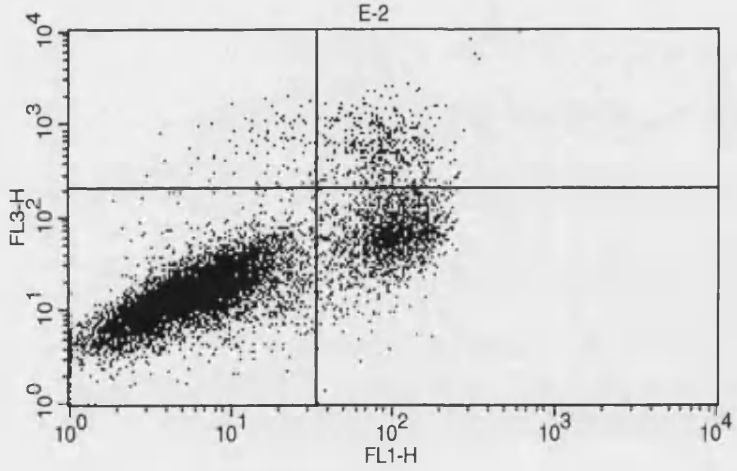


Sample ID: E-2

| Quad | % Gated |
|---|---|
| UL | 0.83 |
| UR | 4.67 |
| LL | 77.37 |
| LR | 17.13 |

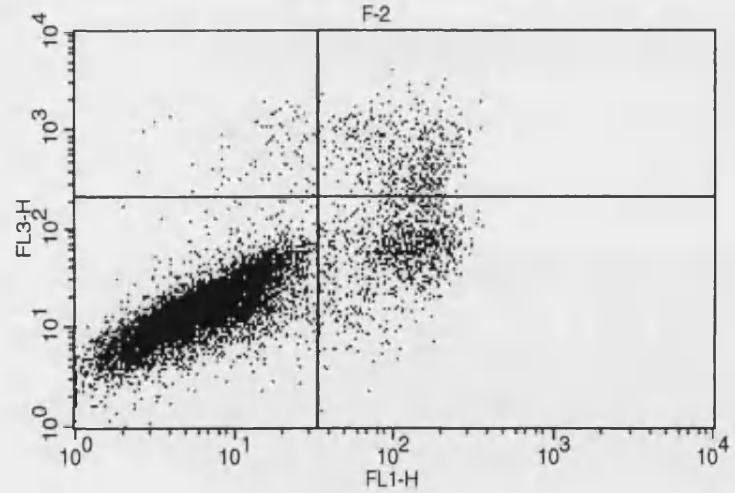


Sample ID: F-2

| Quad | % Gated |
|---|---|
| UL | 0.84 |
| UR | 4.50 |
| LL | 84.58 |
| LR | 10.08 |

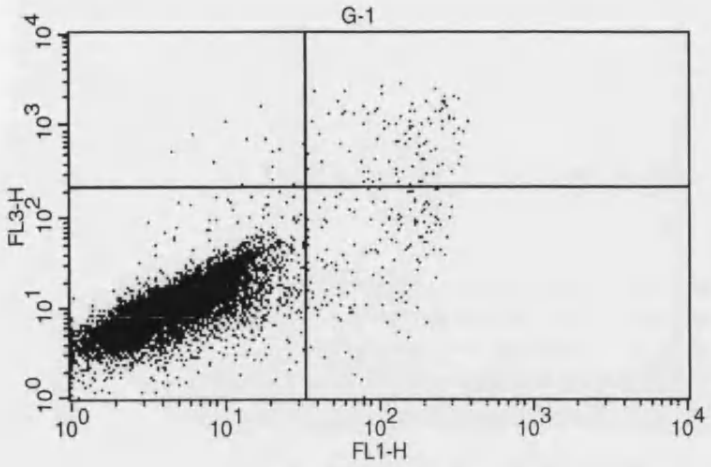


Sample ID: G-1

| Quad | % Gated |
|---|---|
| UL | 0.14 |
| UR | 0.98 |
| LL | 97.36 |
| LR | 1.52 |

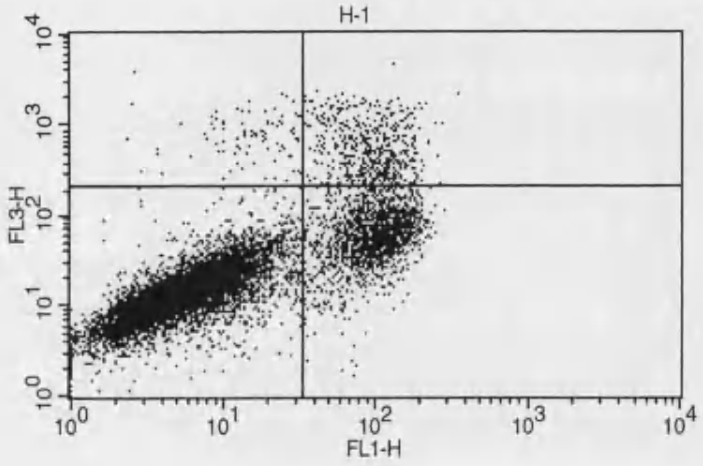


Sample ID: H-1

| Quad | % Gated |
|---|---|
| UL | 0.94 |
| UR | 5.45 |
| LL | 76.00 |
| LR | 17.61 |

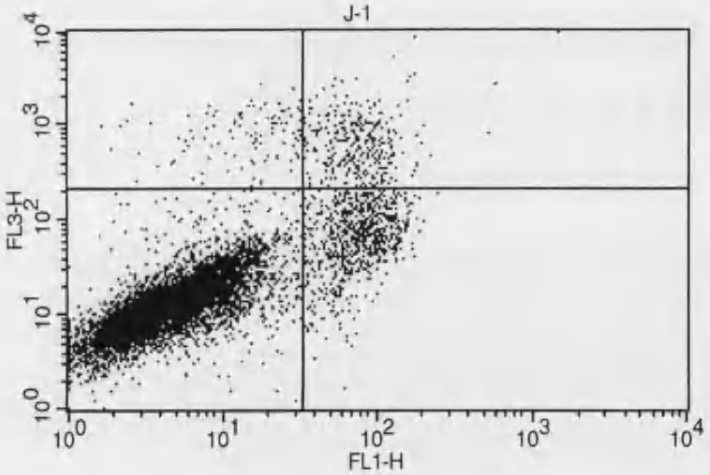


Sample ID: J-1

| Quad | % Gated |
|---|---|
| UL | 1.13 |
| UR | 3.37 |
| LL | 87.66 |
| LR | 7.84 |

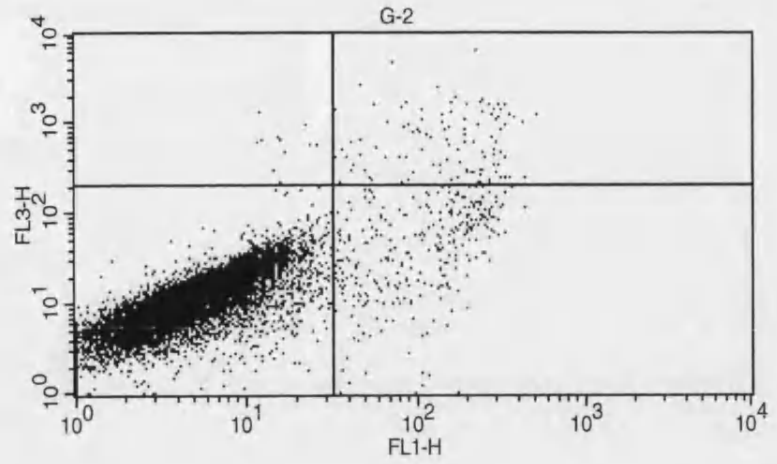


Sample ID: G-2

| Quad | % Gated |
|---|---|
| UL | 0.11 |
| UR | 1.08 |
| LL | 95.82 |
| LR | 2.99 |

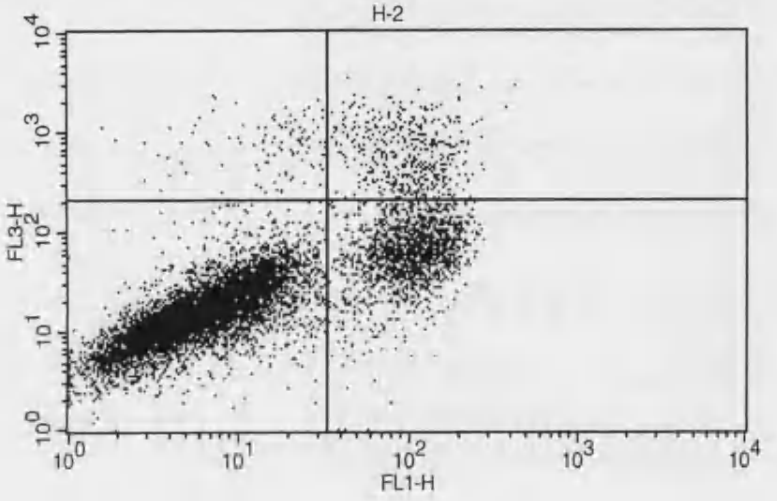


Sample ID: H-2

| Quad | % Gated |
|---|---|
| UL | 1.13 |
| UR | 4.87 |
| LL | 77.44 |
| LR | 16.56 |

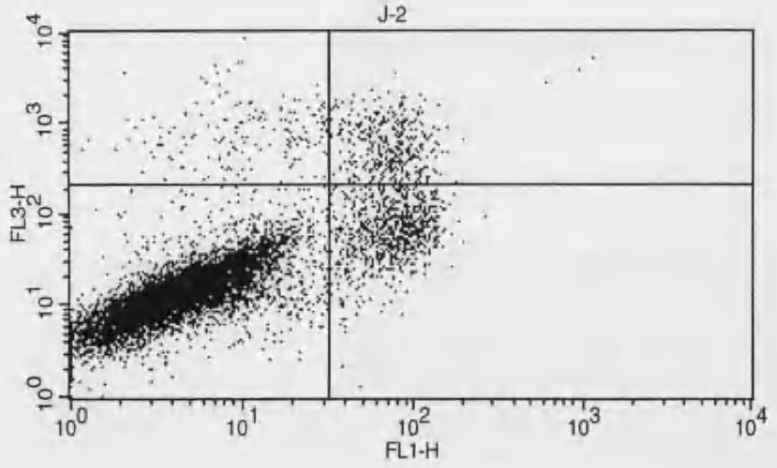


Sample ID: J-2

| Quad | % Gated |
|---|---|
| UL | 1.71 |
| UR | 3.72 |
| LL | 86.44 |
| LR | 8.13 |

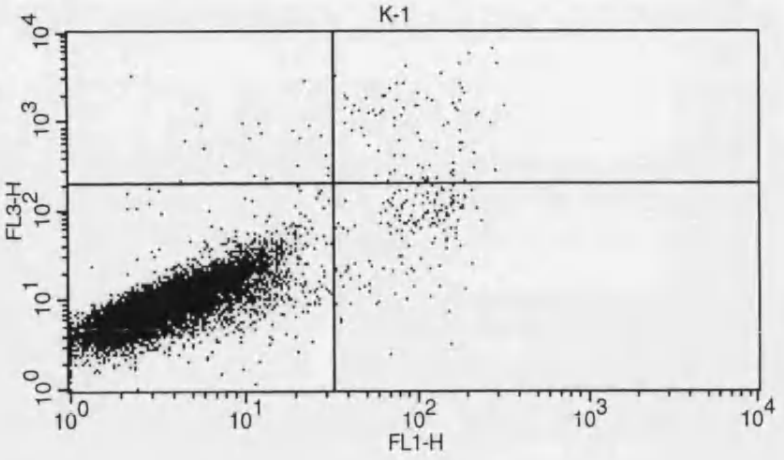


Sample ID: K-1

| Quad | % Gated |
|---|---|
| UL | 0.23 |
| UR | 0.88 |
| LL | 97.27 |
| LR | 1.62 |

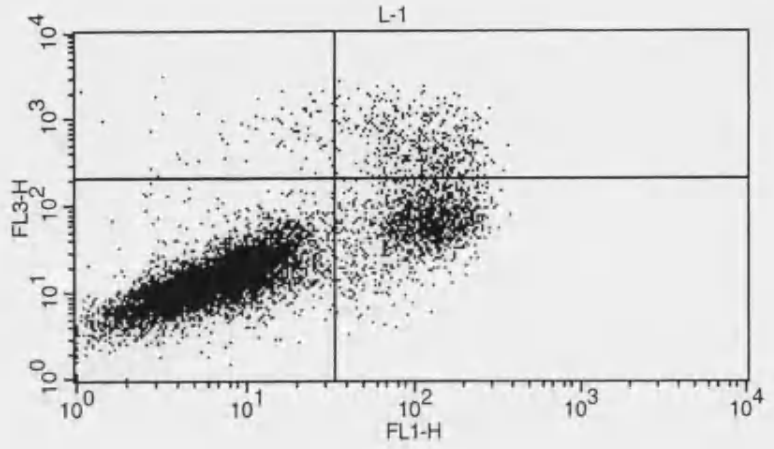


Sample ID: L-1

| Quad | % Gated |
|---|---|
| UL | 0.75 |
| UR | 4.66 |
| LL | 80.32 |
| LR | 14.27 |

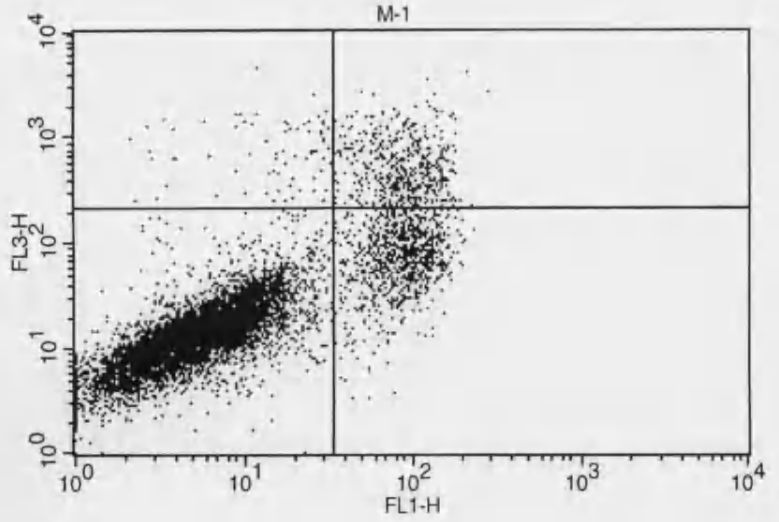


Sample ID: M-1

| Quad | % Gated |
|---|---|
| UL | 0.75 |
| UR | 4.92 |
| LL | 85.32 |
| LR | 9.01 |

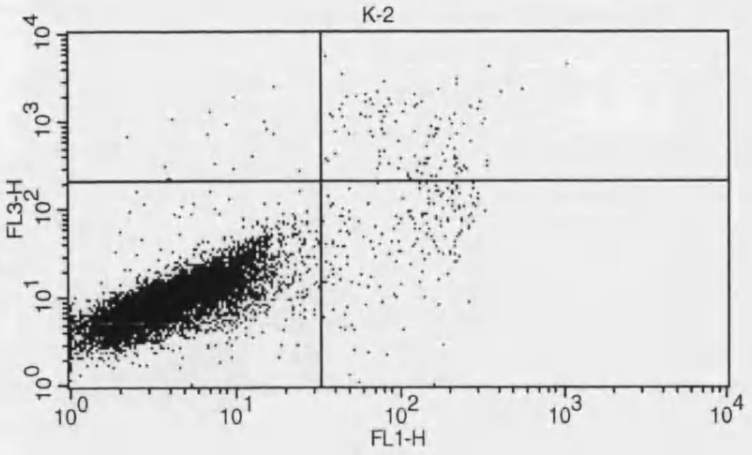


Sample ID: K-2

| Quad | % Gated |
|---|---|
| UL | 0.17 |
| UR | 1.12 |
| LL | 96.84 |
| LR | 1.87 |

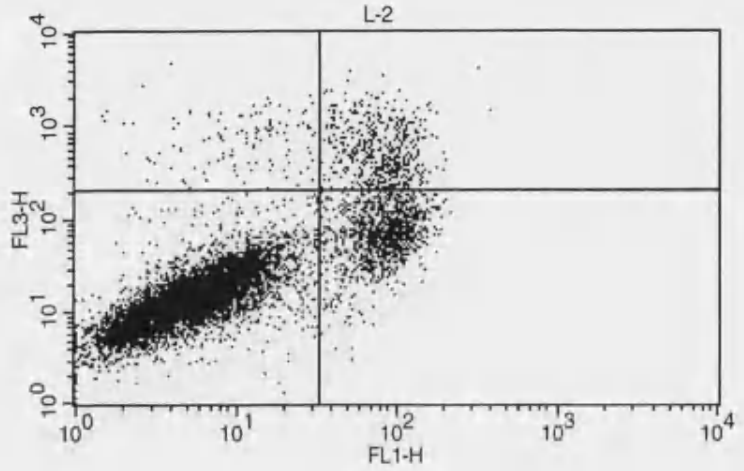


Sample ID: L-2

| Quad | % Gated |
|---|---|
| UL | 1.18 |
| UR | 4.91 |
| LL | 82.71 |
| LR | 11.20 |

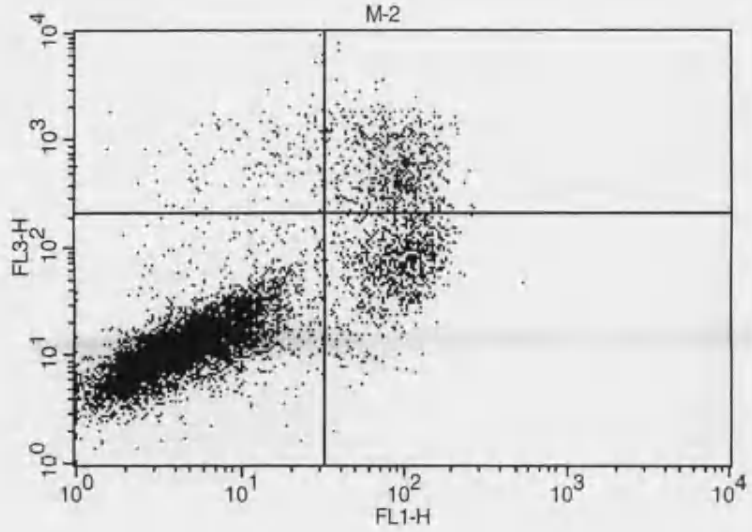


Sample ID: M-2

| Quad | % Gated |
|---|---|
| UL | 1.46 |
| UR | 6.40 |
| LL | 82.37 |
| LR | 9.77 |

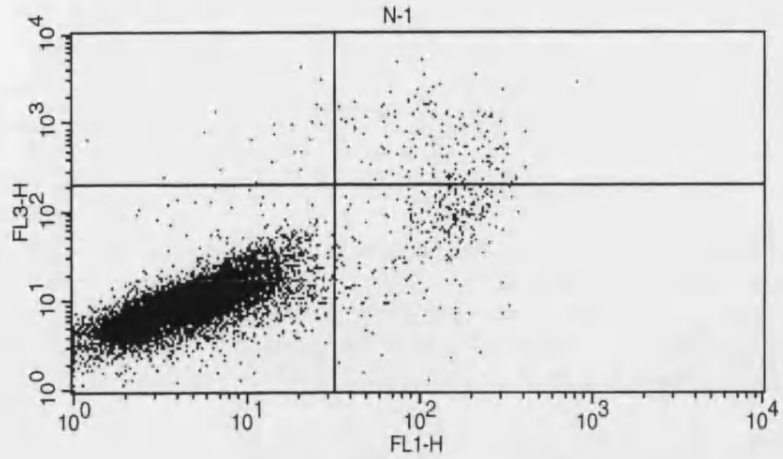


Sample ID: N-1

| Quad | % Gated |
|---|---|
| UL | 0.23 |
| UR | 1.55 |
| LL | 95.44 |
| LR | 2.78 |

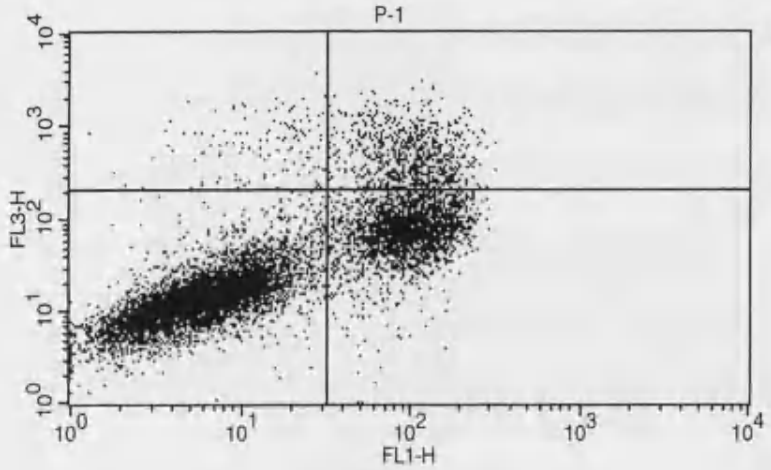


Sample ID: P-1

| Quad | % Gated |
|---|---|
| UL | 1.33 |
| UR | 7.48 |
| LL | 66.10 |
| LR | 25.09 |

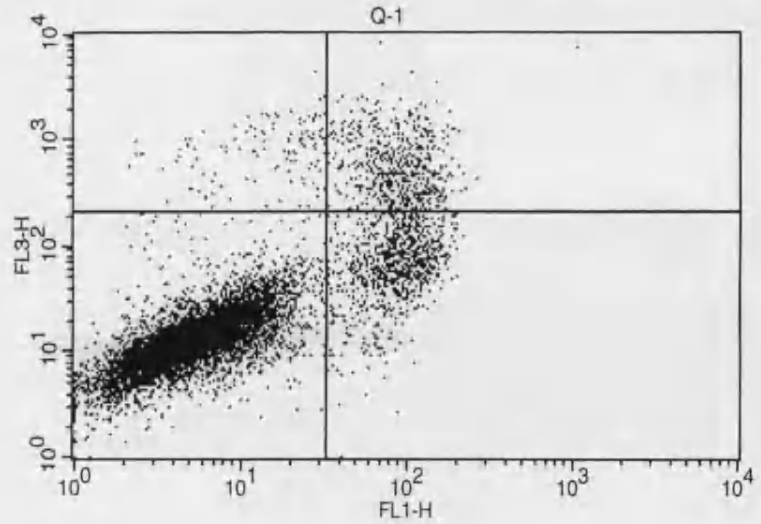


Sample ID: Q-1

| Quad | % Gated |
|---|---|
| UL | 1.30 |
| UR | 5.67 |
| LL | 83.24 |
| LR | 9.79 |

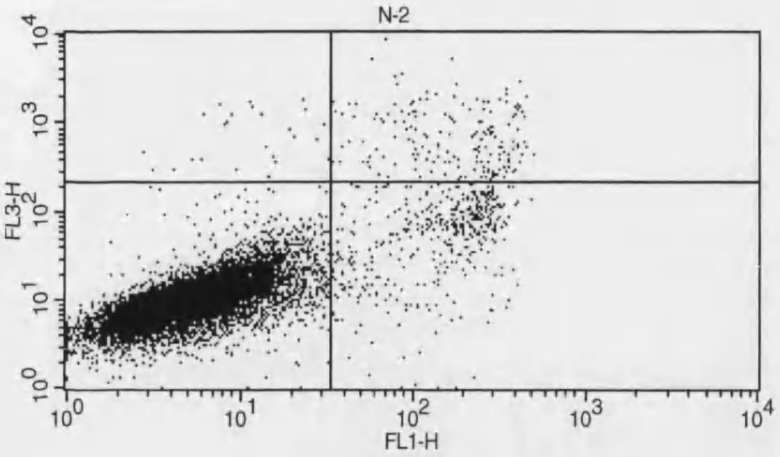


Sample ID: N-2

| Quad | % Gated |
|---|---|
| UL | 0.26 |
| UR | 1.84 |
| LL | 93.44 |
| LR | 4.46 |

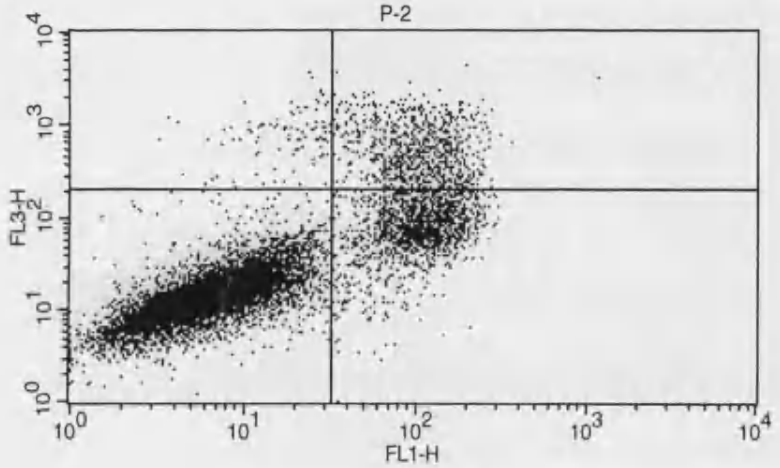


Sample ID: P-2

| Quad | % Gated |
|---|---|
| UL | 1.03 |
| UR | 7.56 |
| LL | 76.76 |
| LR | 14.65 |

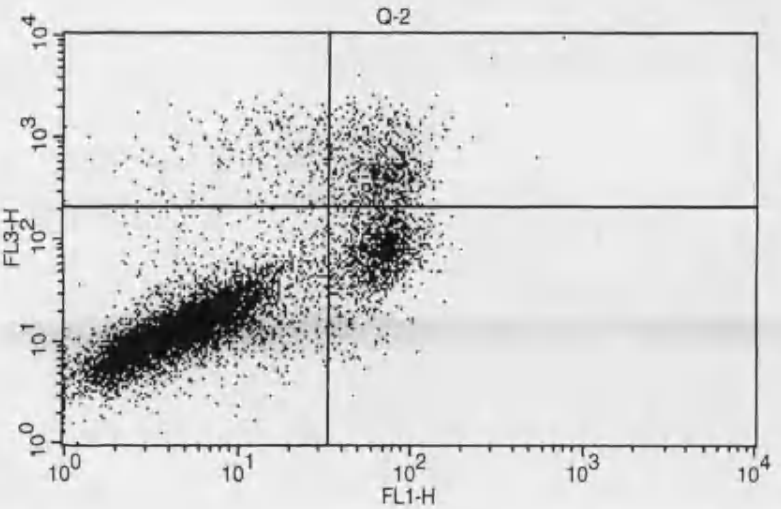


Sample ID: Q-2

| Quad | % Gated |
|---|---|
| UL | 2.35 |
| UR | 7.24 |
| LL | 77.94 |
| LR | 12.47 |

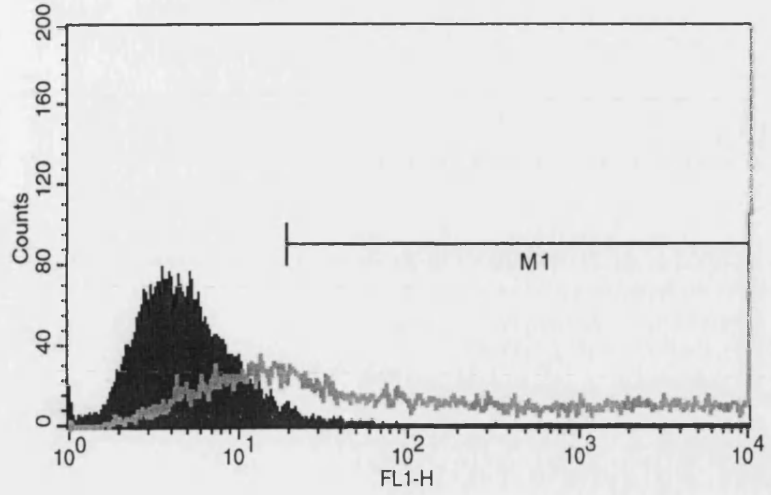


Sample ID: S-1

| Marker | % Total |
|---|---|
| All | 100.00 |
| M1 | 1.96 |

Sample ID: R-1

| Marker | % Total |
|---|---|
| All | 100.00 |
| M1 | 64.76 |

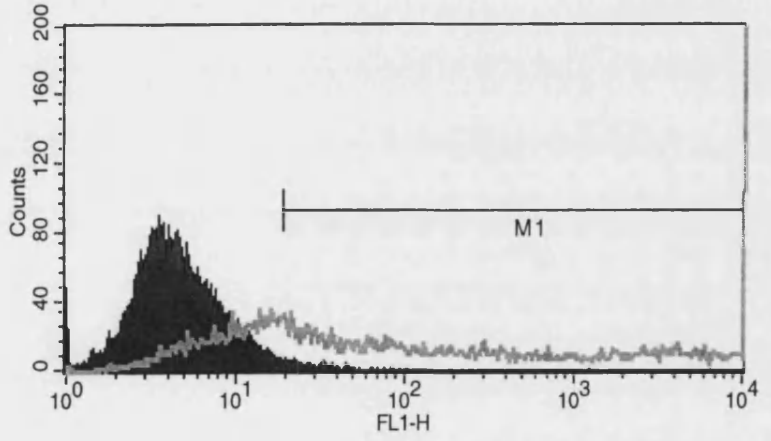


Sample ID: S-2

| Marker | % Total |
|---|---|
| All | 100.00 |
| M1 | 1.71 |

Sample ID: R-2

| Marker | % Total |
|---|---|
| All | 100.00 |
| M1 | 66.54 |

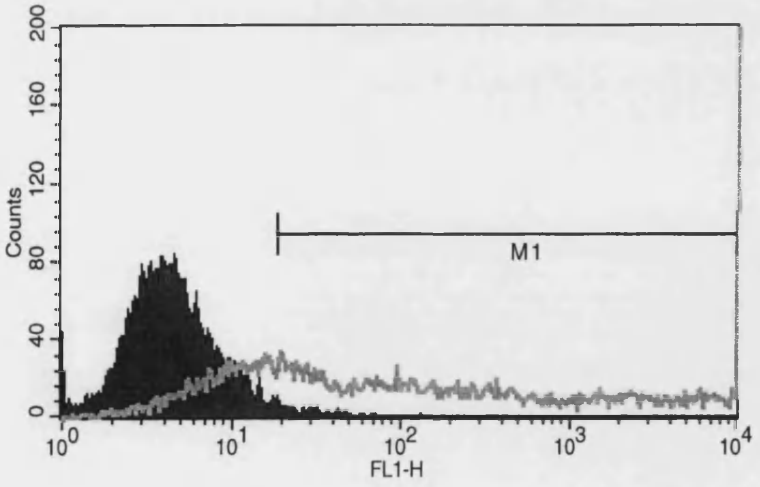


Sample ID: S-3

| Marker | % Total |
|---|---|
| All | 100.00 |
| M1 | 1.53 |

Sample ID: R-3

| Marker | % Total |
|---|---|
| All | 100.00 |
| M1 | 69.50 |